MODELLING THE EFFECTS OF SOIL VARIABILITY AND VEGETATION ON THE STABILITY OF NATURAL SLOPES

by

Yun Hang Chok
B.E. (Hons), MIEAust

Thesis submitted for the degree of
Doctor of Philosophy

The University of Adelaide
School of Civil, Environmental and Mining Engineering

October 2008

ABSTRACT

It is well recognised that the inherent soil variability and the effect of vegetation, in particular the effect of tree root reinforcement, have a significant effect on the stability of a natural slope. However, in practice, these factors are not commonly considered in routine slope stability analysis. This is due mainly to the fact that the effects of soil variability and vegetation are complex and difficult to quantify. Furthermore, the available slope stability analysis computer programs used in practice, which adopt conventional limit equilibrium methods, are unable to consider these factors. To predict the stability of a natural slope more accurately, especially the marginally stable one, the effects of soil variability and vegetation needs to be taken into account.

The research presented in this thesis focuses on investigating and quantifying the effects of soil variability and vegetation on the stability of natural slopes. The random finite element method (RFEM), developed by Griffiths and Fenton (2004), is adopted to model the effect of soil variability on slope stability. The soil variability is quantified by the parameters called the *coefficient of variation* (COV) and *scale of fluctuation* (SOF), while the safety of a slope is assessed using *probability of failure*.

In this research, extensive parametric studies are conducted, using the RFEM, to investigate the influence of COV and SOF on the probability of failure of a cohesive slope (i.e. undrained clay slope) with different geometries. Probabilistic stability charts are then developed using the results obtained from the parametric studies. These charts can be used for a preliminary assessment of the probability of failure of a spatially random cohesive slope. In addition, the effect of soil variability on $c'–\phi'$ slopes is also studied. The available RFEM computer program (i.e. *rslope2d*) is limited to analysing slopes with single-layered soil profile. Therefore, in this research, this computer program is modified to analyse slopes with two-layered soil profiles. The modified program is then used to

investigate the effect of soil variability on two-layered spatially random cohesive slopes. It has been demonstrated that the spatial variability of soil variability has a significant effect on the reliability of both single and two-layered soil slopes.

Artificial neural networks (ANNs), which are a powerful data-mapping tool for determining the relationship between a set of input and output variables, are used in an attempt to predict the probability of failure of a spatially random cohesive slope. The aim is to provide an alternative tool to the RFEM and the developed probabilistic stability charts because the RFEM analyses are computationally intensive and time consuming. The results obtained from the parametric studies of a spatially random cohesive slope are used as the database for the ANN model development. It has been demonstrated that the ANN models developed in this research are capable of predicting the probability of failure of a spatially random cohesive slope with high accuracy. The developed ANN models are then transformed into relatively simple formulae for direct application in practice.

The effect of root reinforcement caused by vegetation is modelled as additional cohesion to the soils, known as *root cohesion*, c_r. The areas affected by tree roots (i.e. root zone) are incorporated in the finite element slope stability model. The extent of the root zone is defined by the *depth of root zone*, h_r. Parametric studies are conducted and the results are used to develop a set of stability charts that can be used to assess the contribution of root reinforcement on slope stability. Furthermore, ANN models and formulae are also developed based on the results obtained from the parametric studies. It has been demonstrated that the factor of safety of a slope increase linearly with the values c_r and h_r, and the contribution of root reinforcement to a marginally stable slope is significant. In addition, probabilistic slope stability analysis considering both the variability of the soils and root cohesion are conducted using the modified RFEM computer program. It has been demonstrated that the spatial variability of root cohesion has a significant effect on the probability of slope failure.

LIST OF PUBLICATIONS

The following publications have been prepared as a result of this research:

Chok, Y. H., Jaksa, M. B. and Griffiths, D. V., Fenton, G.A., and Kaggwa, W. S. (2007). "A parametric study on reliability of spatially random cohesive slopes." *Australian Geomechanics*, 42(2), 79-85.

Chok, Y. H., Jaksa, M. B. and Griffiths, D. V., Fenton, G.A., and Kaggwa, W. S. (2007). "Effect of spatial variability on reliability of soil slopes." *Proc. 10th Australia New Zealand Conference on Geomechanics*, Brisbane, 2, 584-589.

Chok, Y. H., Kaggwa, W. S., Jaksa, M. B. and Griffiths, D. V. (2004). "Modelling the effects of vegetation on stability of slopes." *Proc. 9th Australia New Zealand Conference on Geomechanics*, Auckland, 1, 391-397.

STATEMENT OF ORIGINALITY

This thesis contains no material which has been accepted for the award of any other degree or diploma at any university or other tertiary institution and, to the best of my knowledge and belief, this thesis contains no material previously published or written by another person, except where due reference has been made in the text.

I give consent to this copy of my thesis, when deposited in the University Library, being available for loan and photocopying.

Signed: …….. Date: ……..

ACKNOWLEDGEMENTS

I would like to express my sincere thanks to my principal supervisor, Associate Professor Mark Jaksa, of the School of Civil, Environmental and Mining Engineering, the University of Adelaide, for his enthusiastic guidance, continual support and encouragement throughout this research. His patience and availability for any help is deeply appreciated. His comments and suggestions during the preparation of this thesis are gratefully acknowledged. I would also like to extend my appreciation for the support of my co-supervisor, Dr. William Kaggwa, also of the School of Civil, Environmental and Mining Engineering, the University of Adelaide, for his encouragement, advice and invaluable help throughout this research. His comments, suggestions and thorough review of this thesis are gratefully appreciated.

I wish to thank the School of Civil, Environmental and Mining Engineering, the University of Adelaide for the provision of excellent research support and facilities. I wish to acknowledge the computing support given to me by Dr. Stephen Carr. My thanks are also extended to my fellow postgraduate students for their friendship and encouragement.

The fund given to this research project by the University of Adelaide Scholarship (UAS) is sincerely acknowledged. This research would not have been possible without their financial assistance. My thanks are also extended to the South Australian Partnership Computing (SAPAC) for providing the supercomputer facility called Hydra, which was used to carry out the majority of the numerical studies in this research.

I would also like to acknowledge Professor Vaughan Griffiths, of the Colorado School of Mines, USA, and Professor Gordon Fenton, of the Dalhousie University in Canada, for graciously providing the source code of the random finite element method (RFEM) computer program, i.e. *rslope2d*, which has been used for probabilistic slope stability analysis throughout this research. Their invaluable advice and help in this research are also appreciated.

Finally, I would like to thank my family who have been the source of my strength and inspiration throughout this journey. I will always be indebted to my parents, Tien Siong and Kui Yin, for their sacrifices, love and support throughout my life. I would also like to thank my brother, Yun Vun, and my sister, Yan Lee, for their continual support and encouragement. Lastly, I wish to thank my wife, Lan, for her constant love, understanding and support throughout the period of my candidature.

TABLE OF CONTENTS

Abstract *i*
List of Publications *iii*
Statement of Originality *iv*
Acknowledgements *v*
Table of Contents *vii*
List of Figures *xi*
List of Tables *xvii*
Notation *xix*

CHAPTER 1 INTRODUCTION **1**

1.1 Introduction 1
1.2 Aims and Scope of the Research 2
1.3 Layout of Thesis 3

CHAPTER 2 LITERATURE REVIEW **6**

2.1 Introduction 6
2.2 Methods of Slope Stability Analysis 6
2.2.1 Conventional Slope Stability Analysis 6
2.2.2 Finite Element Method for Slope Stability Analysis 9
2.2.3 Probabilistic Slope Stability Analysis 11
2.3 Soil Variability 15
2.3.1 Classical Statistical Characteristic of Soil Properties 16
2.3.2 Spatial Variability of Soil Properties 21
2.3.3 Published Data for Inherent Soil Variability 25
2.4 Effects of Vegetation on Slope Stability 27
2.4.1 Background 27
2.4.2 Influences of Vegetation 29
2.4.3 Quantifying Effect of Root Reinforcement 33

2.4.4 Modelling Effects of Vegetation on Slope Stability 46
2.4.5 Discussion 50
2.5 Artificial Neural Networks 52
2.5.1 Background 52
2.5.2 Back-Propagation Multi-Layer Perceptrons 53
2.5.3 Development of ANN Model 57
2.6 Summary 61

CHAPTER 3 PROBABILISTIC SLOPE STABILITY ANALYSIS USING RANDOM FINITE ELEMENT METHOD 63

3.1 Introduction 63
3.2 Overview of the Probabilistic Analysis Methodology 63
3.3 Simulation of Soil Profile 64
3.3.1 Soil Parameters 65
3.3.2 Random Field Generation 66
3.3.3 Transformation into Lognormal Random Field 69
3.3.4 Effects of Local Averaging and Variance Reduction 70
3.3.5 Mapping of Simulated Soil Properties onto Finite Element Mesh 72
3.3.6 Cross-correlation between c and ϕ 73
3.4 Finite Element Slope Stability Analysis 74
3.4.1 Determination of Factor of Safety 75
3.4.2 Definition of Slope Failure 76
3.5 Monte Carlo Simulation 76
3.5.1 Probability of Failure 76
3.5.2 Number of Realisations 77
3.6 Validation of Simulated Soil Properties 80
3.6.1 Verification of the Lognormal Distribution 80
3.6.2 Verification of the Correlation Structure 87
3.7 Summary 89

CHAPTER 4 INFLUENCE OF SOIL VARIABILITY ON RELIABILITY OF SINGLE-LAYERED SOIL SLOPES 90

4.1 Introduction 90
4.2 Probabilistic Analysis of Spatially Random Cohesive Slopes 90
4.2.1 Description of Numerical Studies Undertaken 90

4.2.2 Consideration of Computational Resources and Time Constraints 93
4.2.3 Determination of Iteration Limit and Number of Realisations 94
4.2.4 Effect of Mesh Density on Probability of Failure 97
4.2.5 Deterministic Solutions 100
4.2.6 Results of Parametric Studies 100
4.2.7 Effect of Anisotropy of Scale of Fluctuation on Probability of Failure 111
4.2.8 Probabilistic Stability Charts 112
4.3 Probabilistic Analysis of Spatially Random $c' - \phi'$ Slopes 112
4.3.1 Deterministic Solutions 115
4.3.2 Iteration Limit and Number of Realisations 115
4.3.3 Effect of COV and θ/H on Probability of Failure 117
4.3.4 Comparison of Probability of Failure and Factor of Safety 119
4.3.5 Effect of $c'–\phi'$ Correlation on Probability of Failure 121
4.4 Summary 122

CHAPTER 5 INFLUENCE OF SOIL VARIABILITY ON RELIABILITY OF TWO-LAYERED SOIL SLOPES 124

5.1 Introduction 124
5.2 Description of The Two-Layered Soil Slope Model 125
5.3 Validation of the Two-layered Slope Model 128
5.4 Probabilistic Analysis of a Two-Layered Spatially Random Cohesive Slope 129
5.4.1 Description of Numerical Studies Undertaken 129
5.4.2 Deterministic Solutions 130
5.4.3 Results of Numerical Studies 131
5.5 Summary 139

CHAPTER 6 PREDICTION OF RELIABILITY OF SPATIALLY RANDOM COHESIVE SLOPES USING ARTIFICIAL NEURAL NETWORKS 141

6.1 Introduction 141
6.2 Development of ANN Models 142
6.2.1 Input and Output Variables 142
6.2.2 Data Division and Pre-processing 143
6.2.3 Network Architecture and Performance of ANN Models 145
6.3 Development of ANN Model Equation 151

6.4 Sensitivity Analysis of the ANN Model Inputs 154
6.5 Summary 156

CHAPTER 7 SLOPE STABILITY ANALYSIS CONSIDERING EFFECT OF ROOT REINFORCEMENT 157

7.1 Introduction 157
7.2 Assessing Influence of Root Reinforcement on Slope Stability by Finite Element Method 158
7.3 Vegetated Slope Stability Charts 165
7.4 Artificial Neural Networks Modelling 170
7.4.1 Input and Output Variables 170
7.4.2 Database 171
7.4.3 Network Architecture and Performance of ANN Models 172
7.4.4 ANN Model Equation for Vegetated Slope 173
7.5 Probabilistic Study 175
7.5.1 Summary 182

CHAPTER 8 SUMMARY AND CONCLUSIONS 185

8.1 Summary 185
8.2 Recommendations for Further Research 189
8.3 Conclusions 190

REFERENCES 191

APPENDIX A PROBABILISTIC STABILITY CHARTS 211

LIST OF FIGURES

Figure 2.1	Uncertainty in estimation of soil properties (after Kulhawy 1992)	16
Figure 2.2	Normal and lognormal distributions of undrained shear strength, s_u, with mean of 100 kPa and standard deviation of 50 kPa (COV = 0.5)	20
Figure 2.3	Dilatometer lift-off pressure reading P_0 versus depth: (a) measured data points; (b) linear fit and linear regression lines (after DeGroot 1996)	22
Figure 2.4	Reductions in soil moisture near a Poplar tree growing in boulder clay (after Biddle 1983)	31
Figure 2.5	Effect of root reinforcement on the shear strength of soil (after Coppin and Richards 1990)	34
Figure 2.6	Shear strength of root-permeated sand as a function of root density (after Ziemer 1981)	35
Figure 2.7	Comparison of shear strength increase due to root/fibre reinforcement (after Gray and Leiser 1982)	35
Figure 2.8	Root area ratio against depth for different distance from the tree trunk: (a) swamp paperbark and (b) river red gum (after Abernethy and Rutherfurd 2001)	37
Figure 2.9	Relationship between root tensile strength and root diameter for two Australian riparian species (after Abernethy and Rutherfurd 2001)	39
Figure 2.10	Relationship between root tensile strength and root diameter for six vegetation species in Northern Mississippi (after Simon and Collison 2002)	39
Figure 2.11	Perpendicular root reinforcement model (after Wu et al. 1979)	40
Figure 2.12	Root cohesion, c_r (kPa), due to river red gum root reinforcement (after Abernethy and Rutherfurd 2001)	45
Figure 2.13	Root cohesion, c_r (kPa), due to swamp paperbark root reinforcement (after Abernethy and Rutherfurd 2001)	45

Figure 2.14	Forces acting on a slice on a vegetated infinite slope (after Coppin and Richards 1990)	47
Figure 2.15	Influences of vegetation on deep-seated failures (after Coppin and Richards 1990)	48
Figure 2.16	Typical structure and operation of an MLP (after Maier and Dandy 1998)	54
Figure 3.1	Top-down approach for random field generation using LAS method (after Fenton 1990)	67
Figure 3.2	Comparison of estimated and exact correlation between adjacent cells across a parent cell boundary for varying effective averaging lengths 2D/θ (after Fenton 1990)	68
Figure 3.3	Comparison of estimated and exact covariance for generated 2-D LAS process with scales of fluctuation of (a) θ = 4 and (b) θ = 0.5, averaged over 10 realisations (after Fenton 1990)	69
Figure 3.4	Variance reduction over a square finite element (after Griffiths and Fenton 2004)	71
Figure 3.5	Typical finite element mesh used for slope stability analysis	72
Figure 3.6	Typical random field realisations of undrained cohesion, c_u, with scales of fluctuation of (a) θ = 1 m and (b) θ = 10 m	73
Figure 3.7	Minimum number of realisations required versus relative percentage error for 95% and 90% confidence levels, and m = 1	79
Figure 3.8	Frequency density plots for simulated values of c_u with different values of COV and θ/H (based on one realisation)	81
Figure 3.9	Frequency density plots for 'Mean c_u' with different values of COV and θ/H (based on 2,000 realisations)	85
Figure 3.10	Comparison of experimental and theoretical correlation structure for scales of fluctuation (a) θ = 1 m and (b) θ = 10 m	88
Figure 4.1	Geometry of the cohesive slope problem	91
Figure 4.2	Typical finite element mesh for a 1:1 cohesive slope (β = 45°, D = 2)	92
Figure 4.3	Effect of number of iterations on probability of failure (COV = 0.5; θ/H = 1)	96
Figure 4.4	Effect of number of realisations on probability of failure (COV = 0.5; θ/H = 1)	96

Figure 4.5 Effect of number of realisations on computational time (*maxit* = 500) 97

Figure 4.6 Finite element mesh with different mesh density (a) 0.5 m × 0.5 m; (b) 1 m × 1 m; (c) 2 m × 2 m. (β = 45°, D = 2) 98

Figure 4.7 Effect of varying θ/H on probability of failure for different mesh densities with COV fixed at 0.5 and 1.0 (β = 45°, D = 2, N_s = 0.3) 99

Figure 4.8 Typical deformed mesh for the 1:1 cohesive slope with COV of (a) 0.3, (b) 0.5 and (c) 1.0 (β = 45°; D = 2; N_s = 0.3; θ/H = 1) 101

Figure 4.9 Typical deformed meshes for the 1:1 cohesive slope with θ/H of (a) 0.1, (b) 1 and (c) 10 (β = 45°; D = 2; N_s = 0.3; COV = 0.5) 102

Figure 4.10 Effect of varying COV on probability of failure for different values of θ/H with N_s fixed at 0.2 (β = 45°; D = 2) 104

Figure 4.11 Effect of varying COV on probability of failure for different values of θ/H with N_s fixed at 0.3 (β = 45°; D = 2) 104

Figure 4.12 Effect of varying θ/H on probability of failure for different values of COV with N_s fixed at 0.2 (β = 45°; D = 2) 106

Figure 4.13 Effect of varying θ/H on probability of failure for different values of COV with N_s fixed at 0.3 (β = 45°; D = 2) 106

Figure 4.14 Effect of varying θ/H on probability of failure for different values of N_s with COV fixed at 0.1 (β = 45°; D = 2) 107

Figure 4.15 Effect of varying θ/H on probability of failure for different values of N_s with COV fixed at 0.5 (β = 45°; D = 2) 108

Figure 4.16 Effect of varying θ/H on probability of failure for different slopes (D = 2; N_s = 0.2; COV = 0.5) 109

Figure 4.17 Probability of failure versus factor of safety for different values of θ/H with COV fixed at 0.1 (β = 45°; D = 2) 110

Figure 4.18 Probability of failure versus factor of safety for different values of θ/H with COV fixed at 0.5 (β = 45°; D = 2) 110

Figure 4.19 Probability of failure versus factor of safety for different degrees of anisotropy with COV fixed at 0.5 (β = 45°; D = 2; N_s = 0.3; θ_v/H = 1) 111

Figure 4.20 Typical probabilistic stability charts for D = 2 and N_s = 0.2 113

Figure 4.21 Mesh and slope geometry used for the c'-ϕ' slope problem 114

Figure 4.22	Critical slip surface obtained from SLOPE/W using simplified Bishop's method (FOS = 1.2)	115
Figure 4.23	Effect of number of iterations on P_f	116
Figure 4.24	Effect of number of realisations on P_f	116
Figure 4.25	Typical deformed mesh at slope failure for the c'–ϕ' slope with (a) $\theta/H = 0.1$ and (b) $\theta/H = 10$. ($COV_{c'} = 2COV_{\phi'} = 0.3$)	117
Figure 4.26	Effect of varying COV on probability of failure for different values of θ/H	118
Figure 4.27	Effect of varying θ/H on probability of failure for different COVs of c' and ϕ'	119
Figure 4.28	Probability of failure versus factor of safety for different COV of c' and ϕ' ($\theta/H = 1$)	120
Figure 4.29	Probability of failure versus factor of safety for different values of θ/H ($COV_{c'} = 2COV_{\phi'} = 0.5$)	121
Figure 4.30	Probability of failure versus θ/H for different values of COVs of c' and ϕ', and θ/H	122
Figure 5.1	Typical layering profiles of the two-layered soil slope model (a) horizontal layering; and (b) parallel layering	126
Figure 5.2	Simulation of two-layered spatially random soil profile with horizontal layering ($\theta_1/H = 10$, $\theta_2/H = 0.1$)	127
Figure 5.3	Typical simulated two-layered spatially random soil profile with parallel layering ($\theta_1/H = 10$, $\theta_2/H = 0.1$)	127
Figure 5.4	Typical finite element mesh for a 2:1 cohesive slope problem ($\beta = 26.6°$; D = 2)	128
Figure 5.5	Deformed mesh of single-layered cohesive slope ($N_s = 0.25$; COV = 0.5; $\theta/H = 1$)	131
Figure 5.6	Deformed meshes of two-layered cohesive slope with different values of c_{u1}/c_{u2}: (a) 0.5; (b) 0.75; (c) 1.25; and (d) 1.5. (COV = 0.5; θ/H =1)	133
Figure 5.7	Probability of failure versus COV for different values of c_{u1}/c_{u2} with θ/H fixed at 1	134
Figure 5.8	Probability of failure versus θ/H for different values of c_{u1}/c_{u2} with COV fixed at 0.5	135

Figure 5.9	Probability of failure versus θ/H for different values of h/DH with COV and θ/H fixed at 0.5 and 1, respectively	136
Figure 5.10	Typical deformed meshes for a two-layered cohesive slope with different values of COV in each layer: (a) $COV_1 = 0.1$, $COV_2 = 0.5$ ($P_f = 0.014$) and (b) $COV_1 = 0.5$, $COV_2 = 0.1$ ($P_f = 0.081$)	138
Figure 5.11	Typical deformed meshes for a two-layered cohesive slope with different values of θ/H in each layer: (a) $\theta_1/H = 0.1$, $\theta_2/H = 1$ ($P_f = 0.022$) and (b) $\theta_1/H = 1$, $\theta_2/H = 0.1$ ($P_f = 0.151$)	139
Figure 6.1	Data division for ANN model development	143
Figure 6.2	Effect of the numbers of hidden layers nodes on correlation coefficient, *r*, for the validation data set of ANN Models A1 – A12 (learning rate = 0.2; momentum term = 0.8)	147
Figure 6.3	Effect of the learning rate on correlation coefficient, *r*, for the validation data set of the ANN model A3 (momentum term = 0.8)	150
Figure 6.4	Effect of the momentum term on correlation coefficient, *r*, for the validation data set of the ANN model A3 (learning rate = 0.2)	150
Figure 6.5	Structure of the ANN Model A3	151
Figure 7.1	Typical finite element mesh for incorporating effect of root reinforcement	159
Figure 7.2	Vegetated slope with different locations of root zone	160
Figure 7.3	FOS versus root cohesion for different depths of root zone (c' = 1 kPa; ϕ' = 25°)	162
Figure 7.4	FOS versus root cohesion for different values of effective cohesion of soil (ϕ' = 25°; h_r = 1 m)	163
Figure 7.5	FOS versus root cohesion for different values of effective friction angle of soil (c' = 1 kPa; h_r = 1 m)	164
Figure 7.6	Stability charts for 3:1 vegetated slope	166
Figure 7.7	Stability charts for 2:1 vegetated slope	167
Figure 7.8	Stability charts for 1:1 vegetated slope	168
Figure 7.9	Stability charts for 0.5:1 vegetated slope	169
Figure 7.10	Data division for ANN model development	171
Figure 7.11	Structure of the optimal ANN model (Model E2)	174
Figure 7.12	Typical finite element mesh with simulated cohesion value	177

Figure 7.13 Typical deformed meshes for the slopes without considering the effect of root reinforcement: (a) Case 1 and (b) Case 2 178

Figure 7.14 P_f versus COV for different θ/H: (a) Case 1 and (b) Case 2 180

Figure 7.15 P_f versus θ/H for different COV: (a) Case 1 and (b) Case 2 181

Figure 7.16 Typical deformed meshes for the vegetated slope with different values of COV: (a) 0.1 and (b) 1. (θ/H fixed at 10) 182

Figure 7.17 Typical deformed meshes for the vegetated slope with different values of θ/H: (a) 0.1 and (b) 10. (COV fixed at 0.5) 183

LIST OF TABLES

Table 2.1	Typical values for coefficient of variation (after Lee et al. 1983)	26
Table 2.2	Typical values for coefficient of variation (after Lacasse and Nadim 1996)	26
Table 2.3	Suggested guidelines for inherent soil variability (after Phoon and Kulhawy 1999a)	28
Table 2.4	Summary of scale of fluctuation of some geotechnical properties (after Phoon and Kulhawy 1999a)	29
Table 2.5	Root tensile strength for selected plant species (after Coppin and Richards 1990)	38
Table 2.6	Typical values for root cohesion, c_r	43
Table 3.1	Normal standard deviates for different confidence levels	78
Table 3.2	Minimum number of realisations required for achieving desired accuracy	79
Table 3.3	Comparison between sample and target mean and standard deviation of c_u (based on one realisation)	83
Table 3.4	Comparison between sample and target mean and standard deviation of '*Mean* c_u' (based on 2000 realisations)	87
Table 4.1	Input parameters for parametric studies	92
Table 4.2	Cases with shortest and longest computational time	94
Table 4.3	Comparison of P_f and computation time for the slope with different mesh density (COV = 1.0; θ/H = 0.1)	99
Table 4.4	Factor of safety assuming homogenous soil (β = 45°, D = 2)	100
Table 4.5	Input values of COV and θ/H used in the c'-ϕ' slope problem	114
Table 4.6	FOS for c'–ϕ' slope with different mean values of c' and ϕ'	120
Table 5.1	Comparison of estimated values of P_f obtained by using the two-layered model and the original single-layered model	129

Table 5.2	Input parameters for parametric studies of a two-layered cohesive slope	130
Table 5.3	FOS for a two-layered cohesive slope with different c_{u1}/c_{u2} (h/DH = 0.5)	131
Table 5.4	Probability of failure for a two-layered cohesive slope with different values of c_{u1}/c_{u2} (h/DH = 0.5, COV = 0.5, θ/H = 1)	132
Table 5.5	Probability of failure of a two-layered cohesive slope with different values of COV in each soil layer. (h/DH = 0.5, c_{u1}/c_{u2} = 1 and $\theta_1/H = \theta_2/H = 1$)	137
Table 5.6	Probability of failure of a two-layered cohesive slope with different values of θ/H in each soil layer. (h/DH = 0.5, c_{u1}/c_{u2} = 1 and $COV_1 = COV_2 = 0.5$)	138
Table 6.1	Summary of range for input and output variables	143
Table 6.2	Input and output statistic for ANN models	144
Table 6.3	Performance of ANN models with different number of hidden layers and nodes	146
Table 6.4	Performance of ANN models with different learning rates	149
Table 6.5	Performance of ANN models with different momentum terms	149
Table 6.6	Performance of ANN models using different transfer functions	149
Table 6.7	Weights and biases for the ANN Model A3	152
Table 7.1	Computed FOS for the slope with different locations of root zone	161
Table 7.2	Input variables and values for parametric studies undertaken	165
Table 7.3	Summary of range for input and output variables	170
Table 7.4	Input and output statistic for ANN models	172
Table 7.5	Performance of ANN models with different number of hidden nodes	173
Table 7.6	Weights and biases for the ANN Models E2	174
Table 7.7	Input parameters and values for Case 1	177
Table 7.8	Input parameters and values for Case 2	177
Table 7.9	Computed P_f for the slopes considering effect of root reinforcement	179

NOTATION

A	total cross-sectional area of the soil
A_r	total cross-sectional area occupied by roots
ANNs	artificial neural networks
a_i	mean cross-sectional area of roots in size class *i*
$C_{y_j d_j}$	covariance between the model output (y_j) and the desired output (d_j)
COV	coefficient of variation
$\mathrm{Cov}[\ldots]$	covariance operator
c	cohesion
c'	drained or effective cohesion
c_0	autocovariance at lage 0
c_k	autocovariance
c_r	root cohesion
c_{Total}	total cohesion
c_u	undrained cohesion
D	depth factor of a slope
d	root diameter
$\bar{d}$	mean of desired output (d_j)
d_j	desired actual output of node *j*
E	global error function
E_s	Young's modulus
$\mathrm{E}[\cdots]$	expectation operator
F_s	factor of safety
FEM	finite element method
FOS	factor of safety
FOSM	first order second moment method

$f(I_j)$	transfer function of node *j*
$f(x)$	continuous function of *x*
G(*x*)	standard normal random field
H	height of slope
h_r	depth of root zone
I	number of input variables
k	lag distance
k_0	autocorrelation distance
L_{min}	minimum root length
LAS	local average subdivision
MAE	mean absolute error
MLPs	multi-layer perceptrons
MCS	Monte Carlo simulation
MSE	mean squared error
Median_X	median of variable *X*
Mode_X	mode of variable *X*
N_s	stability coefficient
n	number of data points
n_f	number of realisation reaching failure
n_{sim}	number of realisations
P_f	probability of failure
PEM	point estimation method
PDF	probability density function
RAR	root area ratio
RFEM	random finite element method
RMSE	root mean squared error
r	coefficient of correlation
S_w	surcharge due to weight of vegetation
SOF	scale of fluctuation
s	soil shear strength
s_u	undrained shear strength
T	averaging domain

T_r	mean tensile strength of roots
t_i	deterministic trend component
u	pore water pressure
u_a	pore air pressure
$\mathrm{Var}[\ldots]$	variance operator
W	total weight of slice
w_{ji}	connection weight between nodes i and j
X	random variable
$\overline{X}$	average value of variable X
x	input variables
x_i	input from node i
x_{max}	maximum value of input variable x
x_{min}	minimum value of input variable x
x_n	scaled value of input variable x
Y	random variable
$\overline{Y}$	average value of variable Y
$\bar{y}$	average value of variable y
y_j	predicted output of node j
α	shear distortion angle
β	slope angle
Γ^2	variance function
γ	bulk unit weight
Δw_{ji}	weight increment from node i to node j
ε_i	residual component
η	learning rate
θ	scale of fluctuation
θ_j	bias for node j
μ	mean value
μ_X	mean value of variable X
μ_Y	mean value of variable Y
$\mu_{\ln X}$	mean of the normally distributed ln(X)

ν	Poisson's ratio
ρ	correlation coefficient
ρ_k	autocorrelation coefficient
ρ_{XY}	coefficient of correlation of variables X and Y
σ	standard deviation
σ^2	point variance
σ_n	normal stress
σ_T^2	variance of the soil property spatially averaged over an averaging domain T
σ_X	standard deviation of variable X
σ_Y	standard deviation of variable Y
σ_{d_j}	standard deviation of desired output d_j
σ_{y_j}	standard deviation of model output y_j
$\sigma_{\ln X}$	standard deviation of the normally distributed ln(X)
τ_b	limiting bond stress between the root and the soil
ϕ	friction angle
ϕ^b	friction angle of the soil with respect to changes in matric suction
ϕ'	drained or effective friction angle
ψ	dilation angle

Chapter 1

INTRODUCTION

1.1 Introduction

Slope instability is one of the major problems in geotechnical engineering where disasters involving loss of life and property can and do occur. The majority of these slope failures are associated with vegetated or forested *natural slopes*. A natural slope is different from a man-made slope or embankment in that the effects of *soil variability* and *vegetation* may play an important role in its stability. It is well recognised that the underlying soil profiles of a natural slope are unlikely to be completely uniform and homogenous, due largely to the complex deposition process of soil materials. Even within a so-called 'homogenous' soil layer, soil properties tend to vary from one location to another (Vanmarcke 1977a). This inherent variation of soil properties in distance or space is known as *spatial variability*. In addition, vegetation can affect the stability of a slope mainly by the increase in soil shear strength due to *root reinforcement*, although other effects such as surcharge of trees; wind loading on large trees; soil buttressing and arching effects caused by large tree roots; and modification of soil moisture content through the processes of rainfall interception and evapotranspiration may also provide minor effects on slope stability (Gray and Leiser 1982; Greenway 1987; Coppin and Richards 1990). The actual behaviour of natural slopes, as distinct from man-made slopes, is greatly affected by the effects of soil variability and vegetation mentioned above.

In practice, the stability of a slope is usually assessed using the conventional limit equilibrium methods, and the soil profiles are often assumed to be uniform and homogenous. The conventional slope stability analyses are usually performed within a deterministic analysis framework where single best estimates or characteristic values for

soil parameters are used. To account for the variability and uncertainty in soil properties, a higher *factor of safety* is usually adopted. In addition, the effects of vegetation are usually ignored in the stability analysis of a vegetated slope, due mainly to the fact that the physical effects of vegetation are complex and difficult to quantify. Furthermore, engineers claim that ignoring the effects of vegetation is a conservative approach, knowing that vegetation will ultimately enhance the stability of a slope. As a result, the conventional slope stability analysis approach may give a poor estimate of the actual safety of a natural slope because the effects of soil variability and vegetation are not properly modelled and accounted for.

Adopting a higher factor of safety to account for the effects of soil variability and ignoring the influence of vegetation in slope stability analysis appears to be reasonable and acceptable when designing a new slope, where conservatism is necessary. However, when predicting the actual behaviour of an existing slope, for example, the assessment of a marginally stable natural slope, ideally, all aspects should be taken into account. Otherwise, engineers and planners are unaware of the true safety or reliability of the slope. Therefore, there is a need to consider and include the effects of soil variability and vegetation in slope stability analysis so that the actual behaviour of natural slopes can be predicted more accurately.

1.2 Aims and Scope of the Research

This research has aimed to investigate and quantify the effects of soil variability and root reinforcement contributed by vegetation on the stability of natural slopes, and to develop simplified solutions, in the form of charts or equations, which can be readily used in practice for a quick or preliminary assessment of the effects of soil variability and vegetation on slope stability. The results of this research will provide a better understanding of the effects of soil variability and vegetation on the stability of natural slopes. In addition, the simplified solutions (i.e. charts or equations) developed in this research will enable engineers to quantify the effects of soil variability and vegetation on slope stability.

In order to achieve the overall aim of this research, several specific aims or steps are established, as summarised below:

1. Investigate the effects of soil variability on the reliability of single-layered spatially random cohesive slopes (i.e. undrained clay slopes) and $c'-\phi'$ slopes by performing parametric studies using the *random finite element method* (RFEM), developed by Griffiths and Fenton (2000; 2004). For the cohesive slope problem, the results of the parametric studies are used to develop a set of probabilistic stability charts that can be used for predicting the probability of failure of a spatially random slope.

2. The available computer program of the RFEM is limited for analysing slope with only single-layered soil profile. Therefore, this research extends and modifies the available RFEM computer program to model slopes with two-layered soil profiles and the effects of soil variability on the reliability of a two-layered soil slope are investigated.

3. Investigate the feasibility of using *artificial neural networks* (ANNs) for predicting the probability of failure of a spatially random cohesive slope. The objective is to develop ANN models and transform them into relatively simple mathematical equations. These ANN models and equations can serve as an alternative tool to the RFEM and the developed stability charts.

4. Incorporate the effects of root reinforcement into the existing finite element model for slope stability analysis and perform parametric studies to investigate the effect of root reinforcement contributed by vegetation on the stability of a slope. The results of parametric studies are used to develop a set of stability charts for predicting the factor of safety of vegetated slopes considering the effects of root reinforcement. As an alternative tool to the finite element analysis and stability charts, ANN model and mathematical equations are developed.

1.3 Layout of Thesis

In Chapter 2, reviews of literature on the topics that are related to the work in this research are presented including: methods of slope stability analysis; soil variability; effects of vegetation on slope stability; and artificial neural networks.

In Chapter 3, the formulation and implementation of the random finite element method (RFEM) for probabilistic slope stability analysis are described. This includes the

procedures for simulation of spatially random soil profiles, the formulation of the finite element slope stability analysis model, and some important aspects related to Monte Carlo simulation. The soil profiles simulated by RFEM are examined and validated so that the prescribed statistical characteristics are accurately simulated.

In Chapter 4, the parametric studies undertaken, using the RFEM, for investigating and quantifying the effects of soil variability on the reliability of spatially random cohesive and $c'-\phi'$ slopes, are described. For the cohesive slopes, the parametric studies are performed on slopes with different geometries. Probabilistic stability charts are developed for predicting the probability of failure of spatially random cohesive soil slopes.

In Chapter 5, modifications and extension of the available computer model RFEM aimed at analysing slopes with two-layered soil profiles are described. Results of parametric studies to investigate the effect of soil variability on the reliability of a two-layered spatially random cohesive soil slope are also described.

In Chapter 6, the application of ANN techniques for predicting the probability of failure of spatially random cohesive soil slopes is described. The data used for the development of the ANN model are obtained from the results of the parametric studies conducted in Chapter 4. Relatively simple mathematical equations based on the developed ANN model are developed. The relative importance of the input parameters affecting the probability of failure is also investigated.

In Chapter 7, the effect of root reinforcement is incorporated in the existing finite element slope stability model. Parametric studies are conducted to investigate and quantify the effect of root reinforcement on slope stability. A set of stability charts are developed based on the results of the parametric studies, which can be used for a quick evaluation of the factor of safety of a vegetated slope considering the effect of root reinforcement. An ANN model is developed for predicting the factor of safety of a vegetated slope considering the effect of root reinforcement using the data obtained from the parametric studies. This ANN model has been transformed into relatively simple mathematical equation. In addition, the effect of the spatial variability of root cohesion on the probability of failure of a slope is investigated using the two-layered slope model developed in Chapter 5.

In Chapter 8, summary and conclusions of this research are presented, and recommendations for future research are also given.

Chapter 2

LITERATURE REVIEW

2.1 Introduction

In order to predict the stability of a natural slope more accurately, the effects of soil variability and vegetation need to be taken into consideration. In this research, these two aspects have been incorporated into slope stability analysis, and their effects on slope stability have been investigated and quantified. This chapter provides a background for later chapters of this thesis and briefly reviews the relevant literature in: methods of slope stability analysis; soil variability; effects of vegetation on slope stability; and artificial neural networks.

2.2 Methods of Slope Stability Analysis

Slope stability analysis is usually performed to evaluate the safety of natural slopes, excavations, embankments, earth dams and landfills. Over the years, slope stability analysis has evolved from tedious manual calculations to advanced computer solutions and probabilistic analysis. The improvement in the tools for slope stability analysis, in most cases, has improved the engineer's understanding about the slope stability problem. The following sections briefly discuss the available methods of slope stability analysis.

2.2.1 Conventional Slope Stability Analysis

In practice, the stability of a slope is usually assessed using *limit equilibrium methods*. Stability analysis using the limit equilibrium approach involves solving the equilibrium problem by assuming force and/or moment equilibrium. Over the years, many limit equilibrium methods for slope stability analysis have been developed and applied in practice, including the ordinary method of slices (Fellenius 1936), Bishop's modified

method (Bishop 1955), force equilibrium methods (e.g. Lowe and Karafiath 1960), Janbu's generalised procedure of slices (Janbu 1968), Morgenstern and Price's method (Morgenstern and Price 1965) and Spencer's method (Spencer 1967). Slope stability charts based on these limit equilibrium methods have also been developed (e.g. Taylor 1937, 1948; Bishop and Morgenstern 1960; Spencer 1967; Janbu 1968; Hunter and Schuster 1971; Cousins 1978), which are useful for preliminary analysis and quick estimation of the stability of a slope. However, in practice, detailed slope stability analysis is usually performed using a computer program and most of the available computer programs are based on the limit equilibrium approach.

Slope stability analysis can be performed using either *total* or *effective stress*. Total stress analysis is applicable to embankments and multistage loading problems where the short-term condition is critical, while effective stress analysis should be used for excavation problems where the long-term condition is critical (Duncan 1996). In total stress analysis, pore pressures are not considered in the analysis and the shear strength of soil is described by undrained shear strength, s_u (sometimes referred to $\phi_u = 0$ analysis). In effective stress analysis, the shear strength of soil is described by the Mohr-Coulomb failure criterion, as given by:

$$s = c' + (\sigma_n - u)\tan\phi' \tag{2.1}$$

where c' = effective cohesion of the soil; σ_n = normal stress; u = pore water pressure; and ϕ' = effective friction angle of the soil. It should be noted that Equation (2.1) is applicable only to fully saturated soils. For partially saturated or unsaturated soils, the Mohr-Coulomb failure criterion can be extended in the following form (Fredlund et al. 1978):

$$s = c' + (\sigma_n - u_a)\tan\phi' + (u_a - u)\tan\phi^b \tag{2.2}$$

where u_a = pore air pressure; ϕ^b = friction angle of the soil with respect to changes in $(u_a - u)$ when $(\sigma_n - u_a)$ is held constant. The term $(u_a - u)$ is usually known as the

matric suction and is considered as an increase in the apparent soil cohesion (Fredlund and Rahardjo 1993).

In the conventional limit equilibrium approach, the stability of a slope is measured by *factor of safety* (FOS), which is defined as the ratio between the shear strength of the soil to the shear stress required for equilibrium (Duncan 1996). A slip surface, which can be planar, circular or non-circular in shape, is required to be assumed prior to the equilibrium analysis. At the point of failure the shear strength is assumed to be fully mobilised along the slip surface and FOS is assumed to be constant for the entire slip surface. The stability analysis eventually involves an iterative process until the critical slip surface is found, which is the slip surface with the lowest FOS. Over the years, many studies have been conducted to investigate the computational accuracy of different limit equilibrium methods and to develop techniques for searching the critical slip surface (Duncan 1996). However, Duncan (1996) pointed out that the critical slip surface can be assumed to be circular, in most cases, with little inaccuracy unless there are geological layers that constrain the slip surface to a non-circular shape.

It should be noted that most conventional slope stability analyses are performed within a deterministic framework. This means the input parameters (e.g. shear strength parameters, pore pressure, etc.) are based on the single best estimate value of the available field or laboratory test data. In most cases, due to limited test data, engineering judgements based on previous experience are required to generate the best estimate for each parameter. As a result, the calculated FOS not only depends on the accuracy of the chosen method of analysis and the assumed failure mode, but also the uncertainty associated with the input parameters and the reliability of judgmental assumptions made in relation to the input parameters. In practice, the uncertainty and variability in soil parameters are traditionally accounted for by adopting a higher FOS. However, FOS has been proved to be an inadequate tool for quantifying the effects of uncertainty and variability in soil properties (Duncan 2000). Hence, it is readily accepted that more reliable tools to incorporate soil variability and uncertainty into slope stability analysis are required. This has led to the development of probabilistic slope stability analysis in the 1970s (e.g. Wu and Kraft 1970; Alonso 1976; Tang et al. 1976; Vanmarcke 1977b), and this will be discussed later.

2.2.2 Finite Element Method for Slope Stability Analysis

The finite element method (FEM) is a relatively new but powerful technique for slope stability analysis. Although the FEM has been commonly used in deformation analysis of embankments and other geotechnical problems, it is still not widely used for stability analysis of slopes as compared with the conventional limit equilibrium methods (Duncan 1996; Griffiths and Lane 1999). This is because the latter approach is theoretically simple and the available computer programs can usually provide a quick and accurate estimation of the FOS of a slope. In contrast, the FEM involves more complex theory and it usually requires more time for developing model parameters, performing the computer analyses and interpreting the results (Duncan 1996). Despite that, the FEM for slope stability analysis has several advantages over the conventional limit equilibrium methods, as stated by Griffiths and Lane (1999):

1. No assumption is required to be made in advance with respect to the shape and location of the slip surface. Failure occurs 'naturally' through zones where the soil elements with shear strength that is lower than the applied shear stress.

2. There is no need to make assumptions about internal forces, which appear to be one the major sources of inaccuracy for some limit equilibrium methods. The finite element method preserves global equilibrium until 'failure' is reached.

3. The finite element solutions provide information about deformations at pre-failure stress levels if realistic soil stiffness parameters are used.

4. The finite element method is able to provide information on progressive failure up to and including overall shear failure.

One of the earliest studies that used the FEM for stability analysis of slopes was conducted by Smith and Hobbs (1974). Based on the elasto-plastic soil model, they reported results of ϕ_u = 0 slopes and obtained reasonable agreement with Taylor's (1937) charts. Meanwhile, studies were conducted by Zienkiewicz et al. (1975) and Griffiths (1980) to analyse the stability of c'-ϕ' slopes using the FEM. These studies also indicated that the FOS computed by the FEM was in good agreement with that calculated by limit equilibrium methods. Since then, more studies adopting the FEM for slope stability

analysis have been reported (e.g. Potts et al. 1990; Matsui and Sun 1992; Griffiths and Lane 1999; Jeremic 2000; Lane and Griffiths 2000; Lechman and Griffiths 2000; Sainak 2004; Zheng et al. 2006; Griffiths and Marquez 2007; Li 2007).

The first published finite element slope stability analysis software was reported in the second edition of the text by Smith and Griffiths (1988). This two-dimensional (2D), elasto-plastic finite element software was updated to include a better slope geometry routine in the third edition of the text (Smith and Griffiths 1998) and extended to three-dimensional (3D) analysis in the fourth edition of the text (Smith and Griffiths 2004). This finite element slope stability analysis software has been rigorously tested and validated against the limit equilibrium methods by Griffiths and Lane (1999). They demonstrated that the computer program can be applied to slopes under different conditions including undrained clay (ϕ_u = 0) slopes, $c'-\phi'$ slopes, layered slopes and slopes with a free surface. Meanwhile, Lane and Griffiths (2000) used the same computer program to estimate the stability of a slope under a drawdown condition and comparisons were made with the limit equilibrium results published by Morgenstern (1963). Furthermore, Lechman and Griffiths (2000) analysed the progression of failure within a slope under different loading strategies using the same computer program. More recently, Griffiths and Marquez (2007) conducted studies using the 3D version of the FEM computer program for slope stability analysis and made comparisons with other available 3D limit equilibrium methods. The 2D version of this finite element slope stability program will be used throughout this research. The theoretical aspects and formulation of the finite element slope stability model will be discussed in the next chapter.

In addition to the advantages mentioned above, when the FEM is combined with a random field generator, it is capable of analysing slopes with spatially random soil properties. This is due to the nature of the FEM where the entire slope domain is divided into numerous discrete elements and every single element can be assigned a different random variable by the random field generator. The probabilistic analysis methodology that involves combining random fields with FEM to perform Monte Carlo analysis is called the *random finite element method* (RFEM) (Griffiths and Fenton 2004), which is a powerful tool for considering soil variability in slope stability analysis and this will be discussed later. In contrast, the conventional limit equilibrium methods are deficient when explicitly modelling the spatial or point-to-point variation of soil properties.

2.2.3 Probabilistic Slope Stability Analysis

As mentioned in Section 2.2.1, deterministic FOS is inadequate for effectively accounting for the effect of soil variability and other sources of slope stability uncertainty. Probabilistic analysis has been considered as a more rational approach to account for the uncertainty and variability of soil properties in geotechnical analyses. Instead of using FOS as the measure of the safety of a slope, the *probability of failure* or *reliability index* are often used in probabilistic slope stability analysis (Mostyn and Li 1993; U.S. Army Corps of Engineers 1995; Wolff 1996). In the literature, several probabilistic approaches have been applied to slope stability analysis including the: (1) *first order second moment* (FOSM) method; (2) *point estimate method* (PEM) method; (3) *Monte Carlo simulation* (MCS) and (4) *random finite element method* (RFEM). These are described briefly in turn below.

2.2.3.1 First Order Second Moment

The first order second moment (FOSM) method is a relatively simple approach for accounting for the effects of the variability of the input random variables with respect to a *performance function*. In this case, the performance function is the FOS equation of the selected limit equilibrium method (e.g. Bishop's simplified method of slices, Morgenstern and Price's method and Spencer's method). This approach is based on a Taylor series expansion of the performance function at some point to be evaluated. This expansion is truncated after the linear term (i.e. first order). The first two moments (mean and standard deviation) of the input parameters are used to estimate the first two moments of the performance function (Harr 1987):

$$\mathrm{E}[F_s] = \mu_F \approx g\left(\mathrm{E}[X_1], \mathrm{E}[X_2], \cdots, \mathrm{E}[X_n]\right) \tag{2.3}$$

$$\mathrm{Var}[F_s] = \sigma_F^2 \approx \sum_{i=1}^{n}\left[\left(\frac{\partial F}{\partial X_i}\right)^2 \mathrm{Var}[X_i]\right] + 2\sum_{i=1}^{n}\sum_{j=1}^{n}\left[\left(\frac{\partial F}{\partial X_i}\frac{\partial F}{\partial X_j}\right)\mathrm{Cov}[X_i, X_j]\right] \tag{2.4}$$

where $\mathrm{E}[F_s]$ and $\mathrm{Var}[F_s]$ are the mean and variance of the factor of safety, F_s, respectively; $\mathrm{Cov}[X_i, X_j]$ is the covariance between the random variables x_i and x_j; and n is the number of random variables.

The detailed formulations of the FOSM method can be found in several publications (e.g. Harr 1987; U.S. Army Corps of Engineers 1995; Griffiths et al. 2002b). The application of the FOSM method in slope stability analysis has been described by Alonso (1976), Tang et al. (1976), Vanmarcke (1977b), Li and Lumb (1987), Li and White (1987), Mostyn and Soo (1992), Christian et al. (1994a) and Duncan (2000), among others. Although the FOSM method is relatively simple to implement, it has several limitations. The accuracy of the FOSM method diminishes as the nonlinearity of the performance function increases due to the truncation of the Taylor series after the first order term. It should be noted that the FOS equations for most limit equilibrium methods are non-linear in nature. Furthermore, the FOSM method provides no information about the shape of the probability density function (PDF) of the output and the shape of the PDF needs to be assumed in order to estimate any probability (El-Ramly et al. 2002; Griffiths et al. 2002b). In addition, evaluating the partial derivatives in Equation (2.4), for a highly non-linear performance function, can be cumbersome. To overcome this problem, U.S. Army Corps of Engineers (1995) recommends the use of the finite difference approximation of the partial derivatives. Duncan (2000) demonstrated that the FOSM could be applied to many geotechnical problems including slope stability by using this simplified approach.

2.2.3.2 Point Estimate Method

An alternative approach to the FOSM method is the point estimate method (PEM), developed by Rosenblueth (1975; 1981) and discussed in detail by Harr (1987), Wolff (1996), U.S. Army Corps of Engineers (1995), and Griffiths et al. (2002b). In the PEM, the continuous PDFs for the input random variables are replaced by a set of discrete point masses, which are located at plus or minus one standard deviation from the mean values. The discrete point masses are then multiplied by weighted factors to evaluate the first two moments of the performance function. The PEM is a direct method and it can give reasonably accurate results. However, the PEM is less popular for slope stability analysis because the computations become complicated and tedious when there are more than two random variables to be considered. Despite that, some researchers have attempted to use the PEM for probabilistic slope stability analysis (e.g. McGuffey et al. 1982; Nguyen and Chowdhury 1984; Li 1992; Thornton 1994). An excellent summary of the accuracy and limitations of this method has been provided by Christian and Baecher (1999).

2.2.3.3 Monte Carlo Simulation

Another way to estimate the mean and standard deviation of the performance function is the use of Monte Carlo simulation (MCS). Here, random variables are generated based on their assumed PDF, and the performance function is evaluated for each generated set. The process is repeated thousands of times in order to establish the statistic of the performance function. The major advantage of this method is that no assumption is required about the shape of the PDF of the performance function. In addition, MCS is simpler and more straightforward in terms of mathematics as compared with the FOSM and PEM. The major limitation of the MCS is the extensive computational efforts required. As a result, this method is seldom used in practice (El-Ramly et al. 2002). However, several authors have attempted to combine limit equilibrium methods with MCS to perform probabilistic slope stability analysis (e.g. Kim et al. 1978; Nguyen and Chowdhury 1984; Chandler 1996; El-Ramly et al. 2002) to model the uncertainty and variability of the soil properties. It should be noted that, MSC is gaining popularity due to the recent rapid development in computing resources.

2.2.3.4 Considerations for Spatial Correlation

The majority of the probabilistic slope stability analyses that have been reported in the literature, including those mentioned above, have generally ignored the spatial correlation of the soil properties, except the studies conducted by Vanmarcke (1977b); Li and Lumb (1987), Mostyn and Soo (1992) and El-Ramly et al. (2002). In these studies, the spatial correlation of the soil properties along the critical slip surface has been modelled using a random field model and the concept of spatial averaging (Vanmarcke 1977a, 1983). A reduction in the variance of soil properties was considered, based on the assumed scale of fluctuation of the soil. Other studies, however, assumed that the soil property was represented by a single random variable, which implies that the soil property is perfectly correlated over the entire slope geometry. It has been shown that ignoring spatial correlation of soil properties in probabilistic slope stability analysis could significantly overestimate the probability of failure (Li and Lumb 1987; Mostyn and Soo 1992; El-Ramly et al. 2002).

The main limitation of using limit equilibrium methods for probabilistic slope stability analysis is that the spatial correlation of properties cannot be accounted for explicitly, although some authors have attempted to consider it implicitly. This is due to the inherent limitation of the limit equilibrium method itself, where uniform soil properties need to be assumed within each soil layer. Moreover, previous probabilistic slope stability analyses have evaluated the probability of failure based on the critical slip surface obtained from deterministic analysis. However, very often, the critical slip surface obtained from the deterministic analysis may not be the critical slip surface in the probabilistic analysis due to the spatial variability of the soils. In fact, the critical slip surface is not always a traditional circular or wedge shape in a non-homogenous or spatially random soil slope. It is more logical that slope failure will occur at locations with low shear strength or 'weak zones' within the slope geometry due to the fact that shear strength generally varies from one location to another. Consequently, the critical slip surface can be almost any shape, depending on the spatial correlation structure of the soil properties. Hence, for this reason, the studies that consider spatial correlation of soil properties along the critical slip surface may be inadequate as well.

2.2.3.5 Random Finite Element Method

To overcome the limitations of the limit equilibrium methods in accounting for the spatial variability of soil properties, Griffiths and Fenton (2000; 2004) proposed an approach called the random finite element method (RFEM), which incorporates spatially random soil profiles into finite element slope stability analysis. In this approach, the spatially random soil profiles were generated using the local average subdivision (LAS) method (Fenton 1990; Fenton and Vanmarcke 1990) based on random field theory (Vanmarcke 1977a, 1983). The non-linear finite element program was based on that developed by Smith and Griffiths (1998), as previously discussed in Section 2.2.2. The random field and the finite element methods were merged together and combined with Monte Carlo simulation to perform probabilistic analysis of a slope. The RFEM is a powerful tool for considering the spatial variability of soil properties in geotechnical problems. Apart from the applications in slope stability problems, the RFEM has also been applied to other geotechnical problems including the bearing capacity of shallow foundations (e.g. Fenton and Griffiths 2000, 2001; Griffiths and Fenton 2001; Griffiths et al. 2002a; Fenton and Griffiths 2003), settlements of shallow foundations (e.g. Paice et al. 1996; Fenton and Griffiths 2002,

2005); retaining walls and earth pressure problems (e.g. Fenton et al. 2005; Griffiths et al. 2005), and seepage (Griffiths and Fenton 1993; Fenton and Griffiths 1996, 1997; Griffiths and Fenton 1997, 1998). The RFEM will be used for probabilistic slope stability analysis throughout this research so that the effect of soil variability can be investigated. The theoretical aspects and formulation of the RFEM will be discussed in the next chapter.

Although Griffiths and Fenton (2000; 2004) have made a significant contribution in developing a powerful and advanced method (i.e. RFEM) for considering the spatial variability of soil properties in probabilistic slope stability analysis, more work is required to be done so that this method can be readily accepted and used in the practice. The major limitation of the RFEM is the theoretical complexity of the method and it is also time consuming to perform the finite element analysis and Monte Carlo simulation. Practising engineers may be delaying in adopting the RFEM for probabilistic slope stability analysis due to these limitations. Therefore, there is a need to transform the RFEM solutions into more simplified and straightforward solutions, either in the forms of charts or simple equations, which can be readily adopted by practising engineers. Furthermore, the available computer model of RFEM is limited to analysing slopes with single-layer soil profiles, the model is yet to be extended to analyse slopes with layered soil profiles. The soil profiles of natural vegetated slopes often consist of distinct layers of soil with different properties due to natural deposition process.

2.3 Soil Variability

It is well recognised that the properties of natural soils are inherently variable from one location to another, even within a relatively homogenous deposit. This is due mainly to the complex nature of geological deposition process and loading history. Vanmarcke (1977a) identified *inherent soil variability* as one of the three primary sources of uncertainty in soil property characterisation. The other two sources of uncertainty are *statistical uncertainty* due to limited sampling data and *measurement errors* which arise from testing equipment and procedures. *Transformation model uncertainty* that is introduced when field or laboratory measurements are transferred into design soil properties using empirical or other correlation models has also been identified as another major sources of uncertainty in relation to soil property characterisation (Phoon and Kulhawy 1999a, 1999b). Estimated soil properties, which are used in geotechnical design and analysis, are affected by the

above-mentioned sources of uncertainty, as shown in Figure 2.1. As a result, outcomes of geotechnical design and analysis are always associated with a certain level of uncertainty and risk governed by the assumptions made in relation to the input soil parameters. The present research focuses primarily on the effect of inherent soil variability on slope stability. The following sections present the techniques used to quantify inherent soil variability and published data associated with it.

NOTE:
This figure is included on page 16 of the print copy of the thesis held in the University of Adelaide Library.

Figure 2.1 Uncertainty in estimation of soil properties (after Kulhawy 1992)

2.3.1 Classical Statistical Characteristic of Soil Properties

Variability or uncertainty in soil properties can be quantified by treating the soil properties as *random variables* (e.g. denoted by X and Y). Instead of having a single deterministic value, such a soil property will now have a range of values as defined by its *probability density function* (PDF). Several classical statistical measures used for describing random variables are presented below.

2.3.1.1 Mean of a Random Variable

For a random variable X, with a PDF defined by a function $f(x)$, the mean, μ_X, or expected value, $\mathrm{E}[X]$, is defined by:

$$\mathrm{E}[X] = \mu_X = \int_{-\infty}^{\infty} x\, f(x) dx \tag{2.5}$$

for continuous functions, or

$$\mathrm{E}[X] = \mu_X = \frac{1}{n}\sum x_i \tag{2.6}$$

for discrete functions, where *n* is the number of data points.

2.3.1.2 Variance of a Random Variable

The variance measures the dispersion or uncertainty of data about the mean value and is calculated by:

$$\mathrm{Var}[X] = \sigma_X^2 = \mathrm{E}\left[(X - \mu_X)^2\right] = \int_{-\infty}^{\infty} (x - \mu_X)^2\, f(x)\, dx \tag{2.7}$$

for continuous functions, or

$$\mathrm{Var}[X] = \frac{1}{n-1}\sum (x_i - \mu_X)^2 \tag{2.8}$$

for discrete functions, , where *n* is the number of data points.

2.3.1.3 Standard Deviation of a Random Variable

The standard deviation is, σ_X , is related to the variance, $\mathrm{Var}[X]$, by:

$$\sigma_X = \sqrt{\mathrm{Var}[X]} \tag{2.9}$$

2.3.1.4 Coefficient of Variation of a Random Variable

Variability of soil properties is often expressed by the parameter known as the *coefficient of variation*, COV, which is the ratio of the standard deviation to the mean value, as given by:

$$\mathrm{COV} = \frac{\sigma_X}{\mu_X} \tag{2.10}$$

In the literature, many researchers have reported values of COV for various soil properties, which will be discussed later.

2.3.1.5 Correlation of Two Random Variables

If a pair of random variables (e.g. X and Y) depends on each other, the variables X and Y are considered to be correlated, and their correlation is measured by the *covariance*, $\mathrm{Cov}[X,Y]$, as described by:

$$\mathrm{Cov}[X,Y] = \mathrm{E}[(X-\mu_X)(Y-\mu_Y)] \tag{2.11}$$

for continuous functions, or

$$\mathrm{Cov}[X,Y] = \frac{1}{n}\sum (x_i-\mu_X)(y_i-\mu_Y) \tag{2.12}$$

for discrete functions, where n is the number of data points.

The *coefficient of correlation*, ρ_{XY}, is obtained by normalising the covariance by the standard deviation of variables X and Y, as given by:

$$\rho_{XY} = \frac{\mathrm{Cov}[X,Y]}{\sigma_X \sigma_Y} \tag{2.13}$$

The correlation coefficient is bounded by –1 and +1 (i.e. $1- \le \rho_{XY} \le +1$), where $\rho_{XY} = \pm 1$ indicates a perfect correlation between the variables *X* and *Y* (either positive or negative), while $\rho_{XY} = 0$ indicates the two random variables are linearly independent.

2.3.1.6 Probability Density Function

The probability density function (PDF) defines the distribution of a random variable and the most commonly used PDFs in geotechnical applications are the normal and lognormal distributions. For example, Lumb (1966) used the χ^2 test, and data from vane shear tests and unconfined compression tests, to show that the undrained shear strength, s_u, follows a normal distribution. Similar findings about s_u have also been reported by other researchers (e.g. Hooper and Butler 1966; Chiasson et al. 1995). Lumb (1966) also demonstrated that normal distributions were suitable for other soil properties (e.g. effective cohesion and friction angle). The applicability of the normal distribution for soil properties was also supported by Lee et al. (1983). In contrast, Brejda et al. (2000) found it difficult to fit a normal distribution to sampled soil properties, but a lognormal distribution showed a better fit to their data. Fenton (1999) also pointed out that most soil properties are strictly non-negative, in that case a lognormal distribution is more suitable. He assumed that the cone tip resistance was lognormally distributed. In addition, there are available field data that indicate some soil properties are well represented by a lognormal distribution (e.g. Hoeksema and Kitanidis 1985; Sudicky 1986; Cherubini 2000). Other distributions such as triangular, beta and gamma distributions are also gaining popularity (Abramson et al. 2002; Baecher and Christian 2003).

The PDF for the normal distribution with mean, μ, and standard deviation, σ, is defined by:

$$f(x) = \frac{1}{\sigma\sqrt{2\pi}} \exp\left[-\frac{1}{2}\left(\frac{x-\mu}{\sigma} \right)^2 \right] \tag{2.14}$$

The normal distribution is in a bell shape which is symmetrical about the mean value, and the random variable can take on values between -∞ to +∞. Despite this vast range, 99.7 percent of the values will be found within $\pm 3\sigma$ of the mean (Abramson et al. 2002). Thus, 99.7 percent of the values will be positive if the mean value is positive and is at least

greater than 3σ. Figure 2.2 shows a typical normal distribution for undrained shear strength, s_u, with a mean of 100 kPa and standard deviation of 50 kPa (i.e. COV = 0.5).

For a lognormally distributed random variable, X, with a mean, μ_X, and a standard deviation, σ_X, its natural logarithm, ln(X), will be normally distributed. The mean and standard deviation of the normally distributed ln(X) are given by:

$$\mu_{\ln X} = \ln \mu_X - \tfrac{1}{2}\sigma^2_{\ln X} \tag{2.15}$$

and

$$\sigma_{\ln X} = \sqrt{\ln\left(1+\mathrm{COV}_X^2\right)} \tag{2.16}$$

The PDF of a lognormal distribution is then given by:

$$f(x) = \frac{1}{x\sigma_{\ln X}\sqrt{2\pi}} \exp\left[-\frac{1}{2}\left(\frac{\ln(x)-\mu_{\ln X}}{\sigma_{\ln X}}\right)^2\right] \tag{2.17}$$

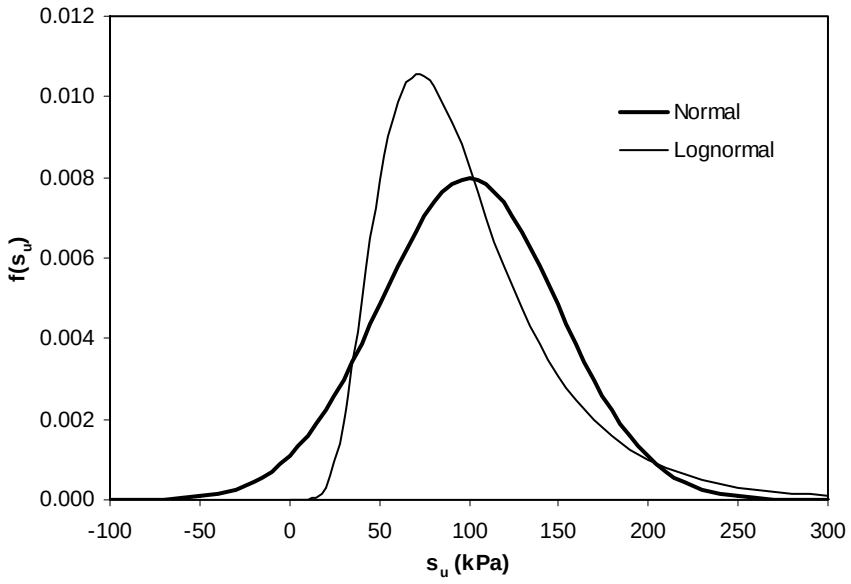

Figure 2.2 Normal and lognormal distributions of undrained shear strength, s_u, with mean of 100 kPa and standard deviation of 50 kPa (COV = 0.5)

The lognormal distribution ranges between zero and infinity, thus includes no negative values. A typical lognormal distribution for undrained shear strength, s_u, with a mean of 100 kPa and standard deviation of 50 kPa (i.e. COV = 0.5) is also plotted in Figure 2.2, together with the normal distribution that has the same mean and standard deviation, as previously mentioned. Rearrangement of Equations (2.15) and (2.16) will give the mean and standard deviation of the lognormal field:

$$\mu_X = \exp\left(\mu_{\ln X} + \tfrac{1}{2}\sigma^2_{\ln X}\right) \tag{2.18}$$

$$\sigma_X = \mu_X \sqrt{\exp\left(\sigma^2_{\ln X}\right) - 1} \tag{2.19}$$

The median and the mode of a lognormal distribution is related to a normal distribution by:

$$\text{Median}_X = \exp\left(\mu_{\ln X}\right) \tag{2.20}$$

$$\text{Mode}_X = \exp\left(\mu_{\ln X} - \sigma^2_{\ln X}\right) \tag{2.21}$$

2.3.2 Spatial Variability of Soil Properties

The inherent variations in soil properties from point to point is not a completely random process, rather it is spatially correlated and is controlled by location in space. The magnitudes of a soil property at two adjacent locations are likely to be strongly correlated. As the distance between the two locations increases, the correlation weakens until it vanishes. Vanmarcke (1977a) pointed out that such *spatial correlation* should be considered in modelling of soil properties.

The spatial variation of soil properties, x_i, at any locations, i, can be divided into a deterministic *trend* component, t_i, and a *residual* component, ε_i, (Vanmarcke 1977a; DeGroot and Baecher 1993; Baecher and Christian 2003), as shown in Figure 2.3, and described by:

$$x_i = t_i + \varepsilon_i \tag{2.22}$$

The trend component represents the change in average soil properties as a function of location. In practice, the trend function is often estimated using regression analysis. The method of ordinary least squares is the most widely used method for trend estimation in geotechnical literature (Lumb 1974; DeGroot 1996; Baecher and Christian 2003), with polynomial trends to order 4 being reported.

NOTE:
This figure is included on page 22 of the print copy of the thesis held in the University of Adelaide Library.

Figure 2.3 Dilatometer lift-off pressure reading P_0 versus depth: (a) measured data points; (b) linear fit and linear regression lines (after DeGroot 1996)

The residual component is the random variation from the trend, which can be estimated from the scatter of observations around the trend. This residual component is commonly modelled as a *stationary* random field with a probability density function of zero mean and constant variance (Vanmarcke 1977a; DeGroot and Baecher 1993; Baecher and Christian 2003). A random field is considered to be stationary if (Brockwell and Davis 1987):

- The mean is constant with distance (i.e. no spatial tend in the data);
- The variance is constant with distance (i.e. homoscedastic);
- There are no seasonal variations; and

- There are no irregular fluctuations.

Since the trend is considered deterministic, spatial variability is concerned with the correlation between residuals. *Random field theory* (Vanmarcke 1977a, 1983) is the most commonly used mathematical technique for modelling the spatial variability of soil properties. In a stationary random field, i.e. a soil profile with constant mean trend and whose properties vary spatially, the soil property can be described stochastically using three parameters (Vanmarcke 1977a): (i) the mean; (ii) the standard deviation (or the variance); and (iii) the *scale of fluctuation*. The mean and the standard deviation are the point statistical measures with no consideration of their spatial correlation structure. The scale of fluctuation (SOF) was introduced as an additional statistical parameter for describing the spatial correlation of soil properties. The SOF is defined as the distance within which the soil properties show strong correlation from point to point (Vanmarcke 1977a). Thus, a large value of SOF implies a smoothly varying field, suggesting a more continuous soil mass, while a small value of SOF implies one that varies more randomly.

2.3.2.1 Autocovariance and Autocorrelation Function

The spatial correlation of soil properties can be described by the statistical measures called the *autocovariance,* c_k, and *autocorrelation coefficient,* ρ_k, which measure the similarity between data separated by a lag distance, *k*, as given by:

$$c_k = \mathrm{Cov}[X_i, X_{i+k}] = \mathrm{E}[(X_i - \overline{X})(X_{i+k} - \overline{X})] \tag{2.23}$$

and

$$\rho_k = \frac{c_k}{c_0} \tag{2.24}$$

where c_0 is the autocovariance at lag 0. At a separation or lag distance of $k = 0$, the residuals are the same and the autocovariance reduces to the variance of the data, $\mathrm{Var}[X]$. Therefore, Equation (2.24) can be re-written as follow:

$$\rho_k = \frac{\mathrm{Cov}[X_i, X_{i+k}]}{\mathrm{Var}[X]} = \frac{\mathrm{E}[(X_i - \overline{X})(X_{i+k} - \overline{X})]}{\mathrm{Var}[X]} \tag{2.25}$$

The plots of autocovariance and autocorrelation coefficient against lag distance, *k*, are known as the *autocovariance function* and *autocorrelation function*, respectively. Monotonically decaying functions are usually used to describe the autocovariance and autocorrelation functions. The exponential and Gaussian (squared exponential) are the functions that are most commonly used in practice (Vanmarcke 1977a, 1983; Li and White 1987; DeGroot 1996; Lacasse and Nadim 1996), as given by Equations (2.26) and (2.27), respectively:

$$\rho_k = e^{-|k|/k_0} \tag{2.26}$$

$$\rho_k = e^{-(k/k_0)^2} \tag{2.27}$$

where k_0 is called the *autocorrelation distance*, which is the distance at which the autocorrelation function decays from 1 to 1/*e* (i.e. 0.3679) (DeGroot 1996; Lacasse and Nadim 1996). For the exponential and Gaussian autocorrelation function, the SOF is equal to 2 and $\sqrt{\pi}$ (i.e. 1.77) times the autocorrelation distance, respectively (Vanmarcke 1977a, 1983).

2.3.2.2 Spatial Average and Variance Function

The spatial variability of soil properties has been included in geotechnical analysis through the concept of *spatial* or *local averaging* (Vanmarcke 1977a, 1983). It is assumed that geotechnical performance is controlled by the average soil properties rather than soil properties at discrete locations. For example, the stability of a slope tends to be controlled by the average shear strength rather than the shear strength at a particular location along the slip surface (Li and Lumb 1987). As a result, local averages over a spatial domain are of more interest than the point-to-point variation in a random field. The process of spatial averaging results in a reduction of variance because the fluctuations in soil properties tend to cancel out within the averaging domain. This implies that the variance of an average soil property is usually less than the variance of its point property. Vanmarcke (1977a)

proposed the dimensionless *variance function*, Γ^2, to measure the reduction in the point variance under local averaging, as given by:

$$\Gamma^2(\mathrm{T}) = \frac{\sigma_{\mathrm{T}}^2}{\sigma^2} \tag{2.28}$$

where σ_{T}^2 = the variance of the soil property spatially averaged over an averaging domain T; σ^2 = the point variance. At relatively large values of T, the variance function will take the following form (Vanmarcke 1977a):

$$\Gamma^2(\mathrm{T}) = \frac{\theta}{\mathrm{T}} \tag{2.29}$$

where θ = scale of fluctuation. Equation (2.29) can be re-written to give the expression for scale of fluctuation:

$$\theta = \Gamma^2(\mathrm{T})\,\mathrm{T} \tag{2.30}$$

Vanmarcke (1977a) proposed that the variance function may be approximated by the following expression:

$$\Gamma^2(\mathrm{T}) = \begin{cases} 1 & \mathrm{T} \le \theta \\ \dfrac{\theta}{\mathrm{T}} & \mathrm{T} \ge \theta \end{cases} \tag{2.31}$$

This model indicates that no reduction to the point variance is required if the averaging domain is smaller than or equal to the scale of fluctuation.

2.3.3 Published Data for Inherent Soil Variability

Limited in-situ soil data, in most practical cases, is the obstacle for incorporating the spatial variability of soil properties into geotechnical design and analysis. However, in the absence of adequate data, the statistical parameters of soil data can be estimated from the values published in the literature. Extensive efforts have been made by several

investigators to compile the values of coefficient of variation (COV) for various soil properties. For example, Lee et al. (1983) compiled reported values of COV for a wide variety of soil properties, and the soil properties that are relevant to slope stability analysis are summarised in Table 2.1. In addition, Lacasse and Nadim (1996) have also published a table of suggested PDF and COV for various soil properties, as shown in Table 2.2.

Table 2.1 Typical values for coefficient of variation (after Lee et al. 1983)

NOTE:
This table is included on page 26 of the print copy of the thesis held in the University of Adelaide Library.

Table 2.2 Typical values for coefficient of variation (after Lacasse and Nadim 1996)

NOTE:
This table is included on page 26 of the print copy of the thesis held in the University of Adelaide Library.

Furthermore, Phoon and Kulhawy (1999a) produced suggested guidelines of COV for inherent soil variability based on a comprehensive review on various test measurements, as shown in Table 2.3. Other researchers (e.g. Lumb 1966; Asaoka and Grivas 1982; Soulie et al. 1990; Chiasson et al. 1995) also reported values of COV based on in-situ testings.

The scale of fluctuation (SOF) and autocorrelation distance is less well documented in the literature as compared with the values of COV, especially in the horizontal direction. Despite that, Phoon and Kulhawy (1999a) have reported values of SOF, as summarised in Table 2.4. It can be seen that vertical SOF generally ranges between 0.1 and 12.7 m, while horizontal SOF generally ranges between 3 and 80 m. It is also noted that the horizontal SOF is much higher than the vertical SOF (i.e. at least 10 times). This is due mainly to the nature of the soil and geological deposition process.

2.4 Effects of Vegetation on Slope Stability

2.4.1 Background

Incorporating the effects of vegetation in slope stability analysis was first attempted in the 1960s although grass, shrubs and trees have been used to stabilise slopes for many years. Vegetation has been traditionally considered to have a minor effect on the stability of slopes, and it is usually ignored in conventional slope stability analysis. This assumption has been proved not always to be correct. Terzaghi (1950) considered deforestation to be a possible cause of the landslide that occurred in 1915 at Hudson, New York. Although the effect of vegetation had been qualitatively appreciated at that time, the influences of vegetation were only well recognised after the pioneer quantitative research on this subject by several investigators (Bethlahmy 1962; Bishop and Steven 1964; Endo and Tsuruta 1969). Bethlahmy (1962) and Bishop and Stevens (1964) quantitatively investigated the effects of timber harvesting on the stability of slopes. Bishop and Stevens (1964) noted a significant increase in the frequency of landslides after forest clearing. Endo and Tsuruta (1969) determined the reinforcing effect of tree roots on soil shear strength through large-scale, in-situ direct shear tests on soil blocks containing live tree roots. These pioneer studies all showed that vegetation has a significant influence on the stability of slopes. Since then, research on this topic has continued to become more widespread.

Table 2.3 Suggested guidelines for inherent soil variability (after Phoon and Kulhawy 1999a)

NOTE:
This table is included on page 28 of the print copy of the thesis held in the University of Adelaide Library.

Table 2.4 Summary of scale of fluctuation of some geotechnical properties (after Phoon and Kulhawy 1999a)

NOTE:
This table is included on page 29 of the print copy of the thesis held in the University of Adelaide Library.

2.4.2 Influences of Vegetation

The influences of vegetation can be generally classified into hydrological and mechanical effects. Hydrological effects refer to the modification of soil moisture content caused by the hydrological cycle when vegetation is present. Mechanical effects arise from the physical interaction between the vegetation and the soil slope, i.e. soil-vegetation interaction. The following sections briefly discuss these effects and a more comprehensive review on this subject can be found in many publications (e.g. Gray and Leiser 1982; Greenway 1987; Coppin and Richards 1990; Gray and Sotir 1996).

2.4.2.1 Hydrological Effects

Vegetation may influence the soil moisture content in several ways. The foliage intercepts part of the rainfall and from there it evaporates back to the atmosphere. This process ultimately reduces the amount of rainfall that infiltrates into the soil slope. In addition,

plant roots extract moisture from the soil through the process of transpiration. The evaporation of intercepted rainfall from the plant surface and the removal of moisture from a plant by transpiration are often known as the process of *evapotranspiration* (Coppin and Richards 1990). Rainfall interception and evapotranspiration by plants have the effect of reducing the soil moisture content, which leads to a decrease of pore water pressure in saturated soils or an increase in matric suction in unsaturated soils. Both the decrease of pore water pressure and increase of matric suction will ultimately improve the stability of a slope by increasing the effective stress and hence soil shear strength.

Many studies have shown that vegetation has a significant influence on the soil moisture content and soil suction. Biddle (1983) conducted soil moisture studies near five tree species growing in clayey soils in the UK. The species investigated were poplar, horse chestnut, lime, silver birch and cypress. Soil moisture was measured by means of a neutron moisture meter extending to a maximum depth of 4 m below ground surface. The results showed that poplar trees caused the deepest drying effect to a depth of 4 m, and the drying effect extended to a radius equal to the height of the tree, as shown in Figure 2.4. The average height of the poplar trees studied was 17 m.

Richards et al. (1983) measured the total soil suction for a site in Adelaide, South Australia, which was affected by three different species of tree (i.e. eucalypts, casuarinas and pines). It was found that, for all tree species, soil suctions were significantly higher near the trees than in adjacent land without trees. More recently, similar studies were carried out by other researchers (e.g. Cameron 2001; Jaksa et al. 2002; Blight 2005). These studies together showed that soil moisture content and/or soil suction were significantly influenced by vegetation.

Although the ability of vegetation to reduce soil moisture is well recognised, its influence on the stability of slopes has yet to be quantified. In the literature, most studies assume that the major effects of vegetation on slope stability are mechanical rather than hydrological (e.g. Wu et al. 1979; Gray and Leiser 1982; Coppin and Richards 1990). It is generally accepted that root reinforcement is the most important factor to be considered in assessing the effect of vegetation on the stability of slopes. The hydrological effects are often considered to have a minimal or negligible influence on slope stability.

However, recent field studies by Simon and Collision (2002) have demonstrated the importance of the hydrological effects of riparian vegetation in controlling riverbank stability. They measured the pore water pressure and matric suction in soils, and the response to rainfall over one cycle of a dry and wet period (i.e. 14 months), under different vegetation covers. Based on field data, their stability analysis results showed that the significance of hydrological effects on riverbank stability depended on the types of vegetation and antecedent rainfall. It was found that trees are more efficient in removing soil moisture and preventing rainfall infiltration into soils compared to grasses. It was also shown that the beneficial effect of hydrological factors was more significant in the dry period than in the wet period.

NOTE:
This figure is included on page 31 of the print copy of the thesis held in the University of Adelaide Library.

Figure 2.4 Reductions in soil moisture near a Poplar tree growing in boulder clay (after Biddle 1983)

2.4.2.2 Mechanical Effects

Plant roots can reinforce the soil due to their tensile strength and adhesional properties. The inclusion of plant roots with high tensile strength increases the confining stress in the soil mass by its closely spaced root matrix system. The soil mass is bound together by the plant roots and the soil shear strength is increased by providing additional apparent

cohesion to the soils (Coppin and Richards 1990). Over the past three decades, a significant amount of work has been done to quantify the effect of root reinforcement and this will be discussed later.

The weight of large trees may give an additional surcharge to the slope, hence, increases both the down-slope forces and confining stress of the soil at the potential slip surface. The effect of surcharge could be either adverse or beneficial depending on the location of the trees (Coppin and Richards 1990). If trees are located at the top of slope, the overall stability of the slope will be reduced due to the increase in down-slope forces. On the other hand, if trees are located at the bottom or toe of slope, the stability of slope will be improved due to the fact that the additional vertical load will increase the frictional component of the soil shear strength. In the literature, the total weight of the trees growing on a slope is usually considered to be uniformly distributed. For example, Bishop and Stevens (1964) estimated an average surcharge of 2.5 kPa for Sitka Spruce (*Picea sitchensis*) forest cover, Greenway (1987) reported an average surcharge of 0.5 kPa for Candlenut (*Aleurites moluccana*) trees on slopes in Hong Kong and Wu et al. (1979) computed an average value of 3.8 kPa for Sitka Spruce trees in Alaska.

Furthermore, large trees may be subjected to wind loading which increase the driving forces acting on the slopes. It has been found that the pressure exerted on a tree by wind can be transmitted to the soil as increased loading which ultimately reduces its resistance to failure (Hsi and Nath 1970; Brown and Sheu 1975). The wind force acting on the trees may create a destabilising moment to the slope if the magnitude of the wind is sufficiently large.

Large tree roots may also penetrate deeply into the firm strata causing them act as stabilising piles. When the anchored tree roots are closely spaced they may also yield buttressing and arching effects, which ultimately restrain the downhill movement of the slope and improve slope stability (Gray 1978; Coppin and Richards 1990). Wang and Yen (1974) developed a theoretical model for soil arching in long slopes created by piles or trees. They showed that soil arching would be developed when the piles or trees are spaced within a critical spacing, which is a function of soil properties (i.e. c' and ϕ'), slope angle and the at-rest earth pressure.

The effects of buttressing and arching, surcharge, and wind loading are usually considered only in the case of large trees, since these effects are insignificant for small trees, shrubs and grasses. Although the mechanical effects of vegetation comprise various aspects as discussed above, the available literature has generally focused on investigating the influence of root reinforcement on the stability of slopes. This is a reasonable trend because root reinforcement has been considered as one of the most cost effective slope stabilisation methods nowadays.

2.4.3 Quantifying Effect of Root Reinforcement

2.4.3.1 Enhanced Soil Shear Strength

The presence of plant roots in soils can be analogous to reinforced concrete, where the inclusion of high tensile strength materials (i.e. steel bars) is used to enhance the tensile and shear strength of concrete. Soils reinforced by plant roots behave as a composite material in which the root matrix system tend to bind the soil together in a monolithic mass and contribute to an increase in soil shear strength by an additional apparent cohesion, c_r (Endo and Tsuruta 1969; Waldron 1977; Wu et al. 1979). However, plant roots have a negligible effect on the friction angle of soils due to their random orientation (Gray and Leiser 1982). Hence, the enhanced soil shear strength due to root reinforcement, Δs, can be considered equivalent to the increase in apparent soil cohesion, c_r, as shown in Figure 2.5. As a result, the Mohr-Coulomb equation can be modified as follows (Coppin and Richards 1990):

$$s = c' + c_r + (\sigma_n - u)\tan\phi' \tag{2.32}$$

where s = shear strength of the soil; c' = effective soil cohesion; σ_n = normal stress; u = pore water pressure; and ϕ' = effective friction angle.

Many studies have been conducted to quantify the contribution of root reinforcement to soil shear strength. These studies include in-situ direct shear tests on soil blocks with plant roots (e.g. Endo and Tsuruta 1969; O'Loughlin 1974b; Ziemer 1981; Abe and Iwamoto 1988; Wu et al. 1988a; Nilaweera 1994; Wu and Watson 1998; Abernethy 1999;

Abernethy and Rutherfurd 2001), and laboratory direct shear tests of soils with roots (e.g. Waldron 1977; Waldron and Dakessian 1981, 1982; Waldron et al. 1983; Terwilliger and Waldron 1990, 1991) or soils reinforced by fibres that simulate roots (e.g. Gray and Oshashi 1983; Jewell and Wroth 1987; Wu et al. 1988b; Shewbridge and Sitar 1990, 1996).

These studies together give evidence on the increase in soil shear strength due to root reinforcement. It was generally found that the increase in soil shear strength due to root reinforcement is directly proportional to the root density. For example, Ziemer (1981) showed that the shear strength of California sand containing pine roots increased linearly with the root density, as shown in Figure 2.6. Gray and Leiser (1982) also showed that the increase in shear strength with increase in root density for various vegetation species and plastic fibres (Figure 2.7).

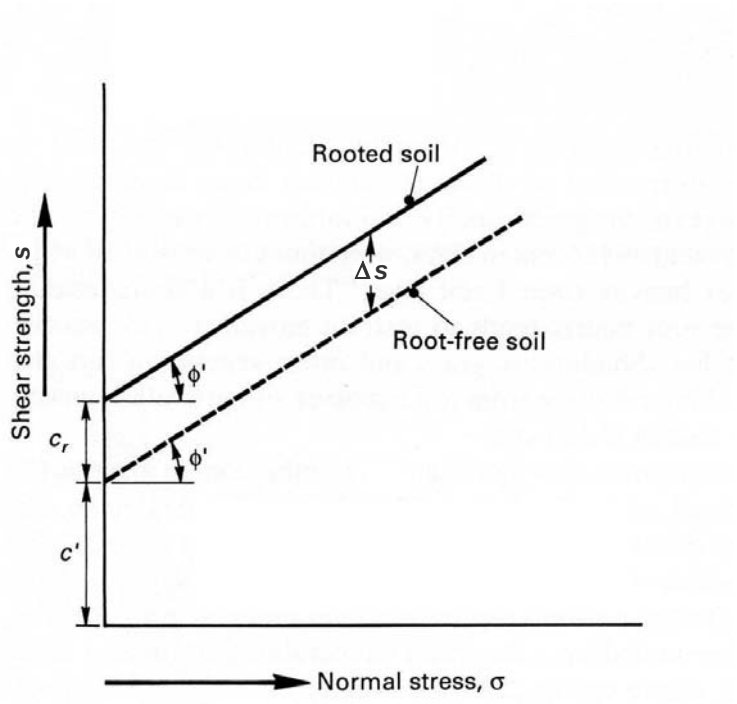

Figure 2.5 Effect of root reinforcement on the shear strength of soil (after Coppin and Richards 1990)

NOTE:
This figure is included on page 35 of the print copy of the thesis held in the University of Adelaide Library.

Figure 2.6 Shear strength of root-permeated sand as a function of root density (after Ziemer 1981)

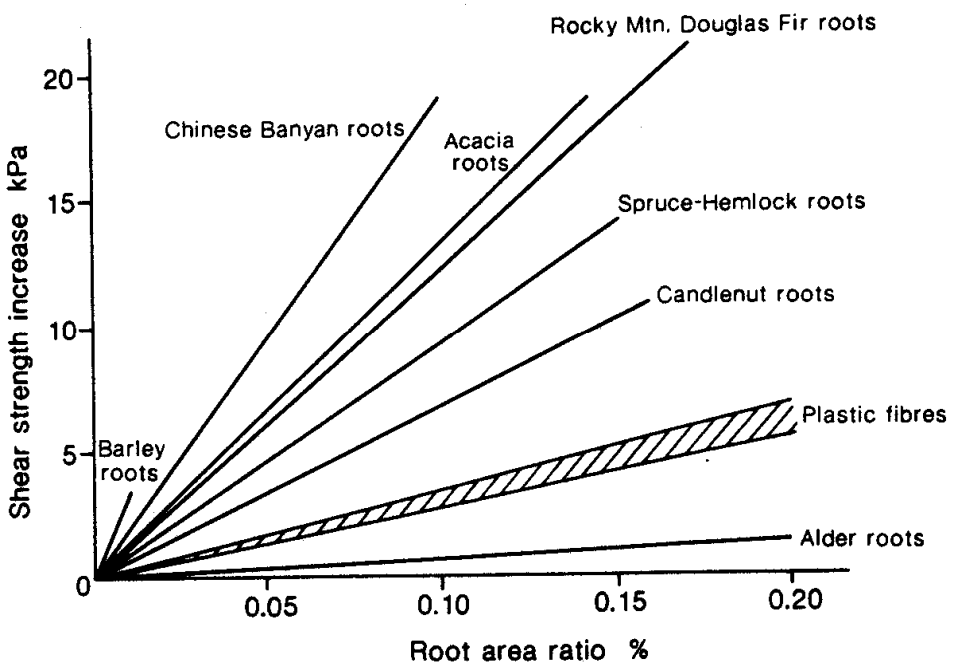

Figure 2.7 Comparison of shear strength increase due to root/fibre reinforcement (after Gray and Leiser 1982)

2.4.3.2 Root Density and Depth

Root density is commonly measured by the term known as *root area ratio*, RAR, which is defined as the ratio of the total cross-sectional area that is occupied by all roots in a given cross-section of soil, A_r, to the total cross-sectional area of the soil being considered, A. RAR can be determined by counting roots by size classes within a given soil area and usually only roots less than 15 mm to 20 mm in diameter are counted (Coppin and Richards 1990):

$$\text{RAR} = \frac{A_r}{A} = \frac{\sum n_i a_i}{A} \tag{2.33}$$

where n_i = number of roots in size class i; and a_i = mean cross-sectional area of roots in size class i.

The depth of root systems varies significantly with vegetation species and their growing environments (Greenway 1987). About 60–80% of grass roots are found in the top 50 mm of soil (Coppin and Richards 1990). For trees and shrubs, the most widely reported range was 1–3 m (Kozlowski 1971). However, deeper root systems had been reported, for example, William and Pidgeon (1983) reported gum tree rooting to 27.5 m. In North America, the depth of rooting is constrained by bedrock at relatively shallow depths (less than 2 m) in many slopes (Schmidt et al. 2001).

Recently, Abernethy and Rutherfurd (2001) conducted a field study to investigate the effect of two Australian riparian trees (i.e. river red gum and swamp paperbark) on riverbank stability at the lower Latrobe River, Victoria. Their field data showed that the range of RAR for the two tree species was found between 0.001% and 0.76%. They also found that RAR decreases as the depth from the soil surface and the distance from the tree trunk increases, as shown in Figure 2.8. It can be seen that the root systems of swamp paperbark and river red gum extend to a depth of 1.2 m and 2.0 m, respectively.

Simon and Collision (2002) also conducted a similar field study to investigate the effect of four riparian tree species (i.e. black willow, sweetgum, river birch and sycamore) and two grass species (i.e. switch grass and gamma grass) on riverbank stability in northern Mississippi. It was found that switch grass has the highest RAR (0.014% averaged over

the upper 1 m of soil), followed by river birch and sycamore (0.010% and 0.012%). For black willow, sweetgum and gamma grass the figures were 0.0087%, 0.0056% and 0.0044% respectively.

The RARs found in the two recent studies (i.e. Abernethy and Rutherfurd 2001; Simon and Collision 2002) are consistent with the results from other previous studies. Typical values of RAR reported by Coppin and Richards (1990) were 0.14–0.93% for tree roots in the 5 to 10 mm diameter class; 0.05–0.17% for Rocky Mountain douglas fir; and 0.1–0.8% for barley.

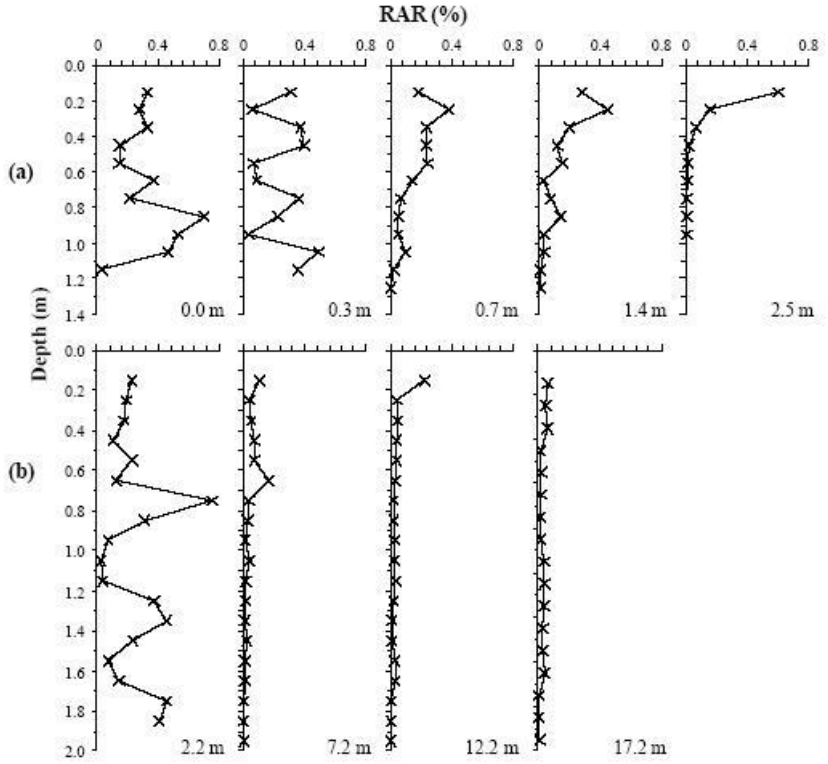

Figure 2.8 Root area ratio against depth for different distance from the tree trunk: (a) swamp paperbark and (b) river red gum (after Abernethy and Rutherfurd 2001)

2.4.3.3 Root Tensile Strength

The tensile strength of tree roots can be measured by tensile tests in the laboratory or in-situ and has been investigated by many researchers. Most authors reported a wide

variation in the root tensile strength depending on species, growing environment, root diameter, and orientation. Coppin and Richards (1990) provided a summary of root tensile strength for different species of plant based on the source from O'Loughlin and Watson (1979) and Schiechtl (1980), as shown in Table 2.5. It can be seen that the root tensile strength for grasses and herbs vary from 0.0 to 86.5 MPa, whereas for trees and shrubs the values vary from 5 to 68 MPa.

Table 2.5 Root tensile strength for selected plant species (after Coppin and Richards 1990)

	Tensile strength (MPa)
Grasses and herbs	
Elymus (Agropyron) *repens* (Cough grass)	7.2–25.3
Campanula trachelium (Bellflower)	0.0–3.7
Convolvulus arvensis (Bindweed)	4.8–21.0
Plantago lanceolata (Plantain)	4.0–7.8
Taraxacum officinale (Dandelion)	0.0–4.4
Trifolium pratense (Red Clover)	10.9–18.5
Medicago sativa (Alfalfa)	25.4–86.5
Trees and shrubs	
Alnus incana (Alder)	32.0
Betula pendula (Birch)	37.0
Cytisus scoparius (Broom)	32.0
Picea sitchensis (Sitka Spruce)	23.0
Pinus radiata (Radiata Pine)	18.0
Populus nigra (Black Poplar)	5.0–12.0
Populus euramericana (Hybrid Poplar)	32.0–46.0
Pseudotsuga menziesii (Douglas Fir)	19.0–61.0
Quercus robur (Oak)	32.0
Robinia pseudoacacia (Black Locust)	68.0
Salix purpurea (Willow)	36.0
Salix cinerea (Sallow)	11.0

There is direct evidence that root tensile strengths vary significantly with root diameter. Most investigators reported a decrease in root tensile strength with increasing root diameter (Wu et al. 1979; Nilaweera and Nutalaya 1999; Abernethy and Rutherfurd 2001; Simon and Collison 2002). Figures 2.9 and 2.10 show the relationship between the root tensile

strength and root diameter reported in the field studies conducted by Abernethy and Rutherfurd (2001) and Simon and Collinson (2002), respectively. Both studies showed that root tensile strength decrease exponentially with root diameter and the majority of the measured tensile strengths were within the range reported by Coppin and Richards (1990).

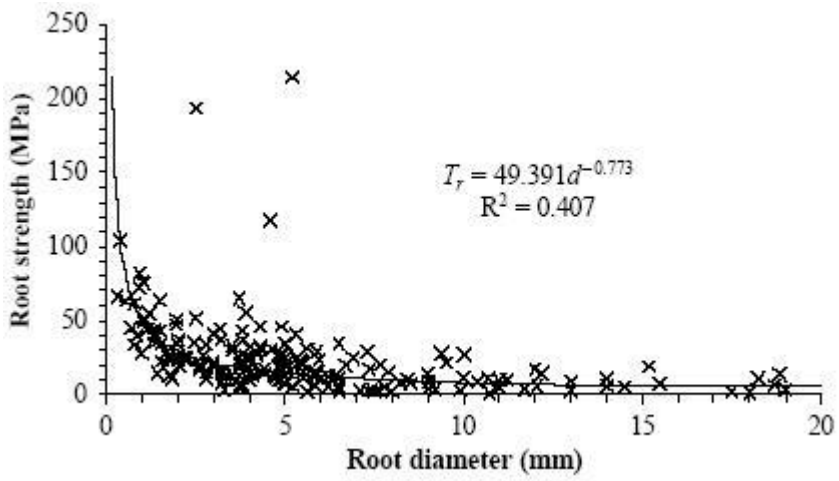

Figure 2.9 Relationship between root tensile strength and root diameter for two Australian riparian species (after Abernethy and Rutherfurd 2001)

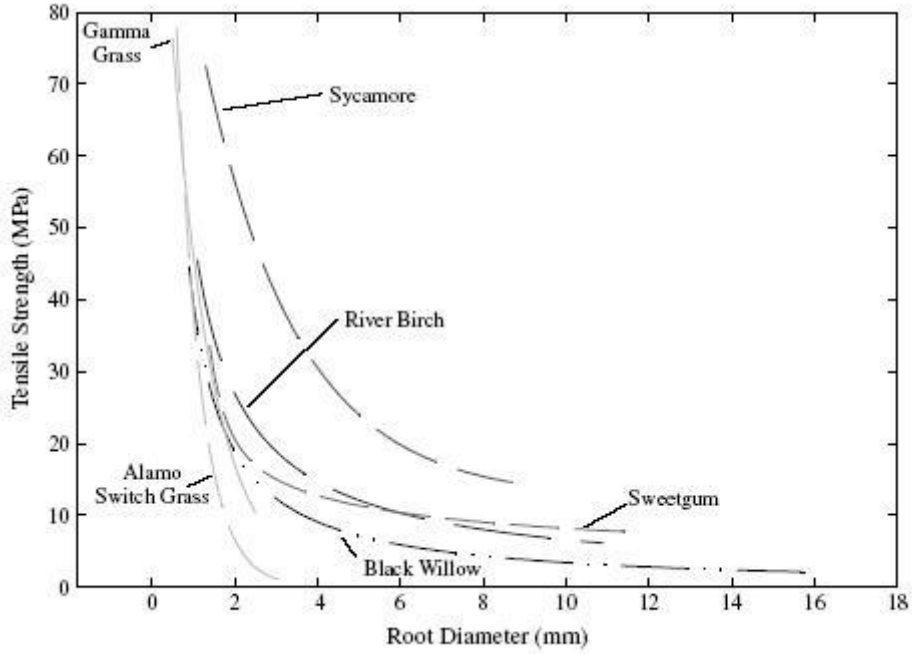

Figure 2.10 Relationship between root tensile strength and root diameter for six vegetation species in Northern Mississippi (after Simon and Collison 2002)

2.4.3.4 Root Reinforcement Model

A simple perpendicular root reinforcement model was developed by Wu et al. (1979) for predicting the increase in shear strength of soil due to the presence of tree roots. This model assumes that a flexible elastic root extends across a potential sliding surface in a slope (Figure 2.11). When the root distorts within the shear zone a tensile force is developed in the root. This force can be resolved into normal and tangential components. The normal component increases the confining stress on the shear plane, while the tangential component directly resists the shear. The increase in shear strength of soil, Δs, predicted by this model is given by the following equation:

$$\Delta s = T_r \left(\frac{A_r}{A} \right) (\cos\alpha \tan\phi + \sin\alpha) \tag{2.34}$$

where T_r = mean tensile strength of the roots; $\frac{A_r}{A}$ = fraction of soil cross-sectional area occupied by roots (i.e the root area ratio, RAR); α = shear distortion angle; and ϕ = friction angle of the soil.

Figure 2.11 Perpendicular root reinforcement model (after Wu et al. 1979)

Observations from the field and laboratory tests indicate that the shear distortion angle, α, is most likely to fall within the range 40° to 70° in most practical situations (Gray and

Leiser 1982). Wu et al. (1979) showed that the second bracketed term in Equation (2.34) is relatively insensitive to normal variations in α and ϕ, as it varied only from 1.0 to 1.3 for $25° < \phi < 40°$ and $40° < \alpha < 70°$. Hence, an average value of 1.2 was suggested and Equation (2.34) may be rewritten as follows:

$$\Delta s = 1.2\ T_r \left(\frac{A_r}{A} \right) \tag{2.35}$$

The assumption of initial root orientation being perpendicular to the shear plane has received some attention in the literature. In nature, tree roots may be inclined at many different angles to the sliding plane. Laboratory direct shear tests on fibre reinforced soils conducted by Gray and Ohashi (1983) have shown that a perpendicular orientation is not optimal. Roots with an initial orientation of 60° to the shear surface yield the greatest increase in shear strength in most sands. However, they showed that perpendicular orientations of reinforcing fibres provided comparable reinforcement to randomly oriented fibres. This finding generally supports the use of the simple perpendicular root reinforcement model in practical applications where tree roots are most likely to be randomly oriented within a soil slope. Although other root reinforcement models have been developed since then, such as the inclined root reinforcement model (Gray and Leiser 1982) and the cable and pile model (Wu et al. 1988b), the perpendicular root reinforcement model still remains widely used because of its simplicity and accuracy.

The perpendicular root reinforcement model assumes that the failure mode for the roots is a tensile failure so that the tensile strength of the roots is fully mobilised. Pullout or bond failure must be prevented for this assumption to be valid. The minimum root length, L_{min}, required to prevent pullout is given by (Wu et al. 1979):

$$L_{\min} = \frac{T_r d}{4\tau_b} \tag{2.36}$$

where T_r = root tensile strength; d = root diameter; and τ_b = limiting bond stress between the root and the soil.

2.4.3.5 Published Data for Root Cohesion

As discussed in Section 2.4.3.1, the increase in shear strength of soil due to root reinforcement is equivalent to an additional apparent cohesion, which is also known as *root cohesion*, c_r, and this value can be estimated based on three different methods: (1) the perpendicular root reinforcement model with the available root density and tensile strength information; (2) field or laboratory direct shear tests; and (3) back analysis on failed slopes. With the estimated value of root cohesion, c_r, the increase in factor of safety (FOS) of a slope can be calculated accordingly using routine slope stability analysis methods. The incorporation of root cohesion in routine slope stability analysis methods is discussed later. In the literature, many investigators have estimated the value of root cohesion for different vegetation species growing in different environments, these typical values are summarised in Table 2.6. It is noted that the typical values for c_r vary from 1.0 to 94.3 kPa depending on the vegetation species and environments. However, the majority of the values fall within the range of 1.0–20.0 kPa. It should be noted that most of these published values were derived from data averaged over the entire soil profile that was affected by vegetation and did not account for any spatial variability. The spatial variability of root cohesion is discussed next.

2.4.3.6 Spatial Variability of Root Cohesion

Root cohesion is spatially variable because the species, age, size, and spacing of trees are usually non-uniform on a slope. Recent field studies conducted by Abernethy and Rutherfurd (2001), at the lower Latrobe River, Australia, indicated that root area ratio, RAR, for two Australian riparian species varied both vertically and laterally, as previously discussed in Section 2.4.3.2 (see Figure 2.8). Based on the measured values of RAR and root tensile strength, they calculated the corresponding values of root cohesion, c_r, using the perpendicular root reinforcement model. Simple linear regression expressions for c_r were developed for the two tree species being investigated (Abernethy and Rutherfurd 2001). For the river red gum:

$$c_r = e^{4.920 - 0.099C - 1.333D} \qquad r^2 = 0.70 \tag{2.37}$$

Table 2.6 Typical values for root cohesion, c_r

Investigators	Vegetation	c_r (kPa)
Endo and Tsuruta (1969)[2]	Alder (Japan)	2.0–12.0
Swanston (1970)[3]	Hemlock, spruce (Alaska, USA)	3.4–4.4
O'Loughlin (1974a)[3]	Conifers (British Columbia, Canada)	1.0–3.0
Burroughs and Thomas (1977)[1]	Conifers (Oregon, USA)	3.0–17.5
Wu et al. (1979)[1]	Conifers (Alaska, USA)	5.9
Gray and Megahan (1981)[3]	Ponderosa pine, Douglas-fir (Idaho, USA)	2.8–6.2
Waldron and Dakessian (1981)[2]	52-month-old yellow pine (Laboratory)	~5.0
Waldron et al. (1983)[2]	54-month-old yellow pine (Laboratory)	3.7–6.4
Ziemer (1981)[2]	Lodgepole pine (California, USA)	3.0–21.0
Sidle and Swanston (1982)[3]	Blueberry, devils's club (Alaska, USA)	2.0
Riestenberg and Sovonick-Dunford (1983)[1]	Sugar maple forest (Ohio, USA)	6.2–7.0
Wu (1984a)[1]	Sphagnum moss (Alaska, USA)	3.5–7.0
Wu (1984b)[1]	Hemlock, sitka spruce (Alaska, USA)	5.6–12.6
Abe and Iwamoto (1986)[2]	Japanese cedar (Japan)	1.0–5.0
Buchanan and Savigny (1990)[3]	Grasses, sedges, shrubs, sword fern (USA)	1.6–2.1
	Red alder, hemlock, Douglas-fir, cedar	2.6–3.0
Abernethy and Rutherfurd (2001)[1]	River red gum (Victoria, Australia)	10.0
	Swamp paperbark	19.0
Schmidt et al. (2001)[1]	Natural forest - conifers (Oregon, USA)	25.6–94.3
	Industrial forest - hardwood	6.8–23.2
	<11-year-old clearcuts	1.5–6.7
Simon and Collision (2002)[1]	Sycamore (Mississippi, USA)	7.0
	River birch	8.0
	Sweetgum	4.0
	Gamma grass	6.0
	Black willow	2.0
	Switch grass	18.0

[1]Based on perpendicular root reinforcement model with measurements of root density and tensile strength

[2]Based on direct shear tests

[3]Based on back analysis

For swamp paperbark:

$$c_r = e^{4.769 - 0.540C - 1.891D} \qquad r^2 = 0.63 \tag{2.38}$$

where C = distance from the tree trunk (m); and D = depth below the soil surface (m).

Based on the developed linear regression expressions, Abernethy and Rutherfurd (2001) plotted isopleths of root cohesion, c_r, for river red gum and swamp paperbark, as shown in Figures 2.12 and 2.13, respectively. It can be seen that the root cohesion reduces dramatically with depth and with distance from the tree trunk.

Other field studies conducted by Schmidt et al. (2001) and Roering et al. (2003), at the Oregon Coast Range, USA, also indicated that the spacing, size and condition of trees controlled the spatial pattern of root network and root strength. It was found that the median lateral root cohesion, c_r, ranges from 6.8–23.2 kPa in industrial forests with significant deciduous vegetation and ranges from 25.6–94.3 kPa in natural forests dominated by coniferous vegetation. It was also found that root cohesion after forest clearing was uniformly less than 10 kPa. In their study sites, it was observed that landslides tend to occur in areas of reduced root strength.

Although spatial variability of root cohesion is well recognised and is verified by recent field measured data, many researchers have ignored it in the past, when considering root reinforcement in slope stability analysis (e.g. Wu et al. 1979; Greenway 1987; Collison et al. 1995; Collison and Anderson 1996), which will be further discussed later. An average root cohesion, which was most probably estimated from an individual tree, was applied to entire slope in the slope stability analysis. This assumption may underestimate or overestimate the root cohesion, hence, gives an incorrect prediction of the safety of the slope. Therefore, there is a need to quantify the spatial variability of root cohesion and consider its effects on slope stability.

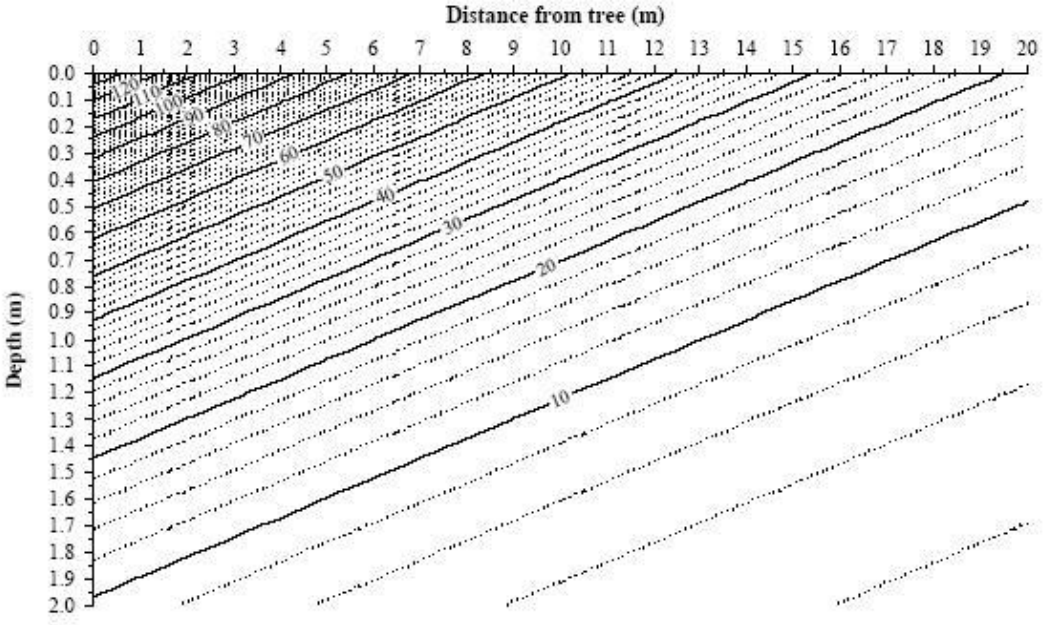

Figure 2.12 Root cohesion, c_r (kPa), due to river red gum root reinforcement (after Abernethy and Rutherfurd 2001)

NOTE:
This figure is included on page 45 of the print copy of the thesis held in the University of Adelaide Library.

Figure 2.13 Root cohesion, c_r (kPa), due to swamp paperbark root reinforcement (after Abernethy and Rutherfurd 2001)

2.4.4 Modelling Effects of Vegetation on Slope Stability

Most researchers have used conventional limit equilibrium methods to quantify the effects of vegetation on the stability of slopes (e.g. Wu et al. 1979; Greenway 1987; Collison et al. 1995; Collison and Anderson 1996; Abernethy and Rutherfurd 2000; Schmidt et al. 2001). Two different types of slope failures have been widely considered in the literature: shallow translational failures and deep-seated rotational failures.

2.4.4.1 Shallow Failures

Most of the vegetated slopes in North America consist of a thin soil layer (usually less than 2 m thick) overlying a bedrock stratum (Schmidt et al. 2001). The length-to-depth ratio for these slopes is usually very high and the failure mode is usually shallow translational or planar. Therefore, the infinite slope analysis method is commonly adopted for slope stability analysis (e.g. Wu et al. 1979; Sidle 1992; Wu and Sidle 1995; Schmidt et al. 2001). The failure plane is normally assumed to be parallel to the bedrock and located at the interface between the rooted soil and the bedrock (Figure 2.14). Wu et al. (1979) modified the original equation for factor of safety (FOS) of an infinite slope to include the effects of vegetation:

$$\mathrm{FOS} = \frac{(c' + c_r)l + [(W + S_w)\cos\beta - ul]\tan\phi'}{(W + S_w)\sin\beta + D} \tag{2.39}$$

where c' = effective cohesion of soil; c_r = root cohesion; l = length of the slice; W = total weight of the slice; S_w = surcharge due to weight of vegetation; β = slope angle; u = pore-water pressure; ϕ' = effective friction angle of soil; and D = wind loading.

Wu et al. (1979) used the modified infinite slope model to investigate the stability of slopes before and after the removal of forest cover in Alaska, USA. An average root cohesion, c_r, of 5.9 kPa was assumed to be contributed by root reinforcement. An average tree surcharge of 3.8 kPa was also assumed in the stability analysis. It was determined that slopes that were originally unstable (i.e. having FOS<1.0) became stable (i.e. having FOS>1.0) when root cohesion was included in the stability analysis. The results indicated that loss of root strength following forest clearing had caused slope instability, which was generally in good agreement with the observed behaviour of the slopes.

Sidle (1992) proposed an infinite slope model that incorporates changes in root cohesion and vegetation surcharge through several forest management cycles. Recovery of root strength and tree surcharge following timber harvest was modelled by a sigmoid relationship, while root deterioration of harvested vegetation was simulated by an exponential decay function. The probability of slope failure was related to the changes in root strength and the probability of occurrence of a landslide-triggering storm. The model was used to study the effects of specific forest management practices over long time periods for selected hillslopes located in coastal Alaska and areas in the western United States. Wu and Sidle (1995) later integrated the infinite slope model proposed by Sidle (1992) with a contour line-based topographic analysis and a geographic information system (GIS) that was used to extract spatial data for soil and vegetation. This distributed, physically-based slope stability model was called dSLAM and it was applied to hillslopes in the Oregon Coast Ranges using actual spatial patterns of timber harvesting and measured rainfall which triggered widespread landslides in that area in 1975. The model was able to produce a map of spatial distribution of factor of safety (FOS) for the entire region being considered. However, Wu and Sidle (1995) pointed out that the accuracy of the results was greatly affected by limited information about spatial distribution of some parameters (e.g. soil depth, saturated hydraulic conductivity, cohesion and friction angle).

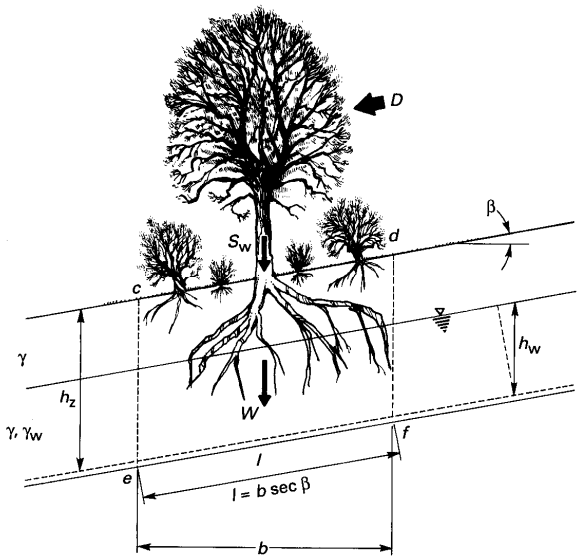

Figure 2.14 Forces acting on a slice on a vegetated infinite slope (after Coppin and Richards 1990)

2.4.4.2 Deep-Seated Failures

Shallow failures are more commonly found in the temperate environment (e.g. North America) where the infinite slope model is considered appropriate for slope stability analysis. However, in the humid tropical environment, the soil profiles are much deeper, reaching depths of up to 30 m (Collison and Anderson 1996). In this case, tree roots are unlikely to occupy the entire soil profile and the failure mode may be circular, or non-circular, rotational rather than shallow translational where potential slip surfaces may pass beneath the root zone, as shown in Figure 2.15. In addition, the ground water table may be very deep below the ground surface, and matric suction or negative pore-water pressure may develop in the unsaturated zone. In the case of deep-seated failures, the infinite slope method is considered inappropriate.

Figure 2.15 Influences of vegetation on deep-seated failures (after Coppin and Richards 1990)

To consider the effects of vegetation on deep-seated slope failures, Greenwood (1983) proposed a simple equation based on the ordinary method of slices (Fellenius 1936) where the original stability equation was modified to include the effects of vegetation. More recently, Greenwood (2006) developed a spreadsheet-based program, called SLIP4EX, where the ordinary method of slices (Fellenius 1936), Bishop's simplified method (Bishop 1955), and Janbu's method (1954) were modified and used for considering effects of

vegetation on slope stability. The modifications to the stability equations were carried out in a fashion similar to that of the infinite slope method where root cohesion, surcharge and wind loading were added to the original equation. The hydrological effects were simply considered as changes in the pore-water pressure.

Several researchers from the University of Bristol, UK, developed a combined hydrologic and stability model, called CHASM, in order to study the effects of rainfall infiltration on the stability of vegetated slopes in the humid tropical environment (Lloyd 1990; Anderson and Kemp 1991; Anderson and Lloyd 1991; Collison 1993; Collison et al. 1995; Collison and Anderson 1996; Wilkinson 2000; Wilkinson et al. 2000; Wilkinson et al. 2002a; Wilkinson et al. 2002b). The CHASM model comprises integrated hydrology, vegetation and stability components. The hydrological system is modelled by a forward explicit finite difference scheme where the rainfall infiltration is calculated using Darcy's Law (Darcy 1856). The unsaturated vertical flow is computed using the Richard's equation (Richards 1931) with the unsaturated conductivity defined by the Millington-Quirk (1959) procedure. Evapotranspiration and root water uptake ae modelled using the Penman-Monteith equation (Monteith 1973). Root reinforcement is modelled by an increase in apparent soil cohesion using the perpendicular root reinforcement model (Wu et al. 1979). Surcharge can be also considered in the stability analysis. The methods of slope stability analysis used in CHASM were Bishop's simplified circular method (Bishop 1955) and Janbu's non-circular method (Janbu 1954).

The Wedge method was more commonly used in the studies investigating the effects of vegetation on riverbank stability (e.g. Abernethy 1999; Abernethy and Rutherfurd 2000; Simon and Collison 2002). Abernethy and Rutherfurd (2000) modified the generalised wedge model, called GWEDGEM (Donald and Zhao 1995), to include the effect of root reinforcement in the stability analysis of riverbanks along the Latrobe River, Australia. Instead of assuming an average value of root cohesion, c_r, the spatial distribution of root cohesion was considered in the stability analysis. Root cohesion was assumed to decrease exponentially from the tree trunk, in both the vertical and lateral directions, based on the empirical relationships obtained from their field test data.

2.4.4.3 Considerations for Parameter Uncertainty

The accuracy of the factor of safety (FOS) calculated by any method of slope stability analysis is affected by the uncertainty in the input parameters. Similar to soil properties, the input parameters related to vegetation such as root cohesion, surcharge and matric suction are subjected to significant uncertainty due to the inherent variable nature of the vegetation system, as well as the errors encountered when their effects are quantified. Very limited studies in the literature have considered the variability in the vegetation input parameters on the estimated FOS of a slope. Wilkinson (1999) performed stochastic analyses, using the CHASM model, to investigate the effect of parameter uncertainty on the FOS of a slope. Input parameters such root cohesion, surcharge, saturated soil hydraulic conductivity, interception and evapotranspiration were considered normally distributed with coefficients of variation (COV) of 0.1, 0.2 and 0.3. It was found that the standard deviation of the FOS was relatively small compared to the standard deviation of the input parameters and it was concluded that, in that case, parameter uncertainty has an insignificant effect on the FOS. However, Wilkinson (1999) only considered a specific case study in his stochastic analyses, where only one set of mean values for each input parameter was used. He pointed out that it is incorrect to state that parameter variability is not important, based on his analysis, because parameter variability may have an important effect on other combinations of mean values of the input parameters.

Chandler (1992; 1996) developed a computer program to perform Monte Carlo simulation using the infinite slope equation for modelling the variability of input parameters including the soil properties, vegetation parameters and rainfall data on the FOS of a slope. The analyses were conducted in a topographic scale to predict the probability of occurrence of shallow slope failure in a selected region. The limitation of this model, as pointed out by Chandler (1992), was large quantities of data were required to perform a meaningful analysis, which could be difficult to obtain.

2.4.5 Discussion

Although many researchers have attempted to incorporate the effect of root reinforcement in slope stability analysis, the spatial variability of root cohesion has not been systematically considered in these analyses. Recent research has focused on considering

the spatial variability of root cohesion through quantifying the spatial distribution of vegetation on a slope on a regional scale (e.g. Wu and Sidle 1995; Schmidt et al. 2001; Roering et al. 2003). All these studies have adopted the simple infinite slope model for slope stability analysis due to the fact that shallow translational failure is the most common failure mode encountered in these regions (i.e. North America).

For deep-seated slope failures, Collison et al. (1995) investigated the effect of vegetation distribution on the factor of safety (FOS) of a slope using the CHASM model. Vegetation was assumed to be located at different locations on a slope, such as the slope toe, slope crest, combined slope toe and crest, slope face and the entire slope. It was found that the case with vegetation located at the slope toe yielded the highest FOS, which was equivalent to the FOS obtained from the case with vegetation located along the entire slope. Abernethy and Rutherfurd (2000) also considered the spatial variability of root cohesion using the wedge method of slope stability analysis. Instead of assuming an average value, root cohesion was varied vertically and laterally based on the linear regression expressions obtained from field data. These analyses eventually yielded a more realistic FOS for the slopes being considered.

To date, there has been no study attempting to incorporate effects of vegetation into finite element slope stability analysis. All the previous studies have adopted the conventional limit equilibrium methods. The advantages of the finite element method are well recognised and has been discussed previously in Section 2.2.2. One of the advantages is the finite element method determines the most critical failure surface or failure mode with no *a priori* assumption. This is particularly useful when root reinforcement is considered because circular or non-circular failure may not be the most critical failure mode. Furthermore, combining the finite element method with random fields, i.e. the random finite element method (RFEM), allows the spatial variability of soil properties and root cohesion to be accounted together in the probabilistic slope stability analysis. Again, no study has considered the effect of spatial variability of soil properties and root cohesion simultaneously in slope stability analysis. The above-mentioned issues will be addressed in this research (Chapter 7).

2.5 Artificial Neural Networks

2.5.1 Background

Artificial neural networks (ANNs) are a class of non-linear computational tools that attempt to simulate the way in which the human brain processes information (Zurada 1992; Fausett 1994). It is a powerful tool for pattern recognition and modelling of non-linear relationships involving a large number of variables. ANNs learn 'by example', in which an actual measured set of input variables and their corresponding outputs are presented to an ANN to determine the relationship between the input and output variables. The most widely used ANNs in the field of geotechnical engineering are the *multi-layer perceptrons* (MLPs) that are trained with the *back-propagation algorithm* (Rumelhart et al. 1986). Adeli (2001) has provided a comprehensive review on the historical applications of ANNs in the field of civil engineering. Meanwhile, Shahin et al. (2001) reviewed the applications of ANNs specifically in the field of geotechnical engineering including pile capacity, settlement of foundations, soil properties and behaviour, liquefaction, site characterisation, earth retaining structures, slope stability, and tunnels and underground openings. It is generally accepted that ANN models are a useful alternative to many analytical and empirical models provided quality data for model development are available.

The application of ANNs to slope stability problems is significantly lower when compared with other geotechnical problems. Shahin et al. (2001) cited only one previous study (i.e. Ni et al. 1996) that applied ANNs to a slope stability problem. Ni et al. (1996) proposed a methodology of combining fuzzy sets theory with ANNs for evaluating the stability of slopes. In this approach, the input variables were gradient, horizontal profile, vertical profile, location, slope height, geological origin, soil texture, depth of weathering, direction of the slope, vegetation, land use, maximum daily precipitation and hourly precipitation. However, more studies on the application of ANNs to slope stability problems have been reported more recently (e.g. Neaupane and Achet 2004; Sakallariou and Ferentinou 2005; Wang et al. 2005).

Neaupane and Achet (2004) used back-propagation MLPs to predict slope movements in a higher Himalayan highway slope. In their study, the input variables included the antecedent rainfall, rainfall intensity, infiltration coefficient, shear strength, groundwater

and slope gradient. The data used for ANN model development were obtained from field measurements and observations. Meanwhile, Sakellariou and Ferentinou (2005) utilised back-propagation MLPs to predict the factor of safety (FOS) and the stability status (i.e. either 'failed' or 'stable') of a slope based on the input variables of unit weight, cohesion, friction angle, slope angle, slope height, and pore water pressure. A total of 46 different case records of slopes with a circular failure mechanism were used in the ANN model development process. The factors of safety of these slopes were previously evaluated using conventional limit equilibrium methods. These recent studies together show that ANNs can be used to predict slope stability and movements.

2.5.2 Back-Propagation Multi-Layer Perceptrons

The topology and algorithm details of back-propagation MLPs have been described in many publications (e.g. Eberhart and Dobbins 1990; Zurada 1992; Fausett 1994; Hassoun 1995). In brief, MLPs consists of a number of interconnected neurons, commonly known as *processing elements* (PEs) or *nodes*. The PEs are logically arranged into multiple layers: an input layer, one or more intermediate layers called hidden layers, and an output layer, as shown in Figure 2.16. Each PE is connected to all the PEs in the next layer via weighted connections. The scalar weights determine the strength of influence between the interconnected neurons.

The input from each PE in the previous layer is multiplied by an adjustable connection weight. The weighted input values, at each PE, are then summed and a threshold value or bias is added or subtracted. The result of this combined summation is then passed through a non-linear transfer function (e.g. logistic sigmoid or hyperbolic tangent functions) to produce the output of the PE. The output of one PE provides the input to the PEs in the next layer. For node *j*, this process is summarised in Equations (2.40) and (2.41), and illustrated in Figure 2.16.

$$I_j = \sum_{i=1}^{n} w_{ji} x_i + \theta_j \tag{2.40}$$

$$y_i = f(I_j) \tag{2.41}$$

where I_j = the activation level of node *j*; w_{ji} = the connection weight between nodes *i* and *j*; x_i = the input from node *i*, *i* = 0, 1, …, *n*; θ_j = the bias for node *j*; y_j = the output of node *j*; and $f(I_j)$ = the transfer function.

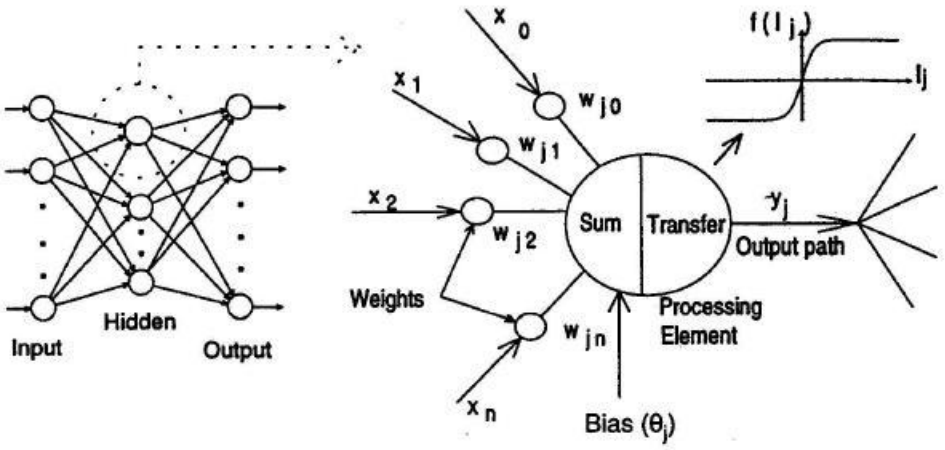

Figure 2.16 Typical structure and operation of an MLP (after Maier and Dandy 1998)

The logistic sigmoid and hyperbolic tangent transfer functions are given in Equations (2.42) and (2.43), respectively:

$$f(I_j) = \frac{1}{1+e^{-(I_j)}} \tag{2.42}$$

$$f(I_j) = \frac{e^{(I_j)} - e^{-(I_j)}}{e^{(I_j)} + e^{-(I_j)}} \tag{2.43}$$

'*Learning*' or '*training*' of the neural networks involves adjusting the connection weights by repeatedly presenting a historical set of model inputs and the corresponding (desired) outputs. The objective of this process is to minimise the errors between the predicted and desired output values. The number of training samples presented to the weight updates is called an *epoch*. This iterative process of correcting the weights at the completion of each epoch, until the errors are minimal, is based on the gradient-descent technique. The global

error between the predicted and desired output is calculated using an error function. The most commonly used error function is the mean square error (MSE) function, which is defined as:

$$E = \frac{1}{2}\sum (y_j - d_j)^2 \tag{2.44}$$

where E = global error function; y_j = the predicted output; and d_j = the desired output.

The global error function, E, is minimised by modifying the weight using the gradient decent rule as follows:

$$\Delta w_{ji} = -\eta \frac{\partial E}{\partial w_{ji}} \tag{2.45}$$

where Δw_{ji} = weight increment from node i to node j; and; η = *learning rate*, by which the size of the step taken along the error surface is determined.

The weights are then updated by adding the delta weight, Δw_{ji}, to the corresponding previous weight as follows:

$$w_{ji}(n+1) = w_{ji}(n) + \Delta w_{ji} \tag{2.46}$$

where $w_{ji}(n)$ = the value of a weight from node i to node j at step n (before adjustment); and $w_{ji}(n+1)$ = the value of the weight at step (n+1) (after adjustment).

The choice of learning rate, η, is critical and the optimal learning rate is usually determined by trial-and-error. A small learning rate will usually result in a very slow convergence. On the other hand, if a large learning rate is chosen, convergence will never occur. To solve this problem, Rumelhart et al. (1986) proposed to add a *momentum term*, μ, to the weight adjustment that is proportional to the amount of the previous weight change. By doing so, the weight change of the current step will carry some momentum of

the weight change from the previous step. The modified adjustment equations are as follows:

$$\Delta w_{ji}(n+1) = -\eta \frac{\partial E}{\partial w_{ji}} + \mu \Delta w_{ji}(n) \tag{2.47}$$

and

$$w_{ji}(n+1) = w_{ji}(n) + \Delta w_{ji}(n+1) \tag{2.48}$$

Shahin et al. (2002b) investigated the effect of the learning rate and momentum term on the performance of the ANN model developed for settlement prediction. They found that the performance of the ANN model was relatively insensitive to the learning rate and momentum term. It was determined that a learning rate of 0.2 and a momentum value of 0.8 produced the best prediction. Neaupane and Achet (2004) also used different learning rates (i.e. 0.001, 0.05, and 0.01) in the development of an ANN model used for the prediction of slope movement. In their case, it was found that a learning rate of 0.01 was optimal. In addition, Basma and Kallas (2004) determined that the optimal values of the learning rate and momentum term were 0.03 and 0.9, respectively, when the ANNs were used to predict the soil collapse potential. It can be seen that there is no consensus, in the literature, in relation to the selection of the values of learning rate and the momentum term, which could be due mainly to fact that they are problem dependent. Therefore, the best way to determine the optimal values of the learning rate and momentum term is through trial-and-error.

In the back-propagation algorithm, the adjustment of the weights is carried out in a backward manner. The weights between the hidden layers and the output layer are adjusted first, followed by the weights between the hidden layer and the input layer. This is an iterative process until some stopping criterion is met so that the network can obtain a set of weights, which will produce the input/output mapping that has the minimum error. One common stopping criterion is the *cross-validation* technique proposed by Stone (1974). The advantage of this technique is to ensure that '*overfitting*' or '*overtraining*' does not occur (Smith 1993). Overfitting may occur when the network starts to learn 'noise' contained in the training data and the model might no longer fit the general trend.

2.5.3 Development of ANN Model

The development of an artificial neural network (ANN) model essentially involves a number of steps, which are carried out in a systematic manner as outlined by Maier and Dandy (2000). This systematic approach has been successfully adopted and applied to geotechnical problems (e.g. Shahin et al. 2002a; Shahin et al. 2002b; Shahin 2003; Shahin and Jaksa 2005). First, the input and output variables for the ANN model need to be identified. This usually requires a good understanding of the physical problem. A number of techniques have been suggested in the literature in relation to the selection of input variables. In the field of geotechnical engineering, one common approach is that a fixed number of input variables are used in advance and assumed to be the most effective input variables in relation to the model output variables (e.g. Jan et al. 2002; Shahin et al. 2002b; Sakallariou and Ferentinou 2005). Another approach is to train many neural networks with different combinations of input variables and to select the network that has the best performance (e.g. Goh 1994; Saka and Ural 1998). Other useful techniques include the use of statistical methods (Stein 1993) and genetic algorithms (NeuralWare 1997) to identify the most significant variables in the model.

The next step involves gathering the data required for calibrating and validating the ANN model. The database will contain numerous case records that have different input patterns with their corresponding expected outputs. In geotechnical problems, these case records could be obtained from field measurements, laboratory test results, or data generated by numerical analysis. It is common practice to divide the available data into two subsets: a training set to construct the ANN model and a validation set to test the generalisation ability of the model within the limits set by the training data. If cross-validation is used as the stopping criterion for training, in order to avoid overfitting, the data need to be divided into three sets: training, testing, and validation. The training set is used in the training process to adjust the connection weights. The testing set is used to decide when to stop training, and training is normally stopped when the error of the testing sets starts to increase. The validation set is used to test the performance of the trained network in the deployed environment using data that were not used in the model development phase.

There are no guidelines found in the literature in relation to the optimal proportion of the data to use for training, testing and validation sets. However, Hammerstrom (1993)

suggested that two-thirds of the data are to be used for model calibration (i.e. training and testing sets) and one-third for model validation. Shahin et al. (2004) investigated the effect of using different proportions of data for training, testing and validation on the performance of ANN models developed for settlement prediction. It was found that there was no clear relationship between the data proportion and the model performance. The best result was obtained when 20% of the data were used for validation and the remaining data were divided into 70% for training and 30% testing.

In the majority of ANN applications in geotechnical engineering, the data are divided into their subsets arbitrarily. Recent studies have found that the way the data are divided can have a significant impact on the results obtained (Tokar and Johnson 1999; Shahin et al. 2004). It is well understood that ANNs perform best when they do not extrapolate beyond the extreme values of the data used for calibration (Minns and Hall 1996; Tokar and Johnson 1999). Therefore, in order to develop a reliable ANN model, the case records of the extreme values should be included in the calibration set. In addition, the statistical properties (e.g. mean and standard deviation) of the various data subsets need to be similar to ensure that each subset represents the same statistical population (Masters 1993).

Pre-processing of the data is usually required before they are applied to the neural networks. This is essential because the transfer function adjusts the output of each neuron to its limiting values (e.g. –1.0 and 1.0 for the hyperbolic tangent function; and 0 and 1 for the logistic sigmoid function). Various scaling and normalisation methods have been proposed in the literature (Masters 1993; Stein 1993). The simple linear mapping of the variables' extreme to the neural network's practical extreme is adopted for scaling, as it is the most commonly used method for this purpose (Masters 1993). For a variable, x, with a maximum and minimum values of $x_{\max}$ and $x_{\min}$, respectively, the scaled value, x_n, is calculated as follows:

$$x_n = \frac{x - x_{\min}}{x_{\max} - x_{\min}} \tag{2.49}$$

After all the data are divided into their respective subsets (i.e. training, testing and validation) and pre-processed, the next step is to determine the model or network architecture. Determination of model architecture is one of the most important and

difficult tasks in the ANN model development process (Maier and Dandy 2000). This is because there is currently no rule for determining the optimal number of hidden layers and the number of nodes of in each of these hidden layers. A common strategy is to train the ANN model several times, starting with the least number of layers and nodes and then increasing the number while monitoring the model performance. It has been shown that one hidden layer is sufficient to approximate any continuous function provided that sufficient connection weights are given (Cybenko 1989; Hornik et al. 1989). In contrast, some researchers (Flood and Kartam 1994; Ripley 1996) stated that the use of more than one hidden layer provides the flexibility needed to model complex functions in many situations. However, using more than one hidden layer often increases the training time (Masters 1993). It has also been shown in the literature (e.g. Maren et al. 1990; Masters 1993; Rojas 1996) that neural networks with a large number of connection weights or nodes are more likely to be subject to overfitting and poor generalisation.

Training or learning is then carried out using the back-propagation algorithm, as discussed in the previous section. The aim of the training process is to optimise the connection weights so that they can be used to define the relationship between the input and output variables. This process is equivalent to the parameter estimation phase in conventional statistical models. Cross-validation (Stone 1974), by using a testing data set, is commonly used to decide when to stop training in order to avoid overfitting. Once the neural network is trained by optimising the weights, the performance of the trained model needs to be validated. The validation of the trained model is conducted using an independent data set (i.e. validation set), which has not been used in the model calibration phase. The aim is to test the predictive and generalisation ability of the ANN model within the limits or ranges set by the training data.

The *coefficient of correlation*, *r*, the *root mean squared error*, RMSE, and the *mean absolute error*, MAE, are the main criteria that are often used to evaluate the prediction performance of ANN models. The coefficient of correlation is a standard statistical measure that is used to determine the relative correlation and goodness-of-fit between the predicted and observed data and can be calculated as follows:

$$r = \frac{C_{y_j d_j}}{\sigma_{y_j} \sigma_{d_j}} \tag{2.50}$$

and

$$C_{y_j d_j} = \frac{1}{n-1}\sum_{j=1}^{n}(y_j - \bar{y})(d_j - \bar{d}) = \frac{1}{n-1}\left(\sum_{j=1}^{n} y_j d_j - \frac{\sum_{j=1}^{n} y_j \sum_{j=1}^{n} d_j}{n}\right) \tag{2.51}$$

$$\sigma_{d_j} = \sqrt{\frac{\sum_{j=1}^{n}(d_j - \bar{d})^2}{n-1}} \tag{2.52}$$

$$\bar{y} = \frac{\sum_{j=1}^{n} y_j}{n} \tag{2.53}$$

$$\bar{d} = \frac{\sum_{j=1}^{n} d_j}{n} \tag{2.54}$$

where y_j = model (predicted) output $= y_1, y_2, y_3, \ldots, y_n$; d_j = desired (observed) output $= d_1, d_2, d_3, \ldots, d_n$; $C_{y_j d_j}$ = covariance between the model output (y_j) and the desired output (d_j); σ_{y_j} = standard deviation of the model output, y_j; σ_{d_j} = standard deviation of the desired output, d_j; $\bar{y}$ = mean of the model output, y_j; $\bar{d}$ = mean of the desired output, d_j; and n = number of data.

Smith (1986) suggested the following guide for values of $|r|$ between 0.0 and 1.0:

- $|r| \geq 0.8$ strong correlation exists between the two sets of variables;
- $0.2 < |r| < 0.8$ correlation exists between the two sets of variables; and
- $|r| \leq 0.2$ weak correlation exists between the two sets of variables.

The RMSE is the most popular measure of error and has the advantage that large errors receive much greater attention than small errors (Hecht-Nielsen 1990). RMSE is calculated as follows:

$$\text{RMSE} = \left\{ \frac{1}{n} \sum_{j=1}^{n} (y_j - d_j)^2 \right\}^{\frac{1}{2}} \tag{2.55}$$

In contrast with RMSE, MAE eliminates the emphasis given to the large errors. Both RMSE and MAE are desirable when the evaluated output data are smooth or continuous (Twomey and Smith 1997) and is calculated as follows:

$$\text{MAE} = \frac{1}{n} \sum_{j=1}^{n} \left| y_j - d_j \right| \tag{2.56}$$

Based on the values of *r*, RMSE and MAE, an optimum ANN model can be selected. This ANN model can then be used as a forecasting tool in practice. With the optimal connection weights in place, it is also possible to develop a mathematical expression relating the input and output variables. This mathematical expression or formula is more useful and portable in practice. In the field of geotechnical engineering, ANN-based equations that can be used for predicting the settlement of shallow foundations on granular soils and the pullout capacity of marquee ground anchors have been developed by Shahin et al. (2002a) and Shahin and Jaksa (2005), respectively.

2.6 Summary

The treatment of the relevant literature in this chapter has indicated that inherent soil variability and effects of vegetation are not commonly considered in routine slope stability analysis although their effects on slope stability are well recognised. This is because quantifying the effects of soil variability and vegetation is usually a complicated task. The available tools for slope stability analysis in practice (i.e. limit equilibrium methods) are not well established to account for the effects of soil variability and vegetation. Furthermore, there is currently no simple or straightforward solution available (either in the form of equations or charts) for this problem. Engineers are usually left to manipulating the factor of safety in order to take such effects into consideration. Despite

the complexity, it has been demonstrated that the effects of soil variability and vegetation can be quantified by various methods found in the literature. In addition, the random finite element method (RFEM) has emerged as a powerful tool that capable of considering spatially varying soil properties in slope stability analysis through a probabilistic framework. The RFEM can also be used to consider the effects of root reinforcement on slope stability, in particular considering the spatially varying root cohesion. The implementation of the RFEM in probabilistic slope stability analysis is discussed in the next chapter.

Chapter 3

PROBABILISTIC SLOPE STABILITY ANALYSIS USING RANDOM FINITE ELEMENT METHOD

3.1 Introduction

This chapter discusses the formulation and implementation of the random finite element method (RFEM) for probabilistic slope stability analysis. The RFEM combines a random field generator with a non-linear finite element slope stability analysis algorithm to perform a probabilistic analysis using the Monte Carlo simulation method. This probabilistic methodology was developed by Griffiths and Fenton (2000; 2004) and it has been fully implemented in a computer model known as *rslope2d*.

Throughout this research, the computer model *rslope2d* has been adopted to investigate the effect of soil variability on slope stability. However, the available version (i.e. version 1.98) of *rslope2d* was limited to analysing slopes with single-layered soil profiles. Therefore, this computer model was modified and further developed to consider slopes with two-layered soil profiles. This computer model was also extended in order to analyse the effect of root reinforcement. These developments of the computer model are discussed in subsequent chapters.

3.2 Overview of the Probabilistic Analysis Methodology

Probabilistic analysis is a more realistic approach to the assessment of slope stability because the uncertainty and variability in soil properties can be explicitly taken into account. Unlike deterministic analysis, which is based on assumed characteristic values of

soil properties, probabilistic analysis considers the variable nature of soil properties, based on their statistical characteristics. The latter approach leads to a more realistic measure of the stability of a slope, which is usually characterised by the probability of failure, P_f. As previously mentioned in Chapter 2, the random finite element method (RFEM) is a powerful probabilistic method for slope stability analysis because the spatial correlation of soil properties is modelled explicitly and no assumption about the shape or location of the failure surface is required to be made in advance. Failure occurs through soil elements whose shear strength is lower than the applied shear stresses.

The procedures for probabilistic slope stability analysis adopted in *rslope2d* can be summarised as follows:

1. Simulate a 2-dimensional (2-D) spatially random soil profile based on the prescribed statistical parameters of the chosen soil properties;

2. Perform finite element slope stability analysis on the simulated soil profile to determine whether the slope 'fails' under specific convergence criteria; and

3. Repeat Steps 1 and 2 many times as part of the Monte Carlo simulation process to establish the probability of failure, P_f.

Detailed descriptions of each process are presented in the following sections.

3.3 Simulation of Soil Profile

To incorporate soil variability in slope stability analysis, it is essential to generate a soil profile that can represent the variability and spatial correlation of the properties in real soil deposits. In *rslope2d*, a 2-D spatially random soil profile is generated based on random field theory (Vanmarcke 1977a, 1983), which makes use of three statistical properties: the mean, μ, a measure of the variance (e.g. standard deviation, σ, or coefficient of variation, COV), and the scale of fluctuation, θ. The scale of fluctuation (SOF), as previously discussed in Chapter 2, is a parameter describing the spatial correlation of soil properties with distance. A small value of SOF implies rapid fluctuation of the soil property in space about the mean, whereas a large value of SOF implies a smoothly varying field.

3.3.1 Soil Parameters

Prior to the random field generation process, it is important to identify the soil parameters that are required to be treated as random variables. The soil model used in the elastoplastic finite element slope stability analysis algorithm in *rslope2d* consists of the following input parameters:

1. Cohesion, c;
2. Friction angle, ϕ;
3. Dilation angle, ψ;
4. Young's Modulus, E_s;
5. Poisson's ratio, ν; and
6. Unit weight, γ.

The parameters c and ϕ are commonly referred to as soil shear strength parameters and the soil shear strength is commonly described by the Mohr-Coulomb failure criterion, as discussed in Chapter 2. The parameters c and ϕ can be expressed in two different stress states, depending on whether a '*total*' or '*effective*' stress analysis is assumed. A total stress analysis is applied to short-term stability problems where no dissipation of excess pore water pressure has taken place, such as a newly cut or newly constructed slope in fully saturated clay. Stability analyses should be carried out in terms of effective stresses for problems where changes in pore pressures have taken place, for example, an existing embankment. In total stress analysis, the cohesion is assumed to be completely undrained and the shear strength is given by the undrained shear strength, s_u, or undrained cohesion, c_u, (i.e. $\phi_u = 0$). In effective stress analysis, the drained cohesion, c', and drained friction angle, ϕ', are used in the slope stability analysis. The research contained in this thesis considers both total and effective stress analysis of the slope stability problem, where the results and discussions are presented in Chapter 4.

While the dilation angle, ψ, affects the volume change of the soil during yielding and the elastic parameters (i.e. Young's modulus, E_s, and Poisson's ratio, ν) influence the

computed deformations prior to failure in slope stability analysis, they have little influence on the predicted factor of safety (Griffiths and Lane 1999). Griffiths and Lane (1999) also concluded that the most important parameters in finite element slope stability analysis are the same as those used in the traditional limit equilibrium approach, namely the strength parameters c and ϕ, unit weight, γ, and the geometry of the slope. Hence, it is logical to assume that, in a probabilistic analysis, only the variability of the cohesion, friction angle and unit weight influences the probability of failure of a slope.

However, a previous probabilistic study conducted by Alonso (1976) concluded that the influence of the soil density or unit weight on the probability of failure of a clay slope is relatively small compared with the shear strength parameters. This is due to the fact that the variability of soil unit weight is usually small, as published in the literature (e.g. Lee et al. 1983; Phoon and Kulhawy 1999a; Duncan 2000; Baecher and Christian 2003). Therefore, throughout this research, only the shear strength parameters c and ϕ are modelled as random fields, while the other parameters are held constant and treated deterministically to reduce the complexity of the problem. The variability of the shear strength parameters c and ϕ is characterised by a lognormal distribution. This is because lognormal distribution avoids the generation of negative values of strength parameters c and ϕ that a normal distribution allows. Furthermore, available field data indicate that some soil properties are well represented by a lognormal distribution (e.g. Hoeksema and Kitanidis 1985; Sudicky 1986; Cherubini 2000), as previously discussed in Chapter 2. The characteristic of a lognormal distribution has been discussed in Section 2.3.1.6.

3.3.2 Random Field Generation

To generate random fields of a soil property (i.e. c or ϕ), random field theory is implemented in *rslope2d* using the local average subdivision (LAS) method developed by Fenton and Vanmarcke (1990). This method produces correlated local averages of the soil property based on a standard normal distribution function (i.e. having zero mean and unit variance) and a spatial correlation function. An isotropic exponentially decaying (Markovian) correlation function is assumed in this research, and it can be expressed as:

$$\rho(k) = \exp\left(-\frac{2|k|}{\theta}\right) \tag{3.1}$$

where ρ = correlation coefficient between the underlying random field values at any two points separated by a lag distance *k*.

The LAS methodology has been described in detail by Fenton (1990) and Fenton and Vanmarcke (1990). Briefly, the one-dimensional (1-D) LAS method proceeds in a top-down recursive manner, as indicated in Figure 3.1. In Stage 0, a normally distributed global average is generated for the process. In subsequent stages, the parent cell from previous stage is subdivided into two equal regions such that the local averages of these two new cells must average to the parent cell value, which in turn preserves upward averaging. The normally distributed values in the two new cells are generated so that the following four criteria are satisfied:

1. They have the correct variance according to local averaging theory;
2. They are properly correlated with each other;
3. Their average is equal to the parent cell value; and
4. They are properly correlated with other new cells.

Figure 3.1 Top-down approach for random field generation using LAS method (after Fenton 1990)

Fenton (1990) investigated the accuracy of the 1-D LAS method for estimating a zero mean Ornstein-Uhlenbeck process, and the results of comparing the exact correlation with that estimated by LAS are given in Figure 3.2. The correlation structure is exponentially decaying and based on an averaging dimension, D, and a scale of fluctuation, θ. It can be seen from Figure 3.2 that the error is typically very small. Fenton (1990) also pointed out that the errors are self-correcting and the estimated correlation structure tends to the exact correlation function when averaged over several realisations. The rate of convergence of the estimated statistic to the exact one is $1/n$, where n is the number of realisations.

Figure 3.2 Comparison of estimated and exact correlation between adjacent cells across a parent cell boundary for varying effective averaging lengths $2D/\theta$ (after Fenton 1990)

In simulating a 2-D random field, the parent cell is subdivided into four equal regions at each stage. As in the 1-D case, the values in the four new cells are selected so that the upward averaging is preserved and they are properly correlated with each other, as well as with other new cells. The comparisons of the estimated and exact covariance structure of a generated 2-D LAS process with scales of fluctuation of $\theta = 4$ and $\theta = 0.5$ are shown in Figures 3.3 (a) and (b), respectively. The results have been averaged over 10 realisations and indicate that the exponentially decaying correlation structure has been estimated by 2-D LAS method with a reasonable accuracy.

Figure 3.3 Comparison of estimated and exact covariance for generated 2-D LAS process with scales of fluctuation of (a) θ = 4 and (b) θ = 0.5, averaged over 10 realisations (after Fenton 1990)

3.3.3 Transformation into Lognormal Random Field

If a soil property X (i.e. c or ϕ) is assumed to be characterised statistically by a lognormal distribution defined by a mean, μ_X, and a standard deviation, σ_X, the standard normal random field, $G(x)$, generated by the LAS method is then necessary to be transformed into a lognormal distribution using the relationship:

$$X_i = \exp\{\mu_{\ln X} + \sigma_{\ln X} G(x_i)\} \tag{3.2}$$

where x_i is the vector containing the coordinates of the centre of the ith element; X_i is the soil property value assigned to that element; $\mu_{\ln X}$ and $\sigma_{\ln X}$ are the mean and standard deviation, respectively, of the underlying normally distributed $\ln X$. $\mu_{\ln X}$ and $\sigma_{\ln X}$ can be

computed using Equations (2.15) and (2.16), respectively, as previously shown in Section 2.3.1.6.

3.3.4 Effects of Local Averaging and Variance Reduction

The input statistical parameters such as the mean, standard deviation and scale of fluctuation are assumed to be defined at the point level. Within the context of the LAS methodology, the point variance is reduced due to the local averaging process and the reduction is governed by a *variance function*, Γ^2. The variance reduction is a function of the size of the averaging domain and the scale of fluctuation (Vanmarcke 1983), and for an exponentially-decaying correlation function, it is given by:

$$\Gamma^2(\mathrm{T}) = 2\left(\frac{\theta}{2\mathrm{T}}\right)^2\left(\frac{2\mathrm{T}}{\theta} - 1 + e^{-\frac{2\mathrm{T}}{\theta}}\right) \tag{3.3}$$

where T is the size of the averaging domain. For a square finite element, T is the element size.

Griffiths and Fenton (2004) show that the variance function for a square finite element of side length $\alpha\theta$ can be expressed as follows:

$$\Gamma^2 = \frac{4}{\alpha\theta}\int_0^{\alpha\theta}\int_0^{\alpha\theta}\exp\left(-\frac{2}{\theta}\sqrt{x^2+y^2}\right)(\alpha\theta - x)(\alpha\theta - y)\,dx\,dy \tag{3.4}$$

The variance function for a square finite element, based on an exponentially decaying correlation function, is given in Figure 3.4. This figure indicates that elements that are small relative to the scale of fluctuation ($\alpha \to 0$) lead to very little reduction in variance ($\Gamma^2 \to 1$), while elements that are large relative to the scale of fluctuation lead to very significant variance reduction ($\Gamma^2 \to 0$). In other words, if the element size is fixed, a larger scale of fluctuation leads to less reduction in variance, while a smaller scale of fluctuation leads to greater reduction in variance.

NOTE:
This figure is included on page 71 of the print copy of the thesis held in the University of Adelaide Library.

Figure 3.4 Variance reduction over a square finite element (after Griffiths and Fenton 2004)

Griffiths and Fenton (2004) also point out that, if the point distribution is normal, local averaging results in reduction in variance but the mean is unaffected. However, in a lognormal distribution, local averaging reduces both the mean and the standard deviation. This is because the mean and variance of a lognormal distribution being dependent on both the mean and variance of the underlying normal distribution, as indicated by Equations (2.18) and (2.19) (see Section 2.3.1.6). When the effects of local averaging are included, Equations (2.18) and (2.19) can be rewritten to define the 'sample' mean and standard deviation of a lognormal field as:

$$\hat{\mu}_X = \exp\left(\mu_{\ln X} + \tfrac{1}{2}\Gamma^2\sigma^2_{\ln X}\right) \tag{3.5}$$

$$\hat{\sigma}_X = \hat{\mu}_X\sqrt{\exp\left(\Gamma^2\sigma^2_{\ln X}\right)-1} \tag{3.6}$$

From Equations (3.5) and (3.6), when $\Gamma^2 \to 0$, $\hat{\mu}_X \to \exp\left(\mu_{\ln X}\right)$ = Median $_X$; and $\hat{\sigma} \to 0$. This implies that with significant variance reduction due to local averaging, the sample mean tends to the median and the sample standard deviation tends to zero.

3.3.5 Mapping of Simulated Soil Properties onto Finite Element Mesh

Once the random field is transformed into the desired lognormal field, it is then mapped onto the finite element mesh, which is established according to the user-defined slope geometry. A typical finite element mesh for a 1:1 slope with a height, H = 10 m, is shown in Figure 3.5. A fixed base is assumed at the lower boundary and rollers are assumed at the two vertical boundaries. Each element within the slope geometry is 1 m by 1 m in size and it is assigned a random variable of the particular soil property (i.e. c or ϕ).

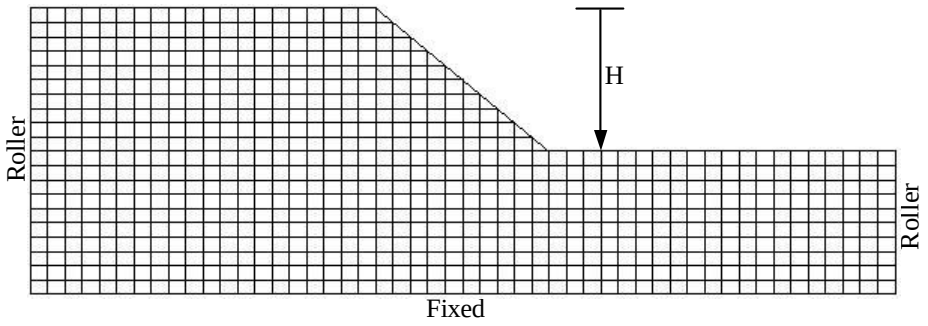

Figure 3.5 Typical finite element mesh used for slope stability analysis

Figure 3.6 shows typical random field realisations of undrained cohesion, c_u, for the slope with different scales of fluctuation, θ. Figure 3.6(a) shows a relatively small scale of fluctuation of θ = 1 m, while Figure 3.6(b) shows a relatively large scale of fluctuation of θ = 10 m. It should be noted that both random field realisations have the same mean and standard deviation of μ_{c_u} = 60 kPa and σ_{c_u} = 30 kPa, respectively, i.e. COV = 0.5. Dark and light regions indicated 'strong' and 'weak' soil elements, respectively. It can be observed from Figure 3.6 that a smaller value of θ generates a more rapidly varying soil profile with distance (i.e. a more spatially random soil profile), while a larger value of θ generates a more continuously varying soil profile (i.e. a more uniform soil profile).

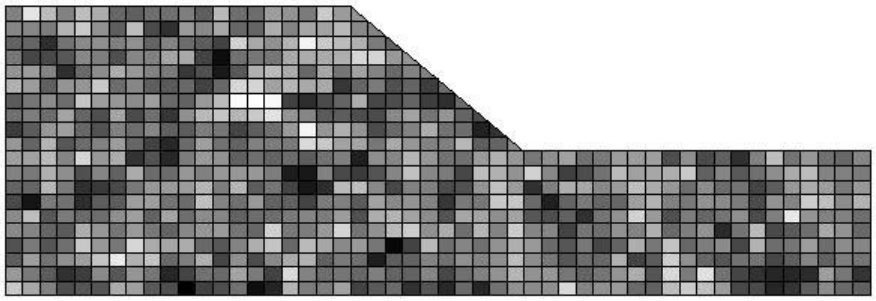

(a)

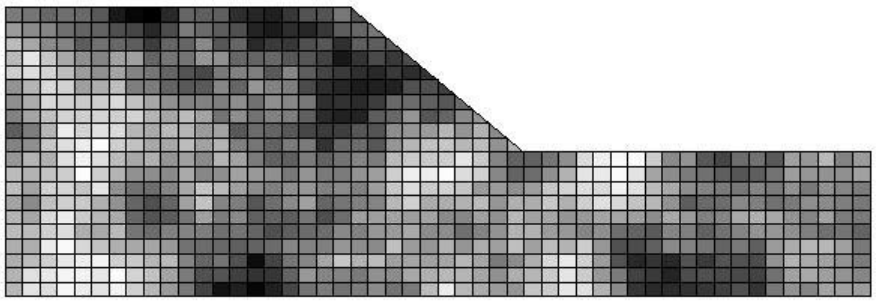

(b)

Figure 3.6 Typical random field realisations of undrained cohesion, c_u, with scales of fluctuation of (a) θ = 1 m and (b) θ = 10 m

3.3.6 Cross-correlation between *c* and ϕ

The relationship or cross-correlation between the strength parameters *c* and ϕ is poorly understood and no consensus is provided by literature. In addition, it is strongly dependent on the soil being studied (Fenton and Griffiths 2003). However, Cherubini (2000) reported values of cross-correlation between *c* and ϕ ranging from –0.24 to –0.70. In *rslope2d*, cross-correlation between *c* and ϕ is implemented using the covariance matrix decomposition approach (Fenton 1994). The algorithm is summarised as follows:

1. Specify the cross-correlation coefficient, $\rho_{c\phi}$ ($-1 \le \rho_{c\phi} \le 1$). Values of $\rho_{c\phi}$ of –1, 0, and 1 correspond to completely negatively correlated, uncorrelated, and completely positively correlated, respectively;

2. Form the correlation matrix between $G_{\ln c}(x)$ and $G_{\ln \phi}(x)$, assumed to be stationary (i.e. the same at all points *x* in the field):

$$\rho = \begin{bmatrix} 1.0 & \rho_{c\phi} \\ \rho_{c\phi} & 1.0 \end{bmatrix} \tag{3.7}$$

3. Compute the Cholesky decomposition of ρ. That is, find the lower triangular matrix L, such that $LL^T = \rho$;

4. Generate two independent standard normally distributed random fields, $G_1(x)$ and $G_2(x)$, each having a scale of fluctuation of θ;

5. At each spatial point, x, form the underlying point-wise correlated random fields:

$$\begin{Bmatrix} G_{\ln c}(x_i) \\ G_{\ln \phi}(x_i) \end{Bmatrix} = \begin{bmatrix} L_{11} & 0.0 \\ L_{21} & L_{22} \end{bmatrix} \begin{Bmatrix} G_1(x_i) \\ G_2(x_i) \end{Bmatrix} \tag{3.8}$$

6. Transform the standard normal random field of c and ϕ to the final lognormal random field using Equation (3.2).

3.4 Finite Element Slope Stability Analysis

The finite element slope stability analysis algorithm in *rslope2d* assumes 2-D and plain strain conditions. It uses an elastic-perfectly plastic stress-strain law with a Mohr-Coulomb failure criterion. It utilises 8-node quadrilateral elements with reduced integration in the gravity loads generation, stiffness matrix generation and stress redistribution phases of the algorithm. The theoretical basis of the method is described fully by Smith and Griffiths (1998; 2004) and the application of the finite element method in slope stability problems is described by Griffiths and Lane (1999).

In brief, the analyses involve the application of gravity loading and the monitoring of stresses at all Gauss points. The forces generated by the self-weight of the soil are modelled by a standard gravity 'turn-on' procedure. This procedure generates normal and shear stresses at all Gauss points within the mesh and the soil is initially assumed to be elastic. These stresses are then compared with the Mohr-Coulomb failure criterion, which can be written in terms of principal stresses as follows:

$$F = \frac{\sigma_1 + \sigma_3}{2} \sin\phi - \frac{\sigma_1 - \sigma_3}{2} - c\cos\phi \tag{3.9}$$

where σ_1 and σ_3 are the major and minor principal stresses.

If the stresses at a particular Gauss point lie within the Mohr-Coulomb failure envelope ($F < 0$), then that location is assumed to remain elastic. If the Mohr-Coulomb failure criterion is violated ($F \geq 0$), then that location is assumed to be yielding. Yielding stresses are redistributed to neighbouring elements that still have reserves of strength. The plastic stress redistribution is accomplished by using a visco-plastic algorithm (Zienkiewicz and Cormeau 1974). This is an iterative process which continues until the Mohr-Coulomb failure criterion and global equilibrium are both satisfied at all Gauss points within the mesh.

3.4.1 Determination of Factor of Safety

The finite element algorithm in *rslope2d* computes a deterministic factor of safety, FOS, based on the mean values of the shear strength parameters using the strength reduction method (Matsui and Sun 1992). The FOS of a slope is defined as the factor that the original shear strength parameters must be divided by in order to bring the slope to the point of failure. The strength parameters at the point of failure, c_f and ϕ_f, are therefore given by:

$$c_f = \frac{c}{\text{FOS}} \tag{3.10}$$

and

$$\phi_f = \arctan\left(\frac{\tan\phi}{\text{FOS}}\right) \tag{3.11}$$

This definition of the factor of safety is essentially the same as that used in limit equilibrium methods, which is defined as the ratio of shear strength of soil to shear stress required for equilibrium (Duncan 1996). Validation studies conducted by Griffiths and Lane (1999) indicate good agreement between the FOS computed by the finite element method and that obtained from the stability charts developed by Taylor (1937) and Bishop and Morgenstern (1965).

3.4.2 Definition of Slope Failure

Several definitions of slope failure used in finite element slope stability analysis have been discussed by Wong (1984) and Abramson et al. (2002) including:

1. Some test of bulging of the slope profile (Snitbhan and Chen 1976);
2. Limiting of the shear stresses on the potential failure surface (Duncan and Dunlop 1969); and
3. Non-convergence of the solution (Zienkiewicz and Taylor 1989).

In *rslope2d*, non-convergence of the algorithm within a user-specified maximum number of iterations or iteration limit is used as an indicator of slope failure. A slope is considered to have "failed" when no stress distribution can be found that simultaneously satisfies both the Mohr-Coulomb failure criteria and global equilibrium (Griffiths and Lane 1999). This is usually accompanied by a dramatic increase in the nodal displacements within the mesh. Griffiths and Fenton (2004) reported that an iteration limit of 500 was adequate to ensure convergence of solutions for a case study of a 2:1 undrained clay slope. The iteration limit required for the case studies considered in this research is investigated and discussed further in Chapter 4.

3.5 Monte Carlo Simulation

This section covers two important aspects of Monte Carlo simulation, namely the probability of failure and the number of realisations. Treatment of each of these follows.

3.5.1 Probability of Failure

Based on a given set of soil property statistics (mean, standard deviation and scale of fluctuation), there are an infinite number of possible random fields that can be generated. Although these random fields have the same statistics, the arrangement of the 'strong' and 'weak' soil elements is different in each random field realisation, which in turn yields different outcomes in the finite element analyses. Hence, probabilistic analysis involves the repeated finite element examination of every single realisation of the generated random

fields, as part of the Monte Carlo simulation process. The probability of failure, P_f, of a slope is estimated by the following relationship:

$$P_f = \frac{n_f}{n_{sim}} \tag{3.12}$$

where n_f = number of realisations reaching failure; and n_{sim} = total number of realisations in the simulation process.

3.5.2 Number of Realisations

The accuracy of the estimated probability of failure depends on the number of realisations in the Monte Carlo simulation process. In general, the accuracy increases as the number of realisations increases. However, it is important to determine the minimum number of realisations to produce a reliable and reproducible result. The reason is that repetitive finite element analysis is very time consuming and the estimation of P_f usually converges within a certain number of realisations. Any further increase in the number of realisations will not improve the estimation greatly, but will adversely affect the computational time and effort.

Hahn and Shapiro (1967) suggest that the minimum number of realisations required is dependent on the number of component random variables and the desired level of confidence, as given by:

$$n_{\min} = m\left(\frac{100d}{\varepsilon}\right)^2 \frac{\left(1-P_f\right)}{P_f} \tag{3.13}$$

where $n_{\min}$ = minimum number of realisations for the Monte Carlo simulation process; m = number of random variables; ε = relative percentage error in estimating P_f ; and d = normal standard deviate according to the desired confidence levels, as shown in Table 3.1.

Table 3.1 Normal standard deviates for different confidence levels

Confidence Level	Normal Standard Deviate, *d*
80%	1.282
90%	1.645
95%	1.96
99%	2.576

To use Equation (3.13), a value of P_f is required before the simulation process takes place, but this is not always available. Hahn and Shapiro (1967) suggest the use of $P_f = 0.5$ as a first estimate of the $n_{\min}$. By using $P_f = 0.5$, Table 3.2 lists the minimum number of realisations, $n_{\min}$, required for various percentage errors, ε, and for 95% and 90% confidence levels with number of random variables, m, equals to 1 and 2. It is shown that, in order to achieve a relative percentage error of less than 5%, for a 95% confidence level, the number of realisations must be greater than 1,500 for single random variable problems and 3,000 for two random variables problems. The variation of the minimum number of realisations with relative percentage errors for the single random variable problem (m = 1) and for 95% and 90% confidence levels is also plotted in Figure 3.7.

By rearranging Equation (3.13), the relative percentage error can be back-calculated after a Monte Carlo simulation that involved n_{sim} realisations, based on the computed probability of failure, P_f:

$$\varepsilon = d\sqrt{\frac{m(1-P_f)}{n_{sim}\ P_f}} \times 100\% \tag{3.14}$$

By examining Equation (3.14), it can be seen that the relative percentage error is directly proportional to the square root of $(1 - P_f)$, and inversely proportional to the square root of n_{sim}. Therefore, it should be expected that a larger number of realisations is required for smaller probabilities of failure, if the relative percentage error and confidence level are fixed at a prescribed value.

Griffiths and Fenton (2004) reported that 1,000 realisations of the Monte Carlo simulation process was adequate for a 2:1 undrained clay slope in order to produce converged estimations of the probability of failure. The minimum number of realisations required for the case studies considered in this research is investigated and discussed further in the next chapter.

Table 3.2 Minimum number of realisations required for achieving desired accuracy

Relative error, ε (%)	m = 1		m = 2	
	95% Confidence	90% Confidence	95% Confidence	90% Confidence
0.5	153,664	108,241	307,328	216,482
1	38,416	27,060	76,832	54,121
5	1,537	1,082	3,073	2,165
10	384	271	768	541
50	15	11	31	22

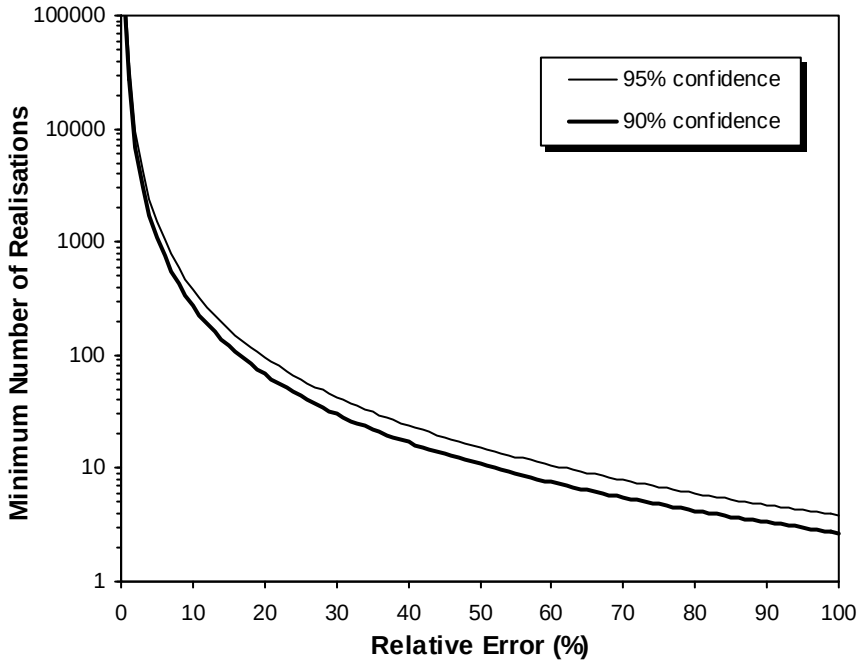

Figure 3.7 Minimum number of realisations required versus relative percentage error for 95% and 90% confidence levels, and m = 1

3.6 Validation of Simulated Soil Properties

It is important to ensure that the soil profile simulated by *rslope2d*, using the local average subdivision (LAS) method, conforms to the prescribed statistical properties such as probability density function (PDF), mean, standard deviation, and scale of fluctuation. It is also necessary to ensure that the simulated random fields conform to the local averaging theory based on random field theory (Vanmarcke 1983). As a result, a verification study was undertaken based on the 1:1 undrained clay slope, as shown previously in Figure 3.7.

3.6.1 Verification of the Lognormal Distribution

The first part of the verification study involves examining the distribution, mean and standard deviation of the simulated soil properties. For the 1:1 undrained clay slope, the simulated soil property is the undrained cohesion, c_u. Random fields of c_u with different values of coefficient of variation, COV, and scale of fluctuation, θ, were simulated using the LAS method. In this study, the scale of fluctuation was normalised by the slope height (i.e. θ/H). The target mean was fixed at 60 kPa and the values of COV being considered were 0.1, 0.3, 0.5 and 1.0. The target normalised scales of fluctuation, θ/H, being considered were 0.1, 1 and 10.

Figure 3.8 shows the frequency density plots of the simulated values of c_u within the slope geometry for one realisation, which are labelled as 'sample' distributions. The 'target' distributions are obtained by using the theoretical PDF for a lognormal distribution, as given by Equation (2.17) in Section 2.3.1.6. Generally, the lognormal distribution appears to be a reasonable fit of the simulated data, as shown in Figure 3.8. However, it can be seen from Figure 3.8 that the sample distribution does not always match the target distribution. In fact, the closest match is observed when θ/H = 1 and larger discrepancies were observed for the random fields with θ/H = 0.1 and 10, for all values of COV. On visual inspection, it is clear that the shape of the sample distribution is affected by the values of COV and θ/H. This is further verified by computing the sample mean and standard deviation of the simulated values of c_u.

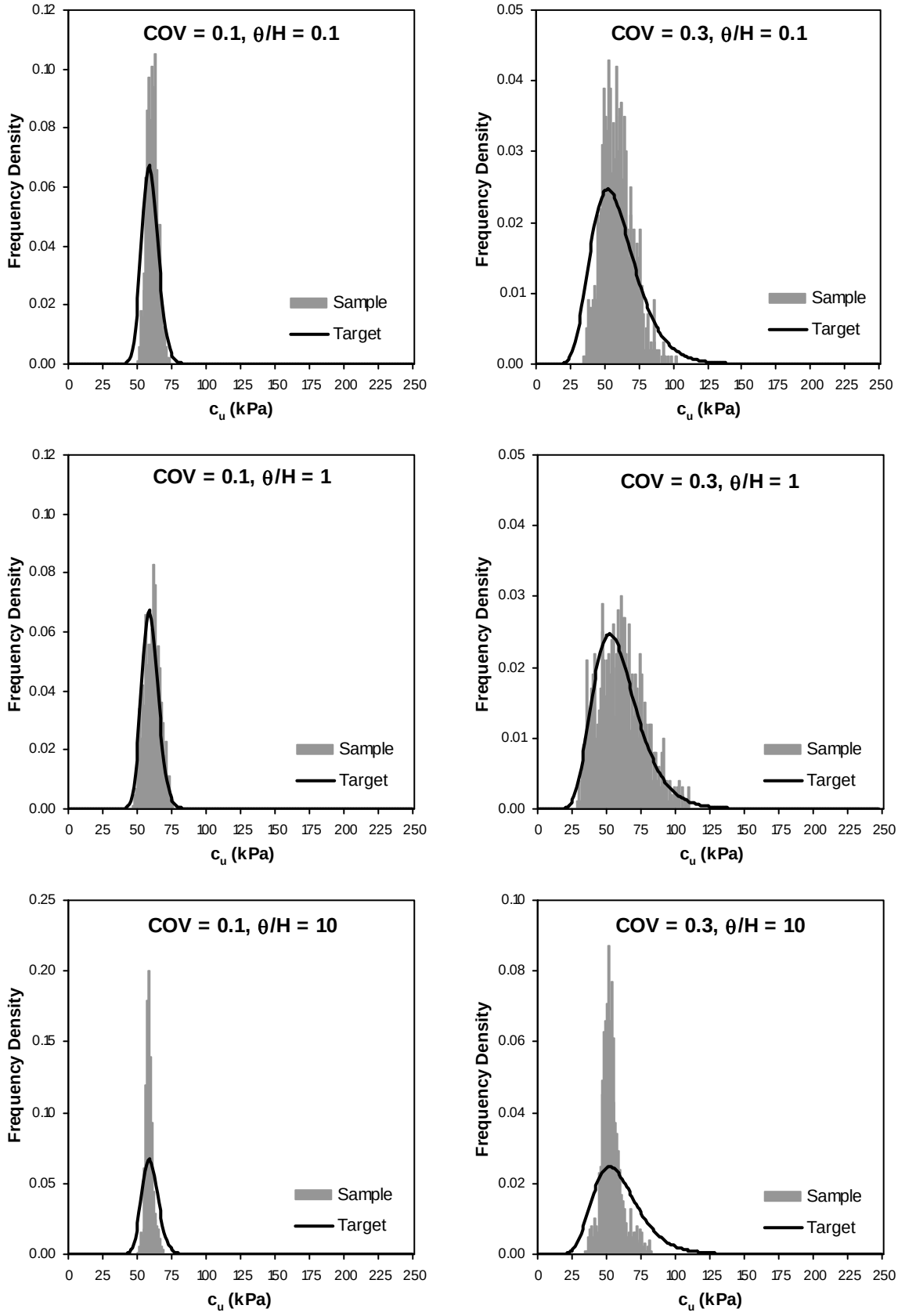

Figure 3.8 Frequency density plots for simulated values of c_u with different values of COV and θ/H (based on one realisation)

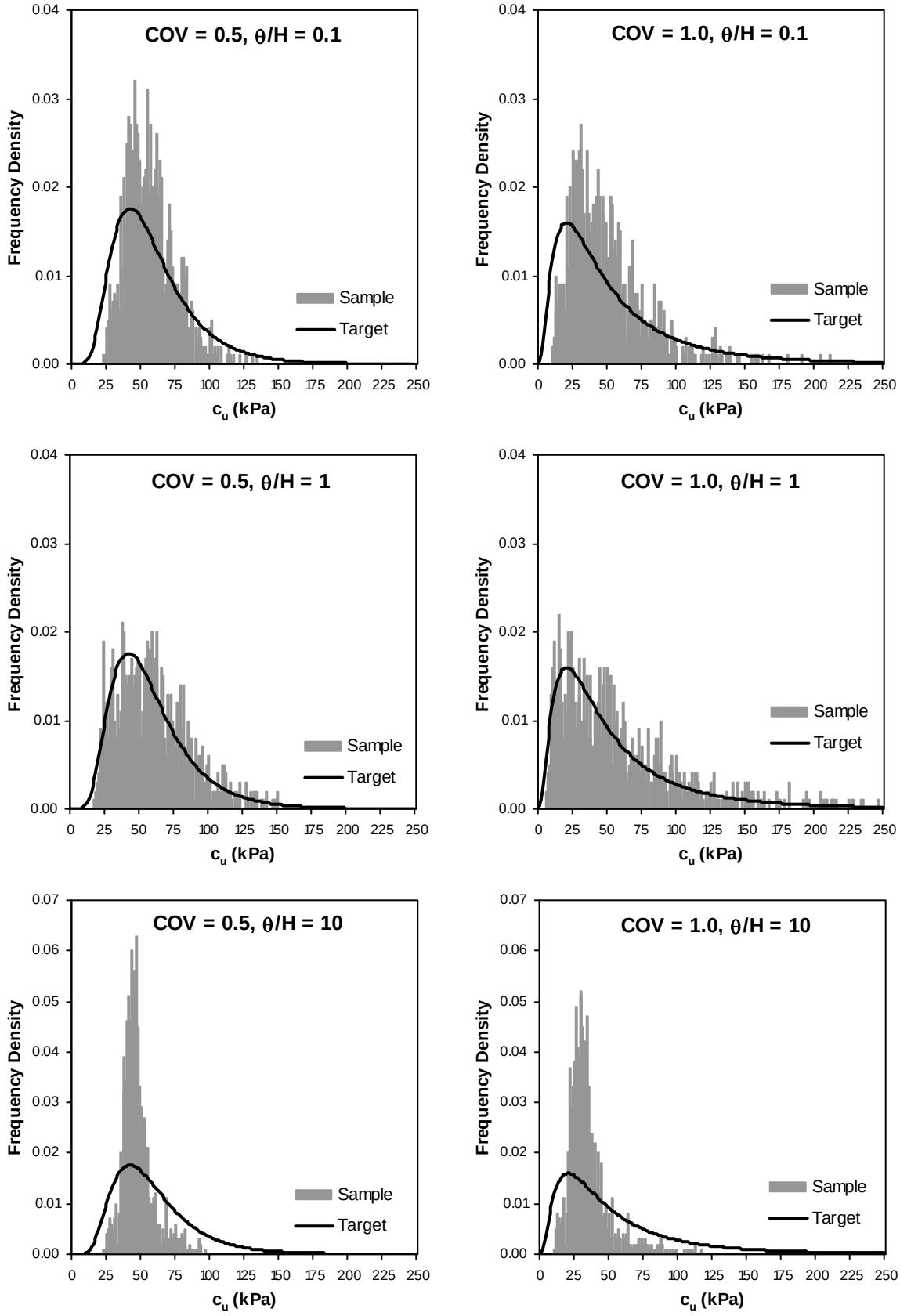

Figure 3.8 Frequency density plots for simulated values of c_u with different values of COV and θ/H (based on one realisation) (continued)

The comparison between the sample and target mean and standard deviation of c_u is summarised in Table 3.3. The results in Table 3.3 confirm that the sample mean and standard deviation of c_u are influenced by the values of COV and θ/H. If the value of θ/H is fixed the difference between the target and sample mean and standard deviation of c_u increases as the value of COV increases. For example, when θ/H is fixed at 0.1, the difference between the target and sample mean of c_u increases from 0.3% to 18.3%, while the difference between the target and sample standard deviation of c_u increases from 34.7% to 52.9%. However, when the value of COV is fixed, the largest difference between the target and sample mean and standard deviation of c_u is observed when θ/H = 10, while the smallest difference is observed when θ/H = 1.

Table 3.3 Comparison between sample and target mean and standard deviation of c_u (based on one realisation)

COV	θ/H	Mean (kPa)		Difference (%)	Std. Dev. (kPa)		Difference (%)
		Target	Sample		Target	Sample	
0.1	0.1	60	59.8	0.3	6	3.9	34.7
0.1	1	60	59.9	0.1	6	5.6	6.3
0.1	10	60	57.7	3.8	6	2.8	53.7
0.3	0.1	60	58.5	2.5	18	11.3	37.1
0.3	1	60	59.6	0.7	18	16.3	9.4
0.3	10	60	52.4	12.6	18	7.6	57.6
0.5	0.1	60	56.2	6.3	30	17.7	41.0
0.5	1	60	59.0	1.7	30	26.0	13.5
0.5	10	60	46.8	22.1	30	11.3	62.2
1	0.1	60	49.1	18.3	60	28.3	52.9
1	1	60	56.5	5.8	60	44.6	25.7
1	10	60	34.6	42.4	60	16.0	73.3

Since the Monte Carlo simulation process essentially involves simulating thousands of realisations of random soil profiles, it is important to investigate the distribution of the 'Mean c_u' computed for each realisation. For this purpose, 2,000 realisations of c_u fields were simulated and the sample mean for each realisation were computed. The frequency

density plots for the computed sample 'Mean c_u' with different values of COV and θ/H are shown in Figure 3.9. The theoretical or target lognormal distribution is also included in each plot.

In can be seen that, for all values of COV, the closest match between the sample and target distribution are observed when θ/H = 10. It is also noted that the scatter of the sample 'Mean c_u' decreases as the values of COV and θ/H decreases. The sample mean and standard deviation of 'Mean c_u' are computed and summarised in Table 3.4. It can be seen that both the sample mean and standard deviation of 'Mean c_u' are reduced from their target values. If the value of θ/H is fixed the difference between the target and sample mean of 'Mean c_u' increases as the value of COV increases. For example, when θ/H = 0.1, the difference between the target and sample mean of 'Mean c_u' increases from 0.5% to 19% as the value of COV increases from 0.1 to 1.0. Similarly, the difference between the target and sample standard deviation of 'Mean c_u' also increases as the values of COV increase when the values of θ/H are fixed. For example, when θ/H = 0.1, the difference between the target and sample standard deviation of 'Mean c_u' increases from 95.3% to 96.9% as the value of COV increases from 0.1 to 1.0.

On the other hand, if the values of COV are fixed, the difference between the target and sample mean of 'Mean c_u' decreases as the value of θ/H increases. For example, the case with COV = 0.1, the difference between the target and sample mean of 'Mean c_u' decreases from 0.5% to 0.2% as the value of θ/H increases from 0.1 to 10. Similarly, the difference between the target and sample standard deviation of 'Mean c_u' also decreases as the values of θ/H increases when the value of is COV fixed. For example, the case with COV = 0.1, the difference between the target and sample standard deviation of 'Mean c_u' decreases from 95.3% to 14.9% as the value of COV increases from 0.1 to 10.

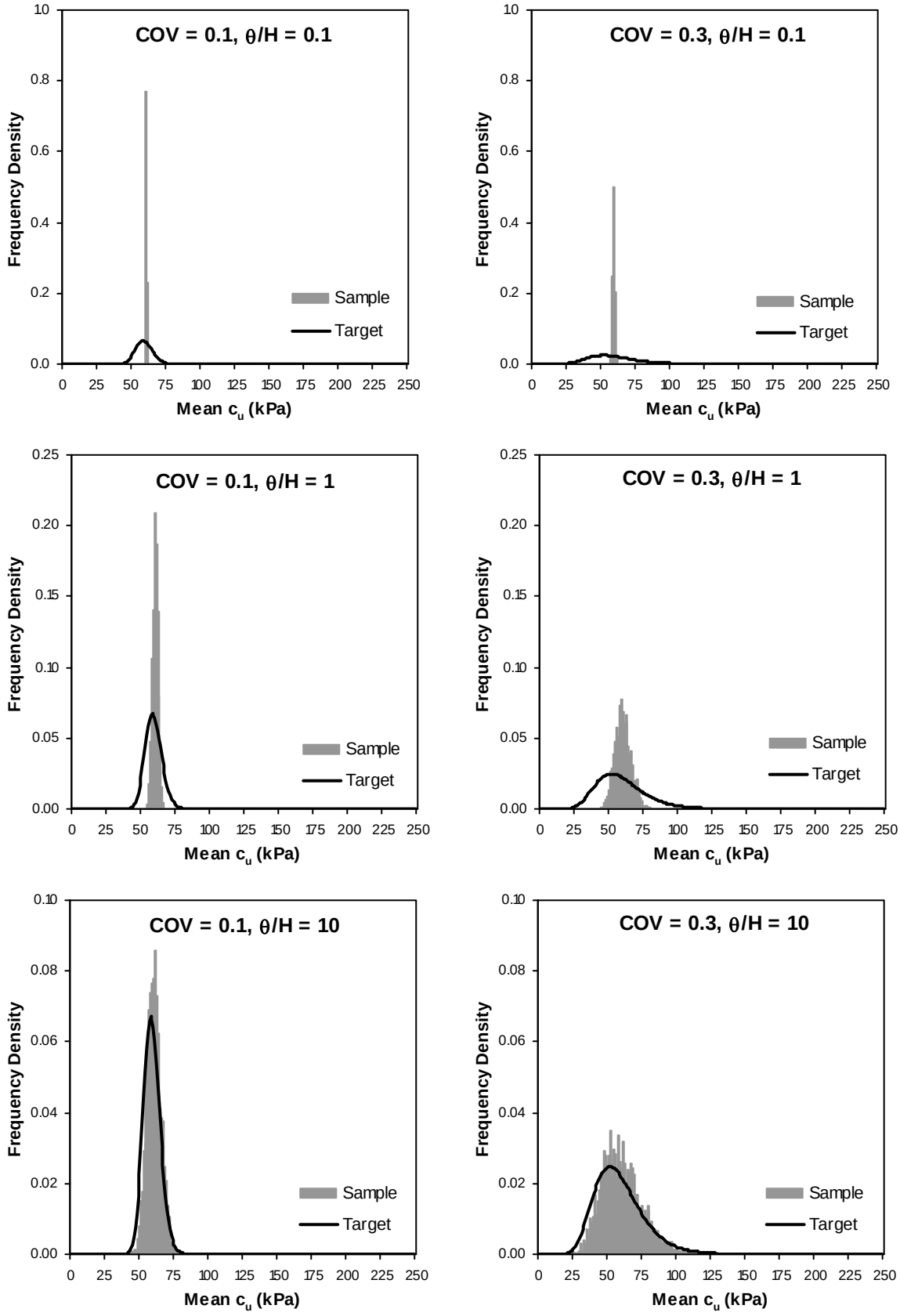

Figure 3.9 Frequency density plots for 'Mean c_u' with different values of COV and θ/H (based on 2,000 realisations)

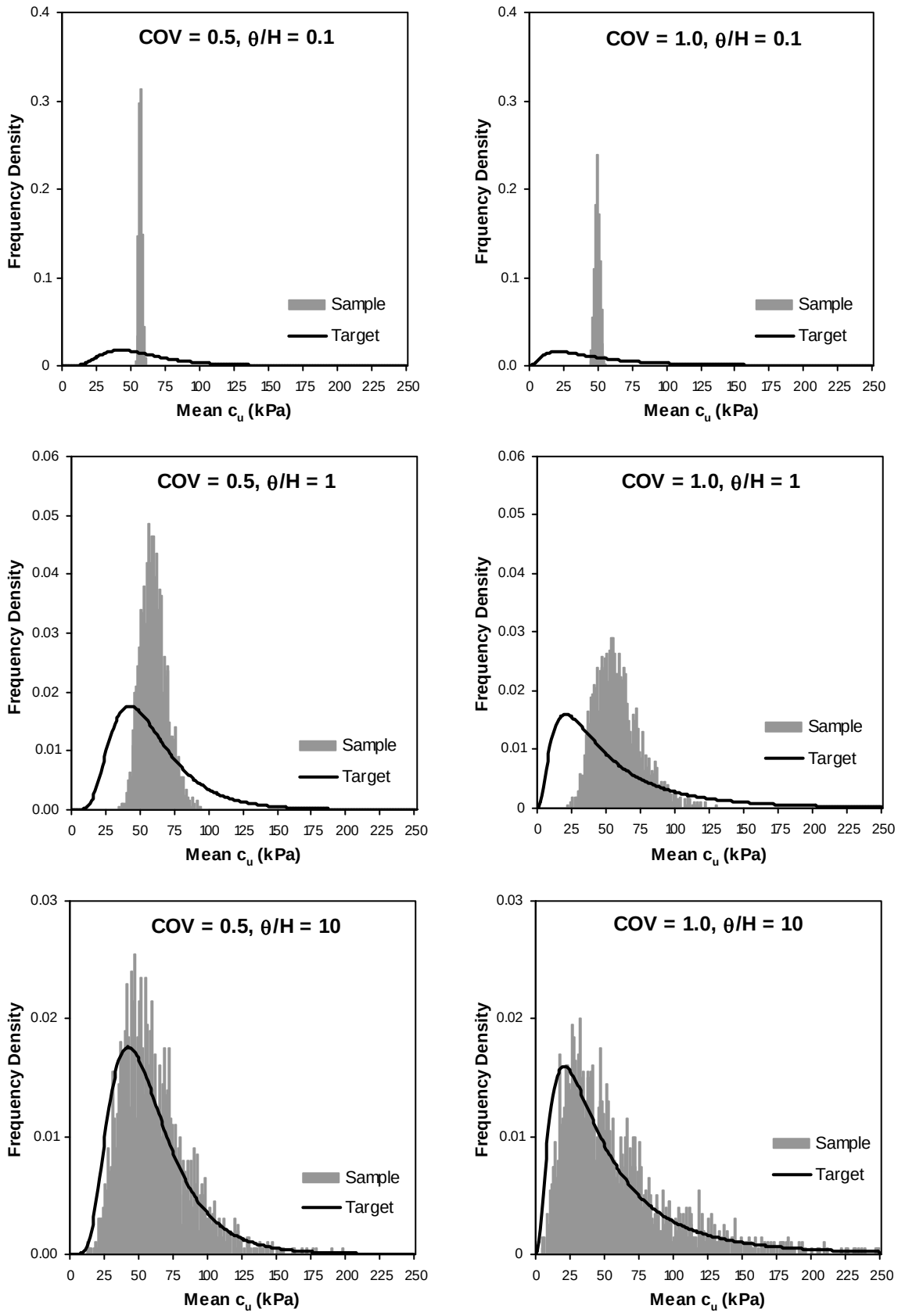

Figure 3.9 Frequency density plots for 'Mean c_u' with different values of COV and θ/H (based on 2,000 realisations) (continued)

Table 3.4 Comparison between sample and target mean and standard deviation of '*Mean* c_u' (based on 2000 realisations)

COV	θ/H	Mean (kPa)		Difference (%)	Std. Dev. (kPa)		Difference (%)
		Target	Sample		Target	Sample	
0.1	0.1	60	59.7	0.5	6	0.3	95.3
0.1	1	60	59.7	0.5	6	2.0	66.4
0.1	10	60	59.9	0.2	6	5.1	14.9
0.3	0.1	60	58.4	2.6	18	0.8	95.8
0.3	1	60	59.6	0.8	18	5.8	67.7
0.3	10	60	59.9	0.2	18	14.9	17.0
0.5	0.1	60	56.1	6.6	30	1.2	96.1
0.5	1	60	59.0	1.6	30	9.4	68.8
0.5	10	60	59.7	0.5	30	24.4	18.7
1	0.1	60	48.6	19.0	60	1.8	96.9
1	1	60	57.4	4.3	60	16.6	72.3
1	10	60	59.1	1.5	60	45.8	23.7

The difference between the sample and target distribution is attributed to the effects of local averaging, which was previously discussed in Section 3.3.4. The target mean and standard deviation are point estimates, while the sample mean and standard deviation are local averages that are affected by the size of the averaging domain and scale of fluctuation (Vanmarcke 1983). For a lognormal distribution, both the mean and variance are reduced due to local averaging, which has been shown in Figure 3.9 and Table 3.4. According to the local averaging theory, if the element size is fixed, a larger scale of fluctuation (i.e. as $\theta \rightarrow \infty$) leads to less reduction to the point variance, while a smaller scale of fluctuation (i.e. as $\theta \rightarrow 0$) leads to greater reduction to the point variance.

3.6.2 Verification of the Correlation Structure

As previously discussed in Section 3.3.2, *rslope2d* uses the local average subdivision (LAS) method to produce correlated local averages based on an isotropic exponentially decaying (i.e. Markov) correlation structure. The theoretical correlation function has been

given in Equation (3.1). Figure 3.10 shows the comparison between the experimental correlation structure simulated by *rslope2d* with the theoretical correlation structure for two different scales of fluctuation, i.e. θ = 1 m and 10 m. The results were obtained based on an average over 100 random field realisations. Good agreement between the experimental and theoretical correlation structure is observed.

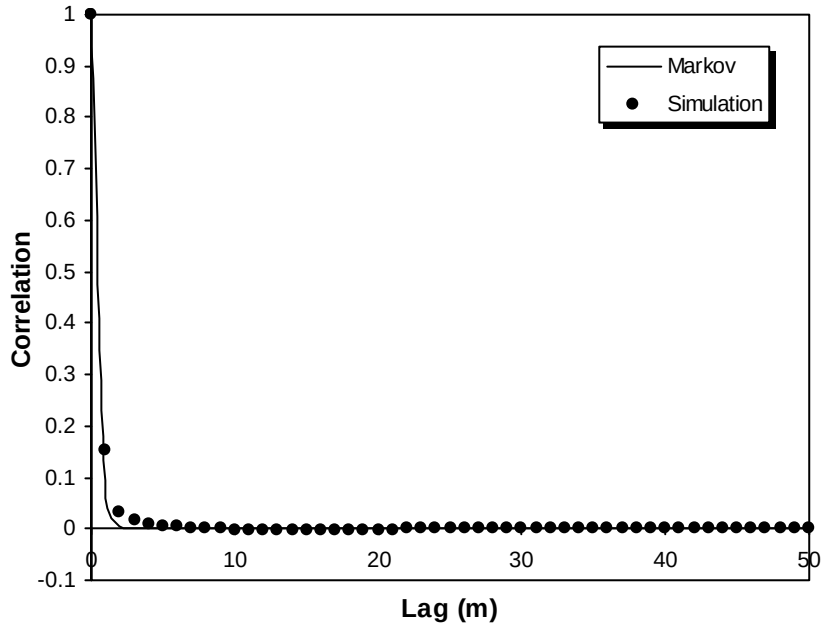

(a)

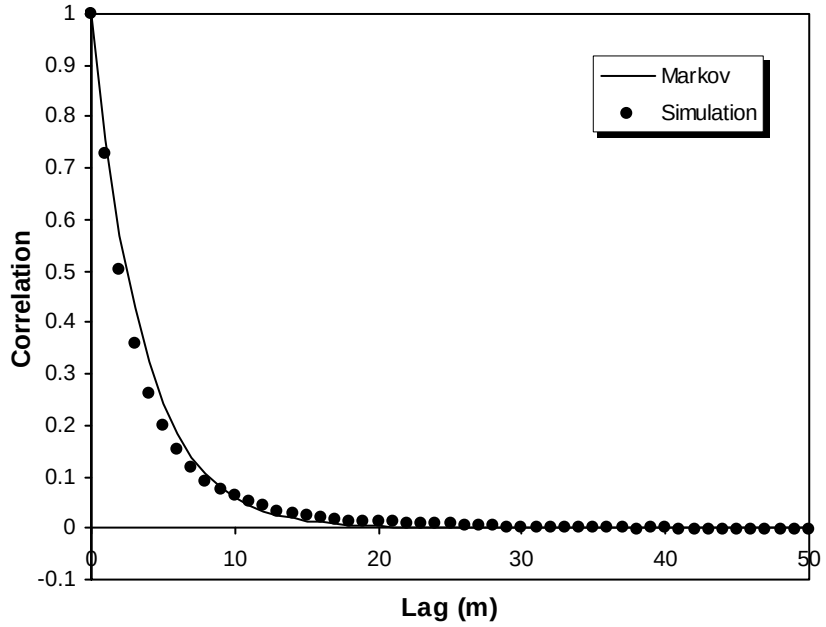

(b)

Figure 3.10 Comparison of experimental and theoretical correlation structure for scales of fluctuation (a) θ = 1 m and (b) θ = 10 m

3.7 Summary

This chapter has described the formulation and implementation of the random finite element method (RFEM), which was used as the probabilistic slope stability analysis tool throughout this research. It has been shown that *rsloped2d*, a computer model that implements RFEM, is capable of modelling the characteristic features of soil variability.

Preliminary studies were undertaken to investigate the effect of varying statistical parameters on the simulated random fields. The results have validated the LAS methodology, which is used for the simulation of random soil profiles in *rslope2d*. The results also indicated that the distribution of a simulated soil property is affected by the coefficient of variation (COV) and the scale of fluctuation, θ. It is anticipated that variations in COV and θ have a significant influence on the probability of failure of a slope. This topic is dealt with in the following chapter.

Chapter 4

INFLUENCE OF SOIL VARIABILITY ON RELIABILITY OF SINGLE-LAYERED SOIL SLOPES

4.1 Introduction

It has been shown in Chapter 3 that the statistical distribution of soil properties is influenced by the soil variability parameters, namely the coefficient of variation (COV) and the scale of fluctuation, θ. It is reasonable to expect that soil variability has a significant influence on the estimated probability of failure, P_f, of a slope. The aim of this chapter is therefore to investigate and quantify the effects of COV and θ on the estimated P_f of a slope. This is achieved by carrying out numerical studies using the computer model *rslope2d*, which is based on the random finite element method (RFEM), as discussed in Chapter 3. Two cases are considered herein: (a) a cohesive slope; and (b) a $c'-\phi'$ slope. This chapter also aims to develop a set of probabilistic stability charts that can be used to evaluate the probability of failure of a slope by taking the effect of soil variability into consideration.

4.2 Probabilistic Analysis of Spatially Random Cohesive Slopes

4.2.1 Description of Numerical Studies Undertaken

The slope problem under consideration is shown in Figure 4.1. The slope geometry is described by the parameters: slope angle, β, depth factor, D, and slope height, H. For a cohesive slope problem, a total stress analysis is assumed and the effect of pore pressure is

not considered. The soil shear strength is described solely by the undrained shear strength, s_u, or undrained cohesion, c_u, (i.e. $\phi_u = 0$). In this study, the undrained cohesion, c_u, was modelled as a random variable, which was described by a lognormal distribution. Meanwhile, the spatial variability of c_u was modelled by the soil variability parameters COV and θ. In the interest of generality, the scale of fluctuation, θ, was normalised by the slope height, H, (i.e. θ/H), while the mean value of undrained cohesion was expressed in terms of a dimensionless stability coefficient, N_s, similar to Taylor's (1937) stability number, and expressed as:

$$N_s = \frac{\mu_{c_u}}{\gamma H} \tag{4.1}$$

where μ_{c_u} = the mean value of c_u; γ = unit weight of the soil; and H = slope height.

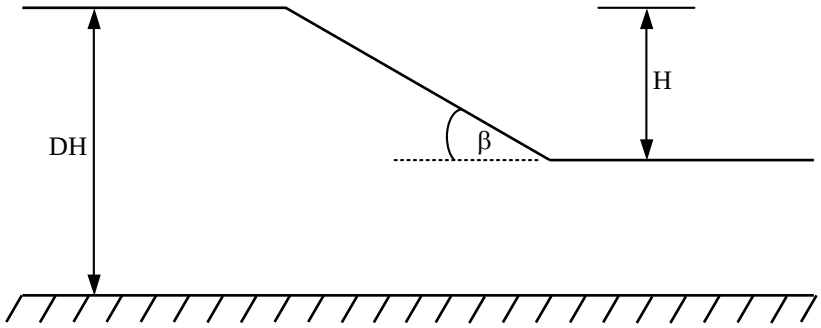

Figure 4.1 Geometry of the cohesive slope problem

In this study, the input parameters β, D, N_s, COV and θ/H were varied systematically, and the values adopted in the parametric studies are given in Table 4.1. The slope angles, β, of 14°, 18.4°, 26.6°, 45° represents slopes of 4:1, 3:1, 2:1, and 1:1, respectively, were adopted. The scale of fluctuation, θ, was assumed to be isotropic, i.e. the horizontal θ and the vertical θ are equal. The effect of anisotropy of θ is investigated and discussed later. Other parameters were held constant at their deterministic values, e.g. slope height, H = 10 m; unit weight, γ = 20 kN/m^3; Young's modulus, $E_s = 1 \times 10^5$ kPa; Poisson's ratio, ν = 0.3; and dilation angle, ψ = 0°.

Figure 4.2 shows a typical finite element mesh for a 1:1 cohesive slope with $\beta = 45°$ and D = 2. The parameter S is dependent on the slope angle, β. For example, in this case, when $\beta = 45°$, the corresponding value of S is 1. An element size of 1 m × 1 m is adopted for the finite element mesh in Figure 4.2. The effect of mesh density on the estimated probability of failure, P_f, is also discussed later.

Table 4.1 Input parameters for parametric studies

Parameters	Input values
β	14°, 18.4°, 26.6°, 45°
D	1, 2, 3
N_s	0.1, 0.2, 0.3, 0.4, 0.5
COV	0.1, 0.3, 0.5, 1.0
θ/H	0.1, 0.5, 1, 5, 10

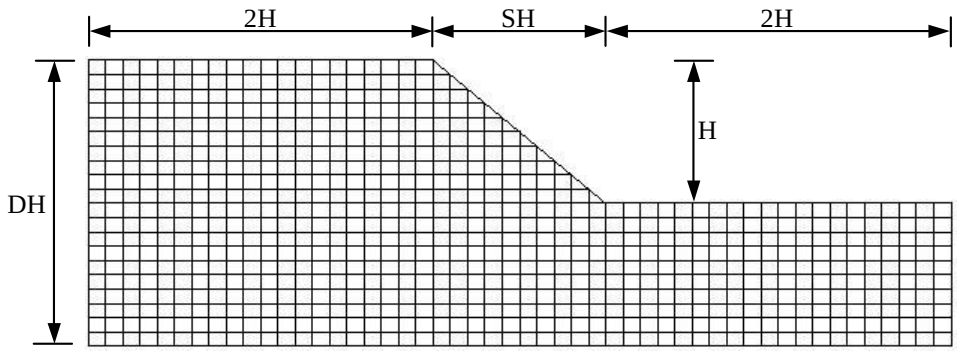

Figure 4.2 Typical finite element mesh for a 1:1 cohesive slope ($\beta = 45°$, D = 2)

Parametric studies of a single-layered cohesive slope problem using the random finite element method (RFEM) were previously conducted by Griffiths and Fenton (2004). These studies, however, focused solely on a 2:1 slope with $\beta = 26.6°$ and D = 2, using a 1 m × 1 m finite element mesh. The values of N_s, COV and θ/H investigated were:

- N_s = 0.15, 0.17, 0.2, 0.25, 0.3;

- COV = 0.25, 0.5, 1, 2, 4, 8; and
- θ/H = 0.1, 0.25, 0.5, 1, 2, 4, 8.

The current parametric studies therefore extend Griffiths and Fenton's studies by investigating slopes with different geometry (i.e. by varying β and D). The current studies also aim at developing a set of probabilistic stability charts, which can be used for a preliminary estimate of P_f of a cohesive slope with spatially random undrained cohesion, c_u. It should be noted that the values of N_s, COV and θ/H being considered in the current studies are not exactly the same as those investigated by Griffiths and Fenton (2004). In the current studies, high values of COV (i.e. COV > 1.0) are not considered due to the fact that these high values of COV are unlikely to be encountered in real soil deposits, based on the published data in the literature (e.g. Lee et al. 1983; Phoon and Kulhawy 1999a; Baecher and Christian 2003). These published data suggested a likely range for COV of c_u of 0.1 – 0.5, as previously shown in Chapter 2. Therefore, the current study sets the upper bound value of COV to 1.0, for the purpose of numerical modelling.

4.2.2 Consideration of Computational Resources and Time Constraints

As discussed in Chapter 3, in order to accurately estimate the probability of failure, P_f, thousands of repetitions of non-linear finite element analyses are required, as part of the Monte Carlo simulation process. The computational time is usually large and dependent on several parameters: iteration limit for the finite element analysis, *maxit*; number of realisations adopted in the Monte Carlo process, n_{sim}; mesh density; problem size and the estimated probability of failure, P_f.

Generally, the computational time increases as *maxit* and n_{sim} increase. The minimum requirement of *maxit* and n_{sim} for producing a reliable and reproducible estimate of P_f is discussed later. The computational time will also increase if a finer mesh is used or the problem size is increased. Moreover, the computational time for a slope with higher P_f is usually greater than that for a slope with lower P_f. This is because a higher P_f means a larger number of Monte Carlo realisations have reached the user-defined iteration limit without converging to a solution, hence, yield more 'failed' slopes. On the other hand, in

the finite element analysis, a 'safe' slope usually converges quickly, before reaching the iteration limit.

In order to investigate the effect of varying each input parameter with the values listed in Table 4.1, a total of 1,200 individual slope problems were analysed. To achieve this, the following computing resources were used:

- IBM eServer 1350 Linux Cluster, named *Hydra*, consisting of 129 nodes with each node having dual 2.4 GHz Xeon Processers (Pentium P4), 2.0 GB RAM and running on RedHat Linux; and
- AMD Athlon 2100+ Dual Servers, named *Terzaghi* and *Vanmarcke*, with 1.0 GB RAM and 60 GB HDD running Linux.

Table 4.2 shows the cases with the shortest and longest computational time out of 1,200 slope problems that were analysed, using the computing facility *Hydra*. It should be noted that, the element size was fixed at 1 m × 1 m, n_{sim} = 2000, and *maxit* = 500. It can be seen that the difference in computational time between these two extreme cases is very large, i.e. approximately 13.5 hours. Clearly, if the element size, n_{sim} and *maxit* are fixed, the computational time is governed by the problem size and the estimated P_f. The slope with β = 14° and D = 3 has a relatively larger problem size and higher P_f than the slope with β = 45° and D = 1, and as a result, it requires a longer computational time.

Table 4.2 Cases with shortest and longest computational time

β	D	N_s	COV	θ/H	FOS	P_f	Runtime (sec)
45	1	0.4	0.1	0.1	2.45	0	50
14	3	0.1	0.5	0.1	0.6	1	48,756

4.2.3 Determination of Iteration Limit and Number of Realisations

Preliminary analyses were conducted to determine the iteration limit, *maxit*, and the number of realisation, n_{sim}, required for producing a reliable and reproducible estimated of

the probability of failure, P_f. The analyses were performed on a 1:1 undrained clay slope with $\beta = 45°$ and D = 2, as previously shown in Figure 4.2. The soil variability parameters COV and θ/H were fixed at 0.5 and 1, respectively. The stability coefficient, N_s, was varied so that slopes with different values FOS and P_f could be investigated. Figure 4.3 shows the effect of the number of iterations on the estimated P_f. It can be seen that iteration limit of 500 appears to be adequate for all cases of slopes with different FOS and P_f.

Figure 4.4 indicates that the estimated P_f, for all cases being considered, starts to converge at 2,000 realisations. Further increment in the number of realisations causes only minor changes in the estimated P_f. Based on the equation suggested by Hahn and Shapiro (1967) (i.e. Equation (3.13)), the number of realisations required to achieve a relative percentage error of less than 5%, for a 95% confidence interval, is 1,500. The results observed in Figure 4.4 are in good agreement with that estimated by the Hahn and Shapiro (1967) equation.

Figure 4.5 shows the effect of varying the number of realisations of Monte Carlo simulation on the computational time for the slopes with different values of FOS, and with COV and θ/H fixed at 0.5 and 1, respectively. It can be seen that, for all cases of FOS, the computational time increases linearly as the number of realisations increases. It is also observed that the slope with a lower FOS (or higher P_f) requires a longer computational time than that with a higher FOS (or lower P_f). It should be noted that the further increase of the number of realisations after 2,000 realisations yielded only minor changes in P_f, as previously shown in Figure 4.4, but the computational time was increased dramatically, as shown in Figure 4.5.

Based on these preliminary analyses, it was concluded that 2,000 realisations to be used for the Monte Carlo simulation to ensure the error in the estimated P_f is minimised, while the iteration limit was fixed at 500.

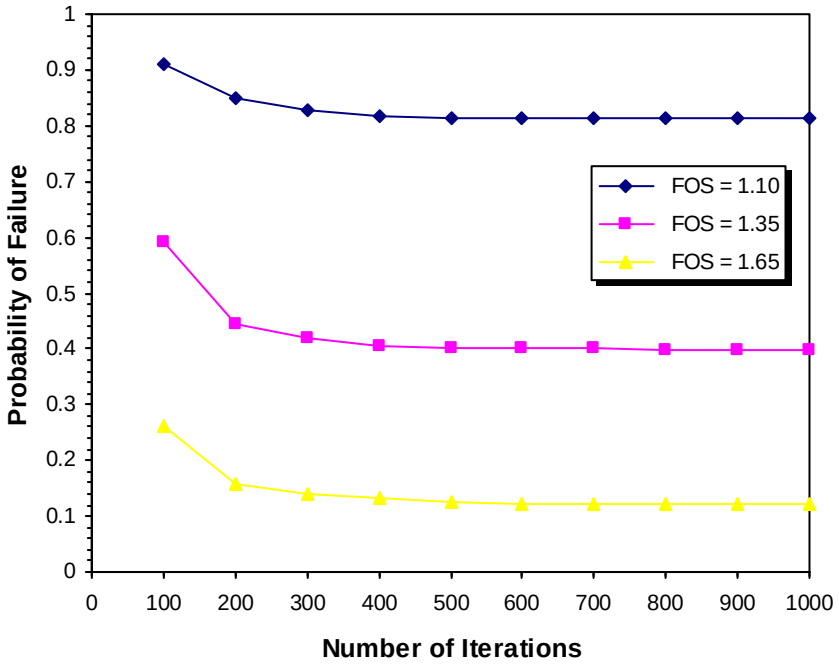

Figure 4.3 Effect of number of iterations on probability of failure (COV = 0.5; θ/H = 1)

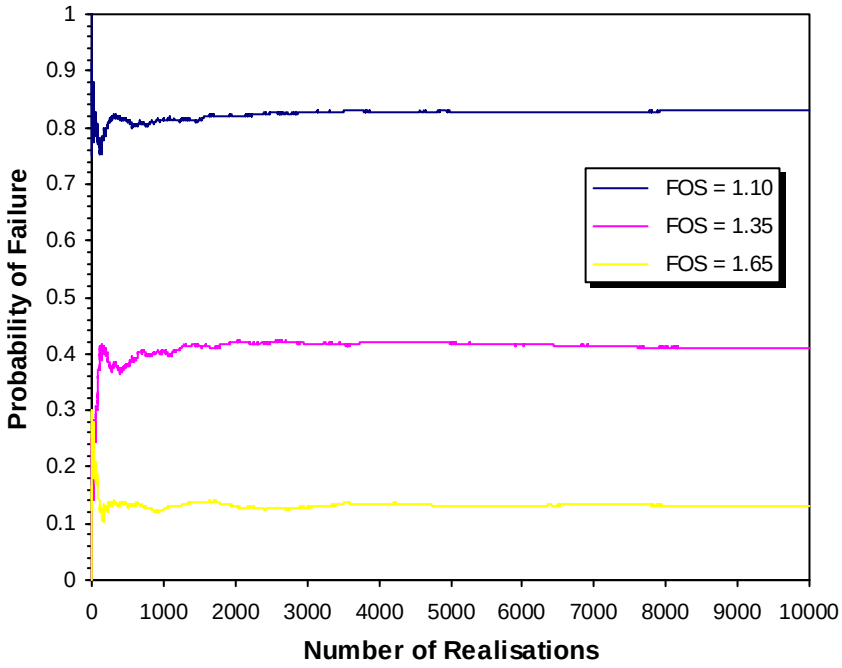

Figure 4.4 Effect of number of realisations on probability of failure (COV = 0.5; θ/H = 1)

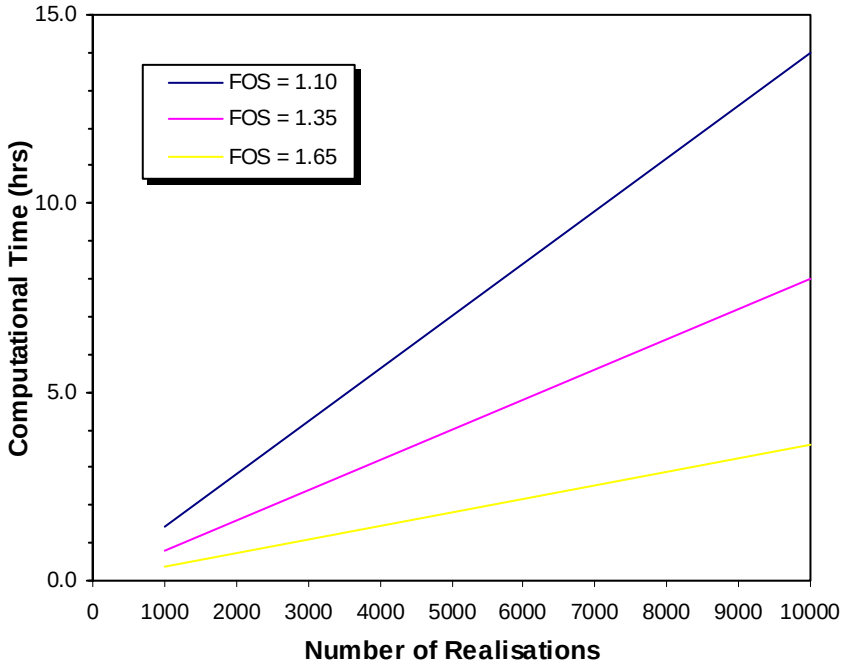

Figure 4.5 Effect of number of realisations on computational time (*maxit* = 500)

4.2.4 Effect of Mesh Density on Probability of Failure

Preliminary analyses were also conducted to investigate the effect of element size of the finite element mesh on the estimated probability of failure, P_f. Three different mesh densities were considered: (a) 0.5 m × 0.5 m; (b) 1 m × 1 m; and (c) 2 m × 2 m, as shown in Figure 4.6. It should be noted that the 1 m × 1 m mesh is the same as that previously shown in Figure 4.2. The finer mesh (0.5 m × 0.5 m) and coarser mesh (2 m × 2 m) have exactly the same slope geometry as the 1 m × 1 m mesh, i.e. $\beta = 45°$ and D = 2. In addition, in this investigation, N_s was held constant at 0.3. Two cases of COV were considered in the analyses, i.e. COV = 0.5 and 1.0, while θ/H was varied between 0.1 and 10.

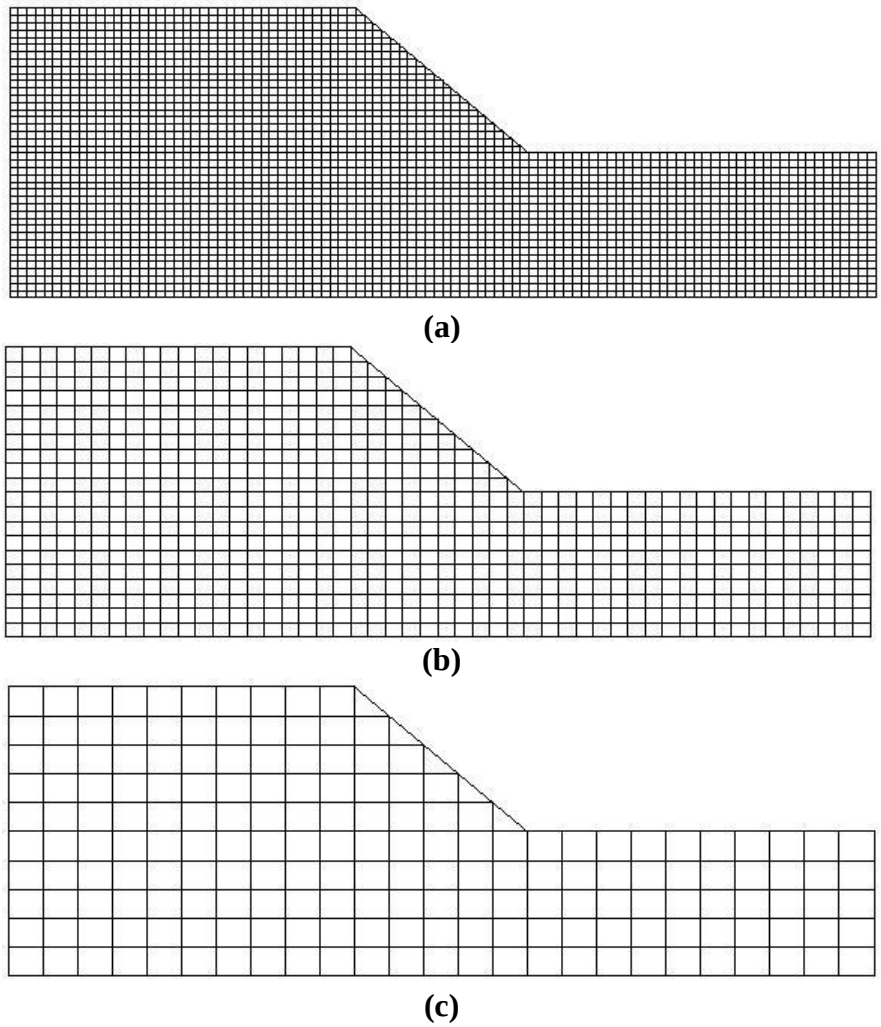

Figure 4.6 Finite element mesh with different mesh density (a) 0.5 m × 0.5 m; (b) 1 m × 1 m; (c) 2 m × 2 m. (β = 45°, D = 2)

Figure 4.7 shows the comparison of the estimated P_f, obtained from 2,000 realisations of the Monte Carlo simulation, by using different mesh densities. It is observed that the estimated P_f is sensitive to mesh density at small values of θ/H. At large values of θ/H, the results seem to converge well. In general, the 1 m × 1 m mesh appears to be reasonable for producing a reliable estimate of P_f, with the exception of when θ/H = 0.1 and when COV is high (i.e. COV = 1.0). The results in Figure 4.7 suggest that, the element size should be much smaller that the scale of fluctuation, θ, in order to produce a reliable estimate of P_f. It was found that the ratio between the element size and scale of fluctuation should be at least 0.5.

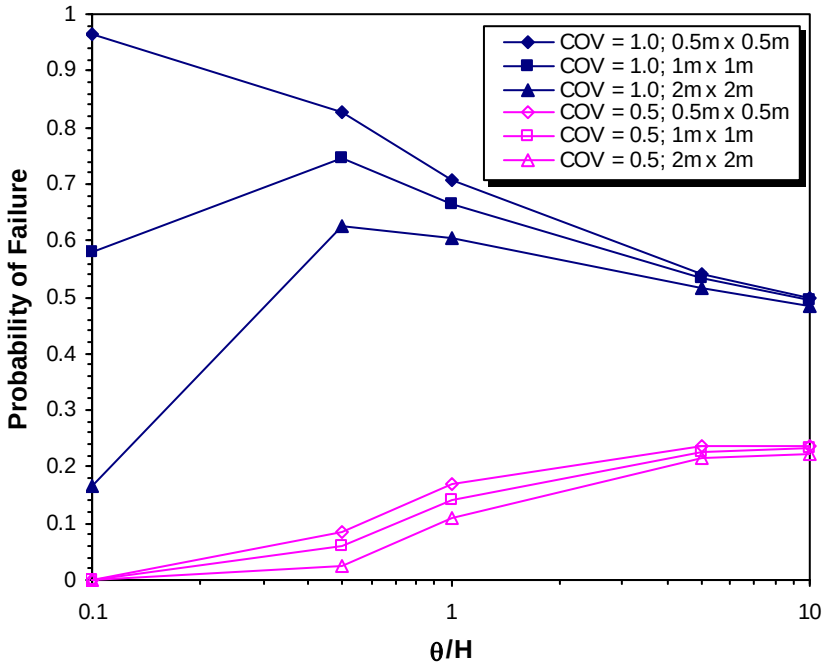

Figure 4.7 Effect of varying θ/H on probability of failure for different mesh densities with COV fixed at 0.5 and 1.0 (β = 45°, D = 2, N_s = 0.3)

Although using a finer mesh produced a better estimate of the P_f, the computational time also increased dramatically, as shown in Table 4.3. Table 4.3 shows the comparison of the estimated P_f and computational time for the worst case observed in Figure 4.7 (i.e. COV = 1.0 and θ/H = 0.1). A significant increase in the computational time is observed, as a finer mesh is used. As a result, in the parametric studies that follow a finer mesh (0.5 m × 0.5 m) was used only for the cases with small θ/H (i.e. θ/H = 0.1 and 0.5) and high COV.

Table 4.3 Comparison of P_f and computation time for the slope with different mesh density (COV = 1.0; θ/H = 0.1)

Mesh density	Estimated P_f	Runtime (hrs)
0.5 m × 0.5 m	0.963	16.3
1 m × 1 m	0.581	2.4
2 m × 2 m	0.166	0.2

4.2.5 Deterministic Solutions

Prior to the probabilistic analyses, deterministic analyses were conducted by assuming the soil profile to be homogeneous. The factor of safety (FOS) was computed, based on the assumed mean value of the undrained cohesion, c_u, using the finite element method (FEM). Griffiths and Lane (1999) reported that FOS predicted by the FEM is in good agreement with those obtained from popular stability charts produced by Taylor (1937) and Bishop and Morgenstern (1960). The comparison between the FOS computed by the FEM and that obtained from Taylor's charts, for the 1:1 undrained clay slope ($\beta = 45°$, $D = 2$) with different values of N_s, is summarised in Table 4.4. It is noted that the FEM solutions are comparable with those obtained from Taylor's charts.

Table 4.4 Factor of safety assuming homogenous soil ($\beta = 45°$, $D = 2$)

N_s	μ_{c_u} (kPa)	FOS (FEM)	FOS (Taylor's charts)
0.1	20	0.55	0.56
0.2	40	1.10	1.12
0.3	60	1.65	1.69
0.4	80	2.15	2.25
0.5	100	2.70	2.81

4.2.6 Results of Parametric Studies

Based on 2,000 realisations of Monte Carlo simulations for each parametric group described in Table 4.1, the influence of each input parameter on the estimated P_f is investigated and discussed in the following sections.

First, the effects of the spatial variability of undrained cohesion, c_u, on the probability of slope failure, P_f, are examined. The results obtained for the slope with $\beta = 45°$ and $D = 2$ are used for this discussion. Figures 4.8 and 4.9 show the typical deformed meshes at slope failure for the 1:1 cohesive slope with $N_s = 0.3$ and different values of COV and θ/H. Again, dark and light regions indicate 'strong' and 'weak' soil elements, respectively.

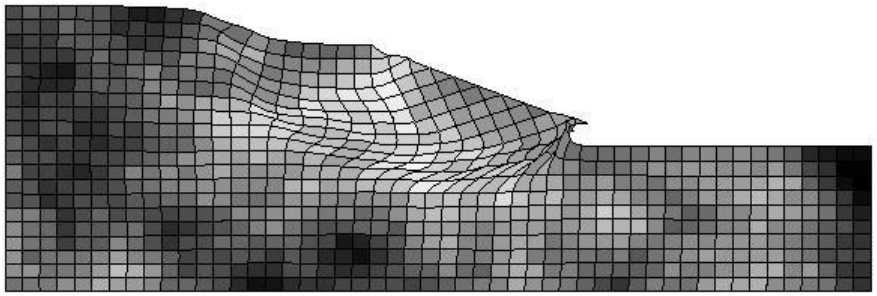

(a)

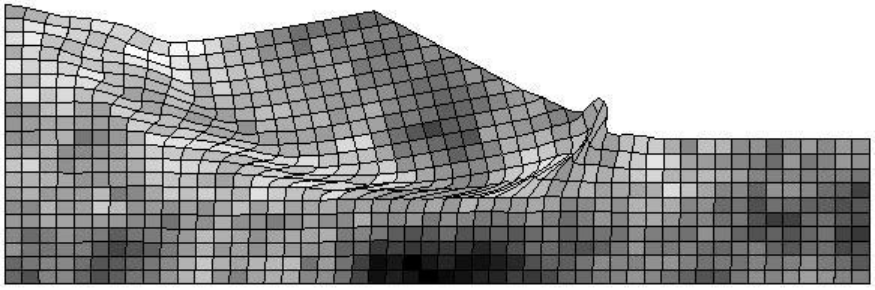

(b)

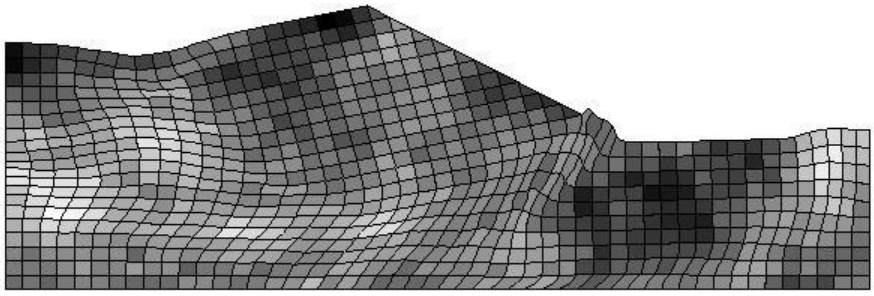

(c)

Figure 4.8 Typical deformed mesh for the 1:1 cohesive slope with COV of (a) 0.3, (b) 0.5 and (c) 1.0 (β = 45°; D = 2; N_s = 0.3; θ/H = 1)

It can be noticed that the failure mode is different for the slope with varying values of COV and θ/H. For example, Figures 4.8(a), (b) and (c) show the failure mechanism of the slope with COV of 0.3, 0.5 and 1.0, respectively with the value of θ/H being held constant at 1 in this case. It can be seen that, when COV = 0.3 and 0.5, a circular 'toe' failure is obtained. However, for COV = 1.0, the failure mode appears to be 'deep-seated'.

It should be noted that the failure mode is not solely dependent on COV but also θ/H. Figures 4.9(a), (b) and (c) show the failure mode of the slope with θ/H of 0.1, 1 and 10,

respectively, with COV fixed at 0.5. When θ/H = 0.1, the soil profile is approaching one that is completely spatially random, and no obvious circular or planar failure surface is observed. In fact, failure occurs through a non-uniform surface delineated by regions of weak soil shear strength. On the other hand, as θ/H increases, the soil profile becomes more uniform, hence, a circular failure mode is more likely to be developed. When θ/H = 10, a 'deep-seated' mode is observed. These observations suggest that, for a cohesive slope, 'deep-seated' failure only occurs when the soil profile is uniform, that is, θ/H is large.

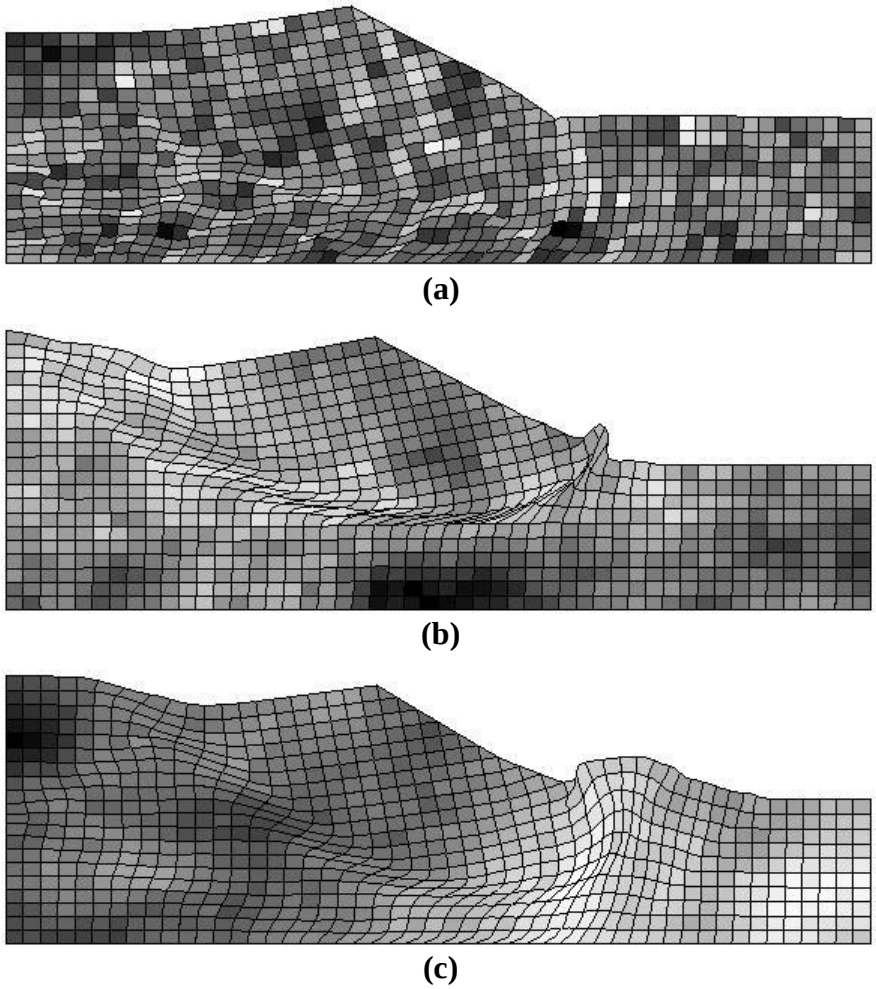

Figure 4.9 Typical deformed meshes for the 1:1 cohesive slope with θ/H of (a) 0.1, (b) 1 and (c) 10 (β = 45°; D = 2; N_s = 0.3; COV = 0.5)

Figures 4.10 and 4.11 show the effects of varying COV on P_f for different values of θ/H, with N_s fixed at 0.2 and 0.3, respectively. It has been previously shown that N_s of 0.2 and 0.3 yielded a FOS of 1.10 and 1.65, respectively (Table 4.4). In practice, FOS = 1.10 would suggest a marginally stable slope which is at the verge of failure, while FOS = 1.65 would suggest a stable slope with a very low likelihood for slope failure. In general, P_f increases as COV increases (i.e. increasing variability in c_u). When N_s = 0.2 and FOS = 1.10 (i.e. a marginally stable slope), P_f increases significantly as COV increases from 0.1 to 0.3 for all values of θ/H (Figure 4.10). However, the increase in P_f becomes lesser as COV increases from 0.3 to 0.5, which is the upper bound value for COV suggested in the literature, as discussed in Chapter 2. As an example, for θ/H = 1, P_f increases significantly from 0.10 to 0.69 as COV increases from 0.1 to 0.3 but P_f increases relatively less from 0.69 to 0.82 as COV increases from 0.3 to 0.5.

On the other hand, for the slope with N_s = 0.3 and FOS = 1.65 (i.e. a stable slope), the rate of increase in P_f as COV increases from 0.1 to 0.3 is smaller than that observed for the slope with N_s = 0.2. However, P_f increases significantly as COV increases from 0.5 to 1.0. In addition, it is also noted that the values of P_f for the slope with N_s = 0.3 are generally smaller than those observed for the slope with N_s = 0.2. This is expected because a higher value of N_s indicates the corresponding *mean* value of c_u is higher as well. Despite that, a P_f of as high as 0.23 was computed for the slope with COV = 0.5 and θ/H = 10. The results in Figures 4.10 and 4.11 suggest that, for a marginally stable slope (i.e. FOS ≈ 1.0), P_f is more sensitive to the lower values of COV (i.e. COV < 0.3), however, for a stable slope (i.e. FOS > 1.5), P_f is more sensitive to the higher values of COV (i.e. COV > 0.3).

Figures 4.10 and 4.11 also show that different values of θ/H lead to different values P_f as COV increases. It can be seen that, for both N_s = 0.2 and 0.3, all the curves intersect at a specific point. For N_s = 0.2, this point occurs when P_f = 0.31 and COV = 0.17, while for N_s = 0.3, the intersection occurs when P_f = 0.31 and COV = 0.66. At the intersection point, the P_f is independent of the values of θ/H. Different behaviour is observed before and beyond these intersection points. As an example, for N_s = 0.3, when COV < 0.66, smaller θ/H leads to lower P_f. On the other hand, when COV > 0.66, smaller θ/H leads to higher P_f. The effect of θ/H on P_f is illustrated more clearly in Figures 4.12 and 4.13.

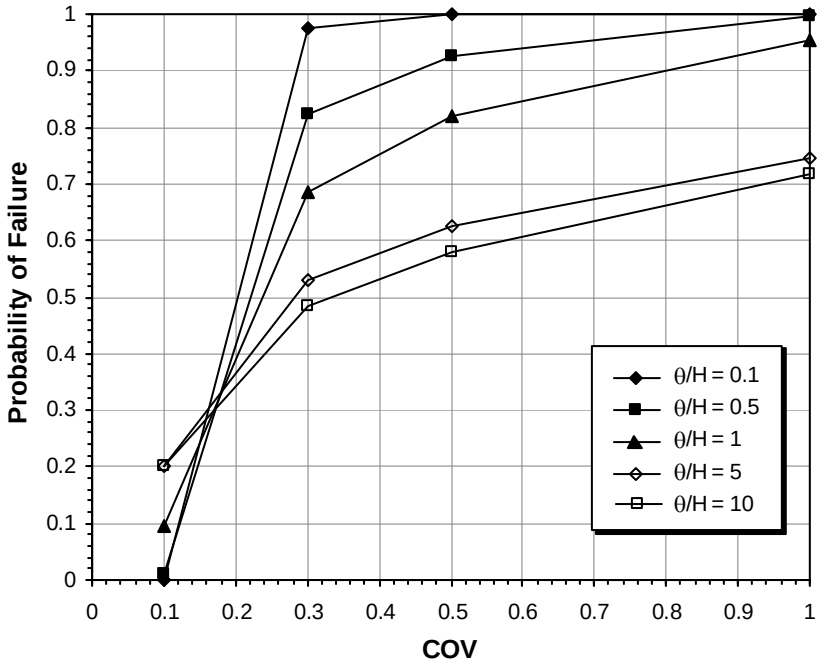

Figure 4.10 Effect of varying COV on probability of failure for different values of θ/H with N_s fixed at 0.2 (β = 45°; D = 2)

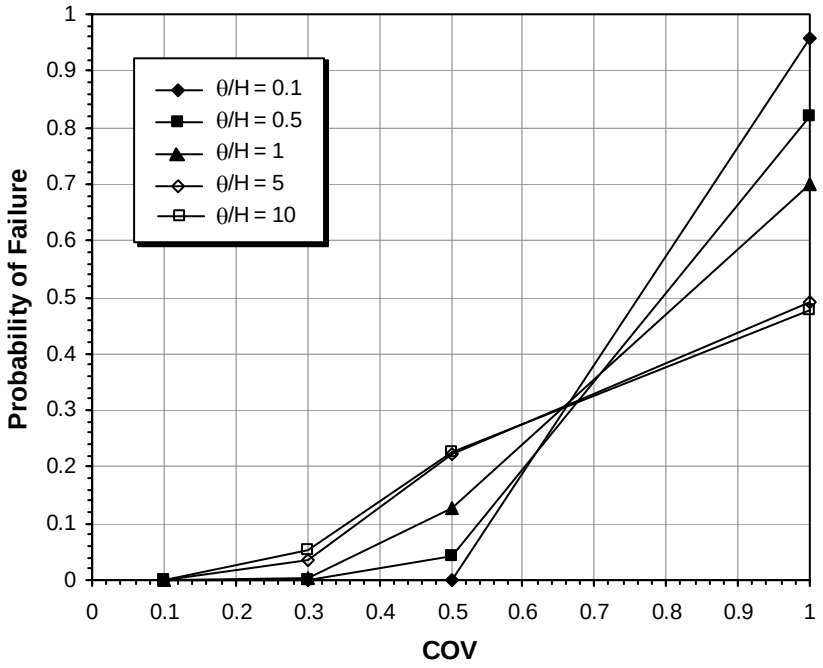

Figure 4.11 Effect of varying COV on probability of failure for different values of θ/H with N_s fixed at 0.3 (β = 45°; D = 2)

Figures 4.12 and 4.13 show the effect of varying θ/H on P_f for different values of COV with N_s fixed at 0.2 and 0.3, respectively. Two different trends are obvious, which are dependent on the values COV, i.e. P_f either increases or decreases as θ/H increases. For N_s = 0.2, P_f increases as θ/H increases when COV = 0.1, but P_f decreases as θ/H increases when COV = 0.3, 0.5 and 1.0 (Figure 4.12). On the other hand, for N_s = 0.3, P_f increases as θ/H increases when COV = 0.1, 0.3, and 0.5, but P_f decreases as θ/H increases when COV = 1.0 (Figure 4.13). It is also noted that P_f converges to either 0 or 1 when θ/H becomes very small (i.e. $\theta/H \rightarrow 0$).

It should be noted that the trends of the results observed in Figures 4.10 to 4.13 are similar to those observed by Griffiths and Fenton (2004) for a 2:1 cohesive slope (β = 26.6°; D = 2) with N_s = 0.25 (i.e. μ_{c_u} = 50 kPa). As previously discussed by Griffiths and Fenton (2004), the two different trends observed with respect to the variation of P_f with θ/H (i.e. P_f either increases or decreases as θ/H increases) are governed by the *median* N_s (or the *median* c_u) of the simulated random fields. The COV values of 0.17 and 0.66, as previously observed at the intersection points in Figures 4.10 and 4.11, are the special values that cause the *median* N_s of the simulated random fields to equal 0.18, which is the critical value that would cause the slope being considered to have FOS = 1.0.

A value of COV lower than the special value will cause the *median* $N_s > 0.18$ and lead to P_f increases as θ/H increases. This is because, as θ/H increases, the scatter of the *mean* c_u of the simulated random fields also increases, as previously shown in Chapter 3. Also, with the simulated *median* $N_s > 0.18$, it is expected that $P_f < 0.5$. Increase in the scatter of *mean* c_u will increase the chances for low values of *mean* c_u to occur, and hence, lead to increase in P_f. In contrast, a value of COV higher than the special value will cause the *median* $N_s < 0.18$ and $P_f > 0.5$, which lead to P_f decreases as θ/H increases. This is because, with *median* $N_s < 0.18$, the chances for a 'failed' slope to occur is very high. Less scatter in the simulated values of N_s means that P_f is expected to remain high (i.e. $P_f \rightarrow 1$). As θ/H increases, the scatter of *mean* c_u increases accordingly, and lead to more realisations with $N_s > 0.18$ to be simulated, thereby increasing the chances of the occurrence of a 'safe' slope, hence, a decrease in P_f is expected.

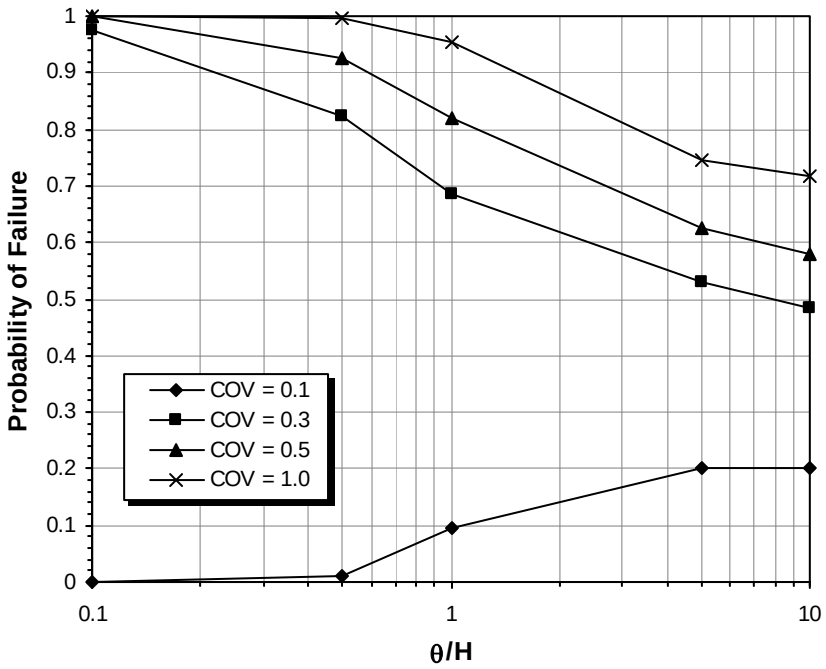

Figure 4.12 Effect of varying θ/H on probability of failure for different values of COV with N_s fixed at 0.2 (β = 45°; D = 2)

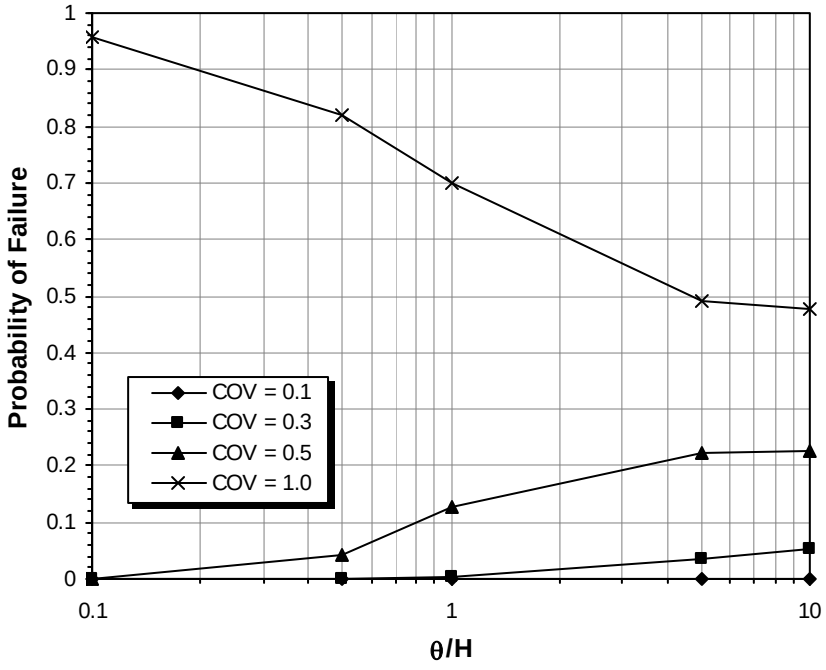

Figure 4.13 Effect of varying θ/H on probability of failure for different values of COV with N_s fixed at 0.3 (β = 45°; D = 2)

Figures 4.14 and 4.15 show the effect of varying θ/H on P_f for the slopes with different values of N_s and FOS, with COV fixed at 0.1 and 0.5, respectively. For COV = 0.1, varying θ/H causes no changes in P_f for the slopes with N_s = 0.1, 0.3, 0.4 and 0.5. For the slopes with N_s = 0.2 (i.e. FOS = 1.10), the value of P_f increases as the value of θ/H increases. These results indicate that, when COV is very small, only the marginally stable slope (i.e. FOS ≈ 1.0) is sensitive to the values of θ/H. On the other hand, when COV = 0.5, the value of P_f increases as the value of θ/H increases for the slopes with N_s = 0.3, 0.4 and 0.5. However, for the slopes with N_s = 0.1 and 0.2, the value of P_f decreases as the value of θ/H increases. This behaviour is also governed by the *median* N_s of the simulated random fields, as discussed above.

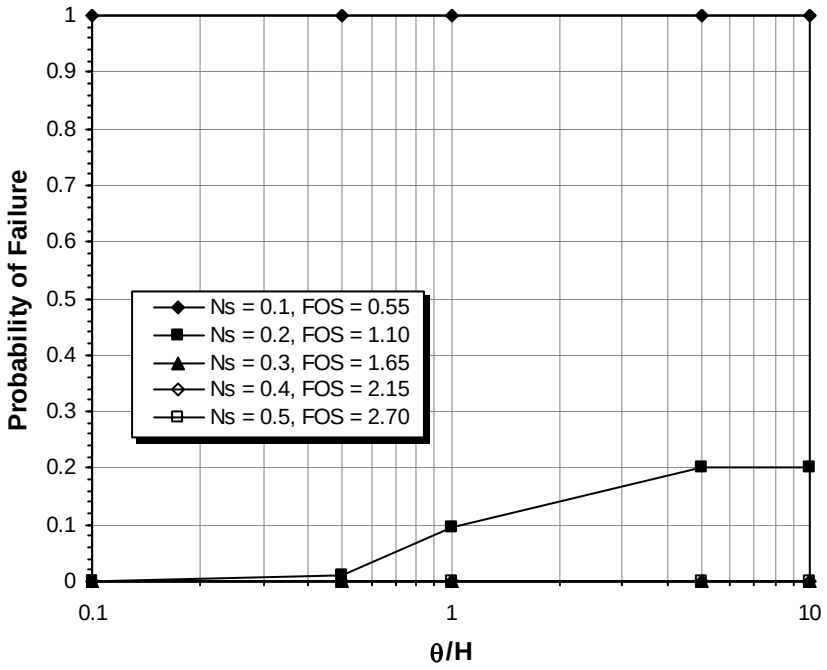

Figure 4.14 Effect of varying θ/H on probability of failure for different values of N_s with COV fixed at 0.1 (β = 45°; D = 2)

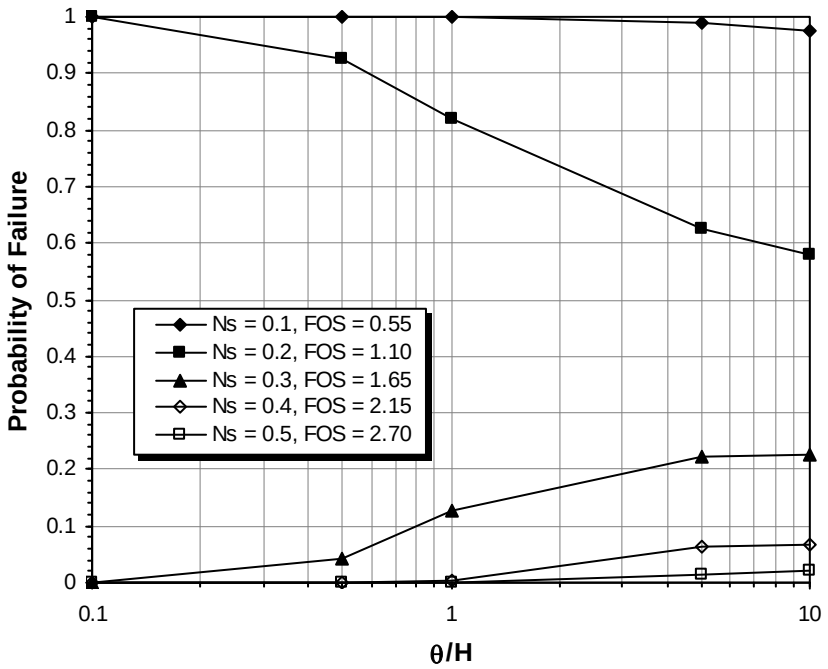

Figure 4.15 Effect of varying θ/H on probability of failure for different values of N_s with COV fixed at 0.5 (β = 45°; D = 2)

Figure 4.16 shows the effect of varying θ/H on the probability of failure, P_f, for different slope angles, with the values of D, N_s and COV fixed at 2, 0.2 and 0.5, respectively. It can be seen that, in this case, P_f increases as θ/H increases for the slopes 3:1 and 4:1. However, P_f decreases as θ/H increases for the slopes 1:1 and 2:1. This is because, as the slope geometry changes, the critical value of N_s that would cause FOS = 1.0 for each slope also varies. In this case, for the slopes 3:1 and 4:1, their *median* N_s is greater than the critical N_s, while for the slopes 1:1 and 2:1, their *median* N_s is smaller than the critical N_s.

It should be noted that assuming a perfectly correlated soil profile (i.e. $\theta/H \rightarrow \infty$) and completely ignoring the spatial correlation in probabilistic slope stability analysis could either overestimate or underestimate the probability of failure of a slope, as observed in Figures 4.12 to 4.16. This is because, as $\theta/H \rightarrow 0$ (i.e. becoming more spatially random), P_f of the slope would either converge to 0 or 1, depending on the values of COV and N_s. In real soil deposits, the scale of fluctuation of soil properties is expected to lie between the two extreme cases: completely random soils (i.e. $\theta/H \rightarrow 0$) and perfectly correlated soil profile (i.e. $\theta/H \rightarrow \infty$).

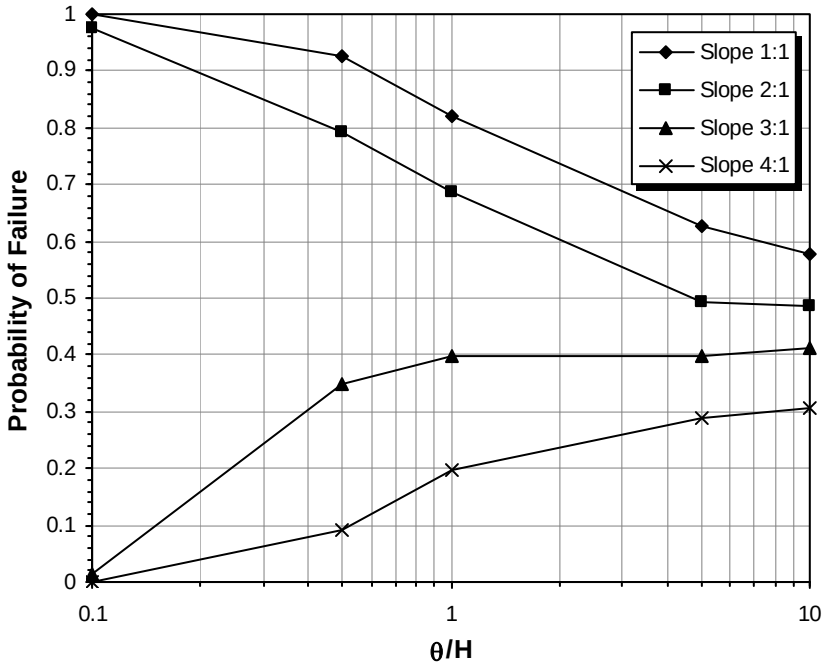

Figure 4.16 Effect of varying θ/H on probability of failure for different slopes (D = 2; N_s = 0.2; COV = 0.5)

Figures 4.17 and 4.18 show the direct comparison between the probability of failure, P_f, and the factor of safety, FOS, for different values of θ/H, and with COV fixed at 0.1 and 0.5, respectively. The different values of FOS were obtained by varying the value of N_s in the range of 0.1 – 0.5, as previously shown in Table 4.4. The corresponding values of FOS were found in the range between 0.55 and 2.75. It can be seen from both Figures 4.17 and 4.18 that, for both COV = 0.1 and 0.5, P_f decreases as FOS increases for all cases of θ/H, which is expected. For COV = 0.5 (Figure 4.18), the curves intersect at the point where P_f = 0.34 and FOS = 1.45. When FOS < 1.45, smaller θ/H leads to higher P_f, and when FOS < 1.45, smaller θ/H leads to lower P_f. It is also noted that, when COV is small (i.e. COV = 0.1), a slope with FOS > 1.65 would have $P_f \rightarrow 0$. However, when COV is large (i.e. COV = 0.5), even with FOS as high as 1.65 there may be still a significant probability of failure, dependent on the values of θ/H. In practice, any slope with FOS > 1.5 would generally be regarded as a stable slope. The results shown in Figures 4.17 and 4.18 suggest that the deterministic FOS is not a reliable measure of the true safety of a slope. In fact, FOS is meaningful only when the COV of the strength parameters is very small (i.e. COV < 0.1).

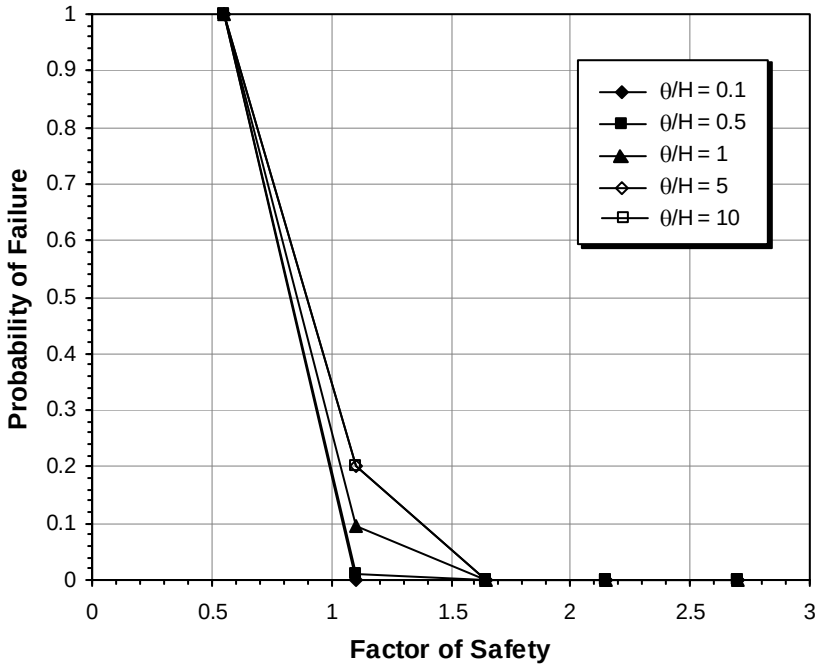

Figure 4.17 Probability of failure versus factor of safety for different values of θ/H with COV fixed at 0.1 (β = 45°; D = 2)

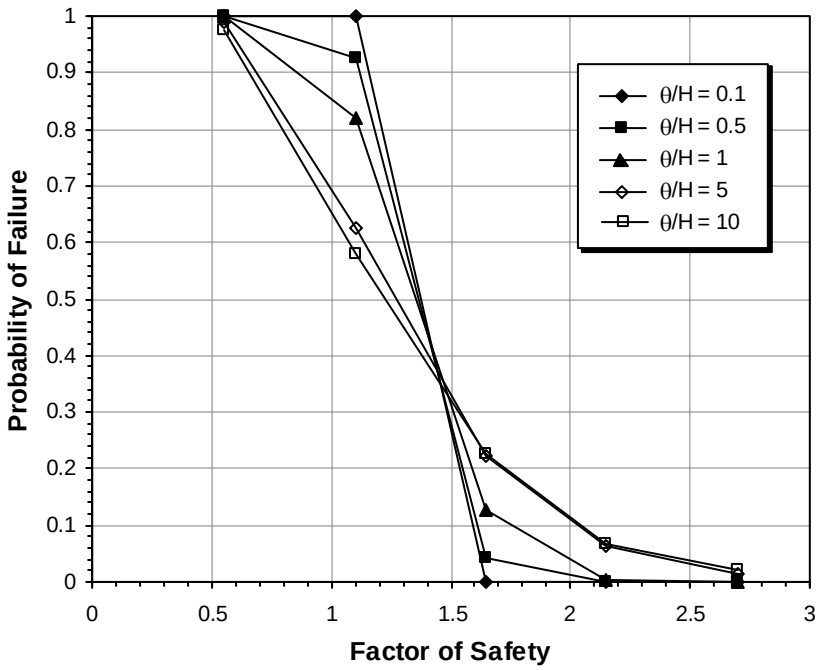

Figure 4.18 Probability of failure versus factor of safety for different values of θ/H with COV fixed at 0.5 (β = 45°; D = 2)

4.2.7 Effect of Anisotropy of Scale of Fluctuation on Probability of Failure

As discussed in Chapter 2, the horizontal scale of fluctuation, θ_h, is generally larger than the vertical scale of fluctuation, θ_v, due mainly to soil depositional processes. The results presented so far are based on the assumption that the scale of fluctuation is isotropic (i.e. $\theta_h = \theta_v$). Numerical studies were conducted to investigate the effect of anisotropy of θ on the P_f. The value of θ_h was assumed to be 1, 5, 10 and 50 times larger than the θ_v. The FOS was varied within the range of 1.0 – 1.5 in this investigation.

Figure 4.19 shows the plots of P_f versus FOS for different degrees of anisotropy (i.e. θ_h/θ_v), with $\theta_v/H = 1$ and COV = 0.5. It is observed that the curves intersect at FOS ≈ 1.42. When FOS < 1.42, the isotropic assumption leads to higher estimate of P_f, which is conservative. In contrast, when FOS > 1.42, the isotropic case becomes unconservative, as a lower P_f is estimated. However, the effects are small compared to the effects of variation in the values COV and θ/H. It is also noted that further increment in the degree of anisotropy will result only small changes to P_f.

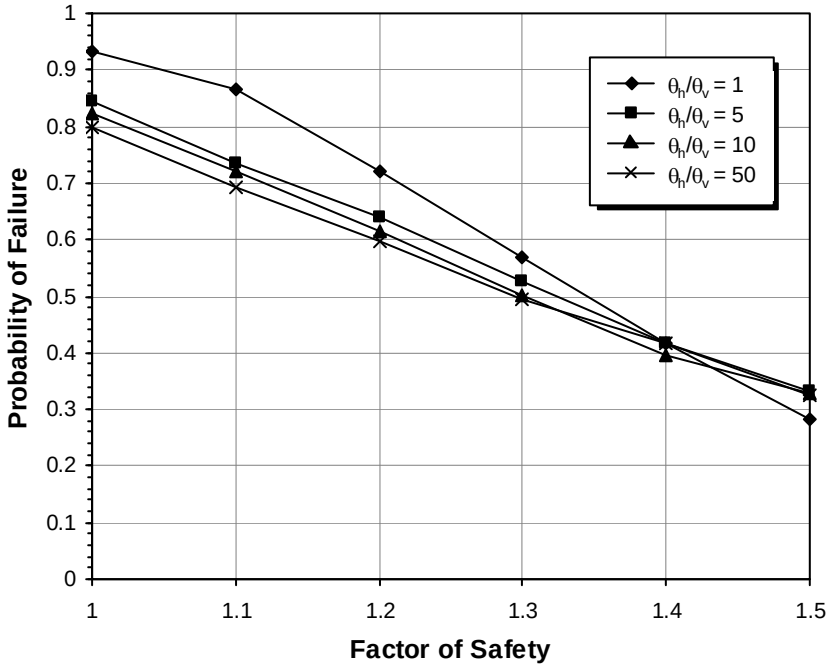

Figure 4.19 Probability of failure versus factor of safety for different degrees of anisotropy with COV fixed at 0.5 (β = 45°; D = 2; N_s = 0.3; θ_v/H = 1)

4.2.8 Probabilistic Stability Charts

It has been shown that, the RFEM analysis is computationally intensive, due mainly to the Monte Carlo simulation process and the non-linear finite element analysis. Therefore, it is worthwhile to develop a set of probabilistic stability charts, which can be used for a quick and preliminary estimation of the P_f of a spatially random cohesive slope. The charts were constructed based on the numerical results obtained from the parametric studies. The values of the input parameters were previously summarised in Table 4.1.

A probabilistic chart of P_f versus θ/H for different values of COV is plotted, for each slope geometry (β and D) and N_s. Figure 4.20 shows a set of typical probabilistic stability charts for the case with D = 2 and N_s = 0.2. The probabilistic stability charts for other combinations of D and N_s are presented in Appendix A. It can be seen from Figure 4.20 that, when the values of D and N_s are fixed, the variations of P_f with respect to θ/H are dependent on the slopes and the values of COV.

4.3 Probabilistic Analysis of Spatially Random $c' - \phi'$ Slopes

This section deals with the c'-ϕ' slope problem, involving an effective stress analysis. Effective or drained cohesion, c', and friction angle, ϕ', are the shear strength parameters. The soil shear strength is defined by the Mohr-Coulomb failure criterion, as previously discussed in Chapter 2. The slope geometry, together with the finite element mesh used is presented in Figure 4.21. The slope has a height, H, of 10 m, a gradient of 1:1 (β = 45°), and a depth factor, D, of 1.5. The element size was fixed at 0.5 m × 0.5 m, for the purpose of modelling soil with small scales of fluctuation, θ. In this study, the slope geometry was fixed and variations in β and D were not considered.

A deep water table was assumed in this study, hence, the effect of pore water pressure was not considered in the analysis. The shear strength parameters c' and ϕ' were modelled as random variables and both were described by a lognormal distribution. Other parameters were held constant, e.g. slope height, H = 10 m; unit weight, γ = 20 kN/m^3; Young's modulus, $E_s^{'}$ = 1 × 10^5 kPa; Poisson's ratio, ν′ = 0.3; and dilation angle, ψ = 0°.

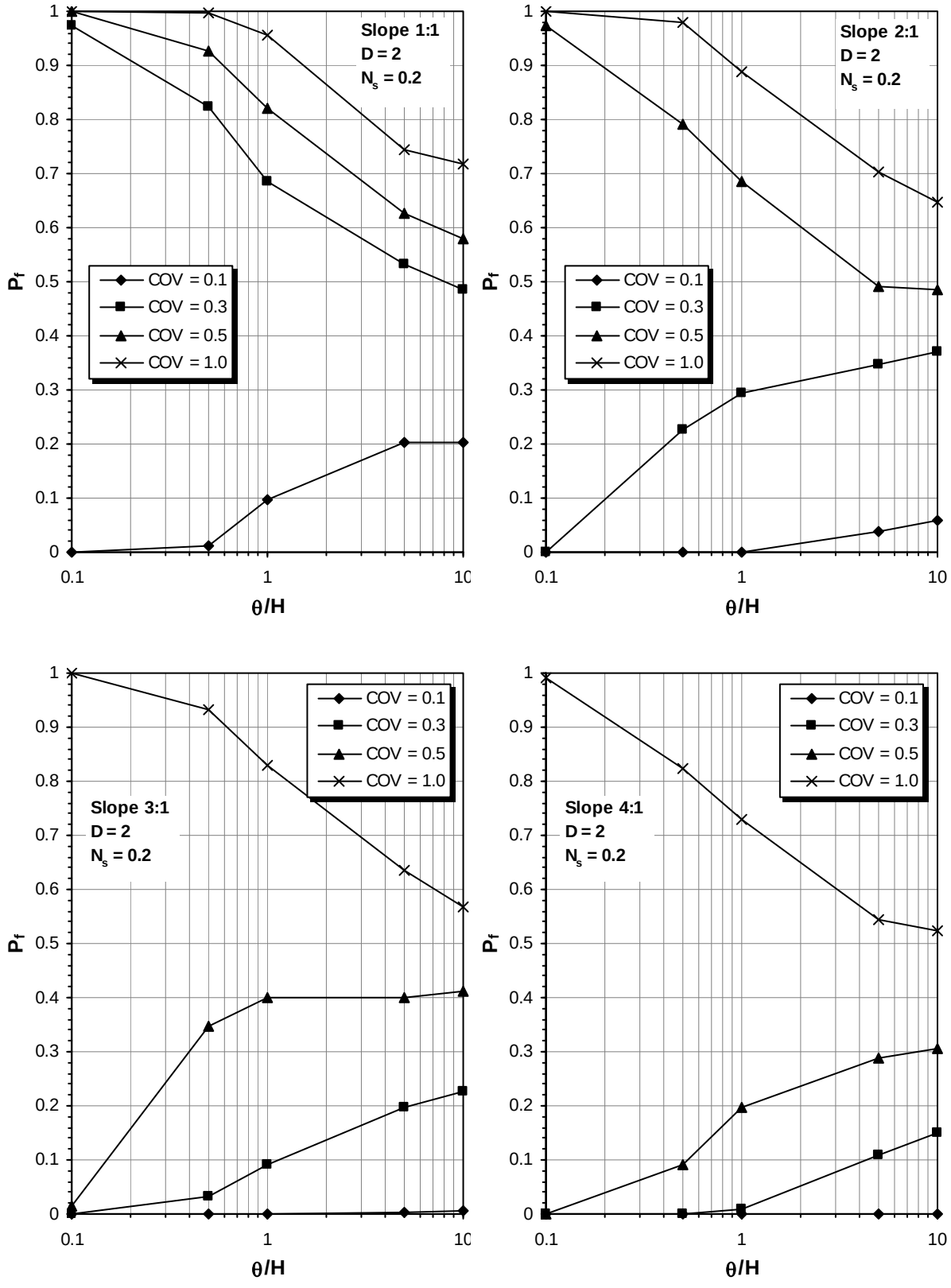

Figure 4.20 Typical probabilistic stability charts for D = 2 and N_s = 0.2

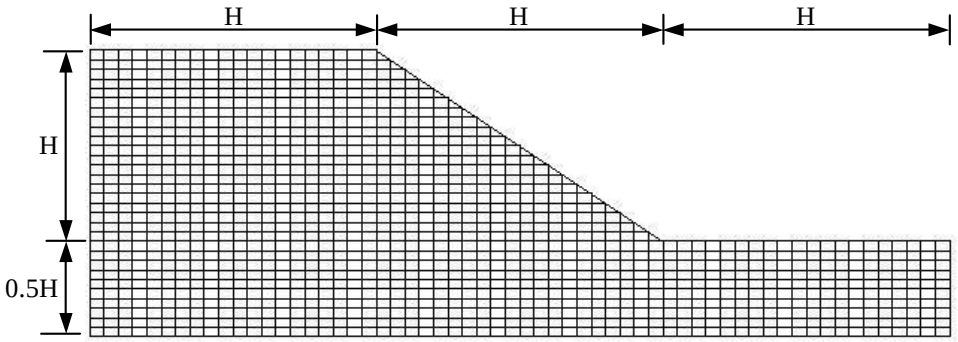

Figure 4.21 Mesh and slope geometry used for the c'-ϕ' slope problem

In the process of simulating the soil profiles, random fields of c' and ϕ' were generated independently, based on their prescribed statistical parameters (i.e. mean, standard deviation, and scale of fluctuation). The mean, μ, and standard deviation, σ, were expressed in terms of the coefficient of variation, COV, while the scale of fluctuation was expressed in the dimensionless form of θ/H.

In the first part of the parametric studies, the mean values of cohesion and friction angle were held constant at 10 kPa and 30°, respectively. The COV of c' and ϕ', and θ/H were varied systematically according to Table 4.5. It is noted that the COV of ϕ' is assumed to be half of the COV of c'. This is due to the fact that the variability of the friction angle is generally smaller than that of cohesion, as previously discussed in Chapter 2. Published data from the literature (e.g. Lee et al. 1983; Phoon and Kulhawy 1999a; Baecher and Christian 2003) indicate that, the COV of cohesion is in the range of 0.1 – 0.5, while the friction angle is in the range of 0.05 – 0.15. No cross correlation between c' and ϕ' was assumed in the first part of analysis. Cross correlation between c' and ϕ' is investigated and discussed later. An isotropic scale of fluctuation was assumed throughout the analysis.

Table 4.5 Input values of COV and θ/H used in the c'-ϕ' slope problem

Parameters	Input values
$COV_{c'}$	0.1, 0.2, 0.3, 0.4, 0.5
$COV_{\phi'}$	0.05, 0.1, 0.15, 0.2, 0.25
θ/H	0.1, 0.5, 1, 5, 10

4.3.1 Deterministic Solutions

Deterministic analyses were conducted using both the finite element method and the limit equilibrium methods, based on the mean values of the shear strength parameters, i.e. c' = 10 kPa and ϕ' = 30°. The limit equilibrium solution was obtained by using the student edition of the commercial slope stability analysis software SLOPE/W (GEO-SLOPE International Ltd 2004). The computed factor of safety (FOS), based on a simplified Bishop's method, was 1.2. The critical slip surface of the slope is shown in Figure 4.22, which indicates a 'toe' failure. Toe failure is generally expected in a c'–ϕ' slope problem due to the low value of effective cohesion. The FOS computed by the finite element method is 1.12, which is comparable with that obtained from the limit equilibrium method.

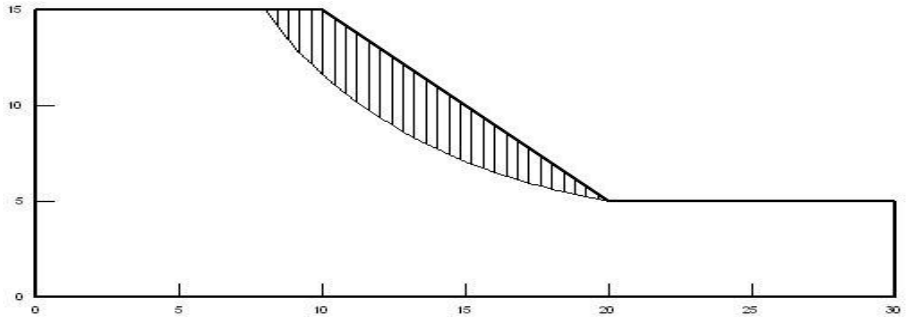

Figure 4.22 Critical slip surface obtained from SLOPE/W using simplified Bishop's method (FOS = 1.2)

4.3.2 Iteration Limit and Number of Realisations

Preliminary analyses were conducted to determine the iteration limit, *maxit*, and number of realisation, n_{sim}, required to produce a reliable estimate of the probability of failure, P_f, similar to that conducted previously for the cohesive slope problem. Figure 4.23 indicates that an iteration limit of 1,000 is required for a c'–ϕ' slope problem in order to obtain a stable estimation of P_f, which is double that required for the cohesive case.

As discussed in Chapter 3, the number of realisations required by Monte Carlo simulation to produce a stable solution is partly dependent on the number of random variables in the problem. Therefore, it is expected that the number of realisations required by a c'–ϕ' slope problem is double that required by a cohesive slope problem. Figure 4.24 indicates that

4,000 realisations would give a reliable and reproducible estimate of P_f. As a result, *maxit* = 1,000 and n_{sim} = 4,000 were used in this study.

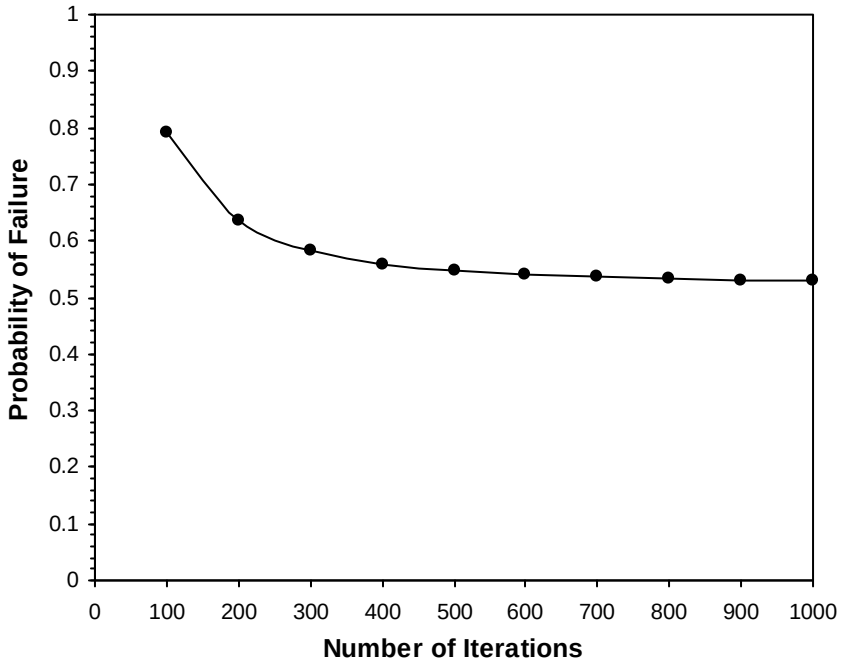

Figure 4.23 Effect of number of iterations on P_f

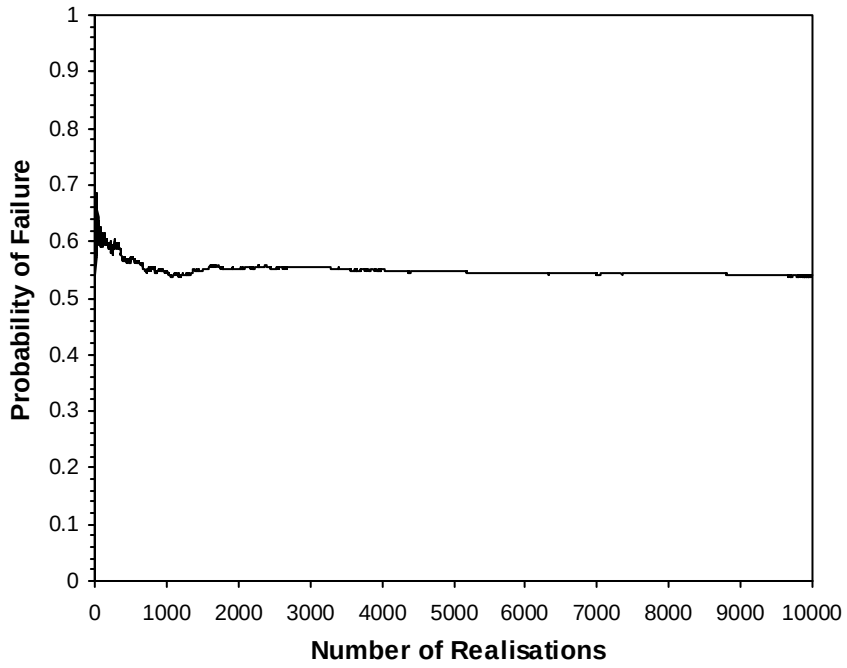

Figure 4.24 Effect of number of realisations on P_f

4.3.3 Effect of COV and θ/H on Probability of Failure

The deterministic FOS computed above by the finite element and limit equilibrium methods are 1.12 and 1.2, respectively, which suggest that the slope is marginally stable. The deterministic solution is based on the assumption that there is no variability of soil properties (i.e. COV $\rightarrow$ 0), as well as the soil profile is uniform and homogenous (i.e. $\theta \rightarrow \infty$). This section deals with the influence of incorporating soil variability on the stability of a c'–ϕ' slope.

Figure 4.25 shows the typical deformed meshes for the c'–ϕ' slope being considered, with θ/H of 0.1 and 10, respectively. The COVs of c' and ϕ' are fixed at 0.3 and 0.15, respectively. It is noted that the finite element method predicted a similar failure mechanism as that obtained from the limit equilibrium method (Figure 4.22). No noticeable difference in the failure mode, between soils with small and large scales of fluctuation, is observed in this case.

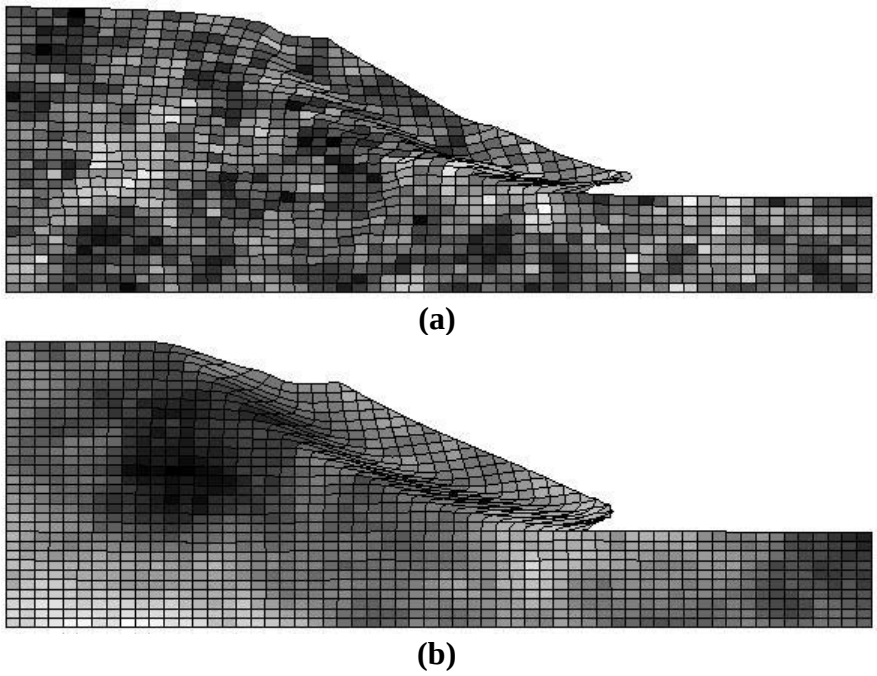

(a)

(b)

Figure 4.25 Typical deformed mesh at slope failure for the c'–ϕ' slope with (a) θ/H = 0.1 and (b) θ/H = 10. ($COV_{c'} = 2COV_{\phi'} = 0.3$)

Figure 4.26 shows the variations of P_f with COV of c'. As discussed earlier, COV of ϕ' was assumed to be equal to half of that of c'. It is observed that, P_f increases as COV increases, for all cases of θ/H. To achieve practically no failure in the slope, the COV of c' and ϕ' must be smaller than 0.1 and 0.05, respectively. When the COV of c' and ϕ' is varied within the range suggested in the literature, P_f as high as 0.38 is obtained, which indicates a high likelihood for slope. As explained earlier, as the COV increases, lower values of shear strength parameters (i.e. c' and ϕ') are likely to be encountered, and more often, in any realisation. These low values tend to control the stability of the slope and the chances of slope failure are increased accordingly.

Figure 4.27 shows the effect of varying θ/H on P_f, for different COVs of c' and ϕ'. It can be seen that, for all cases of COV of c' and ϕ', P_f increases as θ/H increases. This observation is similar to that found in the cohesive case. The similarity in the trends of the results between the cohesive and c'–ϕ' cases suggest that the variations of COV and θ/H with respect to P_f, for the c'–ϕ' cases, are due to the same reasons of the cohesive case, as previously explained in Section 4.2.6. In this c'–ϕ' case, assuming a perfectly correlated soil profile would overestimate the P_f for all the COVs being considered.

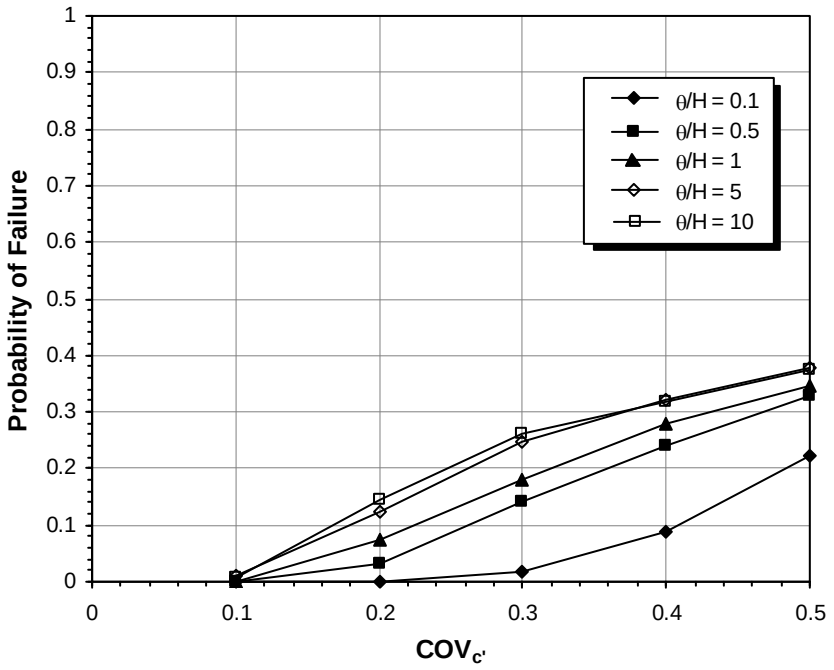

Figure 4.26 Effect of varying COV on probability of failure for different values of θ/H

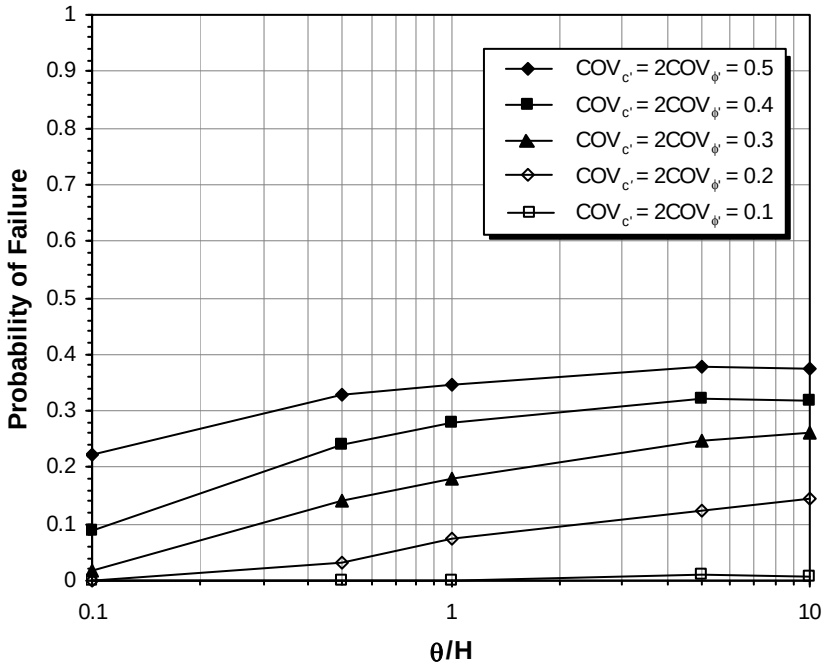

Figure 4.27 Effect of varying θ/H on probability of failure for different COVs of c' and ϕ'

4.3.4 Comparison of Probability of Failure and Factor of Safety

In this section, the mean values of c' and ϕ' are varied, and the P_f is compared directly with the deterministic FOS. The mean values of c' and ϕ' that were considered in the analysis, and their corresponding values of FOS, are summarised in Table 4.6. Figure 4.28 shows the direct comparison between P_f and FOS, for different COV of c' and ϕ'. The value of θ/H was fixed at 1 in this case. It is observed that, P_f decreases as FOS increases, as expected. The curves intersect at the point P_f = 0.75 and FOS = 0.95. When FOS < 0.95, a larger COV leads to a lower value of P_f. In contrast, when FOS > 0.95, a larger COV leads to a higher value of P_f. It is also noted that, for the case with $COV_{c'} = COV_{\phi'} = 0.5$, FOS greater than 1.6 is required to reduce P_f to insignificant levels (i.e. below 1/4000).

Figure 4.29 shows the plots of P_f versus FOS for different values of θ/H, with $COV_{c'} = 2COV_{\phi'} = 0.5$. In this case, the intersection point occurs approximately at P_f = 0.4 and FOS = 1.1. When FOS < 1.1, a larger value of θ/H leads to a lower value of P_f, which indicates that the θ/H = ∞ case is unconservative. On the other hand, when FOS < 1.1, a larger

value of θ/H leads to a higher value of P_f, which indicates that the θ/H = ∞ case is conservative.

Table 4.6 FOS for c'–ϕ' slope with different mean values of c' and ϕ'

$\mu_{c'}$ (kPa)	$\mu_{\phi'}$ (degrees)	FOS
0	20	0.38
0	30	0.60
10	20	0.88
10	30	1.12
20	20	1.25
20	30	1.55

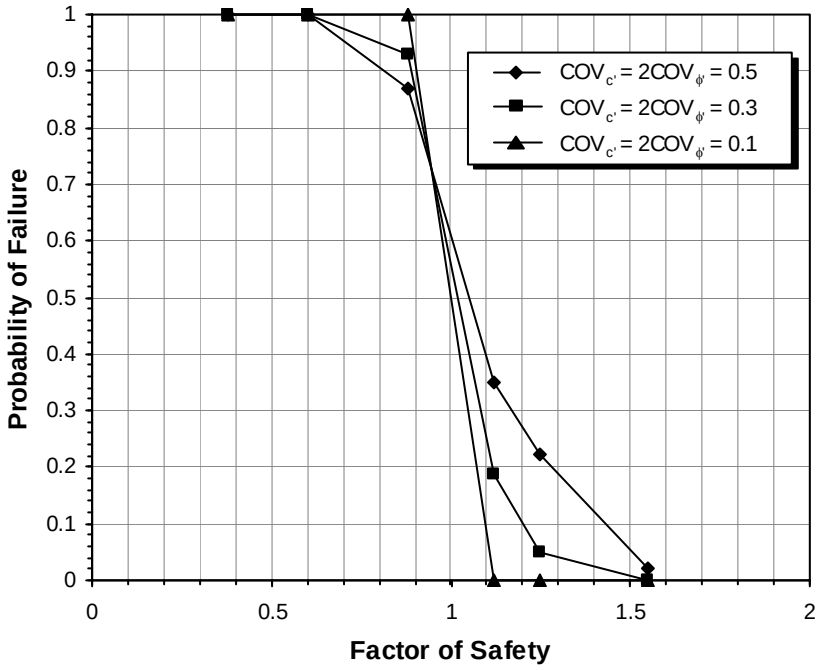

Figure 4.28 Probability of failure versus factor of safety for different COV of c' and ϕ' (θ/H = 1)

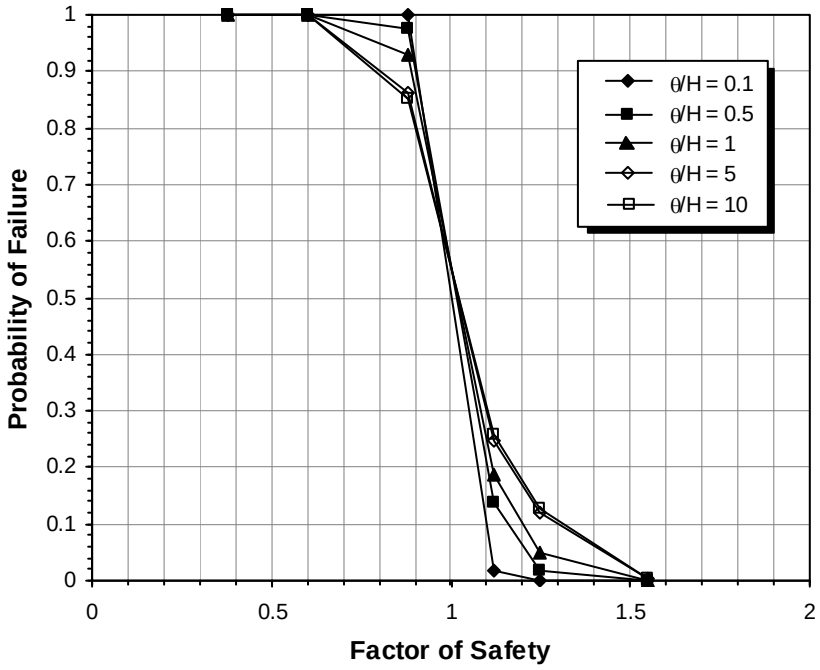

Figure 4.29 Probability of failure versus factor of safety for different values of θ/H ($COV_{c'} = 2COV_{\phi'} = 0.5$)

4.3.5 Effect of c'–ϕ' Correlation on Probability of Failure

The results discussed so far are based on the assumption of no cross-correlation between the parameters c' and ϕ'. Analyses were conducted to investigate the influence of the c'–ϕ' correlation. The cross-correlation between c' and ϕ' is defined by the correlation coefficient, ρ, as previously discussed in Chapter 3 (Section 3.3.6). Values of ρ = –1, 0, and 1, correspond to a completely negatively correlated, uncorrelated, and completely positively correlated soil, respectively. In this study, values of ρ = –1, –0.5, 0, 0.5 and 1 were considered. The COVs of c' and ϕ' were fixed at 0.5 and 0.25, respectively. Cherubini (2000) reported that c and ϕ are negatively correlated, with values ranging from –0.24 to –0.70, as previously discussed in Chapter 3.

Figure 4.30 shows the variations of P_f with respect to c'–ϕ' correlation, ρ, for the slopes with different values of COVs of c' and ϕ', and θ/H. The results indicate that, for all cases of COV and θ/H, negative correlation between c' and ϕ' leads to a lower estimate of P_f, while positive correlation between c' and ϕ' leads to a higher estimate of P_f.

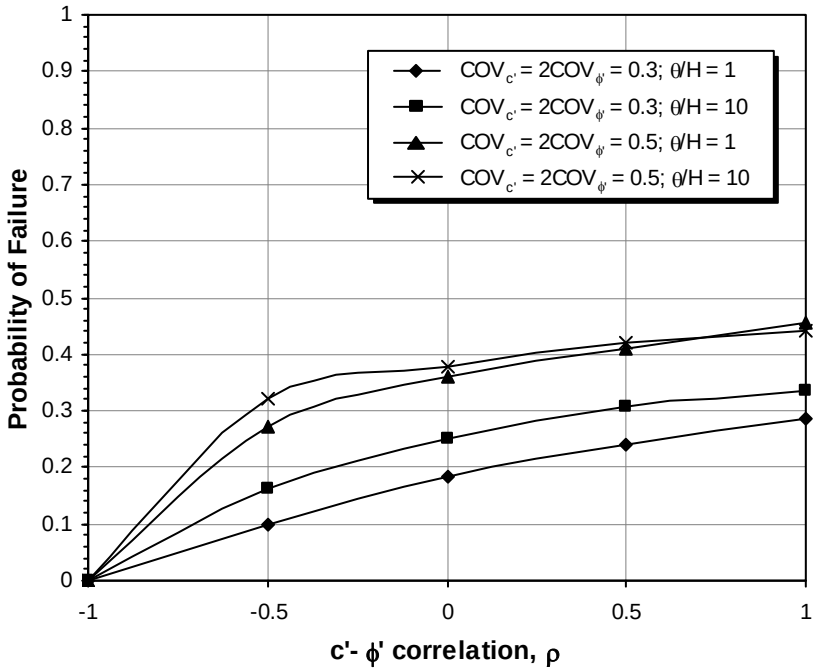

Figure 4.30 Probability of failure versus θ/H for different values of COVs of c' and ϕ', and θ/H

4.4 Summary

The random finite element method (RFEM) was used to investigate the influence of soil variability on the reliability of single-layered soil slopes. The spatial variability of soil properties was modelled by the coefficient of variation (COV) and the scale of fluctuation (SOF). Numerical studies, based on Monte Carlo simulation method, were conducted to investigate the effects of varying COV and SOF on the probability of failure, P_f, of a slope. Two cases were considered in the numerical studies: (a) a cohesive slope problem and (b) a c'–ϕ' slope problem.

To ensure the estimated P_f is reliable and reproducible, preliminary studies were carried out to determine the required iteration limit, *maxit*, for the finite element slope stability analysis and the number of realisations, n_{sim}, for the Monte Carlo simulation process. It was found that *maxit* = 500 and n_{sim} = 2,000 are adequate for a cohesive slope problem. For a c'–ϕ' slope problem, however, *maxit* = 1,000 and n_{sim} = 4,000 are required. Studies were also conducted to investigate the effect of mesh density on the estimated P_f. It was

determined that, in order to obtain a reliable estimate of P_f, the ratio between element size and SOF should be at least 0.5.

For the cohesive slope case study, the undrained cohesion, c_u, was modelled as a random field, which was described by a lognormal distribution. Parametric studies were conducted by varying the slope angle, β, depth factors, D, stability coefficient, N_s, COV and normalised SOF, θ/H. A set of probabilistic stability charts were developed, based on the results of the parametric studies, which can be used as a quick estimation of P_f of a spatially random cohesive slope.

The results of numerical studies indicated that both COV and θ/H have a significant effect on the estimated P_f. It was generally found that, P_f increased as COV increased. However, as θ/H increased, P_f either decreased or increased, dependent on the values of COV, N_s and slope geometry (β and D). It was found that, for slopes with $P_f < 0.5$, P_f decreased as θ/H increased, while for slopes with $P_f > 0.5$, P_f decreased as θ/H increase.

Direct comparison between the probability of failure, P_f, and the deterministic factor of safety (FOS) was made and the results indicated that values of FOS as high as 1.5 were associated with significant chances of failure when the COV was varied within the range suggested in literature. It can be concluded that the deterministic FOS becomes unreliable when the variability in soil properties is significant.

The effects of COV and θ/H on P_f of a c'–ϕ' slope were found to follow the same trends as the cohesive slope. A circular 'toe' type failure was found to be the critical failure mode. It was also determined that, assuming negative correlation between c' and ϕ' leads to a lower estimate of P_f, while positive correlation between c' and ϕ' leads to a higher estimate of P_f.

In the next chapter, the computer model *rslope2d* is extended to examine slopes with two-layered soil profiles. Probabilistic analysis is also conducted to investigate the effects of soil variability on the reliability of two-layered soil slopes.

Chapter 5

INFLUENCE OF SOIL VARIABILITY ON RELIABILITY OF TWO-LAYERED SOIL SLOPES

5.1 Introduction

In the previous chapter, the influence of soil variability on a single-layered soil slope was investigated. However, it is not uncommon that, the real slope soil profiles consist of two or more layers of soil with different properties. There is also a possibility that soil near the ground surface has a higher cohesion due to the apparent cohesion contributed by tree root reinforcement or soil suction, as previously discussed in Chapter 2. In this case, the top layer should be modelled with different values of cohesion.

To model a layered soil slope in traditional limit equilibrium analysis, the soil profile is usually divided into layers with different soil properties. The soil properties within each layer are commonly assumed to be uniform. However, in a real soil profile, the properties within each single layer may vary spatially. In addition, even different soil layers that have the same mean value of a soil property, they may have very different spatial variability (i.e. different COV and θ).

The computer model *rslope2d*, as discussed in Chapter 3 and adopted for the numerical studies in Chapter 4, is capable of modelling soil variability in slope stability analysis. However, the available version of this computer model is limited to analysing slopes with a single-layered soil profile. Therefore, the aim of this chapter is to extend *rslope2d* to incorporate a two-layered soil profile in the probabilistic slope stability analysis. The following sections discuss the development of the two-layered slope model, followed by validation of the developed model. Finally, probabilistic analyses of two-layered soil slopes are performed and the effect of soil variability on layered slopes is examined.

5.2 Description of The Two-Layered Soil Slope Model

As discussed in Chapter 3, it is important to simulate a soil profile that can represent real soil deposits. Therefore, if the real soil profile consists of obvious layers of soil with different properties, it is necessary to model them in the soil profile simulation process. Two different layering profiles are considered in the development of the two-layered soil slope model, as shown in Figure 5.1.

The first layering profile models a slope with two soil layers that are separated by a horizontal boundary, as shown in Figure 5.1(a). This is the most common type of soil layering found in real soil deposits due mainly to the soil deposition process. Similar to a single-layered slope model, the slope geometry is defined by the slope height, H, slope angle, β, and depth factor, D. An additional parameter 'h' is introduced here to define the depth of the upper layer (i.e. layer 2) from the ground surface. The upper layer is underlain by a lower layer (i.e. layer 1), which may consist of a different soil type and hence has different soil properties.

The second type of layering profile models a slope with an upper layer that is parallel to the ground surface, as shown in Figure 5.1(b). This slope profile can be used to model slopes with a thin layer of soil overlying harder materials (e.g. weathered rocks), as found in most natural slopes. In addition, this slope profile is also suitable for modelling the effect of tree root reinforcement or soil suction, such that the upper layer (layer 2) can have a higher cohesion than the lower layer (layer 1). The depth of the upper layer for this profile is also described by the parameter 'h'.

In the process of simulating a two-layered soil profile, two independent random fields are simulated for each soil parameter (e.g. c or ϕ), using the local average subdivision (LAS) method, as discussed previously in Chapter 3. The first random field (RF 1) has the statistical properties (i.e. mean, standard deviation and scale of fluctuation) corresponding to the lower layer (layer 1), while the second random field (RF 2) has properties corresponding to the upper layer (layer 2). These two distinct layers may have different values of mean, standard deviation and scale of fluctuation. The generated random fields are then systematically mapped onto the finite element mesh according the pre-defined depth of the upper layer, h, as illustrated in Figure 5.2.

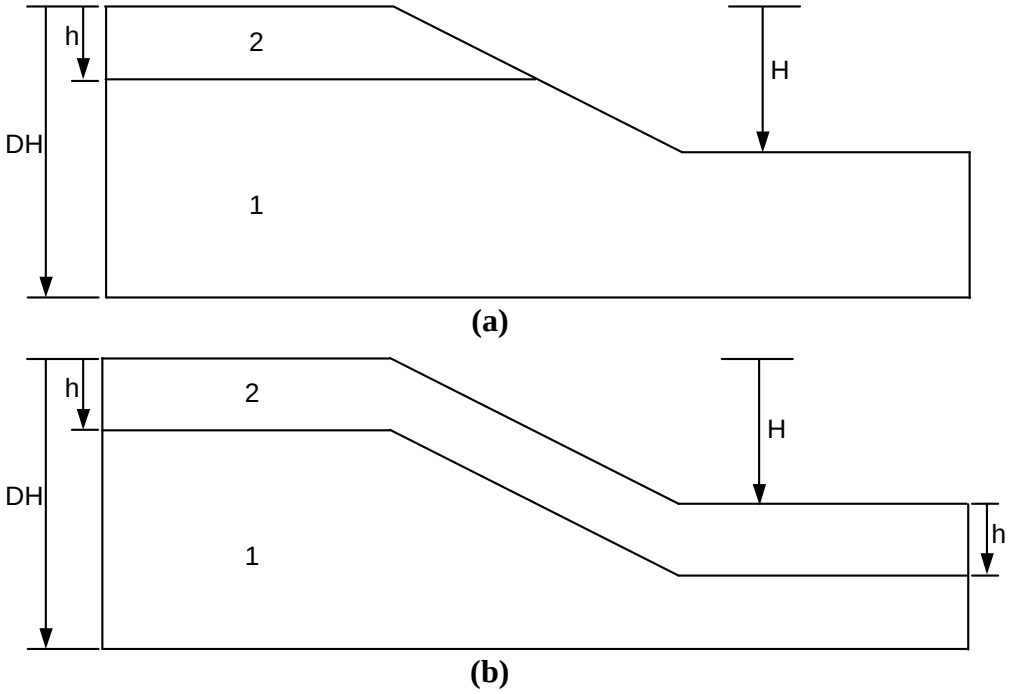

Figure 5.1 Typical layering profiles of the two-layered soil slope model (a) horizontal layering; and (b) parallel layering

Figure 5.2 shows the process of simulation of a two-layered undrained cohesion, c_u, field, with the horizontal layering boundary set at the toe of the slope, such that h/DH = 0.5. In this case, RF 1 is assumed to have a larger scale of fluctuation than RF 2 (i.e. $\theta_1/H = 10$, $\theta_2/H = 0.1$), and for simplicity, the mean and COV of c_u are assumed to be the same for both layers. The simulated soil profile, hence, represents a slope with a more spatially random soil mass overlying a foundation layer with a more continuous soil mass. It can be seen that for RF 1, only the soil elements that are located below the pre-defined horizontal boundary are used to form the desired two-layered soil profile, and on the other hand, for RF 2, only those soil elements that are located above the horizontal boundary are used.

Figure 5.3 shows the typical simulated two-layered spatially random soil profile with parallel layering. The process of simulating the two-layered soil profile with parallel layering is similar to that of the soil profile with horizontal layering except the boundary is defined as being parallel to the slope and ground surface. The simulated two-layered soil profile is then used in the finite element analysis and Monte Carlo simulation. The analysis procedure is exactly the same as that performed on single-layered soil slopes as described in Chapters 3 and 4.

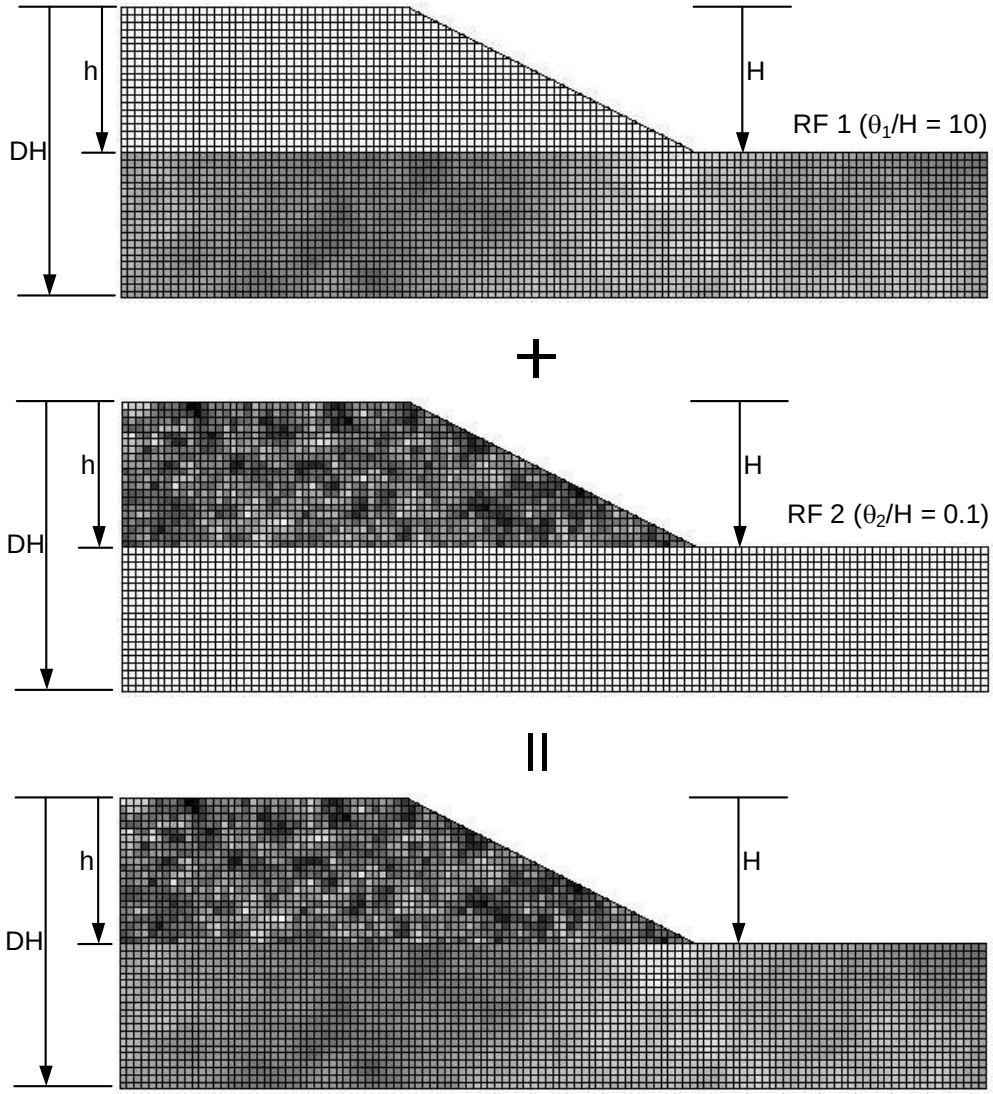

Figure 5.2 Simulation of two-layered spatially random soil profile with horizontal layering (θ_1/H = 10, θ_2/H = 0.1)

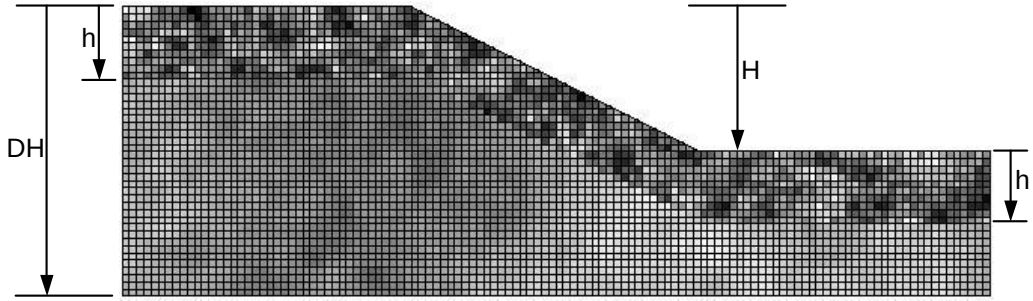

Figure 5.3 Typical simulated two-layered spatially random soil profile with parallel layering (θ_1/H = 10, θ_2/H = 0.1)

5.3 Validation of the Two-layered Slope Model

The developed two-layered slope model was validated against the original single-layered model by simply using the two-layered model to estimate the probability of failure, P_f, of a single-layered soil slope and comparing the result with that obtained by using the original single-layered model (i.e. *rslope2d*). This is achieved by assuming the random fields of the lower (RF 1) and upper (RF 2) layers both have exactly the same statistical properties (i.e. N_s, COV and θ/H). The aim is to confirm that the modified computer program is behaving exactly the same as the original program. The estimated P_f obtained from the two-layered model should be the same or similar to that obtained from the single-layered model. This is because the analysis procedure in the modified program is exactly the same as the original program.

A 2:1 undrained clay slope with a depth factor, D, of 2 was used in this investigation. The slope geometry together with the finite element mesh used in the analyses is shown in Figure 5.4. It is noted that a finer mesh (0.5 m × 0.5 m) was used in this study. The statistical properties of the undrained cohesion, c_u, were held constant at $N_s = 0.25$, COV = 0.5 and $\theta/H = 1$.

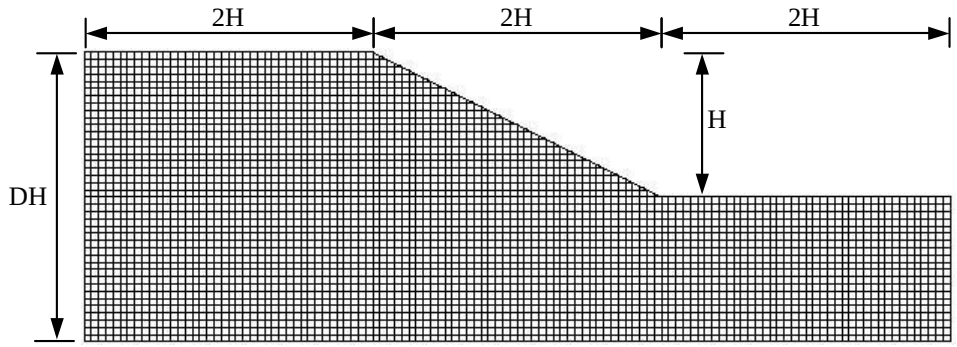

Figure 5.4 Typical finite element mesh for a 2:1 cohesive slope problem ($\beta = 26.6°$; D = 2)

Three different depths of the upper layer were considered when using the two-layered soil slope model, i.e. h/DH = 0.25, 0.5 and 0.75. It should be noted that the statistical properties of c_u (i.e. N_s, COV and θ/H) in each layer of the two-layered soil profile are

exactly the same, although h/DH is different. The only difference is that the random field for each soil layer was generated based on a different random number seed.

The comparison of the estimated P_f obtained by using the different models is shown in Table 5.1. The probability of failure was estimated based on a 2,000 Monte Carlo realisations. It is noted that the estimated values of P_f for this slope, which were computed using the two-layered model, are generally in good agreement with the original single-layered model, with a maximum relative percentage error of 10%. It is noted that the relative percentage error of the estimated P_f of 0.187 is 9% (using a 95% confidence level), as calculated using Equation (3.14). This error is greater than the two-layered slope model with h/DH = 0.25 and 0.5, and slightly less than the model with h/DH = 0.75. Based on this comparison, it is suggested that the relative percentage error between the two-layered and the single-layered models is acceptable.

Table 5.1 Comparison of estimated values of P_f obtained by using the two-layered model and the original single-layered model

Slope Model	Probability of Failure, P_f	Relative Error (%)
Single-layered	0.187	-
Two-layered (h/DH = 0.25)	0.172	8
Two-layered (h/DH = 0.5)	0.179	4
Two-layered (h/DH = 0.75)	0.206	10

5.4 Probabilistic Analysis of a Two-Layered Spatially Random Cohesive Slope

5.4.1 Description of Numerical Studies Undertaken

To investigate the effect of soil variability on the reliability of a two-layered soil slope, numerical studies using the modified version of the computer program *rslope2d* were conducted. In these studies, a 2:1 (β = 26.6°) two-layered cohesive slope with a depth factor, D = 2, was investigated. The slope geometry, together with the finite element mesh used in the analyses, was previously shown in Figure 5.4. The probabilistic analysis

methodology used in these numerical studies is the same as that used for the single-layered cohesive slope problem, as discussed in Chapter 4. The undrained cohesion, c_u, was modelled as a random variable, which was described by a lognormal distribution. The spatial variability of c_u was modelled by the soil variability parameters COV and θ/H.

In the first part of the analyses, both the upper and lower layers were assumed to have the same COV and θ/H (i.e. $COV_1 = COV_2$ and $\theta_1/H = \theta_2/H$). The mean value of c_u for the upper layer (layer 1), $c_{u1,}$ was fixed at 50 kPa (i.e. $N_s = 0.25$). The mean value of c_u for the lower layer (layer 2), $c_{u2,}$ was varied using the ratio c_{u1}/c_{u2} of 0.5, 0.75, 1, 1.25 and 1.5. A value of c_{u1}/c_{u2} of less than one indicates a stronger upper layer overlying a weaker lower layer, while c_{u1}/c_{u2} of greater than one indicates that the lower layer is stronger than the upper layer. In addition, the location of the layering boundary was also varied using the ratio h/DH of 0.25, 0.5 and 0.75. The input parameters c_{u1}/c_{u2}, COV and θ/H were varied systematically in the parametric studies according to the values given in Table 5.2. All other parameters were held constant at their deterministic values, i.e. H = 10 m, γ = 20 kN/m^3, $E_s = 1 \times 10^5$ kPa, ν = 0.3 and ψ = 0°.

In the second part of the study, the ratio of c_{u1}/c_{u2} and h/DH were held constant at 1 and 0.5, respectively, and the effect of varying COV and θ/H between the two layers were investigated.

Table 5.2 Input parameters for parametric studies of a two-layered cohesive slope

Parameters	Input values
c_{u1}/c_{u2}	0.5, 0.75, 1, 1.25, 1.5
h/DH	0.25, 0.5, 0.75
COV	0.1, 0.3, 0.5
θ/H	0.1, 1, 10

5.4.2 Deterministic Solutions

Deterministic factor of safety (FOS) for the two-layered cohesive slope with different ratio of c_{u1}/c_{u2}, with h/DH fixed at 0.5, was determined using the finite element method and the

results are shown in Table 5.3. It is noted that, as expected, FOS increases as c_{u1}/c_{u2} increases. Based on the deterministic FOS, slopes with c_{u1}/c_{u2} = 0.5 would be considered as unstable, slopes with c_{u1}/c_{u2} = 0.75 as marginally stable, and slopes with c_{u1}/c_{u2} greater than 1 as stable.

Table 5.3 FOS for a two-layered cohesive slope with different c_{u1}/c_{u2} (h/DH = 0.5)

c_{u1}/c_{u2}	FOS
0.5	0.86
0.75	1.16
1	1.45
1.25	1.75
1.5	2.03

5.4.3 Results of Numerical Studies

Based on 2,000 realisations of Monte Carlo simulations for each parametric group described in Table 5.2, the effect of each input parameter on the probability of failure, P_f, was examined. However, before examining the results of the two-layered cases, it is worthwhile to look at the deformed mesh of a single-layered cohesive slope with c_u = 50 kPa (i.e. N_s = 0.25), as shown in Figure 5.5. In this case, the values of COV and θ/H were fixed at 0.5 and 1, respectively. The corresponding P_f obtained for this slope was 0.187. Figure 5.5 indicates that the critical failure mechanism is deep-seated.

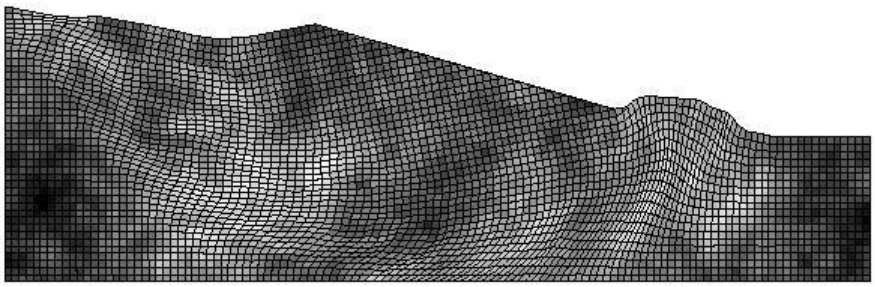

Figure 5.5 Deformed mesh of single-layered cohesive slope (N_s = 0.25; COV = 0.5; θ/H = 1)

5.4.3.1 Effect of Variation of c_{u1}/c_{u2} on Probability of Failure

When the ratio of c_{u1}/c_{u2} was varied, both the P_f and failure mechanism changed accordingly. The P_f of a two-layered cohesive slope with different ratios of c_{u1}/c_{u2} is shown in Table 5.4. The deformed meshes and failure mechanisms of a two-layered cohesive slope with different values of c_{u1}/c_{u2} are shown in Figure 5.6. It should be noted that, in the first part of the analyses, the values of COV and θ/H were assumed to be the same in the two soil layers. The effect of incorporating different values of COV and θ/H in each layer is discussed later.

Table 5.4 Probability of failure for a two-layered cohesive slope with different values of c_{u1}/c_{u2} (h/DH = 0.5, COV = 0.5, θ/H = 1)

c_{u1}/c_{u2}	P_f
0.5	0.986
0.75	0.674
1	0.194
1.25	0.046
1.5	0.021

Table 5.4 shows that P_f decreases as the ratio of c_{u1}/c_{u2} increases. This is expected because as c_{u1}/c_{u2} increases the lower layer becomes stronger, and as a result, the probability of slope failure reduces accordingly. Figure 5.6 shows that different failure mechanisms were observed for different values of c_{u1}/c_{u2}. Figures 5.6(a) and (b) show that when c_{u1}/c_{u2} is less than 1 (i.e. 0.5 and 0.75, respectively), the failure mechanism appears to be deep-seated. The slip surface starts at the top of the upper layer and propagates through the weaker lower layer, and finally exits at the regions near the toe of the slope. However, when c_{u1}/c_{u2} is greater than 1 (i.e. 1.25 and 1.5, respectively), as shown in Figures 5.6(c) and (d), the failure mechanism appears to be a toe failure. It is noted that the slip surface did not propagate through the lower layer as this layer has a larger value of c_u. The higher strength value of the lower layer had eventually prevented the slip surface from propagating through this layer. As a result, the slip surface had to find a weaker path through the soil.

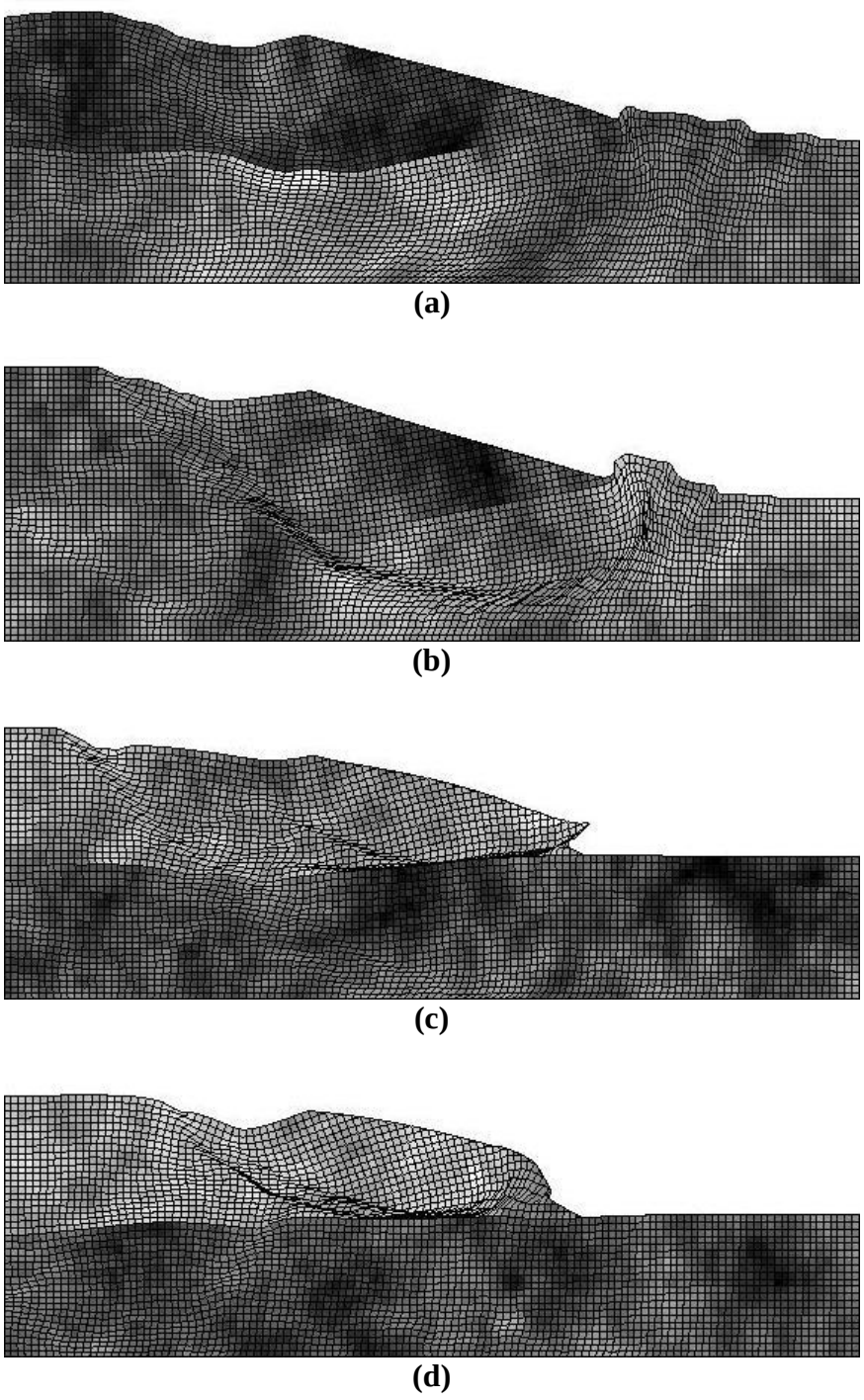

Figure 5.6 Deformed meshes of two-layered cohesive slope with different values of c_{u1}/c_{u2}: (a) 0.5; (b) 0.75; (c) 1.25; and (d) 1.5. (COV = 0.5; θ/H =1)

Figure 5.7 shows the effect of varying the values of COV on P_f for different values of $c_{u1}/c_{u2,}$ with θ/H fixed at 1. It is noted that P_f increases as COV increases for the slopes with $c_{u1}/c_{u2} \geq 0.75$, however, P_f decreases as COV increases for the slopes with c_{u1}/c_{u2} =

0.5. This is because, as COV increases, the scatter of the simulated values of c_u about the mean value increases, and this increases the chances of simulating very low and high values of c_u. It is also observed that, when COV is small (i.e. COV $\rightarrow$ 0), P_f converges to 0 for the slopes with $c_{u1}/c_{u2} \geq 0.75$, while P_f converges to 1 for the slopes with $c_{u1}/c_{u2} = 0.5$.

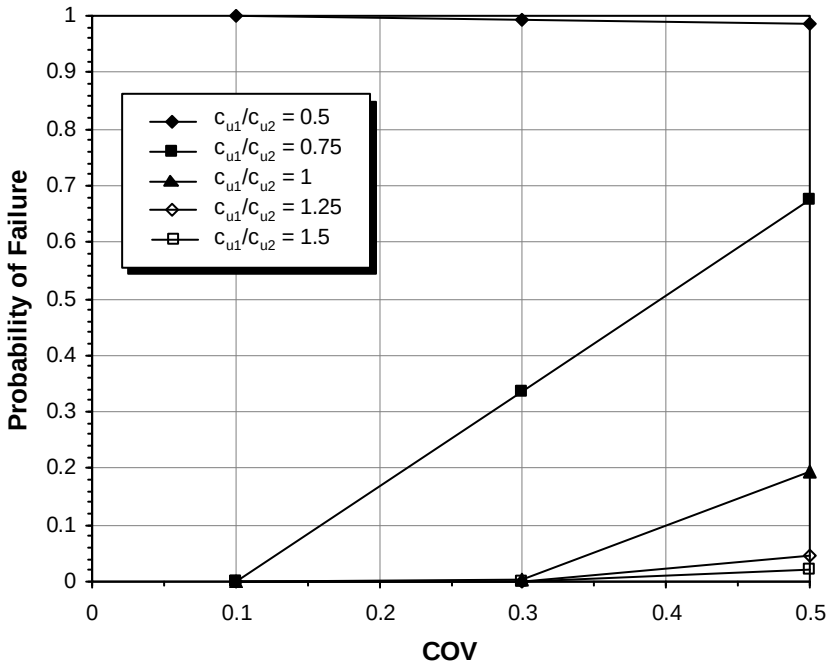

Figure 5.7 Probability of failure versus COV for different values of c_{u1}/c_{u2} with θ/H fixed at 1

Figure 5.8 shows the effect of varying the values of θ/H on P_f for different values of c_{u1}/c_{u2}, with COV fixed at 0.5. It can be seen that P_f increases as θ/H increases for the slopes with $c_{u1}/c_{u2} \geq 1$, but P_f decreases as θ/H increases for the slopes with $c_{u1}/c_{u2} \leq 0.75$. It is also observed that, as θ/H $\rightarrow$ 0, $P_f \rightarrow 0$ for the slopes with $c_{u1}/c_{u2} \geq 1$, but $P_f \rightarrow 1$ for the slopes with $c_{u1}/c_{u2} \leq 0.75$. The results shown in Figure 5.8 indicate that assuming perfectly correlated soil profiles would overestimate the P_f of the slopes with $c_{u1}/c_{u2} \geq 1$, but underestimate the P_f of the slopes with $c_{u1}/c_{u2} \leq 0.5$. The effect of varying θ/H of P_f for the two-layered cohesive slope, as shown in Figure 5.8, is found similar to that observed from the single-layered cohesive slope analyses, as previously described in Chapter 4. The two different trends observed in the variation of P_f with respect to the values of θ/H are

governed by the *median* c_u of the simulated random fields, which was previously discussed in Section 4.2.6.

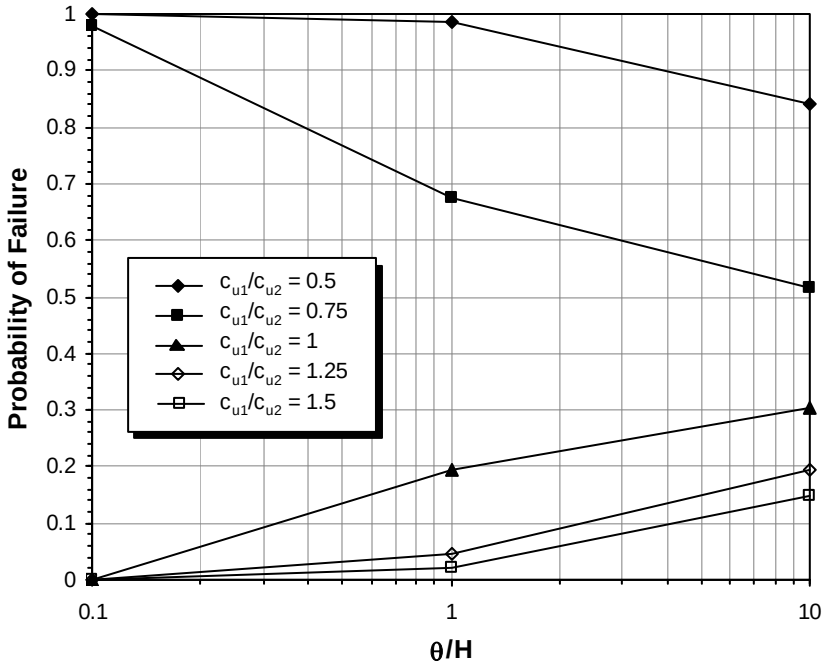

Figure 5.8 Probability of failure versus θ/H for different values of c_{u1}/c_{u2} with COV fixed at 0.5

Figure 5.9 shows a plot of P_f versus c_{u1}/c_{u2} for different cases of h/DH. It is recalled that h/DH represents the location of the horizontal boundary of the layering. The values of COV and θ/H were fixed at 0.5 and 1, respectively. It can be seen that P_f decreases as c_{u1}/c_{u2} increases for all cases of h/DH. The curves intersect at a point where $c_{u1}/c_{u2} = 0.95$ and $P_f = 0.28$. When $c_{u1}/c_{u2} > 0.95$, higher values of h/DH yields a larger P_f, however, when $c_{u1}/c_{u2} < 0.95$, higher values of h/DH yields a lower P_f. This is because a higher value of h/DH means that the thickness of the lower layer is less than the upper layer. Therefore, for the case with a stronger lower layer, as the thickness of the stronger layer diminishes the probability of failure increases.

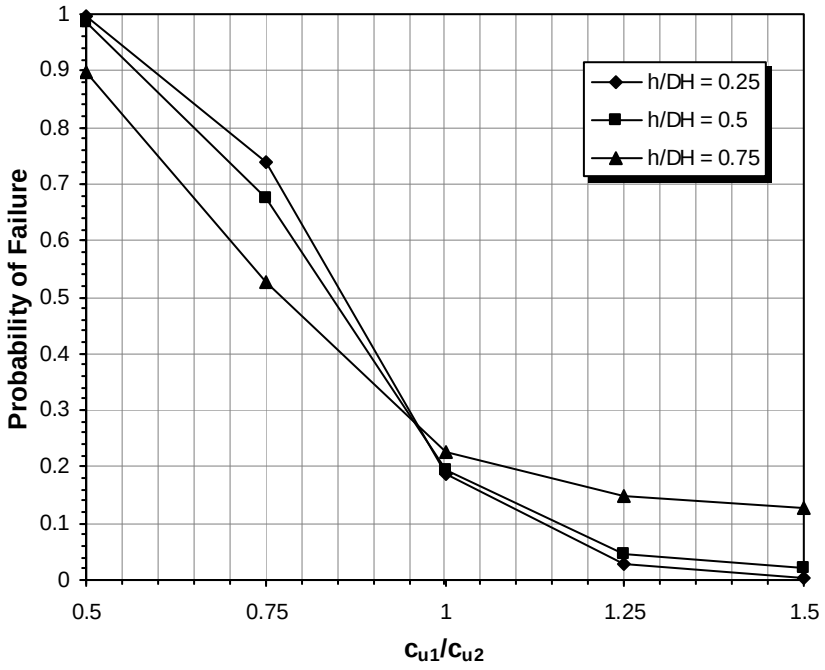

Figure 5.9 Probability of failure versus θ/H for different values of h/DH with COV and θ/H fixed at 0.5 and 1, respectively

5.4.3.2 Effect of Variation of COV and θ/H in Each Soil Layer

In the second part of the analyses, the effect of varying COV and θ/H in each soil layer on P_f was investigated. In these analyses, the location of the layering boundary was fixed at the toe of the slope (i.e. h/DH = 0.5). The mean value of c_u in each soil layer was assumed to be the same (i.e. $c_{u1}/c_{u2} = 1$). Firstly, the effect of varying COV in each layer of a two-layered cohesive slope on P_f was investigated. A total of six cases were considered, for the two-layered cohesive slope, each with different combinations of values of COV in each layer and, the corresponding estimated values of P_f are shown in Table 5.5. It should be noted that θ/H was fixed at 1 for these cases. It can be seen that varying values of COV in each layer has a significant impact on the estimated values of P_f. Bearing in mind that the mean value of c_u in each layer was the same, the only difference was the value of COV. Examination of the results shown in Table 5.5 indicates that a slope with $COV_1 > COV_2$ always has a higher P_f than a slope with $COV_1 < COV_2$, except when COV was small (i.e. Cases 1 and 2). This finding suggests that the lower or base layer is more critical and it is

more sensitive to the variability of c_u. An increase in the variability of this layer will cause a significant effect on the probability of slope failure.

Table 5.5 Probability of failure of a two-layered cohesive slope with different values of COV in each soil layer. (h/DH = 0.5, c_{u1}/c_{u2} = 1 and $\theta_1/H = \theta_2/H = 1$)

Case No.	COV_1	COV_2	P_f
1	0.1	0.3	0
2	0.3	0.1	0
3	0.1	0.5	0.014
4	0.5	0.1	0.081
5	0.3	0.5	0.039
6	0.5	0.3	0.125

Figure 5.10 shows the typical deformed meshes for the two-layered cohesive slope with different values of COV in each layer for: (a) Case 3 and (b) Case 4 (see Table 5.5). It can be seen from Figure 5.10(a) that, when the COV of the upper layer (i.e. COV_2 = 0.5) is higher than the COV of the lower layer (i.e. COV_1 = 0.1), the failure mechanism is a toe failure. The critical slip surface is located in the upper layer and it does not propagate through the lower layer. However, when the COV of the lower layer (i.e. COV_1 = 0.5) is higher than the COV of the upper layer (i.e. COV_2 = 0.1), the failure mechanism is a deep-seated one. The critical slip surface starts at the top of the upper layer and propagates through both the upper and lower layers. This observation suggests that the failure surface is more likely to develop in the soil layer with higher variability, i.e. higher value of COV. It should also be noted that the slope shown in Figure 5.10(b) has a higher P_f than the slope shown in Figure 5.10(a), as shown in Table 5.5, which confirms that deep-seated failure is a more critical failure mechanism.

Next, the effect of varying θ/H in each layer of a two-layered cohesive slope on P_f was investigated. A total of six cases, each with different combinations of θ/H in each layer, were considered and the computed values of P_f are shown in Table 5.6. It should be noted that the COV of each layer was fixed at 0.5 for these analyses. It can be seen from Table 5.6 that a slope with $\theta_1/H > \theta_2/H$ always has a higher P_f than a slope with $\theta_1/H < \theta_2/H$. This again suggests that the lower or base layer has a higher influence on P_f of the slope.

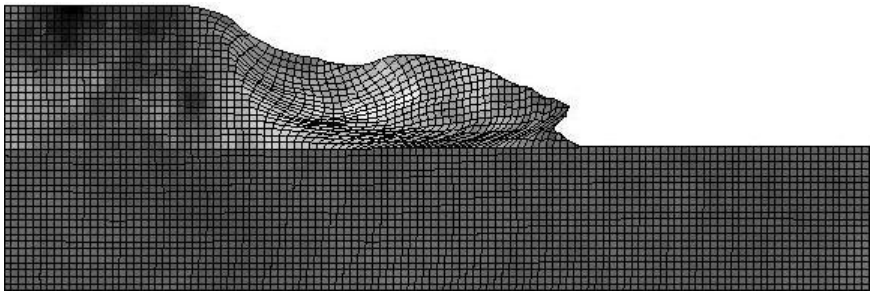

(a)

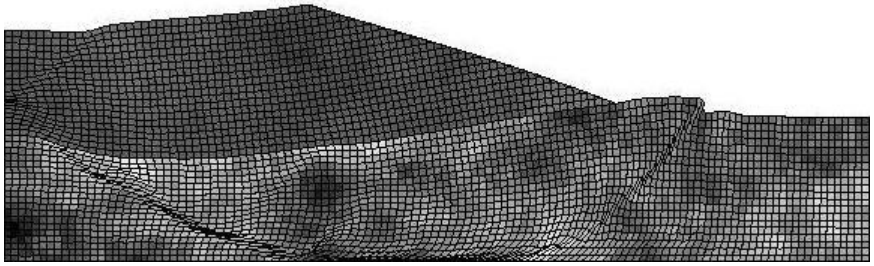

(b)

Figure 5.10 Typical deformed meshes for a two-layered cohesive slope with different values of COV in each layer: (a) COV_1 = 0.1, COV_2 = 0.5 (P_f = 0.014) and (b) COV_1 = 0.5, COV_2 = 0.1 (P_f = 0.081)

Table 5.6 Probability of failure of a two-layered cohesive slope with different values of θ/H in each soil layer. (h/DH = 0.5, c_{u1}/c_{u2} = 1 and COV_1 = COV_2 = 0.5)

Case No.	θ_1/H	θ_2/H	P_f
1	0.1	1	0.022
2	1	0.1	0.151
3	0.1	10	0.098
4	10	0.1	0.278
5	1	10	0.222
6	10	1	0.284

Figure 5.11 shows the typical deformed meshes for the two-layered cohesive slope with different values of θ/H in each layer for: (a) Case 1 and (b) Case 2 (see Table 5.6). It can be seen from Figure 5.11(a) that, when the θ/H of the upper layer (i.e. $\theta_2/H = 1$) is larger than the θ/H of the lower layer (i.e. $\theta_1/H = 0.1$), the failure mechanism is a toe failure. However, when the θ/H of the lower layer (i.e. $\theta_1/H = 1$) is larger than the θ/H of the upper layer (i.e. $\theta_2/H = 0.1$), the failure mechanism is a deep-seated one.

The deformed meshes shown in Figure 5.11 suggest that failure is more likely to occur in the soil layer with a larger θ/H, i.e. a more continuous soil mass. This is because failure will occur along a path of least resistance or low values of c_u. In a more spatially random soil mass (i.e. low θ/H), there is little likelihood for such path because the values of c_u change rapidly and the weaker soil elements are likely to be adjacent to the stronger ones. However, in a more continuous soil mass (i.e. high θ/H), chances of larger zones of low values of c_u are higher. Hence, path of least resistance is more likely to occur.

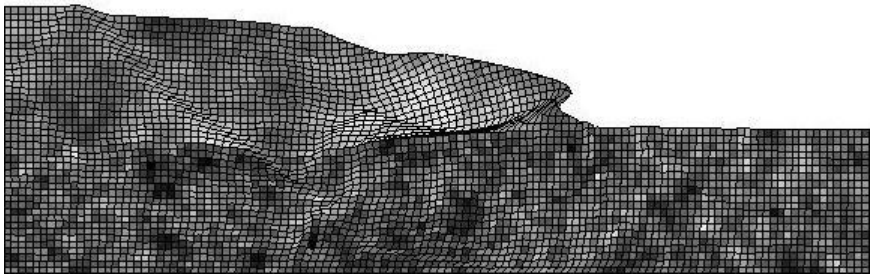

(a)

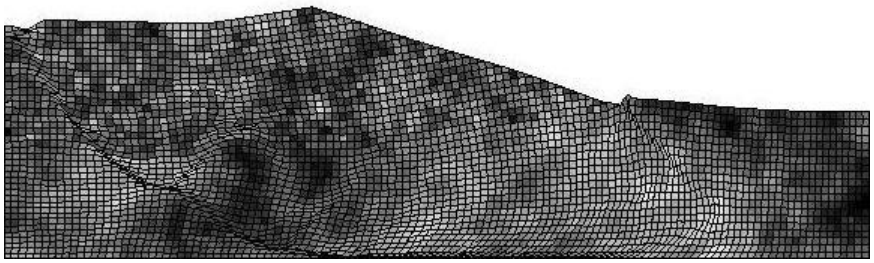

(b)

Figure 5.11 Typical deformed meshes for a two-layered cohesive slope with different values of θ/H in each layer: (a) $\theta_1/H = 0.1$, $\theta_2/H = 1$ ($P_f = 0.022$) and (b) $\theta_1/H = 1$, $\theta_2/H = 0.1$ ($P_f = 0.151$)

5.5 Summary

In this chapter, the random finite element method (RFEM) computer program *rslope2d* was modified so that it could be used to analyse a two-layered soil slope. Two different types of layering profiles were considered: horizontal layering and parallel layering. The modified computer program was validated against the original single-layered program.

The modified program was used in the numerical studies of a two-layered spatially random cohesive slope. A 2:1 slope ($\beta = 26.6°$) with a depth factor, D, of 2 was considered in the numerical studies. In the first part of the analyses, both the upper and lower layers were assumed to have the same COV and θ/H (i.e. $COV_1 = COV_2$ and $\theta_1/H = \theta_2/H$). The parameters c_{u1}/c_{u2}, h/DH, COV and θ/H were varied systematically as part of the parametric studies. The numerical results show that, when the ratio of c_{u1}/c_{u2} was varied, both the P_f and failure mechanism changed accordingly. As expected, P_f reduces as c_{u1}/c_{u2} increases. The failure mechanism for the slopes with c_{u1}/c_{u2} less than 1 appears to be deep-seated. However, a toe failure mechanism was observed for the slopes with c_{u1}/c_{u2} greater than 1. It was found that a deep-seated failure was the critical mechanism as it yielded higher values of P_f.

In the second part of the analyses, the effect of varying COV and θ/H in each soil layer on P_f was investigated. The numerical results suggest that the lower or base layer has a higher influence on P_f of the slope. It was also found that failure surface is more likely to occur in the soil layer with a larger values of COV and θ/H.

Chapter 6

PREDICTION OF RELIABILITY OF SPATIALLY RANDOM COHESIVE SLOPES USING ARTIFICIAL NEURAL NETWORKS

6.1 Introduction

In Chapter 4, a series of parametric studies were conducted, using the random finite element method (RFEM) and the Monte Carlo simulation, to investigate the effect of spatial variability of undrained cohesion, c_u, on the probability of failure, P_f, of a spatially random cohesive slope. These studies provided an insight into the effects of various parameters on the reliability of a spatially random cohesive slope. However, the major drawback of the RFEM and Monte Carlo simulation is that they are computationally intensive. Performing parametric studies or sensitivity analysis is therefore a time-consuming task. Furthermore, the RFEM computer program (i.e. *rslope2d*) is not readily available and widely used in practice, hence, the use of this method to estimate probability of failure of a slope is limited. To overcome this limitation, a series of probabilistic stability charts were developed in Chapter 4, as presented in Appendix A, which can be used for a quick and preliminary estimation of the probability of failure, P_f. However, it would be more useful if a relationship between the input and output parameters of the spatially random cohesive slope problem can be established, ideally in the form of a simple equation so that it can be readily used in practice.

To achieve this aim, this chapter investigates the feasibility of using artificial neural networks (ANNs), a powerful data mapping tool, to establish such an input/output

relationship so that it can be used to predict the probability of failure, P_f, of a spatially random cohesive slope with virtually any combination of input values. As discussed in Section 2.5.2, multi-layer perceptrons (MLPs) that are trained with the back-propagation algorithm are a type of ANN that has a high capability of data mapping, and they have been successfully used in a wide range of geotechnical problems. Therefore, MLPs trained with the back-propagation algorithm are used in this study.

6.2 Development of ANN Models

In this study, the ANN models were developed using the software *Neuframe* Version 4 (Neusciences 2000). The procedures for ANN model development proposed by Maier and Dandy (2000), as given in Section 2.5.3, were used as a guide in this work. The data used to calibrate and validate the ANN model were obtained from the parametric studies that were conducted in Chapter 4 using the random finite element method (RFEM). Additional parametric studies for the slopes with $\theta/H = 0.2$, which were not considered in Chapter 4, were also conducted to obtain more case records for slopes with small θ/H. As a result, there were a total of 1,440 individual case records and each with a different combination of input and output values.

6.2.1 Input and Output Variables

As discussed in Chapter 4, five parameters have a significant impact on the probability of failure, P_f, of a spatially random cohesive slope. They are the slope angle, β, the depth factor, D, stability number, N_s, coefficient of variation, COV, and the normalised scale of fluctuation, θ/H. It should be noted that N_s was previously defined in Chapter 4 (Equation 4.1) as the mean undrained cohesion, μ_{c_u}, normalised by unit weight, γ, and slope height, H. These five parameters were used as the input variables for the ANN model. The model output was therefore the probability of failure, P_f. The range of each parameter examined in the analyses that follow is given in Table 6.1.

Table 6.1 Summary of range for input and output variables

Input/output variables	Range
Slope angle, β	14° – 45°
Depth factor, D	1 – 3
Stability number, N_s	0.1 – 0.5
Coefficient of variation, COV	0.1 – 1.0
Normalised scale of fluctuation, θ/H	0.1 – 10
Probability of failure, P_f	0 – 1

6.2.2 Data Division and Pre-processing

The parametric studies that were performed in Chapter 4 produced a total of 1,440 cases with different combinations of input and output values. Since cross-validation (Stone 1974) was used as the stopping criteria in calibrating the ANN model, the data were randomly divided into three sets: training, testing and validation. In total, 80% (i.e. 1,152 case records) of the data were used for model calibration and 20% (i.e. 288 case records) were used for model validation. The calibration data were further divided into 70% (i.e. 806 case records) for the training set and 30% (i.e. 346 case records) for the testing set. The data division for ANN model development is shown in Figure 6.1.

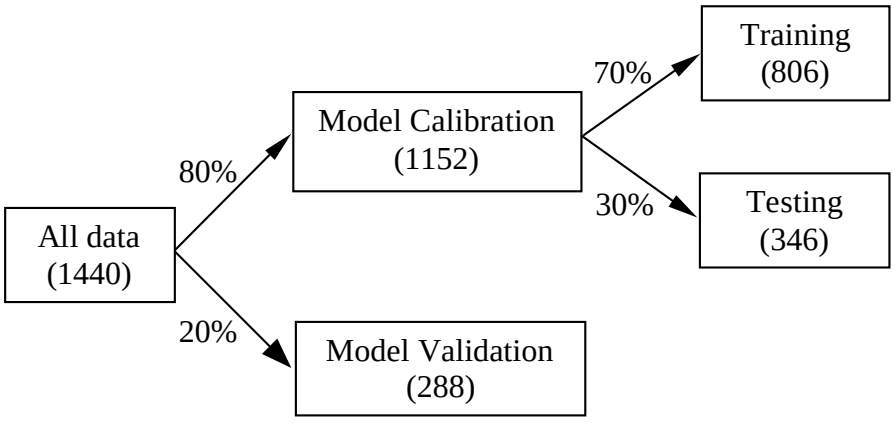

Figure 6.1 Data division for ANN model development

When dividing the data, it is essential to ensure that the data used for training, testing and validation represent the same statistical population, as recommended by Masters (1993). This is achieved by randomly choosing several combinations of the training, testing and validation sets until three statistical consistent data sets are obtained, as proposed by Shahin et al. (2004). The statistics of the data used for the training, testing and validation sets are given in Table 6.2, which includes the mean, standard deviation, maximum, minimum and range. It can be seen that the data used for the training, testing and validation are statistically consistent, which suggests that they represent similar statistical populations.

Table 6.2 Input and output statistic for ANN models

Model variables and data sets	Statistical parameters				
	Mean	**Std. Dev.**	**Minimum**	**Maximum**	**Range**
Slope angle, β (°)					
Training set	25.75	11.75	14.00	45.00	31.00
Testing set	25.97	11.98	14.00	45.00	31.00
Validation set	26.73	12.08	14.00	45.00	31.00
Depth factor, D					
Training set	1.98	0.82	1.00	3.00	2.00
Testing set	2.08	0.80	1.00	3.00	2.00
Validation set	1.95	0.81	1.00	3.00	2.00
Stability number, N_s					
Training set	0.29	0.14	0.10	0.50	0.40
Testing set	0.31	0.14	0.10	0.50	0.40
Validation set	0.31	0.14	0.10	0.50	0.40
Coefficient of variation, COV					
Training set	0.48	0.34	0.10	1.00	0.90
Testing set	0.46	0.32	0.10	1.00	0.90
Validation set	0.49	0.34	0.10	1.00	0.90
Dimensionless scale of fluctuation, θ/H					
Training set	2.87	3.69	0.10	10.00	9.90
Testing set	2.76	3.59	0.10	10.00	9.90
Validation set	2.65	3.53	0.10	10.00	9.90
Probability of failure, P_f					
Training set	0.301	0.413	0.000	1.000	1.000
Testing set	0.268	0.394	0.000	1.000	1.000
Validation set	0.276	0.397	0.000	1.000	1.000

Once the available data have been divided into their subsets, the input and output variables were pre-processed by scaling them to eliminate their dimension and to ensure that all variables receive equal attention during training (Masters 1993), using Equation (2.49), as previously shown in Section 2.5.3.

6.2.3 Network Architecture and Performance of ANN Models

After establishing the required three data sets: training, testing and validation, the next step was to 'train' the ANN model. As previously discussed in Section 2.5.2, 'training' involves repeatedly presenting a series of input/output pattern sets to the networks. The networks gradually learn the input/output relationship by adjusting the weights to minimise the error between the actual and predicted output patterns of the training sets. Cross-validation using the testing data sets was adopted as the stopping criteria for the ANN models to avoid overfitting. The validation data sets were then used to assess the accuracy of the developed ANN model using data that were not used for either training or testing.

As mentioned in Section 2.5.2, neural networks with different numbers of hidden layers and nodes may perform differently. Furthermore, network internal parameters such the learning rate, momentum term, and the use of different transfer functions may also affect the performance of the developed ANN models. The following sections investigate the effects of the above-mentioned factors on the performance of the developed ANN models. The performance of the ANN models was measured by three standard performance measures: the correlation coefficient, r, the root mean square error, RMSE, and the mean absolute error, MAE, as previously discussed in Section 2.5.2.

6.2.3.1 Effect of Numbers of Hidden Layers and Nodes on Performance of ANN Models

The network architecture was determined using a trial-and-error approach in which the ANN models were trained with different numbers of hidden layers and nodes. In this study, networks were developed with 1 and 2 hidden layers and 2, 4, 6, 8, 10, and 12 nodes in each layer. It should be noted that an equal number of nodes was used in each hidden layer for the 2 hidden layers models. The *tanh* and *sigmoid* transfer functions were used in the hidden and output layers, respectively. Other internal parameters such as the learning

rate and momentum term were fixed at the software's default values, i.e. learning rate = 0.2 and momentum term = 0.8. The effect of varying the learning rate and momentum term, and the use of different transfer functions in the hidden and output layer on the performance of ANN models is discussed later.

The performance of the developed ANN models with different numbers of hidden layers and nodes is summarised in Table 6.3. The ANN models developed in this section are designated by the names 'A1' to 'A12'. It should be noted that models that perform better are ones with a higher value of *r* and a lower value of RMSE and MAE. It can be seen from Table 6.3 that models with 2 hidden layers generally perform better than the models with one hidden layer, except for Model A7, which has only 2 nodes in each hidden layer. It is also observed that models with a larger number of hidden layer nodes perform better than the models with a lesser number of nodes in the hidden layers.

Table 6.3 Performance of ANN models with different number of hidden layers and nodes

Model No.	No. hidden layers	No. hidden nodes	Performance measures								
			r			RMSE			MAE		
			T	S	V	T	S	V	T	S	V
A1	1	2	0.971	0.970	0.972	0.100	0.097	0.094	0.051	0.049	0.051
A2	1	4	0.988	0.982	0.982	0.064	0.074	0.075	0.028	0.033	0.034
A3	1	6	0.992	0.987	0.988	0.053	0.064	0.062	0.024	0.029	0.030
A4	1	8	0.994	0.988	0.989	0.046	0.061	0.059	0.021	0.027	0.026
A5	1	10	0.996	0.991	0.990	0.036	0.052	0.056	0.015	0.021	0.024
A6	1	12	0.996	0.991	0.990	0.038	0.054	0.058	0.015	0.023	0.024
A7	2	2	0.969	0.961	0.967	0.103	0.111	0.102	0.054	0.057	0.054
A8	2	4	0.990	0.983	0.983	0.059	0.073	0.073	0.029	0.034	0.036
A9	2	6	0.999	0.994	0.995	0.021	0.045	0.038	0.009	0.017	0.016
A10	2	8	0.998	0.998	0.996	0.024	0.028	0.034	0.010	0.013	0.014
A11	2	10	0.998	0.995	0.996	0.025	0.040	0.037	0.010	0.017	0.016
A12	2	12	0.999	0.996	0.996	0.022	0.035	0.035	0.009	0.015	0.014

T = training; S = testing and V = validation.

The effect of the number of hidden layers and nodes on the performance of ANN models for the validation data is plotted in Figure 6.2. It can be seen that the performance of the ANN models improves significantly when the number of hidden layer nodes increases from 2 to 6. However, the improvement is minimal when the hidden layer nodes further

increases from 6 to 12. Figure 6.2 also shows that the ANN models with 2 hidden layers perform better than the models with only 1 hidden layer when there are 6 or more nodes in the hidden layer. Increasing the number of hidden layers has less impact for models with 2 and 4 nodes in the hidden layer.

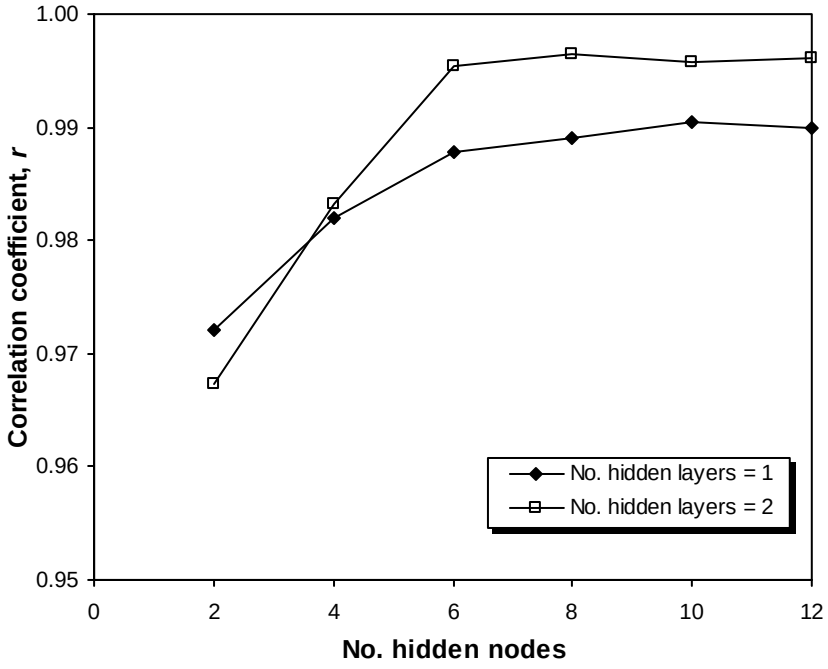

Figure 6.2 Effect of the numbers of hidden layers nodes on correlation coefficient, *r*, for the validation data set of ANN Models A1 – A12 (learning rate = 0.2; momentum term = 0.8)

Based on the results shown in Table 6.3, the optimum ANN model can be determined. According to Shahin and Jaksa (2005), a model is deemed to be optimum if it combines three categories: (i) the model provides good performance with respect to the testing set; (ii) the model has a minimum number of hidden layers and nodes; and (iii) the model has consistent performance on the validation set with that obtained on the training and testing sets. Based on the computed values of *r*, RMSE and MAE of the developed ANN models, Model A12 appears to be the optimum model. However, Model A12 has 2 hidden layers with 12 nodes in each layer, which becomes impractical to transform into formulae. This is because a total of 25 equations are required to describe the relationship between the input and output variables. Therefore, for the purpose of developing a set of practical

equations, Model A3 is considered to be optimum. Model A3 has 1 hidden layer with 6 nodes in each layer, which only requires 7 equations to describe the relationship between the input and output variables. It should be noted that the relative error between the Model A3 and A12, for the correlation coefficient, *r*, is less than 1%, which is insignificant. The details of transforming Model A3 into a set of practical equations for predicting the probability of failure of a spatially random cohesive slope is described later.

6.2.3.2 Effect of Learning Rate and Momentum Term on Performance of ANN Models

The effect of learning rate and momentum term on the performance of ANN models was investigated by varying these two parameters within the range of 0.01 – 0.95 (i.e. 0.01, 0.1, 0.2, 0.4, 0.6, 0.8, 0.9, and 0.95). The number of hidden layers and nodes were fixed at 1 and 6, respectively, which has the same network architecture to that of Model A3, as previously shown in Table 6.3.

The performance of ANN models with different learning rates and momentum terms is summarised in Tables 6.4 and 6.5, respectively. It should be noted that when one parameter was varied the other parameter was kept constant at their default values (i.e. momentum term = 0.8 and learning rate = 0.2). Figures 6.3 and 6.4 shows the effect of varying the learning rate and momentum term on the correlation coefficient, *r*, for the validation data set, respectively. In can be seen from both Figures 6.3 and 6.4 that the effect of varying the learning rate and momentum term on model performance is not as significant as varying the number of hidden layers and nodes. It was found that the optimum learning rate = 0.2 and momentum term = 0.8, which are the software's default values.

6.2.3.3 Effect of Using Different Transfer Functions on Performance of ANN models

The effect of using different transfer functions in the hidden and output layers is shown in Table 6.6. Better performance was observed for the models with a *sigmoid* transfer function in the output layer (i.e. Models D1 and D2). However, Model D1, which uses a *tanh* function in its hidden layer, performs slightly better than Model D2, which uses a *sigmoid* function in its hidden layer.

Table 6.4 Performance of ANN models with different learning rates

Model No.	Learning rate	Performance measures								
		r			RMSE			MAE		
		T	S	V	T	S	V	T	S	V
B1	0.01	0.985	0.983	0.978	0.072	0.074	0.083	0.032	0.034	0.040
B2	0.1	0.987	0.984	0.982	0.066	0.071	0.075	0.029	0.033	0.035
B3	0.2	0.992	0.987	0.988	0.053	0.064	0.062	0.024	0.029	0.030
B4	0.4	0.991	0.985	0.986	0.056	0.069	0.067	0.024	0.032	0.032
B5	0.6	0.993	0.986	0.988	0.050	0.067	0.063	0.022	0.029	0.027
B6	0.8	0.993	0.985	0.986	0.049	0.070	0.067	0.022	0.030	0.029
B7	0.9	0.993	0.984	0.986	0.049	0.071	0.068	0.022	0.030	0.029
B8	0.95	0.993	0.984	0.986	0.050	0.071	0.068	0.022	0.031	0.029

T = training; S = testing and V = validation.

Table 6.5 Performance of ANN models with different momentum terms

Model No.	Momentum term	Performance measures								
		r			RMSE			MAE		
		T	S	V	T	S	V	T	S	V
C1	0.01	0.986	0.984	0.980	0.068	0.071	0.078	0.030	0.033	0.037
C2	0.1	0.987	0.984	0.981	0.066	0.070	0.077	0.030	0.033	0.036
C3	0.2	0.986	0.983	0.979	0.069	0.073	0.081	0.031	0.034	0.037
C4	0.4	0.992	0.987	0.987	0.052	0.063	0.064	0.024	0.029	0.030
C5	0.6	0.987	0.984	0.982	0.066	0.071	0.075	0.029	0.033	0.035
C6	0.8	0.992	0.987	0.988	0.053	0.064	0.062	0.024	0.029	0.030
C7	0.9	0.990	0.982	0.985	0.061	0.076	0.069	0.026	0.035	0.032
C8	0.95	0.989	0.983	0.981	0.060	0.072	0.077	0.029	0.033	0.035

T = training; S = testing and V = validation.

Table 6.6 Performance of ANN models using different transfer functions

Model No.	Transfer function in hidden layer	Transfer function in output layer	Performance measures								
			r			RMSE			MAE		
			T	S	V	T	S	V	T	S	V
D1	Tanh	Sigmoid	0.992	0.987	0.988	0.053	0.064	0.062	0.024	0.029	0.030
D2	Sigmoid	Sigmoid	0.991	0.986	0.985	0.056	0.067	0.069	0.024	0.030	0.031
D3	Tanh	Tanh	0.976	0.970	0.968	0.096	0.103	0.107	0.060	0.064	0.066
D4	Sigmoid	Tanh	0.973	0.959	0.962	0.096	0.112	0.109	0.054	0.061	0.061

T = training; S = testing and V = validation.

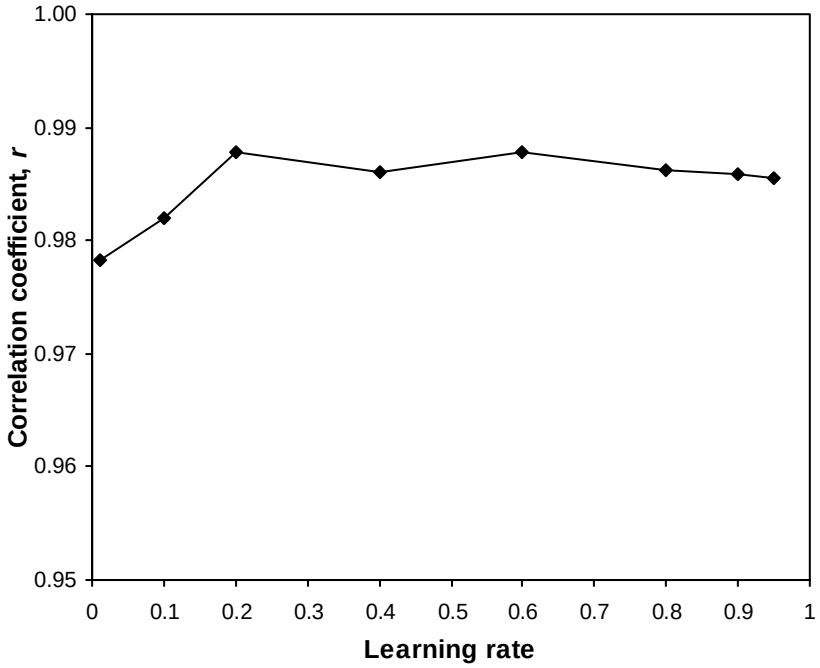

Figure 6.3 Effect of the learning rate on correlation coefficient, *r*, for the validation data set of the ANN model A3 (momentum term = 0.8)

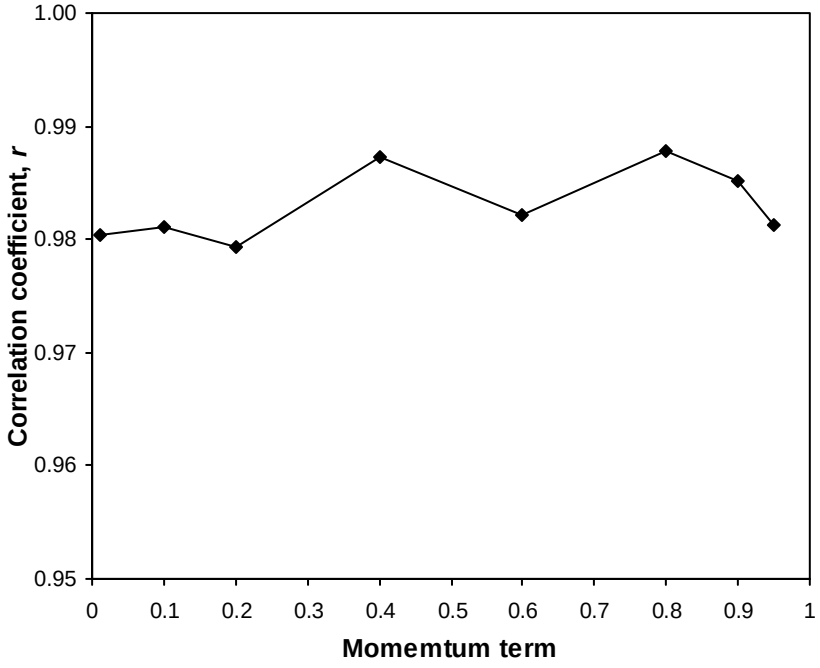

Figure 6.4 Effect of the momentum term on correlation coefficient, *r*, for the validation data set of the ANN model A3 (learning rate = 0.2)

6.3 Development of ANN Model Equation

One of the aims of this chapter is to develop a simple input/output relationship that can be used for prediction of the reliability of a spatially random cohesive slope. It was determined in Section 6.2.3.1 that Model A12, which has 2 hidden layers with 12 hidden nodes in each hidden layer, was the most accurate ANN model. However, as discussed previously, translating this ANN model into simple equation becomes impractical due to the large number of hidden layers and nodes. The use of this ANN model for predicting the probability of failure, P_f, of a cohesive slope is therefore limited to the users who have access to neural network software (e.g. *Neuframe*).

For the purpose of developing a relatively simple equation that can be used for predicting the probability of failure, P_f, of a spatially random cohesive slope, Model A3 is considered suitable. Model A3 has 1 hidden layer with 6 nodes and performs reasonably well, although not as good as Model A12. However, considering the large uncertainties in estimating soil properties, the difference in accuracy between Models A3 and A12 is considered acceptable. The structure of Model A3 is shown in Figure 6.5 and its connection weights and biases are shown in Table 6.7.

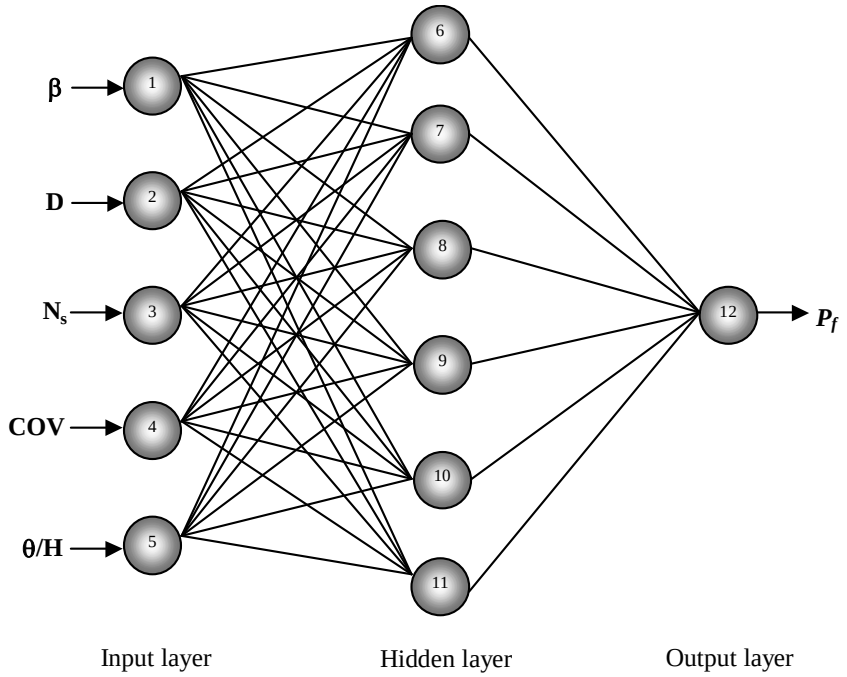

Figure 6.5 Structure of the ANN Model A3

Table 6.7 Weights and biases for the ANN Model A3

Hidden layer nodes	w_{ji} (weight from node i in the input layer to node j in the hidden layer)					Hidden layer bias (θ_i)
	i = 1	i = 2	i = 3	i = 4	i = 5	
j = 6	-1.386	0.936	6.080	3.140	1.006	0.175
j = 7	0.217	0.227	5.689	-4.667	-2.092	-0.943
j = 8	-2.937	-0.719	3.673	-2.058	-1.680	0.642
j = 9	-0.682	-3.259	0.573	-0.916	-0.887	0.846
j = 10	1.136	1.761	-4.868	0.416	-5.032	-0.099
j = 11	0.060	0.560	-4.715	0.177	-0.792	0.152

Output layer nodes	w_{ji} (weight from node i in the input layer to node j in the hidden layer)						Output layer bias (θ_i)
	i = 6	i = 7	i = 8	i = 9	i = 10	i = 11	
j = 12	-5.343	-5.905	-4.3266	-2.126	3.227	3.120	-0.929

Using the connection weights and biases shown in Table 6.7, the predicted probability of failure can be expressed as follows:

$$P_f = \frac{1}{1+e^{(0.929+5.343\tanh H_1+5.905\tanh H_2+4.327\tanh H_3+2.126\tanh H_4-3.227\tanh H_5-3.120\tanh H_6)}} \quad (6.1)$$

where:

$$H_1 = 0.175 - 1.386\beta + 0.936D + 6.08N_s + 3.14COV + 1.006(\theta/H) \quad (6.2)$$

$$H_2 = -0.943 + 0.217\beta + 0.227D + 5.689N_s - 4.667COV - 2.092(\theta/H) \quad (6.3)$$

$$H_3 = 0.642 - 2.937\beta - 0.719D + 3.673N_s - 2.058COV - 1.68(\theta/H) \quad (6.4)$$

$$H_4 = 0.846 - 0.682\beta - 3.259D + 0.573N_s - 0.916COV - 0.887(\theta/H) \quad (6.5)$$

$$H_5 = -0.099 + 1.136\beta + 1.761D - 4.868N_s + 0.416COV - 5.032(\theta/H) \quad (6.6)$$

$$H_6 = 0.152 + 0.06\beta + 0.56D - 4.715N_s + 0.177COV - 0.792(\theta/H) \quad (6.7)$$

It should be noted that, the predicted probability of failure, P_f, obtained from Equation (6.1) is scaled between 0.0 and 1.0 and in order to obtain the actual value, this P_f has to be re-scaled using Equation (2.49) and data ranges in Table 6.1. However, since the data range for P_f is also between 0.0 and 1.0, Equation (6.1) remains unchanged. It should also be noted that, before using Equations (6.2) to (6.7), all input variables (i.e. β, D, N_s, COV and θ/H) need to be scaled between 0.0 and 1.0 using Equation (2.49) and the data ranges in Table 6.1. Accounting for this, Equations (6.2) to (6.7) are hence rewritten as follows:

$$H_1 = 1.494 - 0.045\beta + 0.468D + 15.2N_s + 3.489COV + 0.102(\theta/H) \quad (6.8)$$

$$H_2 = -2.037 + 0.007\beta + 0.114D + 14.223N_s - 5.185COV - 0.211(\theta/H) \quad (6.9)$$

$$H_3 = 1.656 - 0.095\beta - 0.36D + 9.183N_s - 2.287COV - 0.17(\theta/H) \quad (6.10)$$

$$H_4 = 2.752 - 0.022\beta - 1.63D + 1.433N_s - 1.018COV - 0.09(\theta/H) \quad (6.11)$$

$$H_5 = -0.271 + 0.037\beta + 0.881D - 12.17N_s + 0.462COV - 0.508(\theta/H) \quad (6.12)$$

$$H_6 = 1.012 + 0.002\beta + 0.28D - 11.788N_s + 0.197COV - 0.08(\theta/H) \quad (6.13)$$

It should be noted that Equation (6.1) is valid only for the ranges of values of β, D, N_s, COV and θ/H given in Table 6.1. This is because ANN models perform best in interpolation but not extrapolation (Flood and Kartam 1994; Minns and Hall 1996). The developed ANN equations, i.e. Equations (6.1), and (6.8) to (6.13), can therefore be used as an alternative method to the random finite element method (RFEM) for predicting the probability of failure of a spatially random cohesive slope.

6.4 Sensitivity Analysis of the ANN Model Inputs

In an attempt to determine the relative importance of the various input variables, a sensitivity analysis was carried out on the ANN Model A3. This is achieved by using the method proposed by Garson (1991), which has been previously adopted by other researchers (e.g. Goh (1995a), Shahin et al. (2002b)) for the same purpose. This method involves partitioning the hidden-output connection weights of each hidden node into components associated with each input node. As mentioned previously, Model A3 has five input nodes, one hidden layer with six nodes and one output node. The connection weights were previously shown in Table 6.7 and they are rewritten as follows:

Hidden nodes	β	D	N_s	COV	θ/H	P_f
1	-1.386	0.936	6.080	3.140	1.006	-5.343
2	0.217	0.227	5.689	-4.667	-2.092	-5.905
3	-2.937	-0.719	3.673	-2.058	-1.680	-4.327
4	-0.682	-3.259	0.573	-0.916	-0.887	-2.126
5	1.136	1.761	-4.868	0.416	-5.032	-3.227
6	0.060	0.560	-4.715	0.177	-0.792	-3.120

The computation process proposed by Garson (1991) is as follows:

1. For each hidden node *i*, obtain the products P_{ij} (where *j* represent the column number of the weights mentioned above) by multiplying the absolute value of the hidden-output layer connection weight by the absolute value of the hidden-input layer connection weight of each input variable *j*. As an example: $P_{11} = 1.386 \times 5.343 = 7.405$.

Hidden nodes	β	D	N_s	COV	θ/H
1	7.405	5.001	32.485	16.777	5.375
2	1.281	1.340	33.594	27.559	12.353
3	12.708	3.111	15.893	8.905	7.269
4	1.450	6.929	1.218	1.947	1.886
5	3.666	5.683	15.709	1.342	16.238
6	0.187	1.747	14.711	0.552	2.471

2. For each hidden node, divide P_{ij} by the sum for all the input variables to obtain Q_{ij}. As an example: $Q_{11} = 7.405 / (7.405 + 5.001 + 32.485 + 16.777 + 5.375) = 0.110$.

Hidden nodes	β	D	N_s	COV	θ/H
1	0.110	0.075	0.485	0.250	0.080
2	0.017	0.018	0.441	0.362	0.162
3	0.265	0.065	0.332	0.186	0.152
4	0.108	0.516	0.091	0.145	0.140
5	0.086	0.133	0.368	0.031	0.381
6	0.010	0.089	0.748	0.028	0.126

3. For each input node, sum Q_{ij} to obtain S_j. As an example:

   $S_1 = 0.110 + 0.017 + 0.265 + 0.108 + 0.086 + 0.010 = 0.596.$

	β	D	N_s	COV	θ/H
Sum	0.596	0.895	2.465	1.003	1.041

4. Divide S_j by the sum of all the input variables to give the relative importance of all output weights attributed to the given input variable. As an example, the relative importance of input node 1 is equal to:

   $(0.596 \times 100) / (0.596 + 0.895 + 2.465 + 1.003 + 1.041) = 9.9\%$

	β	D	N_s	COV	θ/H
Relative importance (%)	9.9	14.9	41.1	16.7	17.4

The results indicate that the stability number, N_s, has the most significant effect on the predicted probability of failure, P_f, with a relative importance of 41.1%. This is followed by the normalised scale of fluctuation, θ/H, and the coefficient of variation, COV, each with a relative importance of 17.4% and 16.7%, respectively. The slope geometry parameters: depth factor, D, and slope angle, β, has relatively small impact on P_f, each with a relative importance of 14.9% and 9.9%. It should be noted that N_s is the mean undrained cohesion, c_u, normalised by the unit weight and slope height. Furthermore, θ/H and COV are parameters used to model the spatial variability of c_u. Therefore, the sensitivity analysis suggests that spatial variability of soil properties has a more significant impact on the reliability of a slope than the slope geometry parameters, for the geometries examined in the present analysis.

6.5 Summary

This chapter has investigated the feasibility of using artificial neural networks (ANNs) as an alternative approach to the random finite element method (RFEM) and Monte Carlo simulation for predicting the probability of failure, P_f, of a spatially random cohesive slope. Multi-layer perceptrons (MLPs) trained with the back-propagation algorithm were used in this study. The data used for the ANN model development and validation were obtained from the parametric studies conducted in Chapter 4 using RFEM and Monte Carlo simulation. A total of 1,440 case records were used and they were divided into three different data sets: training, testing and validation. The training and testing sets were used for model development or calibration, while the validation set was used for model validation.

The optimum ANN model was determined using a trial-and-error approach where the number of hidden layers and nodes was varied. The performance of the developed ANN models was measured by three standard performance measures: correlation coefficient, r, RMSE and MAE. It was found that the number of hidden layers and nodes has a significant effect on the performance of the ANN models. The ANN model that with 2 hidden layers with 12 nodes in each hidden layers was found to be the most accurate model, which has a correlation coefficient, r, of 0.996 for the validation data set. It was also found that the network internal parameters such as the learning rate and momentum term have less impact on ANN model performance compared to the number of hidden layers and nodes.

A simple equation was developed based on the ANN model that has 1 hidden layer with 6 nodes, which can be used to predict the probability of failure, P_f, of a spatially random cohesive slope. This equation can be used as an alternative approach to the more advanced but computationally intensive approach, i.e. RFEM. The sensitivity analysis of the ANN model inputs indicated the stability number, N_s, was the most important parameter with a relative importance of 41.1%. The other parameters ranked in the order of most to least important were θ/H, COV, D and β.

Chapter 7

SLOPE STABILITY ANALYSIS CONSIDERING EFFECT OF ROOT REINFORCEMENT

7.1 Introduction

As discussed in Chapter 2, it is well recognised that vegetation can have a significant effect on slope stability. Vegetation affects the stability of a slope through various processes, including modification of soil moisture content; root reinforcement; surcharging; buttressing and arching; and wind loading. However, there is a consensus in the literature that root reinforcement provides the most significant and important effect on slope stability. Much research has been conducted, in the past 30 years or so, to quantify the effects of root reinforcement on slope stability. The majority of is research has focussed on field or laboratory studies of root-filled soils and modification of limit equilibrium methods to incorporate the effect of root reinforcement. Despite the considerable amount of research conducted on this topic to date, there are a few issues that have yet to be addressed, as mentioned in Chapter 2.

Firstly, no study has been conducted to consider the effect of root reinforcement on slope stability using a numerical method, such as the finite element method (FEM). All the previous studies were based on limit equilibrium methods. As discussed in Chapter 2 (see Section 2.2.2), the FEM has the advantage of not requiring an advance assumption of the shape and location the critical slip surface. This is particularly useful for considering the effect of root reinforcement in deep-seated type slope failure because the critical slip surface is usually complex and unknown when vegetation is present. Secondly, there is no simple and straightforward solution (i.e. in the form of stability charts or simple formulae) available for the assessment of the stability of deep-seated vegetated slopes considering the

effect root reinforcement. Stability charts or formulae are more useful and practical for preliminary design and the assessment of slopes with a simple geometry. Finally, the spatial variability of root cohesion has not been considered in the previous slope stability analyses, hence, its influence on slope stability is yet to be investigated.

The overall aim of this chapter is to address the above-mentioned issues so that the effect of root reinforcement on slope stability can be modelled more accurately and the behaviour of vegetated slopes can be understood better. The precise objectives of this chapter are as follows:

1. To incorporate the effect of root reinforcement into the existing finite element slope stability model;

2. To investigate the effect of root reinforcement on slope stability using the finite element method;

3. To produce vegetated slope stability charts through parametric studies using the finite element method;

4. To develop an artificial neural network (ANN) model for calculating the factor of safety (FOS) of a slope considering the effect of root reinforcement and to transform the developed ANN model into a relatively simple formula which serves as an alternative tool to the developed stability charts; and

5. To investigate the effect of spatial variability of root cohesion as well as soil properties on slope stability using the random finite element method (RFEM).

7.2 Assessing Influence of Root Reinforcement on Slope Stability by Finite Element Method

It has been discussed in Section 2.4.3 that, the effect of root reinforcement can be modelled as an increase in apparent soil cohesion, called *root cohesion*, c_r. This root cohesion ultimately increases the shear strength of the soil. Various approaches have been established in the past to determine the value of c_r (see Section 2.4.3). Published data in the literature (see Table 2.6) suggested that the average value of c_r is most likely to be within the range of 1 kPa to 20 kPa.

The finite element model used in this study assumes a 2-dimensional plane-strain condition with an elastic-perfectly plastic soil model, which was developed by Smith and Griffiths (1998). The formulation and theoretical aspects of this finite element model has been previously discussed in Section 3.4. The effect of root reinforcement can be taken into account in the finite element slope stability analysis by adding the root cohesion, c_r, to the effective or drained cohesion, c', of the soil to give a total cohesion, c_{Total}, as given by:

$$c_{Total} = c' + c_r \tag{7.1}$$

In the finite element model, the soil elements that are affected by vegetation (known as the *root zone*) are assigned the total cohesion, c_{Total}, while, for other soil elements within the slope geometry, the effective soil cohesion, c', is used. The typical finite element model that consists of a root zone is shown in Figure 7.1. The grey shaded areas indicate the root zone and the extent of this root zone from the ground surface is defined by the parameter called the *depth of root zone*, h_r. This is the effective distance beyond which plant roots are assumed to cause little or no effect on the soil shear strength.

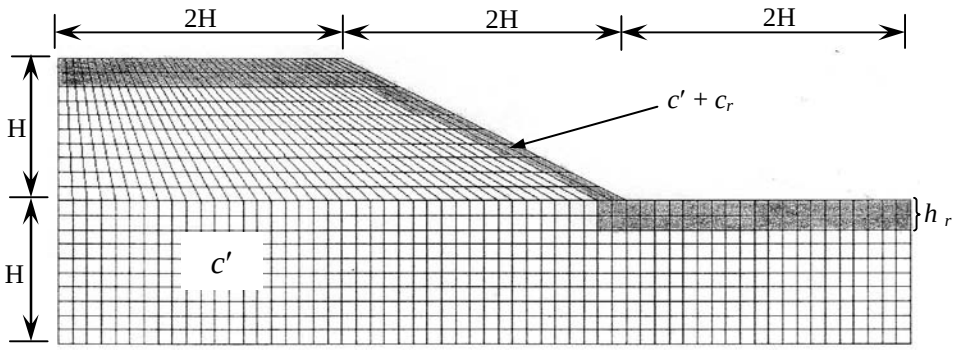

Figure 7.1 Typical finite element mesh for incorporating effect of root reinforcement

Numerical analyses, using the developed finite element model, were carried out to investigate the effect of root reinforcement on slope stability. A 2:1 homogenous slope (β = 26.6°) with a height, H, of 10 m was considered. The assumed soil properties were: γ = 20 kN/m^3; c' = 1 kPa; and ϕ' = 25°. These analyses were performed deterministically,

where a single average value for each parameter was used in the analyses. Considerations for spatial variability of root cohesion and soil properties using probabilistic analysis are discussed later.

It should be noted that vegetation could grow on any region of a natural slope. Therefore, in the first part of the deterministic analyses, the effect of the spatial distribution of vegetation on the stability of a slope was investigated. Vegetation was considered growing on different locations of a slope, as shown in Figure 7.2. In this study, the root cohesion, c_r, and the depth of root zone, h_r, were held constant at 10 kPa and 2 m, respectively. The factor of safety (FOS) for each case of slope shown in Figure 7.2 were computed and summarised in Table 7.1.

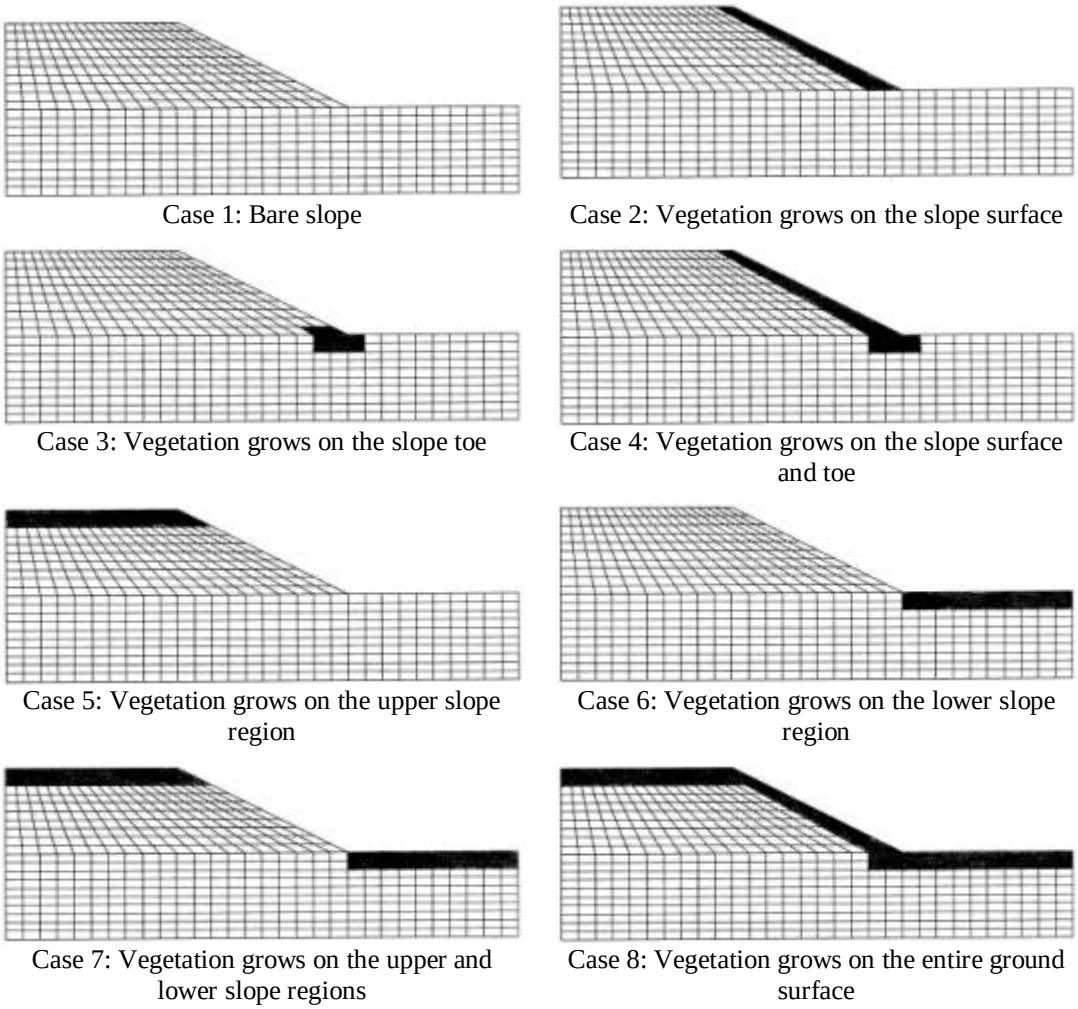

Figure 7.2 Vegetated slope with different locations of root zone

It is noted that, without including the effect of root reinforcement in the slope stability analysis (i.e. Case 1), the computed FOS for the slope is 1.05, which indicates the slope is in a marginally stable state. When vegetation grows on the entire slope (i.e. Case 8), the FOS increases from 1.05 to 1.25 (i.e. 19% increase), which has the most significant increase in FOS among all other cases. This is followed by the case with vegetation grows on the slope surface and toe (i.e. Case 4), in this case, the FOS was increased to 1.2 (i.e. 15% increase). However, when vegetation was grown only on the slope surface (i.e. Case 2) or on the upper slope region (i.e. Case 5), the increase in FOS was only 3%. Furthermore, when vegetation was grown only on the slope toe (i.e. Case 3) or on the lower slope region (i.e. Case 6), no improvement in FOS was observed. These results suggest that vegetation should be grown on entire ground surface of a slope or at least on the slope surface and toe, so that the beneficial effect of the root reinforcement on slope stability can be obtained.

Table 7.1 Computed FOS for the slope with different locations of root zone

Case	FOS	Increase (%)
1	1.05	-
2	1.08	3.0
3	1.05	0.0
4	1.20	15.0
5	1.08	3.0
6	1.05	0.0
7	1.08	3.0
8	1.25	19.0

In the second part of the analyses, vegetation was assumed growing on the entire ground surface (same as Case 8) and the value c_r was varied between 1 kPa and 20 kPa, while a h_r of 1 m and 2 m was considered. The results of these analyses are shown in Figure 7.3. It can be seen that the FOS of a vegetated slope (i.e. $c_r > 0$) is higher than that of a bare slope (i.e. $c_r = 0$). The increase in the FOS is dependent on the values of c_r and h_r. Generally, the FOS increases linearly with the values of c_r and h_r. For example, for an intermediate

value of c_r (i.e. c_r = 10 kPa), the FOS increased from 1.05 to 1.16 for the case with h_r = 1 m, and the FOS increased from 1.05 to 1.25 for the case with h_r = 2 m, or a 10% and 19% increment, respectively. For a high value of c_r (i.e. c_r = 20 kPa), the increments were 19% and 34%, respectively. It is noted that the percentage increase in the FOS is not directly proportional to the increment in the values of c_r. It is expected that the FOS will approach a maximum limiting value as the value of c_r keeps increasing. However, this maximum limiting value for the FOS was not investigated here because the extremely large value of c_r is not likely to be encountered in the real situations. Despite this, the results show that root reinforcement provides a significant improvement on the stability of a slope. The results also indicate that a marginally stable slope could become stable when the effect of root reinforcement is taken into consideration. In other words, an originally stable vegetated slope could become marginally stable after the vegetation is removed.

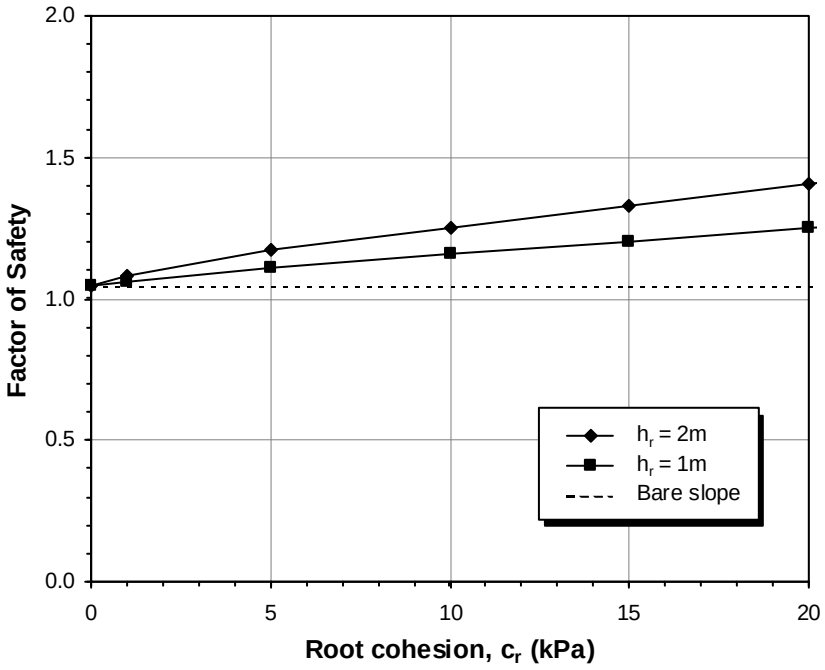

Figure 7.3 FOS versus root cohesion for different depths of root zone (c' = 1 kPa; ϕ' = 25°)

Figure 7.4 shows the effects of varying the values of c_r on the FOS of the slope with different values of effective soil cohesion, c', i.e. 1, 5, 10 and 20 kPa, while the other parameters are held constant at: γ = 20 kN/m^3; ϕ' = 25°; and h_r = 1 m. The computed FOS

for the slopes with c' of 1, 5, 10 and 20 kPa, without considering the effect of root reinforcement (i.e. $c_r = 0$), are 1.05, 1.33, 1.59 and 2.05, respectively. It is noted that the FOS increases as c_r increases for all the cases of c' considered. The maximum percentage increments in the FOS of the slopes with c' of 1, 5, 10 and 20 kPa, which were obtained when c_r = 20 kPa, are 19.4%, 10.6%, 7.8% and 5.3%, respectively.

Clearly, the slope with the lowest value of c' (i.e. lowest FOS) showed the highest percentage increment in the FOS when c_r = 20 kPa. In fact, the same phenomenon is observed for the cases with other values of c_r. This finding suggests that root reinforcement provides greater improvement to the stability of a slope with a lower FOS than a slope with a higher FOS.

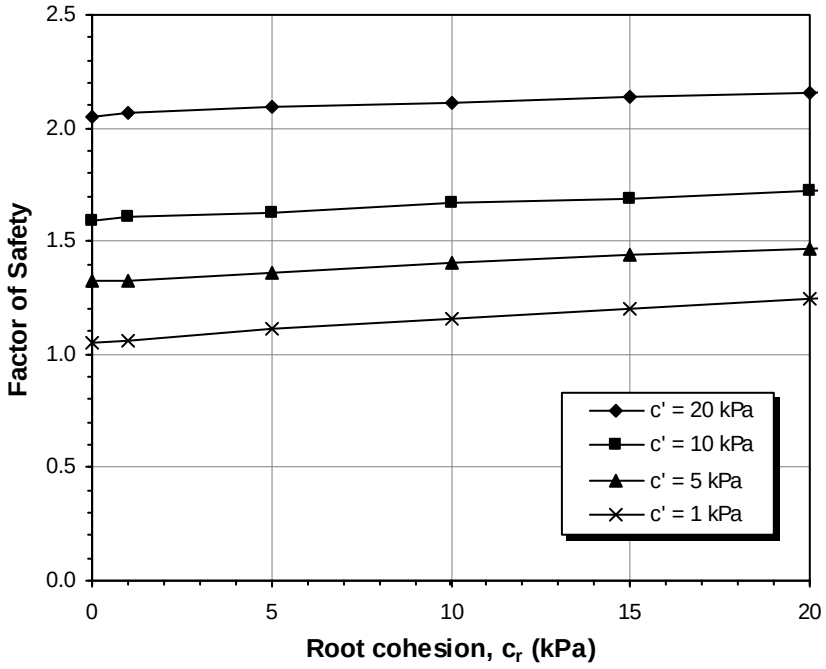

Figure 7.4 FOS versus root cohesion for different values of effective cohesion of soil (ϕ' = 25°; h_r = 1 m)

Figure 7.5 shows the plots of the FOS versus root cohesion, c_r, for the slopes with different values of friction angle, ϕ', i.e. 5°, 15°, 25° and 35°, while the other parameters are held constant at: γ = 20 kN/m^3; c' = 1 kPa; and h_r = 1 m. The FOS for the slopes with ϕ' of 5°, 15°, 25° and 35°, without considering the effect of root reinforcement (i.e. $c_r = 0$), are 0.27,

0.64, 1.05 and 1.53, respectively. It is noted that the slopes that with ϕ' of 5° and 15° are considered to be unstable or 'failed'.

It can be seen from Figure 7.5 that the FOS increases as c_r increases for all cases of ϕ' considered. The maximum percentage increments in FOS of the slopes with ϕ' of 5°, 15°, 25° and 35° are 35.0%, 24.3%, 19.4% and 14.3%, respectively. This observation is similar to that previously found in Figure 7.4 where the slope with a lower FOS obtains a greater in FOS than the slope with a higher FOS. The results in Figure 7.5 once again confirm that root reinforcement provides greater improvement to the stability of a slope with a lower FOS than a slope with a higher FOS.

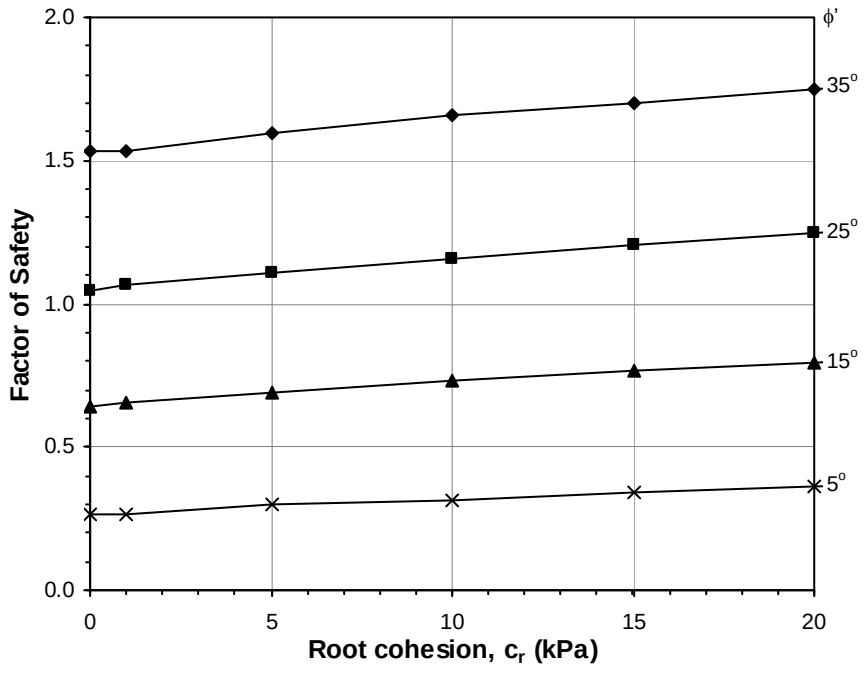

Figure 7.5 FOS versus root cohesion for different values of effective friction angle of soil (c' = 1 kPa; h_r = 1 m)

7.3 Vegetated Slope Stability Charts

In order to construct slope stability charts that can be used for assessing the effect of root reinforcement on slope stability, extensive parametric studies were carried out. The input parameters were systematically varied according to the values shown in Table 7.2. A total of 768 different combinations of input parameters were obtained based on the values shown in Table 7.2. The slope angles, β, of 18.4°, 26.6°, 45.0° and 63.4° correspond to slopes of 3:1, 2:1, 1:1 and 0.5:1, respectively. The depth factor, D, is not considered as a variable because in the case of a c'–ϕ' slope, especially when the value of c' is small, the slip surface will not extend deeper than the toe level. Therefore, a constant depth factor, D, of 2 was used. It is noted that the effective soil cohesion, c', is expressed as a dimensionless stability coefficient, $c'/\gamma H$. For example, when γ = 20 kN/m^3 and H = 10 m, values of $c'/\gamma H$ of 0.1, 0.05, 0.025 and 0.005 correspond to a c' of 20 kPa, 10 kPa, 5 kPa and 1 kPa, respectively. The constructed stability charts are presented in Figures 7.6 to 7.9.

Table 7.2 Input variables and values for parametric studies undertaken

Input variables	Values
Slope angle, β (degrees)	18.4, 26.6, 45.0, 63.4
Friction angle, ϕ' (degrees)	5, 15, 25, 35
Stability coefficient, $c'/\gamma H$	0.1, 0.05, 0.025, 0.005
Root cohesion, c_r (kPa)	0, 1, 5, 10, 15, 20
Depth of root zone, h_r (m)	1, 2

It can be observed from Figures 7.6 to 7.9 that, for all slope angles, FOS increase linearly as root cohesion increases. It also noted that the increase in FOS is more significant for the steeper slopes and those with a lower value of FOS. This observation suggests that vegetation is a useful method of slope stabilisation, especially for steep slopes with a low value of FOS.

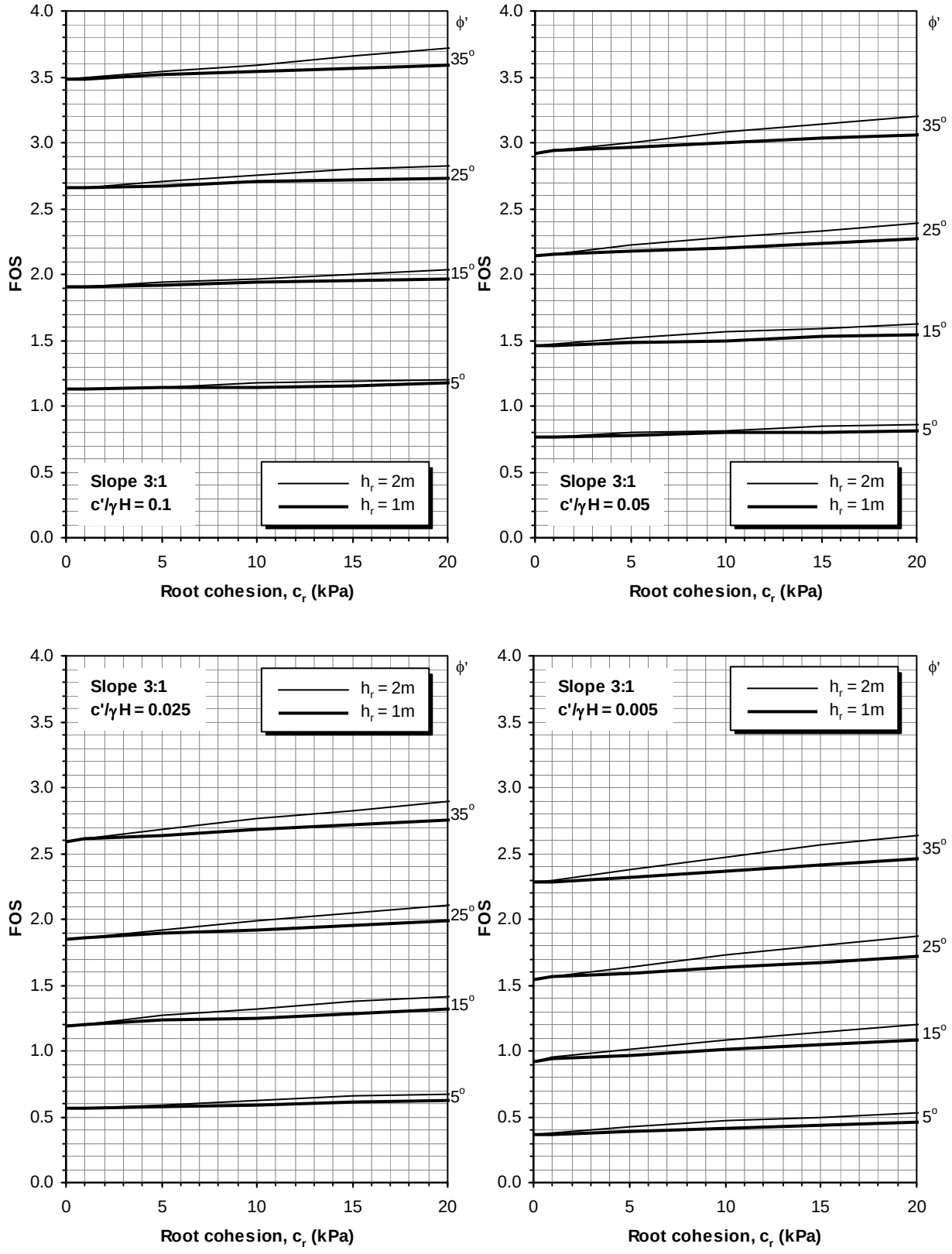

Figure 7.6 Stability charts for 3:1 vegetated slope

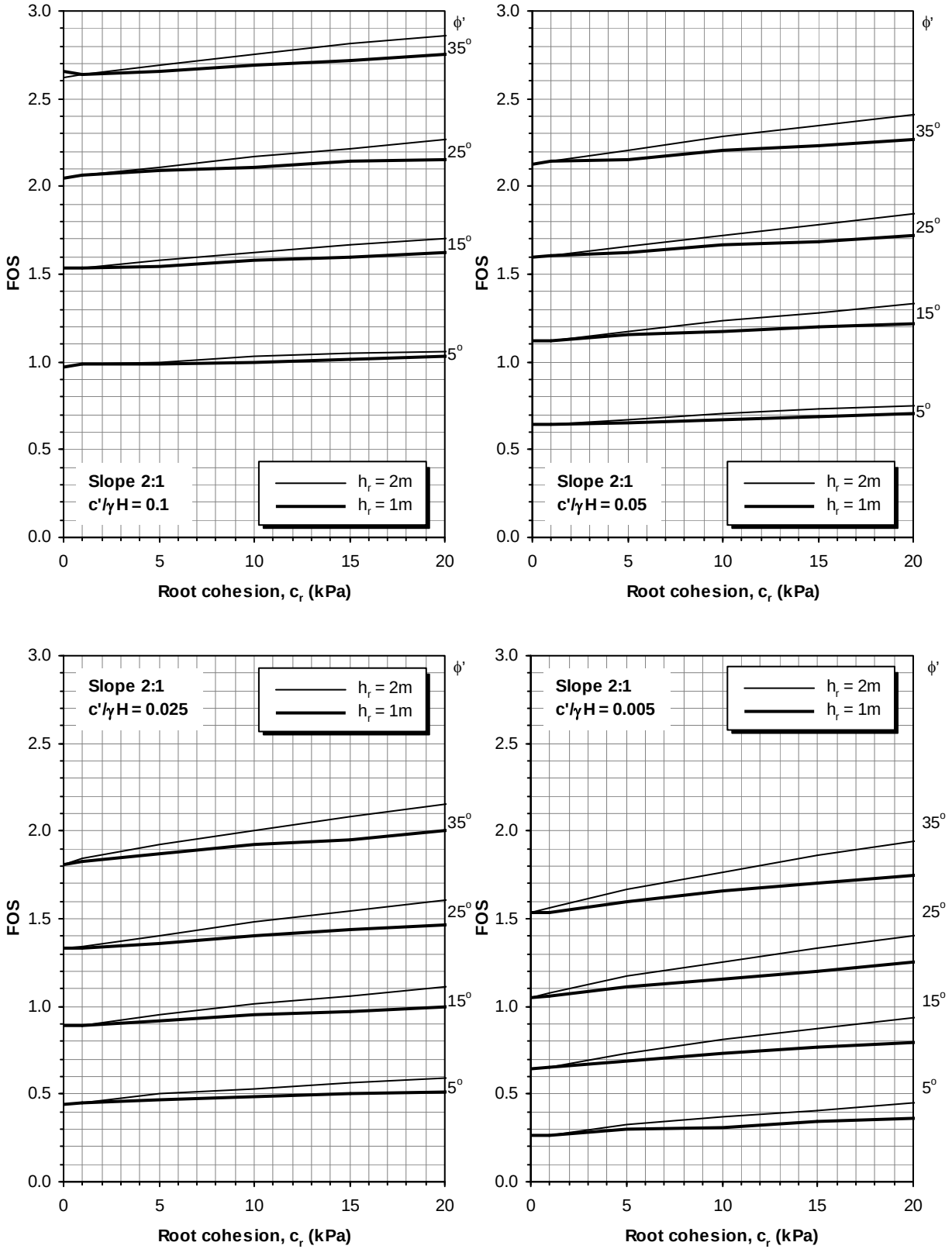

Figure 7.7 Stability charts for 2:1 vegetated slope

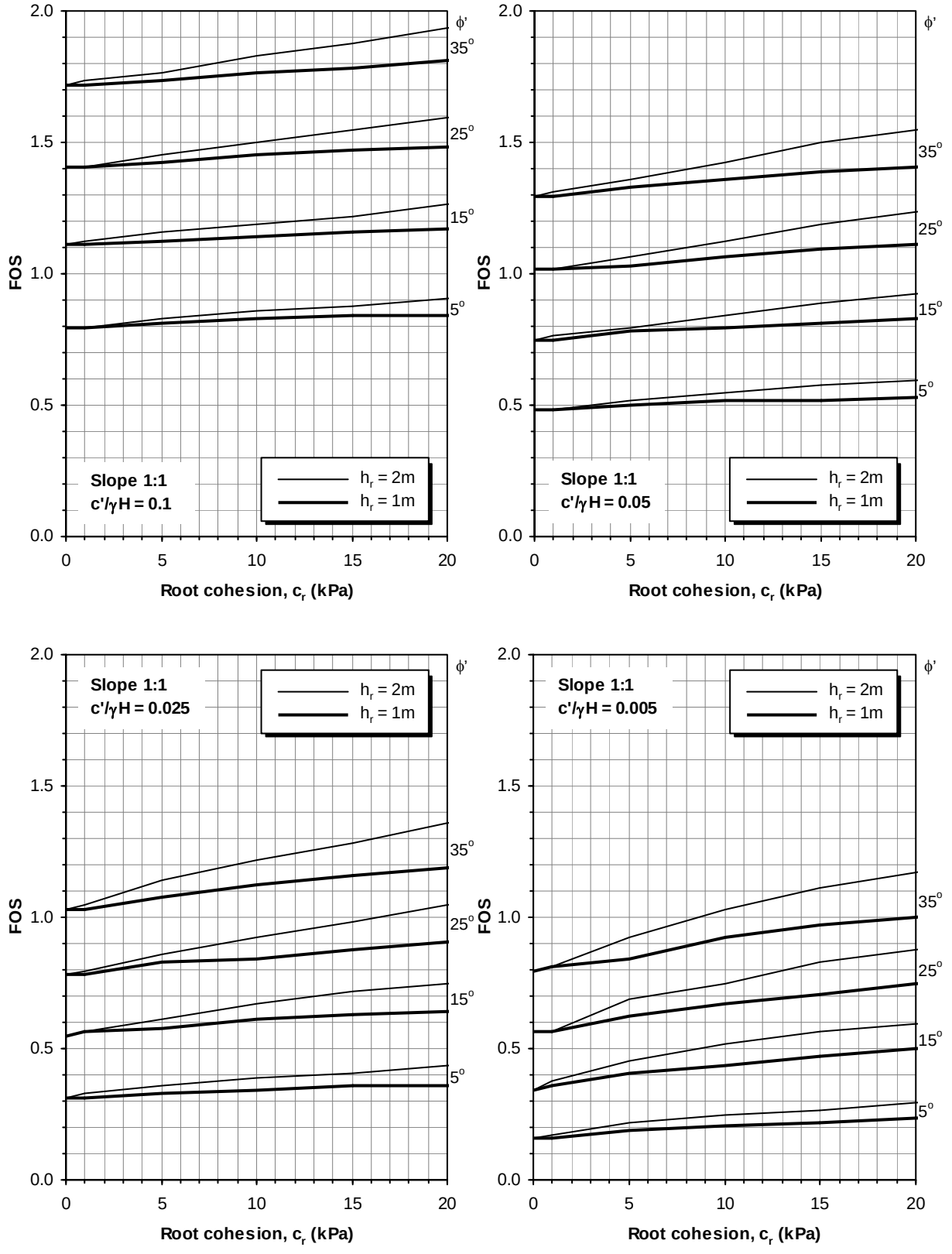

Figure 7.8 Stability charts for 1:1 vegetated slope

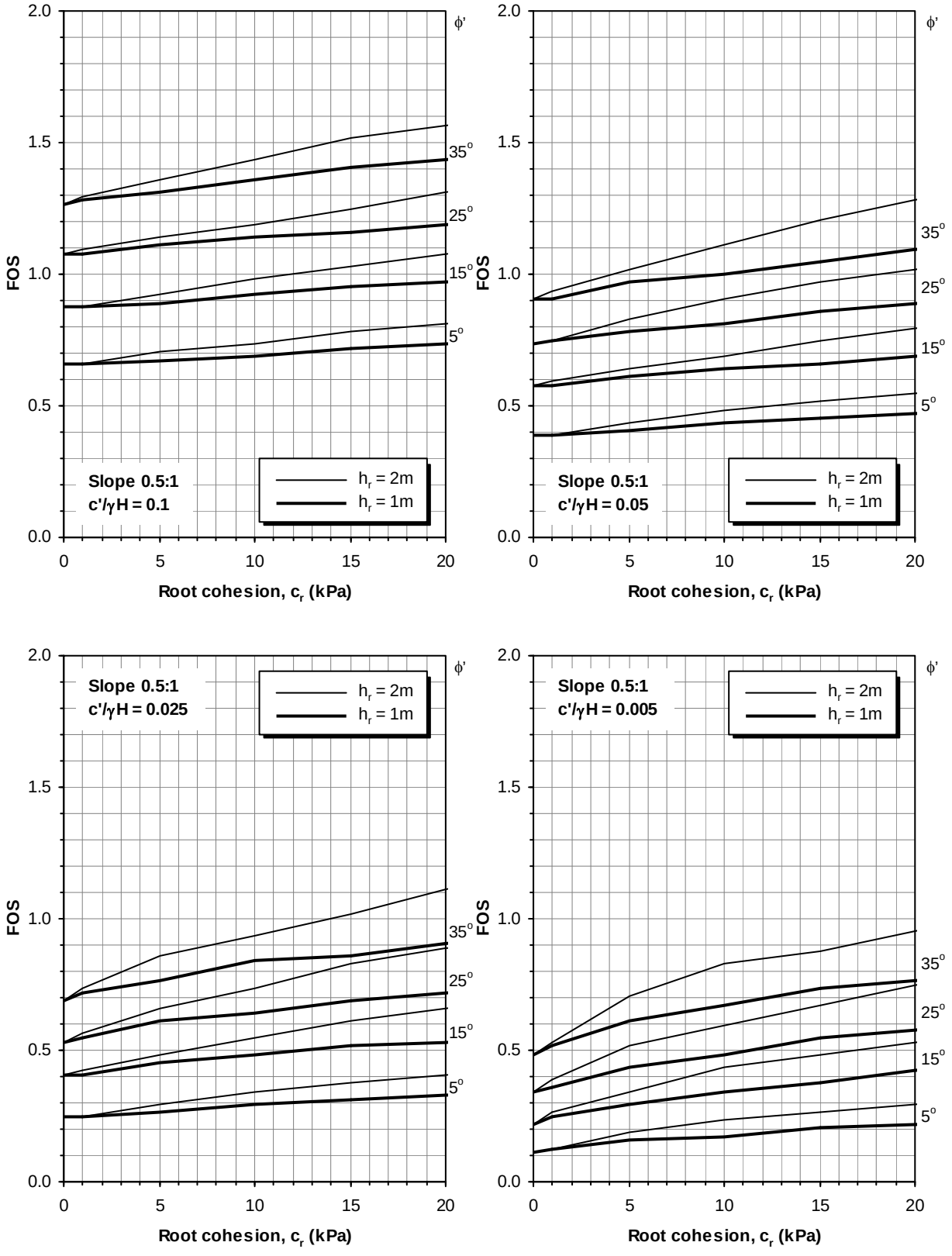

Figure 7.9 Stability charts for 0.5:1 vegetated slope

7.4 Artificial Neural Networks Modelling

This section attempts to develop an artificial neural network (ANN) model for predicting the factor of safety (FOS) of a vegetated slope with considering the effects of root reinforcement. The developed ANN model is then transformed into a simple equation so that it can be readily used in practice. Back-propagation multi-layer perceptrons (MLPs) are used for the ANN model development. The theoretical aspects of back-propagation MLPs have been described in Section 2.5.2. The procedures for ANN model development have also been discussed in Section 2.5.3 and have been adopted in the development of the ANN model for predicting the probability of failure of a spatially random cohesive slope, as presented in Chapter 6. The same procedures for ANN model development are adopted in this section.

7.4.1 Input and Output Variables

As discussed in Section 7.3, five parameters are required to predict the FOS of a vegetated slope with the effect of root reinforcement. They are the slope angle, β, friction angle, ϕ', stability coefficient, $c'/\gamma H$, root cohesion, c_r, and depth of root zone, h_r. These five parameters are used as the input variables for the ANN model. The output for the ANN model is the factor of safety, FOS. The range of each parameter is given in Table 7.3.

Table 7.3 Summary of range for input and output variables

Input/output variables	Range
Slope angle, β (degrees)	18.4 – 63.4
Friction angle, ϕ' (degrees)	5 – 35
Stability coefficient, $c'/\gamma H$	0.005 – 0.1
Root cohesion, c_r (kPa)	0 – 20
Depth of root zone, h_r (m)	1 – 2
Factor of safety, FOS	0.109 – 3.719

7.4.2 Database

In Section 7.3, extensive parametric studies were conducted in order to construct the vegetated slope stability charts. The results of these numerical analyses are used as the data required for ANN model development. As discussed previously in Section 2.5.3, when cross-validation (Stone 1974) is used as the stopping criteria for calibrating the ANN model, the data are randomly divided into three sets: training, testing and validation. In total, 80% (i.e. 614 case records) of the data were used for model calibration and 20% (i.e. 154 case records) were used for model validation. The calibration data were further divided into 70% (i.e. 430 case records) for the training set and 30% (i.e. 184 case records) for the testing set. The schematic representation of data division for ANN model development is shown in Figure 7.10.

The data are randomly divided into several combinations of the training, testing and validation until three statistical consistent data sets are obtained, as proposed by Shahin et al. (2004). The statistics of the data used for the training, testing and validation sets are given in Table 7.4. It can be seen that the data used for training, testing and validation are statistically consistent, which indicates that they represent the same statistical population. The data are then pre-processed using Equation (2.49), as discussed in Section 2.5.3.

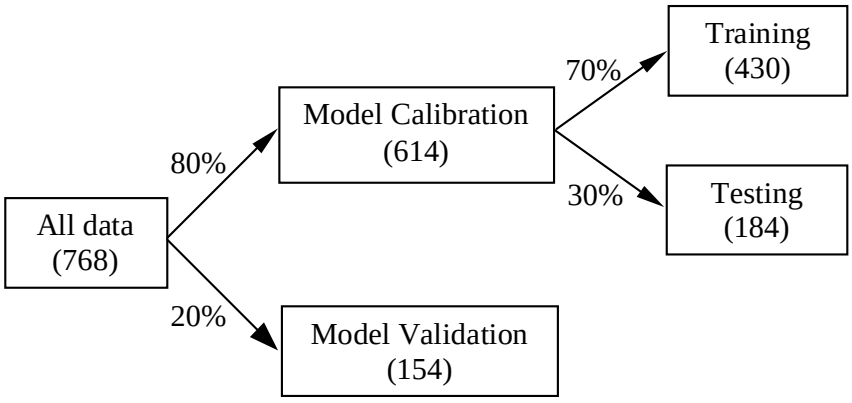

Figure 7.10 Data division for ANN model development

Table 7.4 Input and output statistic for ANN models

Model variables and data sets	Statistical parameters				
	Mean	Std. Dev.	Minimum	Maximum	Range
Slope angle, β (°)					
Training set	38.8	17.4	18.4	63.4	45.0
Testing set	38.4	17.4	18.4	63.4	45.0
Validation set	36.9	17.4	18.4	63.4	45.0
Friction angle, ϕ' (°)					
Training set	20.4	11.4	5.0	35.0	30.0
Testing set	19.4	10.6	5.0	35.0	30.0
Validation set	19.7	11.2	5.0	35.0	30.0
Stability number, $c'/\gamma H$					
Training set	0.046	0.036	0.005	0.100	0.095
Testing set	0.044	0.035	0.005	0.100	0.095
Validation set	0.044	0.035	0.005	0.100	0.095
Root cohesion, c_r (kPa)					
Training set	8.8	7.3	0.0	20.0	20.0
Testing set	7.8	7.3	0.0	20.0	20.0
Validation set	8.6	7.2	0.0	20.0	20.0
Depth of root zone, h_r (m)					
Training set	1.5	0.5	1.0	2.0	1.0
Testing set	1.5	0.5	1.0	2.0	1.0
Validation set	1.5	0.5	1.0	2.0	1.0
Factor of safety, F_s					
Training set	1.216	0.785	0.109	3.719	3.610
Testing set	1.154	0.739	0.156	3.656	3.500
Validation set	1.170	0.662	0.125	3.484	3.359

7.4.3 Network Architecture and Performance of ANN Models

The ANN models were trained with the pre-processed training data set and the testing data set was used to decide when to stop training to avoid overfitting (Stone 1974). In this study, the optimal network architecture of the ANN model was determined by trial-and-error. It was determined that the networks with one hidden layer were able to accurately define the relationship between the input and output variables. However, the performance of the ANN models was affected by the number of nodes in the hidden layer, as shown in Table 7.5. It can be seen that, as the number of hidden layer nodes increases from two to four, the performance of the ANN models improved significantly. However, this

improvement is somewhat reduced when the number of hidden layer nodes was increased from four to six.

Based on the criterion of selecting a network architecture that can be transformed into a practical formula, hence a parsimonious one, the model that with four nodes in the hidden layer (i.e. Model E2) is considered to be the optimal model. It should be noted that the hyperbolic tangent and logistic sigmoid functions were used in the hidden and output layers, respectively. Furthermore, the learning rate and momentum term were fixed at 0.2 and 0.8, respectively.

Table 7.5 Performance of ANN models with different number of hidden nodes

Model No.	No. hidden nodes	Performance measures								
		r			RMSE			MAE		
		T	S	V	T	S	V	T	S	V
E1	2	0.991	0.993	0.990	0.121	0.098	0.119	0.087	0.075	0.090
E2	4	0.995	0.997	0.997	0.079	0.060	0.055	0.047	0.045	0.041
E3	6	0.996	0.998	0.998	0.074	0.052	0.048	0.041	0.038	0.037

T = training; S = testing and V = validation.

7.4.4 ANN Model Equation for Vegetated Slope

It was determined in the previous section that Model E2, which has one hidden layer with 4 nodes, was the optimum ANN model. The structure of the ANN Model E2 is shown in Figure 7.11 and its connection weights and biases are shown in Table 7.6.

Using the connection weights and biases shown in Table 7.6, the predicted FOS, F_s, of a vegetated slope with effect of root reinforcement can be expressed as follows:

$$F_s = \frac{1}{1+e^{(0.346+0.345\tanh H_1-1.381\tanh H_2-3.22\tanh H_3-1.941\tanh H_4)}} \tag{7.2}$$

where:

$$H_1 = 0.653+0.329\beta-0.046\phi'-0.135\frac{c'}{\gamma H}-0.411c_r-0.338h_r \tag{7.3}$$

$$H_2 = 0.445 - 0.843\beta + 0.380\phi' + 1.117\frac{c'}{\gamma H} + 0.305c_r - 0.05h_r \quad (7.4)$$

$$H_3 = -1.794 - 2.357\beta + 1.152\phi' + 0.438\frac{c'}{\gamma H} + 0.018c_r - 0.008h_r \quad (7.5)$$

$$H_4 = 0.356 + 0.008\beta + 1.464\phi' + 0.303\frac{c'}{\gamma H} - 0.083c_r - 0.006h_r \quad (7.6)$$

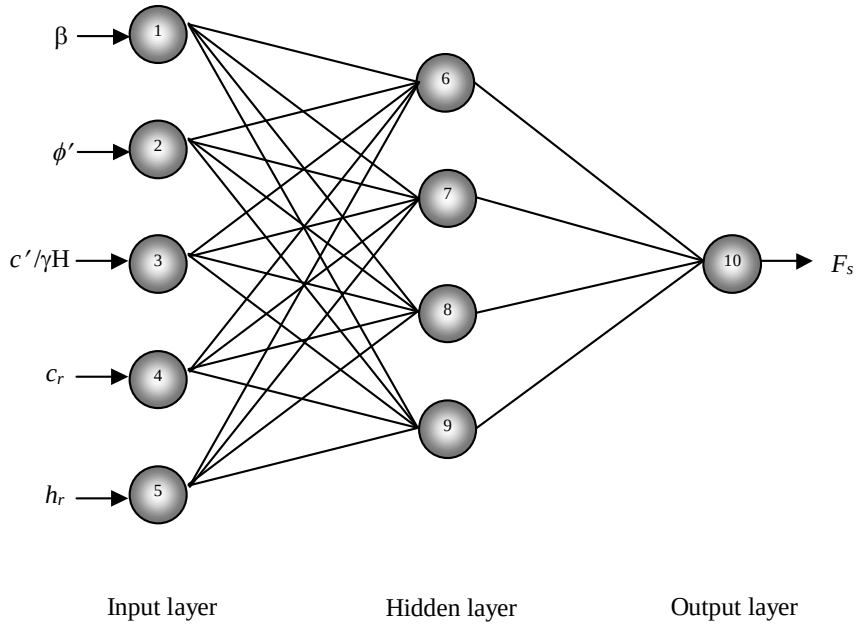

Figure 7.11 Structure of the optimal ANN model (Model E2)

Table 7.6 Weights and biases for the ANN Models E2

Hidden layer nodes	w_{ji} (weight from node i in the input layer to node j in the hidden layer)					Hidden layer bias (θ_i)
	i = 1	i = 2	i = 3	i = 4	i = 5	
j = 6	0.329	-0.046	-0.135	-0.411	-0.338	0.653
j = 7	-0.843	0.380	1.117	0.305	-0.050	0.445
j = 8	-2.357	1.152	0.438	0.018	-0.008	-1.794
j = 9	0.008	1.464	0.303	-0.083	-0.006	0.356
Output layer nodes	w_{ji} (weight from node i in the input layer to node j in the hidden layer)					Output layer bias (θ_i)
	i = 6	i = 7	i = 8	i = 9		
j = 10	-0.345	1.381	3.220	1.941		-0.346

It should be noted that the predicted FOS obtained from Equation (7.2) is scaled between 0.0 and 1.0, and in order to obtain the actual value, this FOS has to be re-scaled using Equation (2.49) and the data ranges in Table 7.3. It should also be noted that, before using Equations (7.3) to (7.6), all input variables (i.e. β, ϕ', c'/γH, c_r and h_r) need to be scaled between 0.0 and 1.0 using Equation (2.49) and the data ranges in Table 7.3. Equations (7.2) to (7.6) are therefore rewritten as follows:

$$F_s = 0.109 + \frac{3.61}{1 + e^{(0.346 + 0.345 \tanh H_1 - 1.381 \tanh H_2 - 3.22 \tanh H_3 - 1.941 \tanh H_4)}} \tag{7.7}$$

$$H_1 = 0.843 + 0.007\beta - 0.002\phi' - 1.421\frac{c'}{\gamma H} - 0.021c_r - 0.338h_r \tag{7.8}$$

$$H_2 = 0.718 - 0.019\beta + 0.013\phi' + 11.758\frac{c'}{\gamma H} + 0.015c_r - 0.05h_r \tag{7.9}$$

$$H_3 = -1.037 - 0.052\beta + 0.038\phi' + 4.611\frac{c'}{\gamma H} + 0.001c_r - 0.008h_r \tag{7.10}$$

$$H_4 = 0.134 + 0.0002\beta + 0.042\phi' + 3.189\frac{c'}{\gamma H} - 0.004c_r - 0.006h_r \tag{7.11}$$

It should be noted that Equation (7.7) is valid only for the ranges of values of β, D, N_s, COV and θ/H given in Table 7.3. This is because ANNs perform best in interpolation but not extrapolation, as discussed previously in Section 2.5.2. The developed ANN equations can therefore be used as an alternative method to the finite element analysis and the vegetated slope stability charts. This is particularly useful for interpolation of the cases that are not considered in the parametric studies and the stability charts.

7.5 Probabilistic Study

It has been discussed in Section 2.4.3.6 that root cohesion, c_r, is most likely to be spatially variable rather than uniform. Therefore, a probabilistic study was conducted to investigate the effect of spatial variability of root cohesion on the stability of a vegetated slope. This was achieved by using the random finite element method (FREM) and the two-layered slope model developed in Chapter 5. As previously discussed in Section 7.2, root

cohesion, c_r, can be modelled as an additional cohesion, which is added to the effective cohesion of soil, c', to give a total cohesion, c_{Total}, in the root zone (Equation (7.1)). In deterministic analyses, such as those performed in Section 7.2, both c_r and c' are assumed to be spatially uniform, however, in probabilistic analysis, they are treated as random variables, and vary spatially within the slope geometry being considered. Coefficients of variation (COV), and the scale of fluctuation (SOF), are used to describe the spatial variability of the root cohesion as well as other soil properties. The probabilistic slope analysis was conducted based on Monte Carlo simulation approach, as previously discussed in Chapter 3.

A 2:1 slope ($\beta = 26.6°$) with a height, H, of 10 m was used in this study, the typical finite element mesh with a realisation of a simulated cohesion random field is shown in Figure 7.12. The darker regions indicate soils with a higher cohesion value. It can be seen that the upper soil layer (i.e. the root zone) has a higher cohesion value than the underlying soil layer. In the first part of the analyses (denoted as Case 1), only the effective cohesion of the soil, c', and root cohesion, c_r, were considered as random variables, which were both described by a lognormal distribution. Other input parameters were assumed to remain constant at their deterministic values, as summarised in Table 7.7. It should be noted that, in the root zone, the effective cohesion of soil, c', was assumed to have the same spatial variability (i.e. same COV and SOF) as the root cohesion, c_r. Therefore, instead of treating c' and c_r as two different random fields, a single random field of total cohesion, c_{Total}, was simulated to represent the cohesion in the root zone.

In this study, the SOF, θ, was normalised by the slope height, H, which was similar to that performed in Chapters 4 and 5. It is noted from Table 7.7 that three different values of COV (i.e. 0.1, 0.5 and 1) and θ/H (i.e. 0.1, 1 and 10) for c_r were considered in the analyses. However, the COV and θ/H of c' for the underlying soil was fixed at 0.5 and 1, respectively. In the second part of the analyses (denoted as Case 2), the effective friction angle of the soil was considered as a lognormally distributed random variable, together with c' and c_r, with a COV of 0.25 and θ/H of 1. Other parameters remained the same values as used in the Case 1 analyses. The input parameters for the Case 2 analyses are summarised in Table 7.8. It should be noted that no correlation between the input parameters was assumed in these analyses.

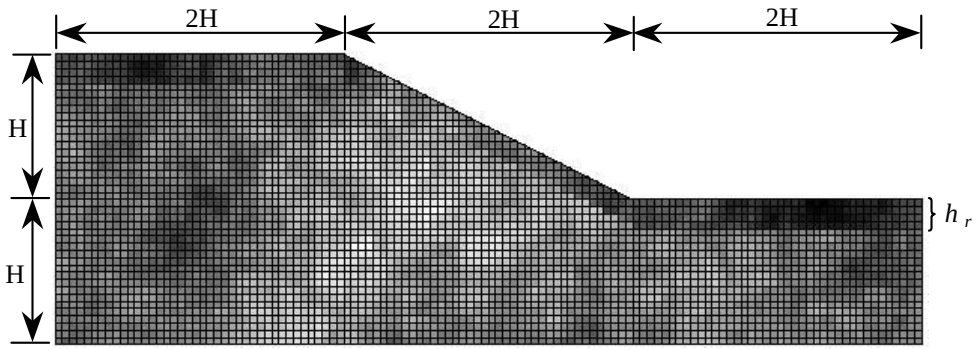

Figure 7.12 Typical finite element mesh with simulated cohesion value

Table 7.7 Input parameters and values for Case 1

Input parameters	Mean	COV	θ/H
Effective cohesion, c'	5 kPa	0.5	1
Effective friction angle, ϕ'	20° (deterministic)	-	-
Unit weight, γ	20 kN/m^3 (deterministic)	-	-
Depth of root zone, h_r	2 m (deterministic)	-	-
Root cohesion, c_r	5 kPa	0.1, 0.5, 1	0.1, 1, 10

Table 7.8 Input parameters and values for Case 2

Input parameters	Mean	COV	θ/H
Effective cohesion, c'	5 kPa	0.5	1
Effective friction angle, ϕ'	20°	0.25	1
Unit weight, γ	20 kN/m^3 (deterministic)	-	-
Depth of root zone, h_r	2 m (deterministic)	-	-
Root cohesion, c_r	5 kPa	0.1, 0.5, 1	0.1, 1, 10

Deterministic analyses, based on the mean values of each input parameter, were conducted to evaluate the factor of safety (FOS) of the slope being considered. It was found that the FOS of the slope without considering the effect of root reinforcement was 1.10. However, when root cohesion of 5 kPa was included in the analysis the FOS increased to 1.18. It should be noted that the deterministic FOS for Cases 1 and 2 were identical because both

cases used the same mean values for input parameters. The FOS indicates that the slope is in a marginally stable condition when the effect of root reinforcement is not considered.

Based on a Monte Carlo simulation involving 2,000 realisations, the computed probability of failure, P_f, of the slope without considering the effect of root reinforcement for Cases 1 and 2 are 0.1555 and 0.4175, respectively. Typical deformed finite element meshes for the slopes of Cases 1 and 2 are shown in Figure 7.13. It can be seen that the failure mechanism of the slope is a typical circular 'toe' failure. It is noted that P_f increased significantly (i.e. approximately 2.7 times) in Case 2 when the spatial variability of the friction angle, ϕ', was considered in the analysis.

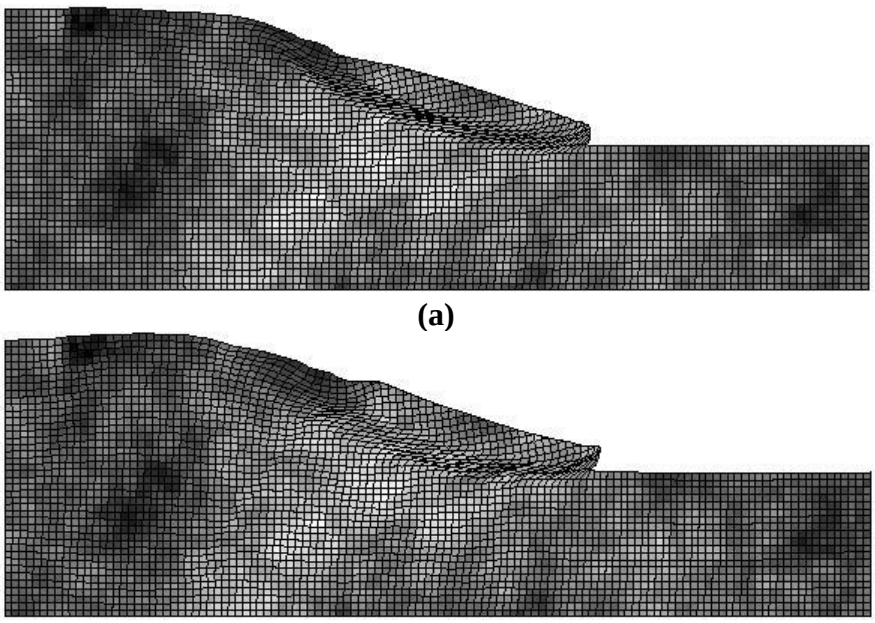

(a)

(b)

Figure 7.13 Typical deformed meshes for the slopes without considering the effect of root reinforcement: (a) Case 1 and (b) Case 2

When the effect of root reinforcement was considered in the probabilistic slope analysis, the probability of failure, P_f, of the slope reduced significantly. The magnitude of the reduction in P_f was governed by the values of COV and θ/H. The computed P_f of the slope with different values of COV and θ/H are summarised in Table 7.9. It can be seen that, in Case 1, P_f reduced from 0.1555 (without root reinforcement) to less than 0.001 when COV of c_r is small (i.e. COV = 0.1). A similar observation was also found in Case 2 where P_f reduced from 0.4175 to less than 0.215 when COV = 0.1. The reduction was also

significant even when the COV was high (i.e. COV = 1), as shown in Table 7.9. These results indicate that the spatial variability of root cohesion has a significant influence on the P_f of a vegetated slope. The effects of variations in COV and θ/H on P_f are shown in Figures 7.14 and 7.15, respectively.

Table 7.9 Computed P_f for the slopes considering effect of root reinforcement

		P_f	
COV	**θ/H**	**Case 1**	**Case 2**
0.1	0.1	0.0010	0.2145
0.1	1	0.0005	0.2140
0.1	10	<1/2000	0.2085
0.5	0.1	0.0055	0.2565
0.5	1	0.0155	0.2375
0.5	10	0.0220	0.2330
1	0.1	0.0490	0.3310
1	1	0.0800	0.3130
1	10	0.1310	0.3030

Figure 7.14 shows the effect of varying the COV of c_r on the P_f of the slope with different values of θ/H, for (a) Case 1 and; (b) Case 2. It can be seen that P_f increases as the COV increases for all values of θ/H. This is because as COV increases the chances of getting extremely low values of c_r are also increases, which ultimately increases P_f, as previously discussed in Section 4.2.6.

Figure 7.15 shows the effect of varying θ/H of c_r on the P_f of the slope with different values of COV. It can be seen that the effect of varying θ/H on P_f is very small when COV = 0.1 and 0.5, for both Cases 1 and 2. However, a more significant effect was observed when COV = 1.0, for both Cases 1 and 2. It is noted that different trends were observed in the variation of θ/H with P_f for Cases 1 and 2. For Case 1, P_f increases as θ/H increases, whereas for Case 2, P_f decreases as θ/H increases. This phenomenon has also been observed when the effect of root reinforcement was not considered in the probabilistic slope analysis, as previously discussed in Section 4.2.6. The results shown in Figures 7.14

and 7.15 indicate that the effect of COV and θ/H on P_f for a vegetated slope follows a similar trend as that for a bare slope (i.e. effect of root reinforcement is not considered).

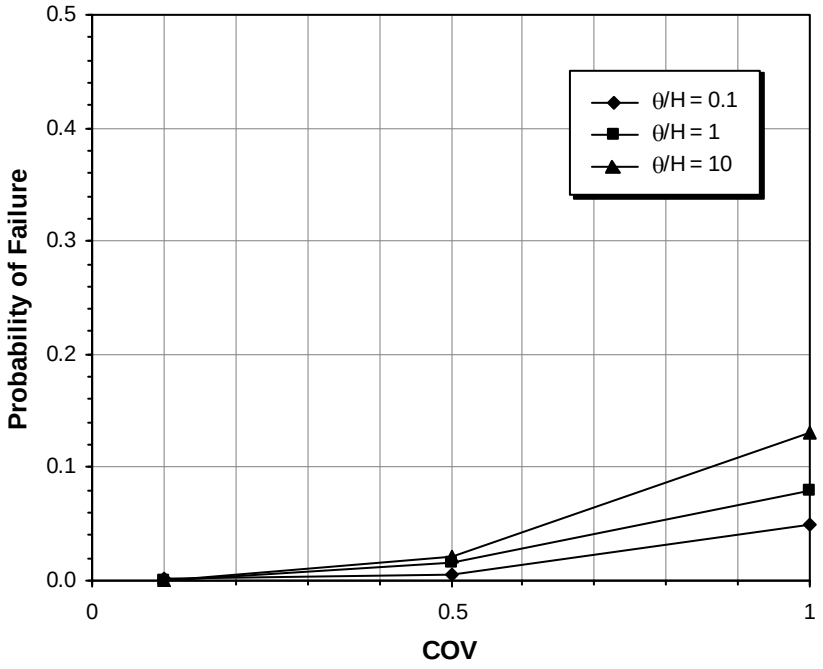

(a)

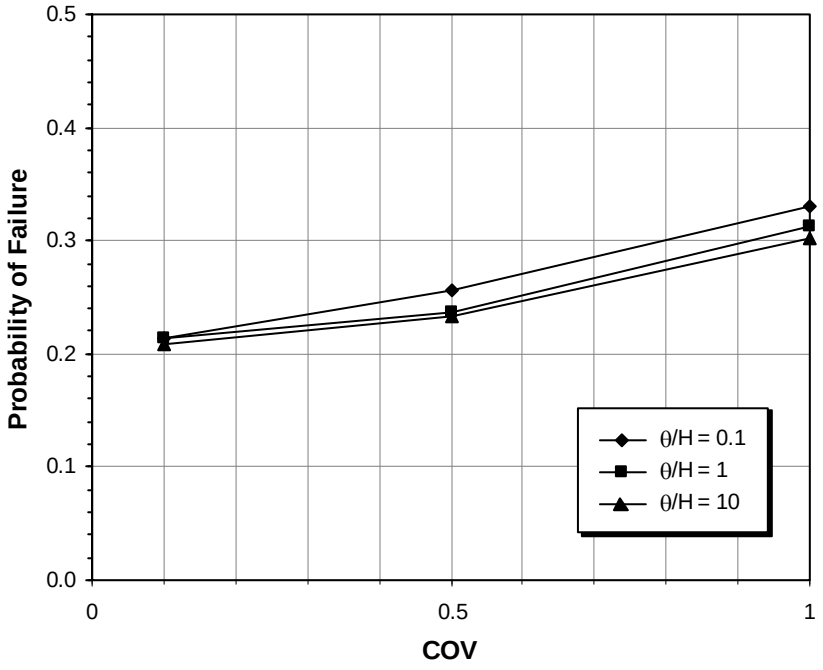

(b)

Figure 7.14 P_f versus COV for different θ/H: (a) Case 1 and (b) Case 2

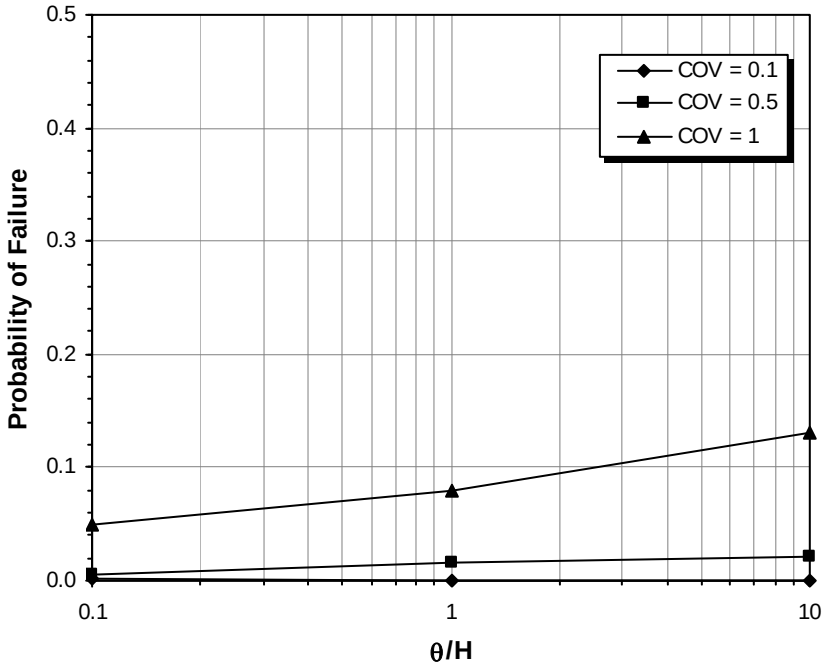

(a)

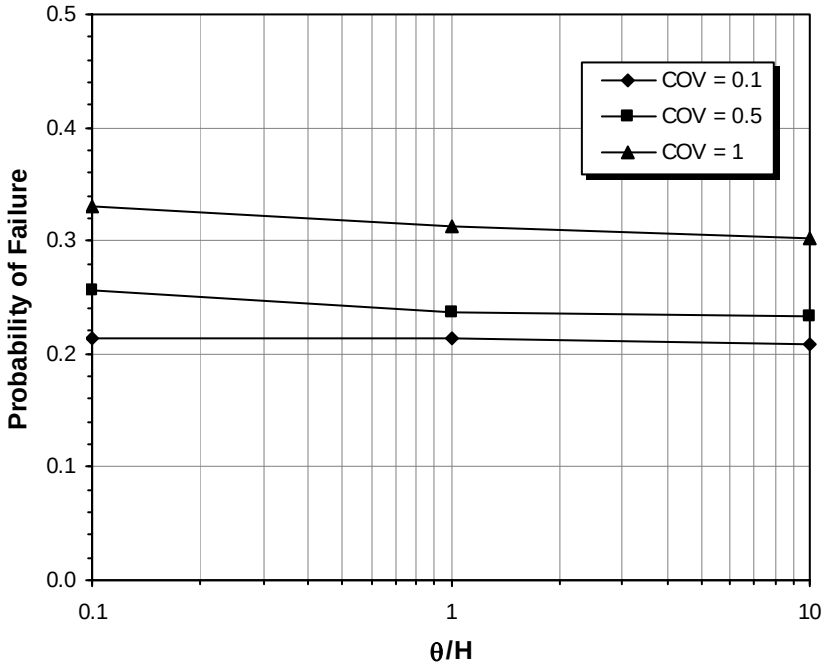

(b)

Figure 7.15 P_f versus θ/H for different COV: (a) Case 1 and (b) Case 2

Figure 7.16 shows the typical deformed finite element meshes for the vegetated slope in Case 1, with different values of COV of c_r: (a) 0.1 and (b) 1, and with θ/H fixed at 10. It can be seen that the failure mechanism for the vegetated slope is a typical 'toe' failure'. It

is also noted that failure surface 'moves' towards the root zone as COV increases, producing a shallow type failure. This is because the extremely low value of c_r in the root zone has controlled the failure mode. Figure 7.17 shows the typical deformed finite element meshes for the vegetated slope with different values of θ/H: (a) 0.1 and (b) 10, and with COV fixed at 0.5. It is noted the failure mode is reasonably consistent, as the values of θ/H varies.

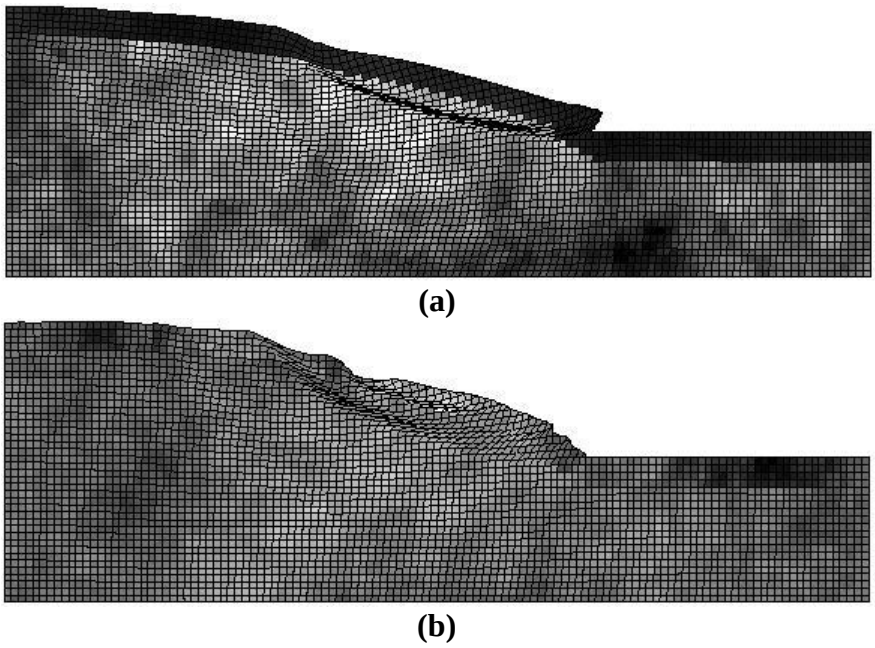

(a)

(b)

Figure 7.16 Typical deformed meshes for the vegetated slope with different values of COV: (a) 0.1 and (b) 1. (θ/H fixed at 10)

7.5.1 Summary

In this chapter, the effect of root reinforcement on slope stability has been modelled using the finite element slope stability analysis method. The *root cohesion*, c_r, has been considered as additional cohesion, which is added to the soil cohesion. The soil elements within the defined slope geometry that are affected by vegetation are known as the *root zone*, and the extent of this root zone is defined by the *depth of root zone*, h_r. The results from the numerical analyses conducted using the finite element method show that the factor of safety (FOS) of a slope increases when the effect of root reinforcement is taken into consideration. In general, the FOS increases linearly with c_r and h_r. It has been found

that the increase in FOS is more significant for the slopes with a lower value of FOS than for those with a higher value FOS.

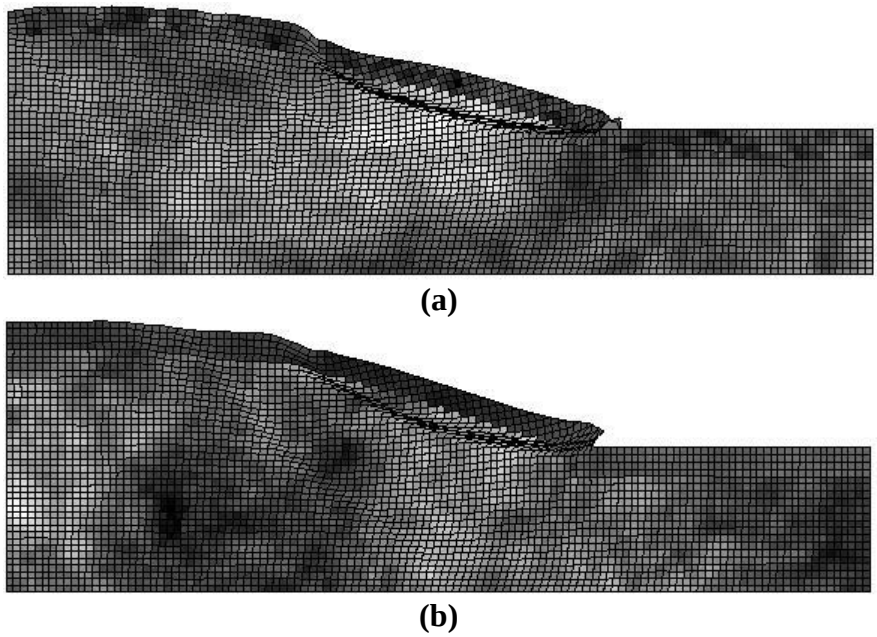

(a)

(b)

Figure 7.17 Typical deformed meshes for the vegetated slope with different values of θ/H: (a) 0.1 and (b) 10. (COV fixed at 0.5)

Extensive parametric studies using the finite element method have been conducted to generate a series of stability charts that can be used for determining the FOS of a vegetated slope. Five variables were varied systematically to determine the corresponding value of FOS for each case. These variables considered are the slope angle, β, friction angle, ϕ', stability coefficient, $c'/\gamma H$, root cohesion, c_r, and depth of root zone, h_r.

An artificial neural network (ANN) model has also been developed to serve as an alternative tool for predicting the FOS of a vegetated slope. The database required for ANN model development is based on the results generated from the parametric studies. The ANN model with one hidden layer and four nodes was found to be the most optimum and parsimonious model. This model has been transformed into a relatively simple formula that can be used in the practice.

Probabilistic studies have been carried out in order to investigate the effect of spatial variability of root cohesion on the stability of a slope. The root cohesion, as well as the

strength parameters (i.e. c' and ϕ'), has been treated as lognormally distributed random variables. The probabilistic slope analysis was performed using the Monte Carlo simulation and the random finite element method (RFEM). It has been demonstrated that spatial variability of root cohesion has a significant effect on the probability of failure, P_f, of a slope. It has been found that P_f increases as the COV of c_r increases for all values of θ/H. However, P_f either increases or decreases as θ/H increases, dependent on the value of COV. These observations are consistent with those found in Chapters 4 and 5, where the effect of root reinforcement was not considered in the probabilistic slope analysis.

Chapter 8

SUMMARY AND CONCLUSIONS

8.1 Summary

This research has examined and quantified the effects of soil variability and vegetation on the stability of natural slopes. A set of probabilistic stability charts has been developed, which can be used for a preliminary assessment of the effect of soil variability on the reliability of spatially random cohesive slopes. Artificial neural network (ANN) models and formulae that can be used to predict the probability of failure of a spatially random cohesive slope have also been developed. In addition, the effect of root reinforcement on slope stability has been examined using the finite element method. A set of stability charts for vegetated slopes, which considers the effect of root reinforcement, has been developed. ANN models and formulae, which can be used for predicting the factor of safety (FOS) of a vegetated slope, have also been developed.

In Chapter 2, it was discussed that inherent soil variability and effects of vegetation are not commonly considered in routine slope stability analysis, although their effects on slope stability are well recognised. The main reason is due to the complexity and difficulty in quantifying the effects of soil variability and vegetation. Furthermore, the available tools for slope stability analysis in practice (i.e. limit equilibrium method) are not well established to account for the effects of soil variability and vegetation. However, the review of relevant literature in this chapter has indicated that the random finite element method (RFEM), developed by Griffiths and Fenton (2004), is capable of considering the effect of soil variability using a probabilistic slope stability analysis approach utilising Monte Carlo simulation. In addition, it was also discussed that ANNs are a powerful computational tool that can be used to determine the relationship between the input and output variables. ANNs are capable of providing relatively simple and straightforward formulae that can be readily used in practice. Such formulae for the assessment of the

effect of soil variability and vegetation on slope stability are not yet available in the literature. Finally, it was also discussed that the effect of root reinforcement can be modelled using the finite element method by considering the effect of root reinforcement as an increase in soil cohesion called *root cohesion*. The spatial variability of root cohesion can also be considered using the RFEM.

Chapter 3 described the formulation and implementation of the random finite element method (RFEM) for probabilistic slope stability analysis. It has been demonstrated that *rslope2d*, a computer model that implementing RFEM, is capable of modelling the effects of soil variability on slope stability. Investigations were undertaken to validate the simulated soil properties and to investigate the effect of varying statistical parameters on the simulated random fields. The results indicated that the statistical distribution of a simulated soil property (e.g. c_u) was affected by the coefficient of variation (COV) and scale of fluctuation (SOF). When the *mean* c_u for each random field (out of 2,000 realisations) was computed, it was observed that the scatter of the computed *mean* c_u increased as either COV or SOF increased. It is also observed that, as SOF $\rightarrow$ 0, both the mean value and standard deviation (or variance) of the computed *mean* c_u, for the simulated random fields, were reduced from their point values due to the effect of local averaging. The reduction was found to increase as COV increased.

In Chapter 4, parametric studies were conducted to examine the influence of the spatial variability of undrained cohesion, c_u, which was described by a lognormal distribution, on the probability of failure, P_f, of a spatially random cohesive slope with different geometries. Based on the results of the parametric studies, a set of probabilistic stability charts were developed for the spatially random cohesive slopes. In addition, probabilistic analysis of a 2:1 spatially random c'-ϕ' slope has also been conducted. The analyses carried out in this chapter yielded the following specific observations:

- In general, P_f increases as COV increases. More specifically, for a marginally stable slope (i.e. FOS $\approx$ 1), P_f is more sensitive to lower values of COV (i.e. COV $\leq$ 0.3). However, for a stable slope (i.e. FOS > 1.5), P_f is more sensitive to higher values of COV (i.e. COV $\geq$ 0.5). This is because, as COV increases, more scatter in the simulated values of c_u is expected and the low values have controlled the failure of the slope.

- P_f either increases or decrease as SOF increases. For a slope with $P_f < 0.5$, P_f increases as SOF increases. On the other hand, for a slope with $P_f > 0.5$, P_f decreases as SOF increases. The effect of SOF on P_f is governed by the reduction in variance of soil properties due to local averaging effect. As SOF increase and approaches infinity, less variance reduction is expected, hence, more scatter in the simulated values of c_u is expected.

- When COV is small (i.e. COV ≤ 0.1), only marginally stable slopes are sensitive to SOF, but when COV is moderate to large (i.e. COV ≥ 0.5), even stable slopes (i.e. FOS > 1.5) are sensitive to SOF.

- P_f decreases as FOS decreases for all values of COV and θ/H. It has been shown that, when COV is small (i.e. COV ≤ 0.1), to achieve $P_f = 0$, FOS needs to be greater than 1.65. However, when COV is large (i.e. COV ≥ 0.5), FOS needs to be greater than 2.75 to achieve $P_f = 0$. This observation suggested that, when COV is large, a high FOS does not necessarily indicate a stable slope.

- It was shown that the effect of anisotropy of SOF on P_f was small compared to the effects of variation in the values COV and θ/H on P_f.

- The results of the probabilistic analysis of a $c'-\phi'$ slope indicated that variations of P_f with respect to COV and SOF were similar to those observed in the cohesive case.

- For all values of COV and θ/H, negative correlation between c' and ϕ' leads to a lower estimate of P_f, while positive correlation between c' and ϕ' leads to a higher estimate of P_f, as compared to the assumption of no correlation between c' and ϕ'.

In Chapter 5, the random finite element method (RFEM) computer program *rslope2d* was modified to analyse a two-layered soil slope. The modified program was then used to study the influence of soil variability on the reliability of a 2:1 two-layered spatially random cohesive slope. The analyses carried out in this chapter yielded the following specific observations:

- When the upper and lower layers were both assumed to have the same COV and θ/H, the failure mechanism changed with respect to the ratio of c_{u1}/c_{u2}. The failure

mechanism for the slopes with c_{u1}/c_{u2} less than 1 appears to be deep-seated. However, a toe failure mechanism was observed for the slopes with c_{u1}/c_{u2} greater than 1. It was found that a deep-seated failure was the critical mechanism as it yielded higher values of P_f.

- When the COV and θ/H were systematically varied, the results indicated that the lower layer has a higher influence on the probability of failure of the slope. It was also shown that failure surface was more likely to occur in the soil layer with a larger value of COV and θ/H.

Chapter 6 investigated the feasibility of using ANNs as an alternative approach to the RFEM and Monte Carlo simulation for predicting the probability of failure, P_f, of a spatially random cohesive slope. Multi-layer perceptrons (MLPs) trained with the back-propagation algorithm were used in this study. The data used for the ANN model development and validation were obtained from the parametric studies conducted in Chapter 4 using RFEM and Monte Carlo simulation. It was concluded that ANNs have the ability of predicting the probability of failure, P_f, of spatially random cohesive slopes with a high degree of accuracy. A relatively simple formula was developed based on the ANN model with 1 hidden layer and 6 nodes, which can be used as an alternative approach to the more advanced but computationally intensive approach (i.e. RFEM). In addition, the sensitivity analysis of the ANN model inputs indicated the stability number, N_s, was the most important parameter with a relative importance of 41.1%. The other parameters ranked in the order of most to least important were θ/H, COV, D and β.

In Chapter 7, the effect of root reinforcement on slope stability was modelled using the finite element slope stability analysis method. The *root cohesion*, c_r, was considered as an additional cohesion, which was added to the soil cohesion. The soil region within the defined slope geometry that is affected by vegetation are known as the *root zone*, and the extent of this root zone is defined by the parameter called the *depth of root zone*, h_r. Based on the results of the parametric studies, a set of stability charts was developed for the vegetated slopes considering the effect of root reinforcement. An ANN model was also developed to serve as an alternative tool for predicting the FOS of a vegetated slope. In addition, probabilistic studies were carried out in order to investigate the effect of spatial variability of root cohesion on the stability of a slope. The analyses carried out in this chapter yielded the following specific observations:

- The FOS increased linearly with c_r and h_r. It was also found that the increase in FOS is more significant for the slopes with a lower value of FOS than for those with a higher value FOS.

- The ANN model with one hidden layer and four nodes was found to be the most optimum and parsimonious model. This model was then transformed into a relatively simple formula that can be used in the practice.

- The spatial variability of root cohesion has a significant effect on the probability of failure, P_f, of a slope. It was found that P_f increases as the COV of c_r increases for all values of θ/H. However, P_f either increases or decreases as θ/H increases, dependent on the value of COV.

8.2 Recommendations for Further Research

The slope stability analyses conducted in this research have assumed a deep water table and the effect of pore water pressure were not considered. It is well known that pore water pressure is one of the variables, in slope stability analysis, that subject to significant uncertainty. Therefore, the variability of pore water pressure is also likely to have a considerable effect on the stability of a natural slope. It is worthwhile to use the random finite element method (RFEM) to analyse slopes with a shallow water table and consider the changes in pore water pressure.

In this research, probabilistic stability charts and ANN model formulae are developed for the spatially random cohesive slopes only, due to time constraints. To construct useful charts for the $c'-\phi'$ slopes with different geometries, more analyses need to be undertaken as more parameters would be involved. Furthermore, in order be more applicable in practice, charts for $c'-\phi'$ slopes should also include water table location. This is a time consuming and computationally intensive task but certainly achievable and desirable.

The RFEM computer model *rslope2d* has assumed a 2-dimensional (2D) plane-strain conditions. Therefore, the spatial variability of soil properties and root cohesion in the third dimension was not considered. Vanmarcke (1977) stated that soil properties vary spatially in 3-dimensions (3D). Furthermore, the spatial distribution of vegetation on a

natural slope is also extended to the third dimension. Hence, it is worthwhile to perform 3D probabilistic slope stability analyses considering the effects of soil variability and vegetation in 3D. As discussed in Chapter 2, the 2D finite element slope stability model, which is used in *rslope2d*, has been recently extended to 3D (Griffiths and Marquez 2007). However, it has yet to be combined with 3D spatially random soil profile simulated by the local average subdivision (LAS) method and incorporated into a Monte Carlo simulation framework.

This research has examined the effect of soil variability and vegetation through parametric studies and the range of the input parameters were based on observed or suggested values found in the literature. It is worthwhile to apply the RFEM and tools developed in this research (i.e. two-layered slope model, stability charts, and ANN models and formulae) to reported case studies of slope failure. However, it should be mentioned that the majority of the case studies reported in the literature do not provide the detailed information required for considering the effects of soil variability and vegetation in slope stability analysis.

8.3 Conclusions

From the analyses presented in this thesis, it can be concluded that the effects of soil variability and root reinforcement have a significant impact on the stability of natural slopes, in particular on marginally stable slopes. Considering these factors in slope stability analysis enables the safety of a slope to be predicted more accurately. In addition, when performing probabilistic slope stability analysis, assuming a perfectly correlated soil profile (i.e. SOF $\rightarrow \infty$) in probabilistic slope stability analysis could either overestimate or underestimate the P_f. For slopes with $P_f < 0.5$, $P_f \rightarrow 0$ as SOF $\rightarrow 0$, hence, the P_f is overestimated. For slopes with $P_f > 0.5$, $P_f \rightarrow 1$ as SOF $\rightarrow 0$, hence, the P_f is underestimated. Finally, it is also concluded that artificial neural networks (ANNs) have the ability to predict the probability of failure of spatially random cohesive and the factor of safety of a vegetated slope taking the effect of root reinforcement into consideration.

REFERENCES

Abe, K., and Iwamoto, M. (1988). "Preliminary experiment on shear in soil layers with a large direct-shear apparatus." *Journal of the Japanese Forestry Society*, 68(2), 61-65.

Abernethy, B. (1999). "On the role of woody vegetation in riverbank stability," Ph.D Thesis, Department of Civil Engineering, Monash University.

Abernethy, B., and Rutherfurd, I. (2000). "The effect of riparian tree roots on the mass-stability of riverbanks." *Earth Surf. Process. Landforms*, 25, 921-937.

Abernethy, B., and Rutherfurd, I. (2001). "The distribution and strength of riparian tree roots in relation to riverbank reinforcement." *Hydrol. Process.*, 15, 63-79.

Abramson, L. W., Lee, T. S., Sharma, S., and Boyce, G. M. (2002). *Slope stability and and stabilization methods, 2nd edition*, John Wiley and Sons, New York.

Adeli, H. (2001). "Neural networks in civil engineering: 1989-2000." *Computer-Aided Civil and Infrastruture Engineering*, 16, 126-142.

Alonso, E. E. (1976). "Risk analysis of slopes and its application to slopes in Canadian sensitive clays." *Geotechnique*, 26(3), 453-472.

Anderson, M. G., and Kemp, M. J. (1991). "Towards an improved specification of slope hydrology in the analysis of slope instability problems in the tropics." *Progress in Physical Geography*, 15(1), 29-52.

Anderson, M. G., and Lloyd, D. M. (1991). "Using a combined slope hydrology-stability model to develop cut slope design charts." *Proc. Inst. Civ. Eng.*, 91(2), 705-718.

Asaoka, A., and Grivas, D. A. (1982). "Spatial variability of the undrained shear strength of clays." *J. Geotech. Eng. Div., ASCE,* 108, 743-756.

Baecher, G. B., and Christian, J. T. (2003). *Reliability and statistics in geotechnical engineering*, John Wiley & Sons Ltd, Chichester.

Basma, A. A., and Kallas, N. (2004). "Modelling soil collapse by artificial neural networks." *Geotechnical and Geological Engineering*, 22, 427-438.

Bethlahmy, N. (1962). "First year effects of timber removal on soil moisture." *Int. Assoc. Sci. Hydrol. Bull.*, 7(2), 34-38.

Biddle, P. G. (1983). "Patterns of soil drying and moisture deficit in the vicinity of trees on clay soils." *Geotechnique*, 33(2), 107-126.

Bishop, A. W. (1955). "The use of slip circle in the stability analysis of slopes." *Geotechnique*, 5(1), 7-17.

Bishop, A. W., and Morgenstern, N. R. (1960). "Stability coefficients for earth slopes." *Geotechnique*, 10, 129-150.

Bishop, D. M., and Steven, M. E. (1964). "Landslides on logged areas in Southeast Alaska." *Research paper NOR-1*, Northern Forest Experiment Station, Juneau, USA.

Blight, G. E. (2005). "Desiccation of a clay by grass, bushes and trees." *Geotechnical and Geological Engineering*, 23, 697-720.

Brejda, J. J., Moorman, T. B., Smith, J. L., Karlen, D. L., Allan, D. L., and Dao, T. H. (2000). "Distribution and variability of surface soil properties at a regional scale." *Soil Science Society of America Journal,* 64, 974-982.

Brockwell, P. J., and Davis, R. A. (1987). *Time series: Theory and methods*, Springer-Verlag, New York.

Brown, C., and Sheu, M. S. (1975). "Effect of deforestation on slopes." *J. Geotech. Eng. Div., ASCE*, 101(GT2), 147-165.

Buchanan, P., and Savigny, K. W. (1990). "Factors controlling debris avalanche initiation." *Can. Geotech. J.*, 27, 659-675.

Burroughs, E. R., and Thomas, B. R. (1977). "Declining root strength in Douglas-Fir after felling as a factor in slope stability." *United states Department of Agriculture Forest Service Intermountain Forest and Range Experimental Station Research Paper*, INT-190, 1-27.

Cameron, D. A. (2001). "The extent of soil desiccation near trees in a semi-arid environment." *Geotechnical and Geological Engineering*, 19, 357-370.

Chandler, D. S. (1992). "An area approach to forest slope stability," Ph.D Thesis, University of Washington.

Chandler, D. S. (1996). "Monte Carlo simulation to evaluate slope stability." *Uncertainty in the geologic environment: From theory to Practice, Proc. Uncertainty'96*, Geotechnical Special Publication No.58, 2, 474-493.

Cherubini, C. (2000). "Reliability evaluation of shallow foundation bearing capacity on c', ϕ' soils." *Can. Geotech. J.*, 37, 264-269.

Chiasson, P., Lafleur, J., Soulie, M., and Law, K. T. (1995). "Characterizing spatial variability of a clay by geostatistics." *Can. Geotech. J.*, 31, 1-10.

Christian, J. T., and Baecher, G. B. (1999). "Point estimate method as numerical quadrate." *J. Geotech. Eng., ASCE*, 125(9), 779-786.

Christian, J. T., Ladd, C. C., and Baecher, G. B. (1994a). "Reliability and probability in stability analysis." *J. Geotech. Eng., ASCE*, 120(2), 1071-1111.

Christian, J. T., Ladd, C. C., and Baecher, G. B. (1994b). "Reliability applied to slope stability analysis." *J. Geotech. Eng., ASCE*, 120(12), 2180-2207.

Collison, A. J. C. (1993). "Assessing the influence of vegetation on slope stability in the tropics," PhD Thesis, University of Bristol.

Collison, A. J. C., and Anderson, M. G. (1996). "Using a combined slope hydrology/stability model to identify suitable conditions for landslide prevention by vegetation in the humid tropics." *Earth Surf. Process. Landforms*, 21, 737-747.

Collison, A. J. C., Anderson, M. G., and Lloyd, D. M. (1995). "Impact of vegetation on slope stability in a humid tropical environment: a modelling approach." *Proc. Inst. Civ. Eng.: Water, Maritime & Energy*, 112, 168-175.

Coppin, N. J., and Richards, I. G. (1990). *Use of vegetation in civil engineering*, Butterworths, London.

Cousins, B. F. (1978). "Stability charts for simple earth slopes." *J. Geotech. Eng. Div., ASCE*, 104(GT-2), 267-279.

Cybenko, G. (1989). "Approximation by superpositions of a sigmoidal function." *Mathematics of Control, Signals, and Systems*, 3, 303-314.

Darcy, H. (1856). *Les Fontaines Publique de la Ville de Dijon*, Dalmont, Paris.

DeGroot, D. J. (1996). "Analyzing spatial variability of in situ soil properties." *Uncertainty in the geologic environment: From theory to Practice, Proc. Uncertainty'96*, Geotechnical Special Publication No. 58, 1, 210-238.

DeGroot, D. J., and Baecher, G. B. (1993). "Estimating autocovariance of in-situ soil properties." *J. Geotech. Eng., ASCE*, 119(1), 147-166.

Donald, I. B., and Zhao, T. (1995). *GWEDGEM: A computer program for slope stability analysis based on the generalised wedge method. User's manual*, Department of Civil Engineeing, Monash University, Melbourne.

Duncan, J. M. (1996). "State of the art: Limit equilibrium and finite-element analysis of slopes." *J. Geotech. Eng., ASCE*, 122(7), 577-596.

Duncan, J. M. (2000). "Factors of safety and reliability in geotechnical engineering." *J. Geotech. Geoenviron. Eng., ASCE*, 126, 307-316.

Duncan, J. M., and Dunlop, P. (1969). "Slopes in stiff fissured clays and soils." *J. Soil Mech. Found. Div., ASCE*, 103(7), 667-676.

Eberhart, R. C., and Dobbins, R. W. (1990). *Neural network PC tools: A practical guide*, Academic Press, San Diego, Calif.

El-Ramly, H., Morgenstern, N. R., and Cruden, D. M. (2002). "Probabilistic slope stability analysis for practice." *Can. Geotech. J.*, 39, 665-683.

Endo, T., and Tsuruta, T. (1969). "Effects of tree root upon the shearing strengths of soils." *Annual Report of the Hokkaido Branch*, Tokyo Forest Experiment Station, 167-179.

Fausett, L. V. (1994). *Fundamentals neural networks: Achitecture, algorithms, and applications*, Prentice-Hall, Englewood Cliffs, New Jersey.

Fellenius, W. (1936). "Calculation of stability of earth dams." *Proc. 2nd Congress on Large Dams*, U.S. Government Printing Office, Washington D.C., 4.

Fenton, G. A. (1990). "Simulation and analysis of random fields," Ph.D. Thesis, Department of Civil Engineering and Operations Research, Princeton University, New Jersey.

Fenton, G. A. (1994). "Error evaluation of three random field generators." *J. Eng. Mech., ASCE*, 120(12), 2478-2497.

Fenton, G. A. (1999). "Random field modeling of CPT data." *J. Geotech. Geoenviron. Eng., ASCE*, 125(6), 486-498.

Fenton, G. A., and Griffiths, D. V. (1996). "Statistic of free surface flow through stochastic earth dam." *J. Geotech. Geoenviron. Eng., ASCE*, 122(6), 427-436.

Fenton, G. A., and Griffiths, D. V. (1997). "Extreme hydraulics gradient statistic in a stochastic earth dam." *J. Geotech. Geoenviron. Eng., ASCE*, 123(11), 995-1000.

Fenton, G. A., and Griffiths, D. V. (2000). "Bearing capacity of spatially random soils." *Proc. 8th ASCE Joint Specialty Conf. on Probabilistic Mechanics and Structural Reliability*, Notre Dame, Indiana.

Fenton, G. A., and Griffiths, D. V. (2001). "Bearing capacity of spatially random *c*-ϕ soils." *Proc. 10th Int. Conf. on Computer Methods and Advances in Geomechanics (IACMAG 01)*, Balkema, Tucson, Arizona, 1411-1415.

Fenton, G. A., and Griffiths, D. V. (2002). "Probabilistic foundation settlement on spatially random soil." *J. Geotech. Geoenviron. Eng., ASCE*, 128(5), 381-390.

Fenton, G. A., and Griffiths, D. V. (2003). "Bearing-capacity prediction of spatially random *c*-ϕ soils." *Can. Geotech. J.*, 40, 54-65.

Fenton, G. A., and Griffiths, D. V. (2005). "Three-dimensional probabilistic foundation settlement." *J. Geotech. Geoenviron. Eng., ASCE*, 131(2), 232-239.

Fenton, G. A., Griffiths, D. V., and Williams, M. B. (2005). "Reliability of traditional retaining wall design." *Geotechnique*, 55(1), 55-62.

Fenton, G. A., and Vanmarcke, E. H. (1990). "Simulation of random fields via local average subdivision." *J. Eng. Mech., ASCE*, 116(8), 1733-1749.

Flood, I., and Kartam, N. (1994). "Neural networks in civil engineering I: Principles and understanding." *J. Comput. Civ. Eng., ASCE*, 8(2), 131-148.

Fredlund, D. G., Morgentern, N. R., and Widger, R. A. (1978). "Shear strength of unsaturated soils." *Can. Geotech. J.*, 15, 313-321.

Fredlund, D. G., and Rahardjo, H. (1993). *Soil mechanics for unsaturated soils*, Wiley Publications, New York.

Garson, G. D. (1991). "Interpreting neural-network connection weights." *AI Expert*, 6(7), 47-51.

Goh, A. T. C. (1994). "Seismic liquefaction potential assessed by neural network." *J. Geotech. Geoenviron. Eng., ASCE*, 120(9), 1467-1480.

Goh, A. T. C. (1995a). "Back-propagation neural networks for modeling complex systems." *Artifiical Intelligence in Engineering*, 9, 143-151.

Gray, D. H. (1978). "Role of woody vegetation in reinforcing soils and stabilising slopes." *Proceeding Symposium Soil Reinforcing & Stabilisation Techniques in Engineering Practice*, Sydney, 253-306.

Gray, D. H., and Leiser, A. T. (1982). *Biotechnical slope protection and erosion control*, Van Nostrand Reinhold Co., New York, N.Y.

Gray, D. H., and Megahan, W. F. (1981). "Forest vegetation removal and slope stability in the Idaho Batholith." *Research Paper INT-271*, Intermountain Forest and Range Experiment Station, Ogden, Utah.

Gray, D. H., and Oshashi, H. (1983). "Mechanics of fiber reinforcement in sand." *J. Geotech. Eng., ASCE*, 109, 335-353.

Gray, D. H., and Sotir, D. B. (1996). *Biotechnical and soil bioengineering slope stabilization*, John Wiley & Sons, New York.

Greenway, D. R. (1987). "Vegetation and slope stability." *Slope Stability*, M. G. Anderson and K. S. Richards, eds., John Wiley & Sons Ltd.

Greenwood, J. R. (1983). "A simple approach to slope stability." *Ground Engeering*, 16(4), 45-98.

Greenwood, J. R. (2006). "SLIP4EX - A program for routine slope stability analysis to include the effects of vegetation, reinforcement and hydrological changes." *Geotechnical and Geological Engineering*, 24, 449-465.

Griffiths, D. V. (1980). "Finite element analysis of walls, footings and slopes," PhD Thesis, Department of Engineering, University of Manchester.

Griffiths, D. V., and Fenton, G. A. (1993). "Seepage beneath water retaining structures foundaed on spatially random soil." *Geotechnique*, 43(6), 577-587.

Griffiths, D. V., and Fenton, G. A. (1997). "Three-dimensional seepage through spatially random soil." *J. Geotech. Geoenviron. Eng., ASCE*, 123(2), 153-160.

Griffiths, D. V., and Fenton, G. A. (1998). "Probabilistic analysis of exit gradients due to steady seepage." *J. Geotech. Geoenviron. Eng., ASCE*, 124(9), 789-797.

Griffiths, D. V., and Fenton, G. A. (2000). "Influence of soil strength spatial variability on the stability of an undrained clay slope by finite elements." *Slope Stability 2000, Proc. GeoDenver Symposium*, Geotechnical Special Publication No. 101, ASCE, 184-193.

Griffiths, D. V., and Fenton, G. A. (2001). "Bearing capacity of spatially random soil: the undrained clay Prandtl problem revisited." *Geotechnique*, 51(4), 351-359.

Griffiths, D. V., and Fenton, G. A. (2004). "Probabilistic slope stability analysis by finite elements." *J. Geotech. Geoenviron. Eng., ASCE*, 130(5), 507-518.

Griffiths, D. V., Fenton, G. A., and Manoharan, N. (2002a). "Bearing capacity of a rough rigid strip footing on cohesive soil: a probabilistic study." *J. Geotech. Geoenviron. Eng., ASCE*, 128(9), 743-755.

Griffiths, D. V., Fenton, G. A., and Tveten, D. E. (2002b). "Probabilistic geotechnical analysis: how difficult does it need to be?" *Proc. Int. Conf. on Probabilistics in GeoTechnics: Technical and Economic Risk Estimation*, Graz, Austria, 3-20.

Griffiths, D. V., Fenton, G. A., and Tveten, D. E. (2005). "Probabilistic earth pressure analysis by the Random Finite Element Method." *Proc. 11th Int. Conf on Computer Methods and Advances in Geomechnics (IACMAG 05)*, Turin, Italy, 4, 235-249.

Griffiths, D. V., and Lane, P. A. (1999). "Slope stability analysis by finite elements." *Geotechnique*, 49(3), 387-403.

Griffiths, D. V., and Marquez, R. M. (2007). "Three-dimensional slope stability analysis by finite elements." *Geotechnique*, 57(6), 537-546.

Hahn, G. J., and Shapiro, S. S. (1967). *Statistical models in engineering*, Wiley, New York.

Hammerstrom, D. (1993). "Working with neural networks." *IEEE Spectrum*, 30(7), 46-53.

Harr, M. E. (1987). *Reliability based design in civil engineering*, McGraw Hill, London.

Hassoun, M. H. (1995). *Fundamentals of artificial neural networks*, MIT Press, Cambridge, Mass.

Hecht-Nielsen, R. (1990). *Neurocomputing*, Addison-Wesely Publishing Company, Reading, M.A.

Hoeksema, R. J., and Kitanidis, P. K. (1985). "Analysis of the spatial structure of properties of selected aquifers." *Water Resour. Res.*, 21(4), 563-572.

Hooper, J. A., and Butler, F. G. (1966). "Some results concerning the shear strength of London clay." *Geotechnique*, 16, 282-304.

Hornik, K., Stinchcombe, M., and White, H. (1989). "Multilayer feedforward networks are universal approximators." *Neural Networks*, 2, 359-366.

Hsi, G., and Nath, J. H. (1970). "Wind drag within a simulated forest." *J. Applied Meteorology*, 9, 592-602.

Hunter, J. H., and Schuster, R. L. (1971). "Chart solutions for analysis of earth slopes." *Highway Research Record*, 345, 77-89.

Jaksa, M. B., Kaggwa, W. S., and Woodburn, J. A. (2002). "Influence of large gum trees on the soil suction profile in expansive soils." *Australian Geomechanics*, 37(1), 23-33.

Jan, J. C., Hung, S. L., Chi, S. Y., and Chern, J. C. (2002). "Neural network forecast model in deep excavation." *J. Comput. Civ. Eng., ASCE*, 16(1).

Janbu, N. (1954). "Stability analysis of slopes with dimensinless parameters." *Harvard Soil Mechanics Series*, Harvard University Press, Cambridge, Mass.

Janbu, N. (1968). "Slope stability computations." *Soil Mechanics and Foundation Engineering Report*, The Technical University of Norway, Trondhein, Norway.

Jeremic, B. (2000). "Finite element emthods for three-dimensional slope stabilty analysis." *Slope Stability 2000, Proc. GeoDenver Symposium*, Geotechnical Special Publication No. 101, ASCE, 224-238.

Jewell, R. A., and Wroth, C. P. (1987). "Direct shear tests on reinforced sand." *Geotechnique*, 37(1), 53-68.

Kim, H. S., Major, G., and Ross-Brown, D. (1978). "Application of Monte Carlo techniques to slope stability analyses." *Proc. 19th US Symposium on Rock Mechanics*, 2, 28-39.

Kozlowski, T. T. (1971). *Growth and development of trees*, vol. 2, Academic Press, New York.

Kulhawy, F. H. (1992). "On evaluation of static soil properties." *Stability and performance of slopes and embankments II (GSP 31)*, R. B. Seed and R. W. Boulanger, eds., ASCE, New York, USA, 95-115.

Lacasse, S., and Nadim, F. (1996). "Uncertainties in characterizing soil properties." *Uncertainty in the geologic environment: From theory to Practice, Proc. Uncertainty'96*, Geotechnical Special Publication No.58, ASCE, 1, 49-75.

Lane, P. A., and Griffiths, D. V. (2000). "Assessment of stability of slopes under drawdown conditions." *J. Geotech. Geoenviron. Eng., ASCE*, 126(5), 443-450.

Lechman, J. B., and Griffiths, D. V. (2000). "Analysis of the progression of failure in earth slopes by finite elements." *Slope Stability 2000, Proc. GeoDenver Symposium*, Geotechnical Special Publication No. 101, ASCE, 250-265.

Lee, I. K., White, W., and Ingles, O. G. (1983). *Geotechnical engineering*, Pitman, London.

Li, K. S. (1992). "A point estimate method for calculating the reliability index of slopes." *Proc. 6th Australia New Zealand Conf. on Geomechanics*, Christchurch, 448-451.

Li, K. S., and Lumb, P. (1987). "Probabilistic design of slopes." *Can. Geotech. J.*, 24, 520-535.

Li, K. S., and White, W. (1987). "Probabilistic characterisation of soil profiles." *Research Report No. 19*, Australian Defence Force Academy, Canberra, ACT, Australia.

Li, X. (2007). "Finite element analysis of slope stability using a nonlinear failure criterion." *Computers and Geotechnics*, 34, 188-195.

Lloyd, D. M. (1990). "Modelling the hydrology and stability of tropical cut slopes," PhD Thesis, University of Bristol.

Lowe, J., and Karafiath, L. (1960). "Stability of earth dams upon drawdown." *Proc. 1st Pan-Am Conf on Soil Mech. and Found. Eng.*, Mexico City, 2, 537-552.

Lumb, P. (1966). "The variability of natural soils." *Can. Geotech. J.*, 3, 74-97.

Lumb, P. (1974). "Application of statistics in soil mechanics." *Soil mechanics - new horizon*, I. K. Lee, ed., American Elsevier, New York, 44-111.

Maier, H. R., and Dandy, G. C. (1998). "The effect of internal parameters and geometry on the performance of back-propagation neural networks: An empirical study." *Environmental Modelling & Software*, 13, 193-209.

Maier, H. R., and Dandy, G. C. (2000). "Neural networks for prediction and forecasting of water resources variables: A review of modelling issues and applications." *Environmental Modelling and Software*, 15(2000), 101-124.

Maren, A., Harston, C., and Pap, R. (1990). *Handbook of neural computing applications*, Academic Press, San Diego, Calif.

Masters, T. (1993). *Practical neural network recipes in C++*, Academic Press, San Diego, Calif.

Matsui, T., and Sun, K. C. (1992). "Finite element slope stability analysis by shear strength reduction technique." *Soils and Foundations*, 32(1), 59-70.

McGuffey, V., Grivas, D., Iori, J., and Kyfor, Z. (1982). "Conventional and probabilistic embankment design." *J. Geotech. Eng. Div., ASCE*, 108(10), 1246-1254.

Millington, R. J., and Quirk, J. P. (1959). "Permeability of porous media." *Nature*, 183, 387-388.

Minns, A. W., and Hall, M. J. (1996). "Artificial neural networks as rainfall-runoff models." *Hydrological Sciences Journal*, 41(3), 399-417.

Monteith, J. L. (1973). *Principles of environmental physics*, Edward Arnold, London.

Morgenstern, N. R. (1963). "Stability charts for earth slopes during rapid drawdown." *Geotechnique*, XIII(2), 121-131.

Morgenstern, N. R., and Price, V. E. (1965). "The analysis of the stability of general slip surfaces." *Geotechnique*, 15(1), 79-93.

Mostyn, G. R., and Li, K. S. (1993). "Probabilistic slope stability - state of play." *Proc. Conf. on Probabilistic Methods in Geotechnical Engineering*, K. S. Li and S. C. R. Lo, eds., Balkema, Rotterdam, The Netherlands.

Mostyn, G. R., and Soo, S. (1992). "The effect of auto-correlation on the probability of failure of slopes." *Proc. 6th Australia-New Zealand Conference on Geomechanics*, 542-546.

Neaupane, K. M., and Achet, S. H. (2004). "Use of backpropagation neural network for landslide monitoring: a case study in the higher Himalaya." *Engineering Geology*, 74, 213-226.

NeuralWare. (1997). "NeuralWorks Predict Release 2.1." NeuralWare Inc., Pittsburgh.

Nguyen, V. U., and Chowdhury, R. N. (1984). "Probabilistic study of spoil pile stability in strip coal mines - two techniques compared." *J. Rock Mech., Mining Sci. and Geomech.*, 21(6), 303-312.

Ni, S. H., Lu, P. C., and Juang, C. H. (1996). "A fuzzy neural network approach to evaluation of slope failure potential." *J. Microcomputers in Civil Eng.*, 11, 59-66.

Nilaweera, N. S. (1994). "Effects of tree roots on slope stability: the case of Khao Luang Mountain area, southern Thailand," Doctor of Technical Science Dissertation, Asian Institute of Technology, Bangkok, Thailand.

Nilaweera, N. S., and Nutalaya, P. (1999). "Role of tree roots in slope stabilisation." *Bulletin of Engineering Geology and the Environment*, 57(4), 337-342.

O'Loughlin, C. L. (1974a). "The effects of timber removal on the stability of forest soils." *J. Hydrology New Zealand*, 13, 121-134.

O'Loughlin, C. L. (1974b). "A study of tree root strength deterioration following clearfelling." *Can. J. For. Res.*, 4, 107-113.

O'Loughlin, C. L., and Watson, A. J. (1979). "Root-wood strength deterioration in radiata pine after clearfelling." *New Zealand Journal of Forestry Science*, 9(3), 284-293.

Paice, G. M., Griffiths, D. V., and Fenton, G. A. (1996). "Finite element modeling of settlements on spatially random soil." *J. Geotech. Geoenviron. Eng., ASCE*, 122(9), 777-779.

Phoon, K. K., and Kulhawy, F. H. (1999a). "Characterization of geotechnical variability." *Can. Geotech. J.*, 36, 612-624.

Phoon, K. K., and Kulhawy, F. H. (1999b). "Evaluation of geotechnical property variability." *Can. Geotech. J.*, 36, 625-639.

Potts, D. M., Dounias, G. T., and Vaughan, P. R. (1990). "Finite element analysis of progressive failure of Carsington embankment." *Geotechnique*, 40(1), 79-102.

Richards, B. G., Peter, P., and Emerson, W. W. (1983). "The effects of vegetation on the swelling and shrinking soils in Australia." *Geotechnique*, 33(2), 127-139.

Richards, L. A. (1931). "Capillary conduction of liquids in porous mediums." *Physics*, 1, 318-333.

Riestenberg, M. M., and Sovonick-Dunford, S. (1983). "The role of woody vegetation in stabilising slopes in the Cincinnati area, Ohio." *Geological Society of America Bulletin*, 94, 506-18.

Ripley, B. D. (1996). *Pattern recognition and neural networks*, Cambridge University Press, Cambridge.

Roering, J. J., Schmidt, K. M., Stock, J. D., Dietrich, W. E., and Montgomery, D. R. (2003). "Shallow landsliding, root reinforcement, and the spatial distribution of trees in the Oregon Coast Range." *Can. Geotech. J.*, 40, 237-253.

Rojas, R. (1996). *Neural networks: A systematic introduction*, Springer-Verlag, Berlin.

Rosenblueth, E. (1975). "Point estimates for probability moments." *Proc. Nat. Acad. Sci. USA*, 10, 3812-3814.

Rosenblueth, E. (1981). "Two-point estimates in probabilities." *Appl. Math. Modelling*, 5, 329-335.

Rumelhart, D. E., Hilton, G. E., and Williams, R. J. (1986). "Learning internal representation by error propagation." *Parallel distributed processing*, D. E. Rumerlhart and J. L. McClelland, eds., MIT Press, Cambridge, Mass., 318-362.

Sainak, A. N. (2004). "Application of three-dimensional finite-element method in parametric and geometric studies of slope stability." *Advamces in geotechnical engineering (Skempton Conf.)*, Thomas Telford, London, 2, 933-942.

Saka, H., and Ural, D. N. (1998). "Liquefaction assessment by neural networks." *Electronic Journal of Geotechnical Engineering*, http://www.ejge.com/1998/Ppr9803/Ppr9803.htm.

Sakallariou, M. G., and Ferentinou, M. D. (2005). "A study of slope stability prediction using neural networks." *Geotechnical and Geological Engineering*, 23, 419-445.

Schiechtl, H. M. (1980). *Bioengineering for land reclamation and conservation*, University of Alberta Press, Edmonton, Canada.

Schmidt, K. M., Roering, J. J., Stock, J. D., Dietrich, W. E., Montgomery, D. R., and Schaub, T. (2001). "The variability of root cohesion as an influence on shallow landslide susceptibility in the Oregon Coast Range." *Can. Geotech. J.*, 38, 995-1024.

Shahin, M. A. (2003). "Use of artificial neural networks for predicting settlement of shallow foundations on cohesionless soils," PhD Thesis, School of Civil and Environmental Engineering, University of Adelaide, Adelaide.

Shahin, M. A., and Jaksa, M. B. (2005). "Neural network prediction of pullout capacity of marquee ground anchors." *Computers and Geotechnics*, 32, 153-163.

Shahin, M. A., Jaksa, M. B., and Maier, H. R. (2001). "Artificial neural network applications in geotechnical engineering." *Aust. Geomech.*, 36(1), 49-62.

Shahin, M. A., Jaksa, M. B., and Maier, H. R. (2002a). "Artificial neural network-based settlement prediction formula for shallow foundations on granular soils." *Aust. Geomech.*, 37(4), 45-52.

Shahin, M. A., Maier, H. R., and Jaksa, M. B. (2002b). "Predicting settlements of shallow foundation using artificial neural networks." *J. Geotech. Geoenviron. Eng., ASCE*, 128(9), 785-793.

Shahin, M. A., Maier, H. R., and Jaksa, M. B. (2004). "Data division for developing neural networks applied to geotechnical engineering." *J. Comput. Civ. Eng., ASCE*, 18(2), 105-114.

Shewbridge, S. E., and Sitar, N. (1990). "Deformation based model for reinforced sand in direct shear." *J. Geotech. Eng., ASCE*, 116(GT7), 1153-7.

Shewbridge, S. E., and Sitar, N. (1996). "Formation of shear zones in reinforced sand." *J. Geotech. Eng., ASCE*, 122(11), 873-885.

Sidle, R. C. (1992). "A theoretical model of the effects of timber harvesting on slope stability." *Water Resources Research*, 28(7), 1897-1910.

Sidle, R. C., and Swanston, D. N. (1982). "Analysis of a small debris slide in coastal Alaska." *Can. Geotech. J.*, 19, 167-174.

Simon, A., and Collison, A. J. C. (2002). "Quantifying the mechanical and hydrologic effects of riparian vegetation on streambank stability." *Earth Surf. Process. Landforms*, 27, 527-546.

Smith, G. N. (1986). *Probability and statistics in civil engineering: an introduction*, Collins, London.

Smith, I. M., and Griffiths, D. V. (1988). *Programming the finite element method*, 2nd edition, John Wiley and Sons, Chichester, New York.

Smith, I. M., and Griffiths, D. V. (1998). *Programming the finite element method*, 3rd edition, John Wiley and Sons, Chichester, New York.

Smith, I. M., and Griffiths, D. V. (2004). *Programming the finite element method*, 4th edition, John Wiley and Sons, Chichester, New York.

Smith, I. M., and Hobbs, R. (1974). "Finite element analysis of centrifuged and built-up slopes." *Geotechnique*, 24(4), 531-559.

Smith, M. (1993). *Neural networks for statistical modelling*, Van Nostrand, Reinhold, New York.

Snitbhan, N., and Chen, W. F. (1976). "Elastic-plastic deformation analysis of soil slopes." *Computers and Structures*, 9, 567-577.

Soulie, M., Montes, P., and Silvestri, V. (1990). "Modelling spatial variability of soil parameters." *Can. Geotech. J.*, 20(3), 453-467.

Spencer, E. (1967). "A method of anlaysis of the stability of embankments assuming parallel inter-slice forces." *Geotechnique*, 17(1), 11-26.

Stein, R. (1993). "Selecting data for neural networks." *AI Expert*, 8(2), 42-47.

Stone, M. (1974). "Cross-validatory choice and assessment of statistical predictions." *J. Royal Statistical Society*, B36, 111-147.

Sudicky, E. A. (1986). "A natural gradient experiment on solute transport in a sand aquifer: Spatial variability of hydraulic conductivity and its role in the dispersion process." *Water Resour. Res.*, 23(13), 2069-2083.

Swanston, D. N. (1970). "Mechanics of debris avalanching in shallow till soils of south Alaska." *US Department of Agriculture Forest Research Paper, PNW-103*, Pacific and Northwest Forest and Range Experimental Station, Portland, Oregon.

Tang, W. H., Yucemen, M. S., and Ang, A. H. S. (1976). "Probabilistic-based short term design of slopes." *Can. Geotech. J.*, 37, 264-269.

Taylor, D. W. (1937). "Stability of earth slopes." *J. Boston. Soc. Civ. Eng.*, 24, 197-246.

Taylor, D. W. (1948). *Fundamentals of soil mechanics*, John Wiley and Sons, Inc., New York, N.Y.

Terwilliger, V. J., and Waldron, L. J. (1990). "Assessing the contribution of roots to the strength of undisturbed, slip prone soils." *Catena*, 17, 151-162.

Terwilliger, V. J., and Waldron, L. J. (1991). "Effects of root reinforcement on soil-slip patterns in the Transverse Ranges of southern California." *Geological Society of America Bulletin*, 103, 775-785.

Terzaghi, K. (1950). "Mechanism of landslides." *Geological Society of America, Engineering Geology (Berkey) Volume*, 83-123.

Thornton, S. I. (1994). "Probability calculation for slope stability." *Proc. Computer Methods and Advances in Geomechanics*, 2505-2509.

Tobutt, D. C. (1982). "Monte Carlo simulation methods for slope stability." *Computers and Geoscience*, 8(2), 199-208.

Tokar, S. A., and Johnson, P. A. (1999). "Rainfall-runoff modeling using artificial neural networks." *J. Hydrol. Eng.*, 4(3), 232-239.

Twomey, J. M., and Smith, A. E. (1997). "Validation and verification." *Artificial neural networks for civil engineers: Fundamentals and applications*, N. Kartam, I. Flood, and J. H. Garrett, eds., ASCE, New York, 44-64.

U.S. Army Corps of Engineers. (1995). "Introduction to probability and reliability methods for use in geotechnical engineering." *ETL 1110-2-547*, Washington D.C.

Vanmarcke, E. H. (1977a). "Probabilistic modelling of soil properties." *J. Geotech. Eng. Div., ASCE*, 103(11), 1227-1246.

Vanmarcke, E. H. (1977b). "Reliability of earth slopes." *J. Geotech. Eng. Div., ASCE*, 103, 1247-1265.

Vanmarcke, E. H. (1983). *Random fields: Analysis and synthesis*, MIT Press, Cambridge, Massachusetts.

Waldron, L. J. (1977). "The shear resistance of root-permeated homogeneous and stratified soil." *Soil Science Society of America Journal*, 41, 843-849.

Waldron, L. J., and Dakessian, S. (1981). "Soil reinforcement by roots: calculation of increased soil shear resistance from root properties." *Soil Science*, 132(6), 427-435.

Waldron, L. J., and Dakessian, S. (1982). "The effect of grass, legume and tree roots on soil shearing resistance." *Soil Science Society of America Journal*, 46, 894-897.

Waldron, L. J., Dakessian, S., and Nemson, J. A. (1983). "Shear resistance enhancement of 1.22-meter diameter soil cross sections by pine and alfalfa roots." *Soil Science Society of America Journal*, 47, 9-14.

Wang, H. B., Xu, W. Y., and Xu, R. C. (2005). "Slope stability evaluation using Back Propagation Neural Networks." *Engineering Geology*, 80, 302-315.

Wang, W. L., and Yen, B. C. (1974). "Soil arching in slopes." *J. Geotech. Eng. Div., ASCE*, 100(GT1), 61-79.

Wilkinson, P. L. (2000). "Investigating the hydrological and geotechnical effects of vegetation on slope stability: Development of a fully integrated numerical model," PhD Thesis, Department of Geographical Sciences, University of Bristol.

Wilkinson, P. L., Anderson, M. G., and Lloyd, D. M. (2002a). "An integrated hydrological model for rain-induced landslide prediction." *Earth Surf. Process. Landforms*, 27, 1285-1297.

Wilkinson, P. L., Anderson, M. G., Lloyd, D. M., and Renaud, J. (2002b). "Landslide hazard and bioengineering: towards providing improved decision support through integrated numerical model development." *Environmental Modelling & Software*, 17, 333-344.

Wilkinson, P. L., Brooks, S. M., and Anderson, M. G. (2000). "Design and application of an automated non-circular slip surface search within a combined hydrology and stability model (CHASM)." *Hydrol. Process.*, 14, 2003-2017.

Williams, A. A. B., and Pidgeon, J. T. (1983). "Evapo-transpiration and heaving clays in South Africa." *Geotechnique*, 33(2), 141-150.

Wolff, T. F. (1996). "Probabilistic slope stability in theory and preactice." *Uncertainty in the geologic environment: From theory to Practice, Proc. Uncertainty'96*, Geotechnical Special Publication No. 58, ASCE, 2, 419-433.

Wong, F. S. (1984). "Uncertainties in modeling of slope stability." *Computers and Structures*, 19, 777-791.

Wu, T. H., Beal, P. E., and Lan, C. (1988a). "In-situ shear test of soil-root systems." *J. Geotech. Eng., ASCE*, 114(12), 1377-1393.

Wu, T. H., and Kraft, L. M. (1970). "Safety analysis of slopes." *J. Soil Mech. Found. Div., ASCE*, 96(2), 609-630.

Wu, T. H., McKinnell, W. P., and Swanston, D. N. (1979). "Strength of tree root and landslides on Prince of Wales Island, Alaska." *Can. Geotech. J.*, 16, 19-33.

Wu, T. H., McOmber, R. M., Erb, R. T., and Beal, P. E. (1988b). "Study of soil-root interaction." *J. Geotech. Eng., ASCE*, 114(12), 1351-1375.

Wu, T. H., and Watson, A. (1998). "In situ shear tests of soil blocks with roots." *Can. Geotech. J.*, 35, 579-590.

Wu, W., and Sidle, R. C. (1995). "A distributed slope stability model for steep forested basins." *Water Resour. Res.*, 31(8), 2097-2110.

Zheng, H., Tham, L. G., and Liu, D. (2006). "On two definitions of the factor of safety commonly used in the finite element slope stability analysis." *Computers and Geotechnics*, 33, 188-195.

Ziemer, R. R. (1981). "The role of vegetation of the stability of forested slopes." *IUFRO 17th World Congress Proceedings-Reference-Exposes*, 297-308.

Zienkiewicz, O. C., and Cormeau, I. C. (1974). "Viscoplasticity, plasticity and creep in elastic solids. A unified numerical solution approach." *Int. J. Num. Met. Eng.*, 8, 821-845.

Zienkiewicz, O. C., Humpheson, C., and Lewis, R. W. (1975). "Associated and non-associated viscoplasticity and plasticity in soil mechanics." *Geotechnique*, 25, 671-689.

Zienkiewicz, O. C., and Taylor, R. L. (1989). *The finite element method*, 4th edition, 1, McGraw-Hill, New York.

Zurada, J. M. (1992). *Introduction to artificial neural systems*, West Publishing Company, St. Paul.

APPENDIX A PROBABILISTIC STABILITY CHARTS

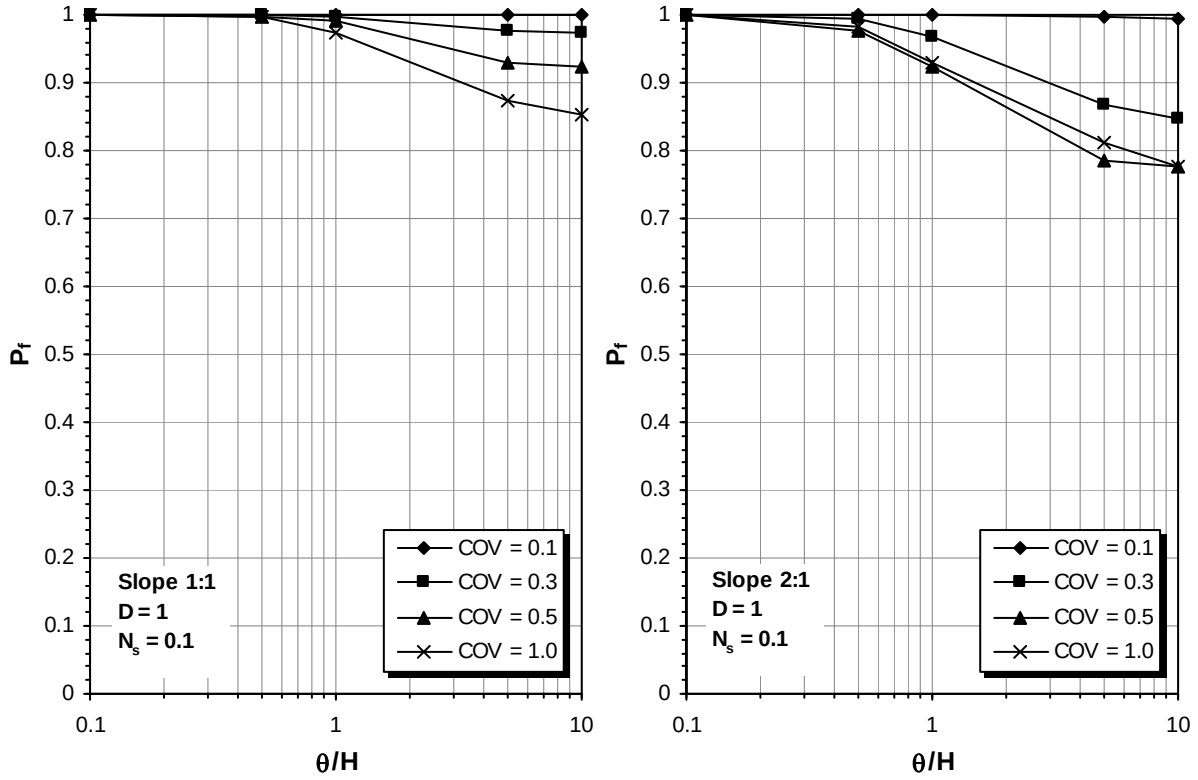
Slope 1:1
D = 1
Ns = 0.1
Slope 2:1
D = 1
Ns = 0.1
COV = 0.1
COV = 0.3
COV = 0.5
COV = 1.0
Pf
θ/H

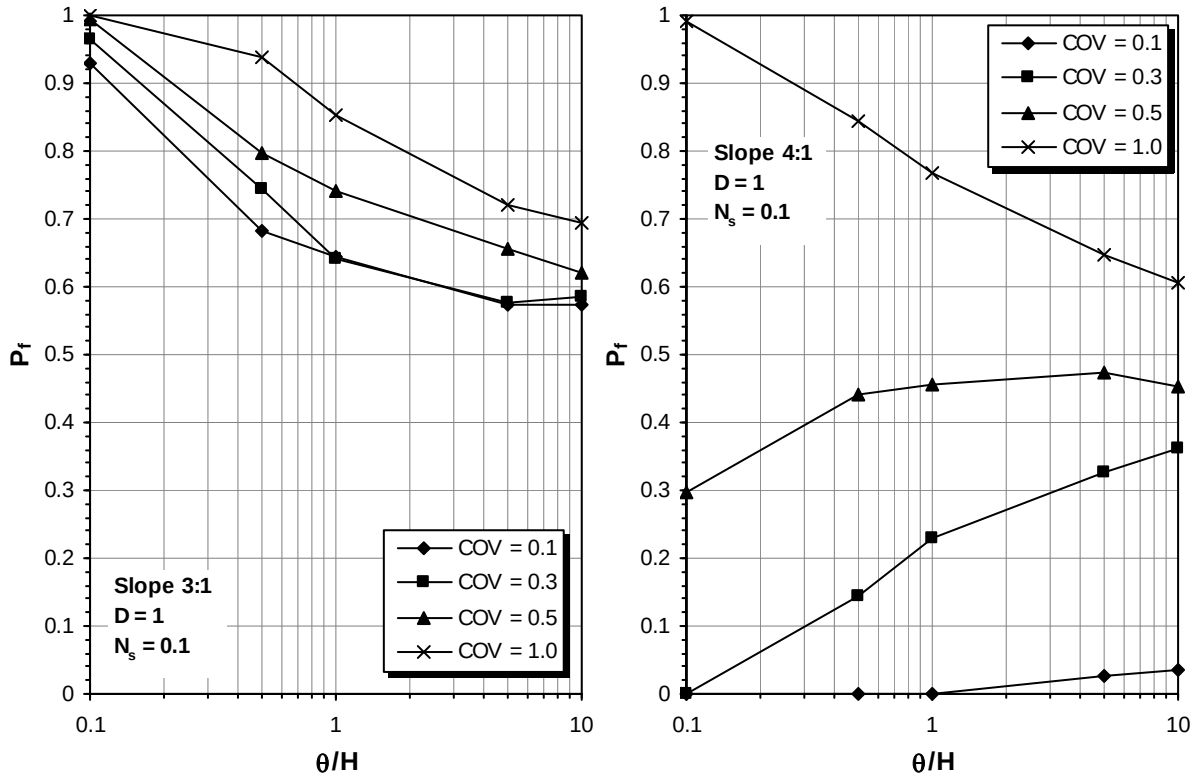
Slope 3:1
D = 1
Ns = 0.1
Slope 4:1
D = 1
Ns = 0.1
COV = 0.1
COV = 0.3
COV = 0.5
COV = 1.0
Pf
θ/H

D = 1; N_s = 0.1

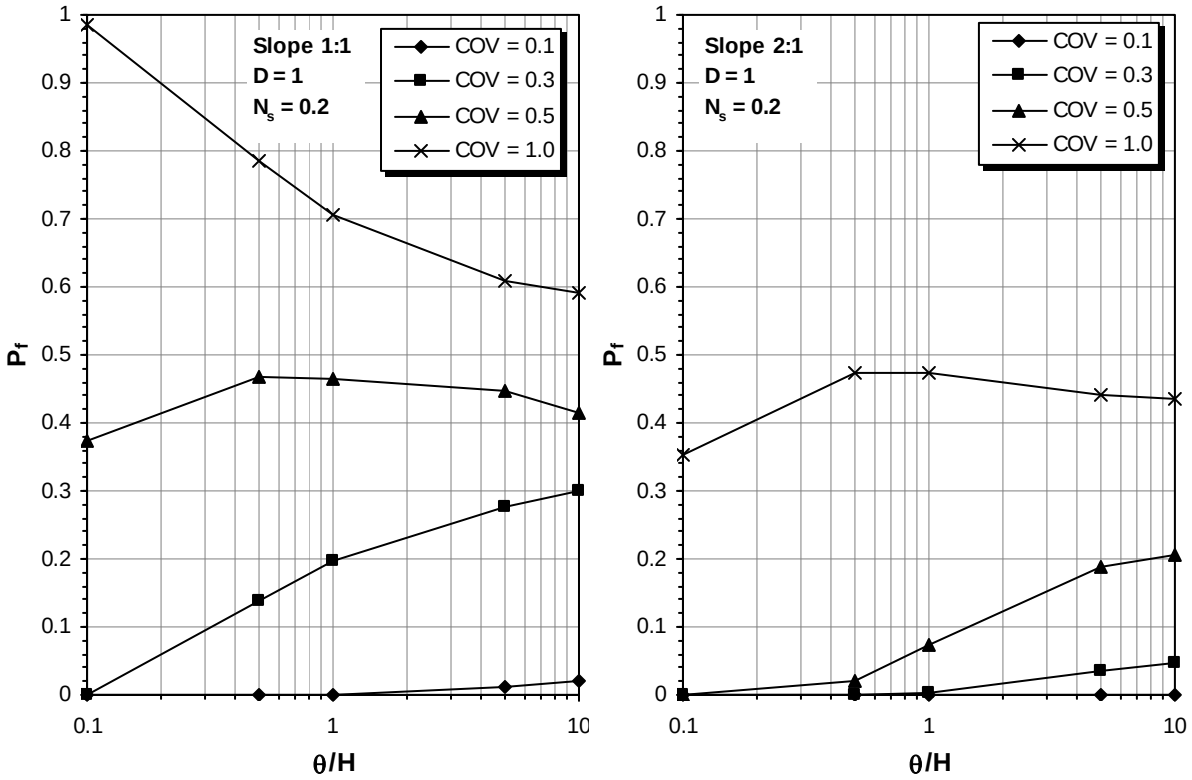
Slope 1:1
D = 1
Ns = 0.2
COV = 0.1
COV = 0.3
COV = 0.5
COV = 1.0
Pf
θ/H
Slope 2:1
D = 1
Ns = 0.2
COV = 0.1
COV = 0.3
COV = 0.5
COV = 1.0
Pf
θ/H

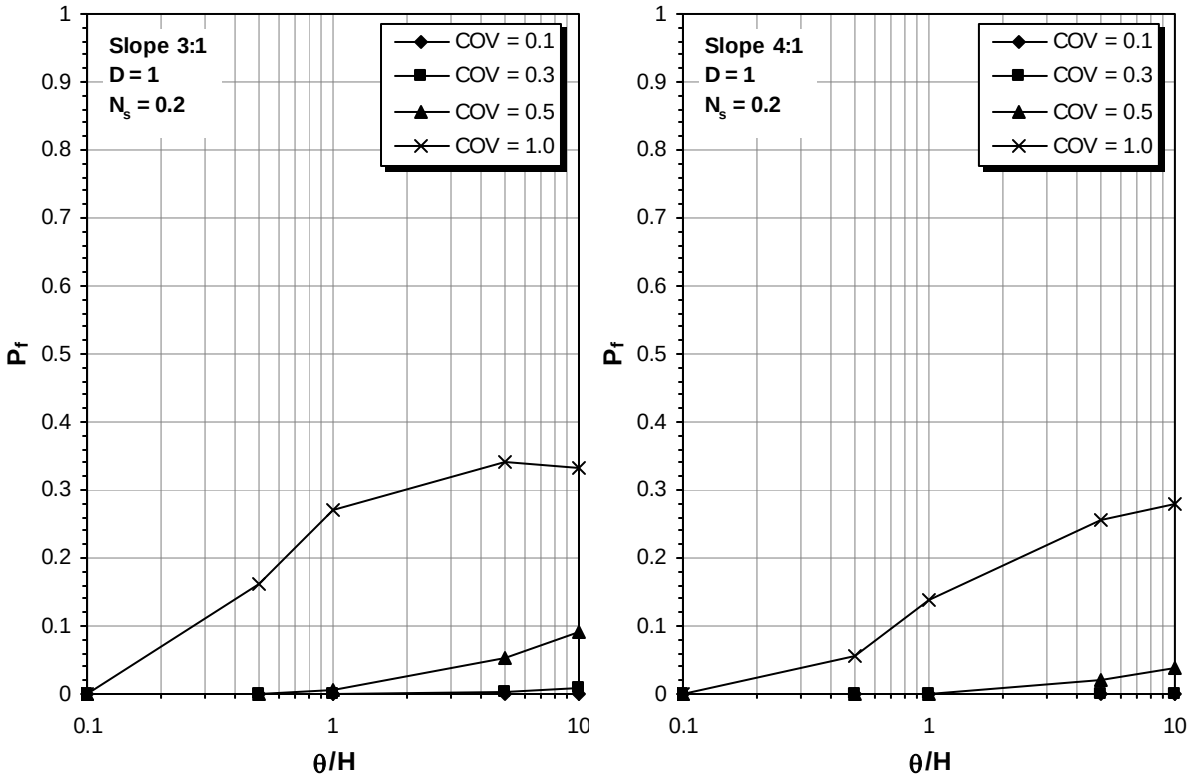
Slope 3:1
D = 1
Ns = 0.2
COV = 0.1
COV = 0.3
COV = 0.5
COV = 1.0
Pf
θ/H
Slope 4:1
D = 1
Ns = 0.2
COV = 0.1
COV = 0.3
COV = 0.5
COV = 1.0
Pf
θ/H

D = 1; N_s = 0.2

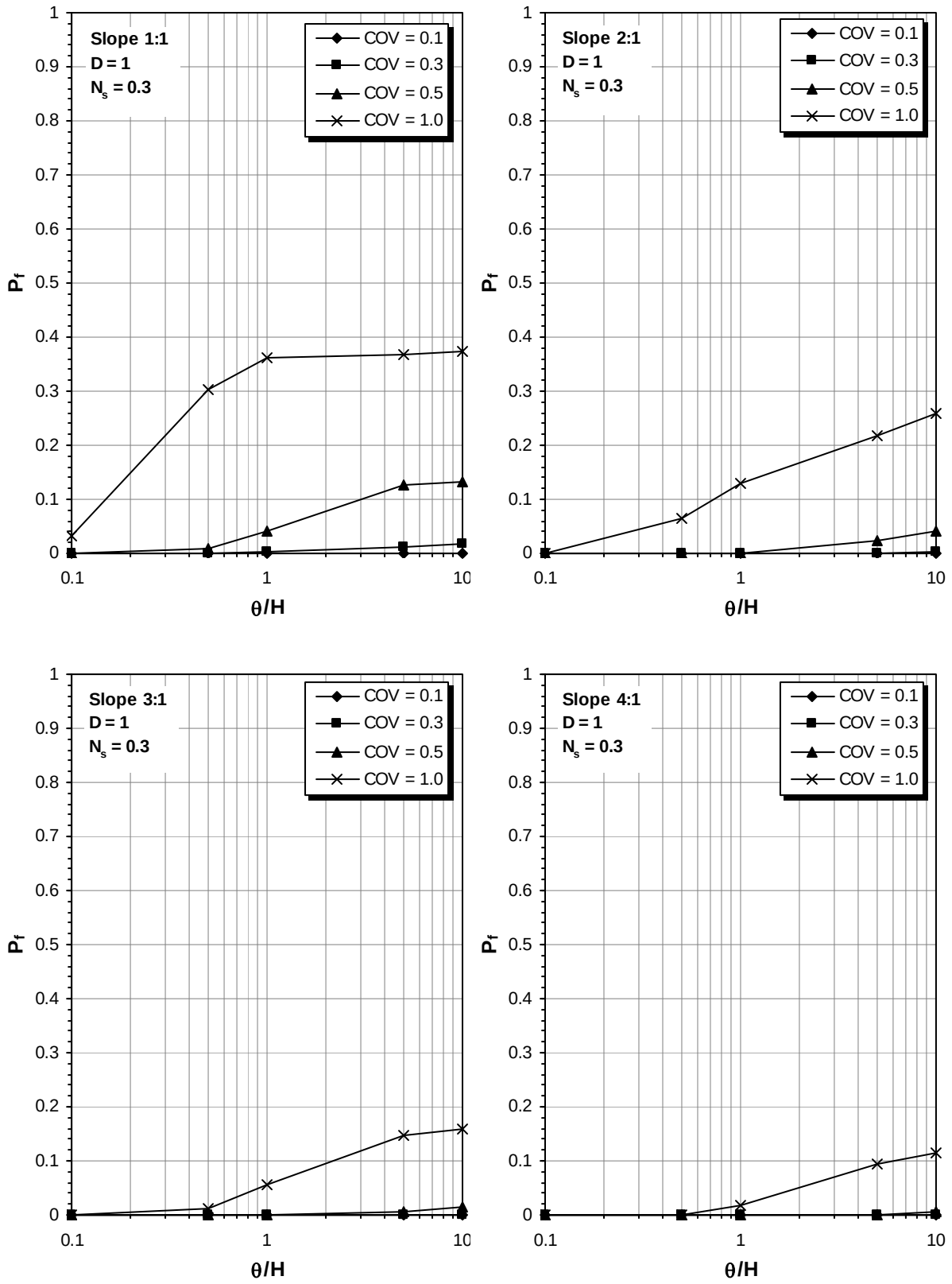
Slope 1:1
D = 1
N_s = 0.3
Slope 2:1
D = 1
N_s = 0.3
Slope 3:1
D = 1
N_s = 0.3
Slope 4:1
D = 1
N_s = 0.3
COV = 0.1
COV = 0.3
COV = 0.5
COV = 1.0
P_f
θ/H
0
0.1
0.2
0.3
0.4
0.5
0.6
0.7
0.8
0.9
1
0.1
1
10

D = 1; N_s = 0.3

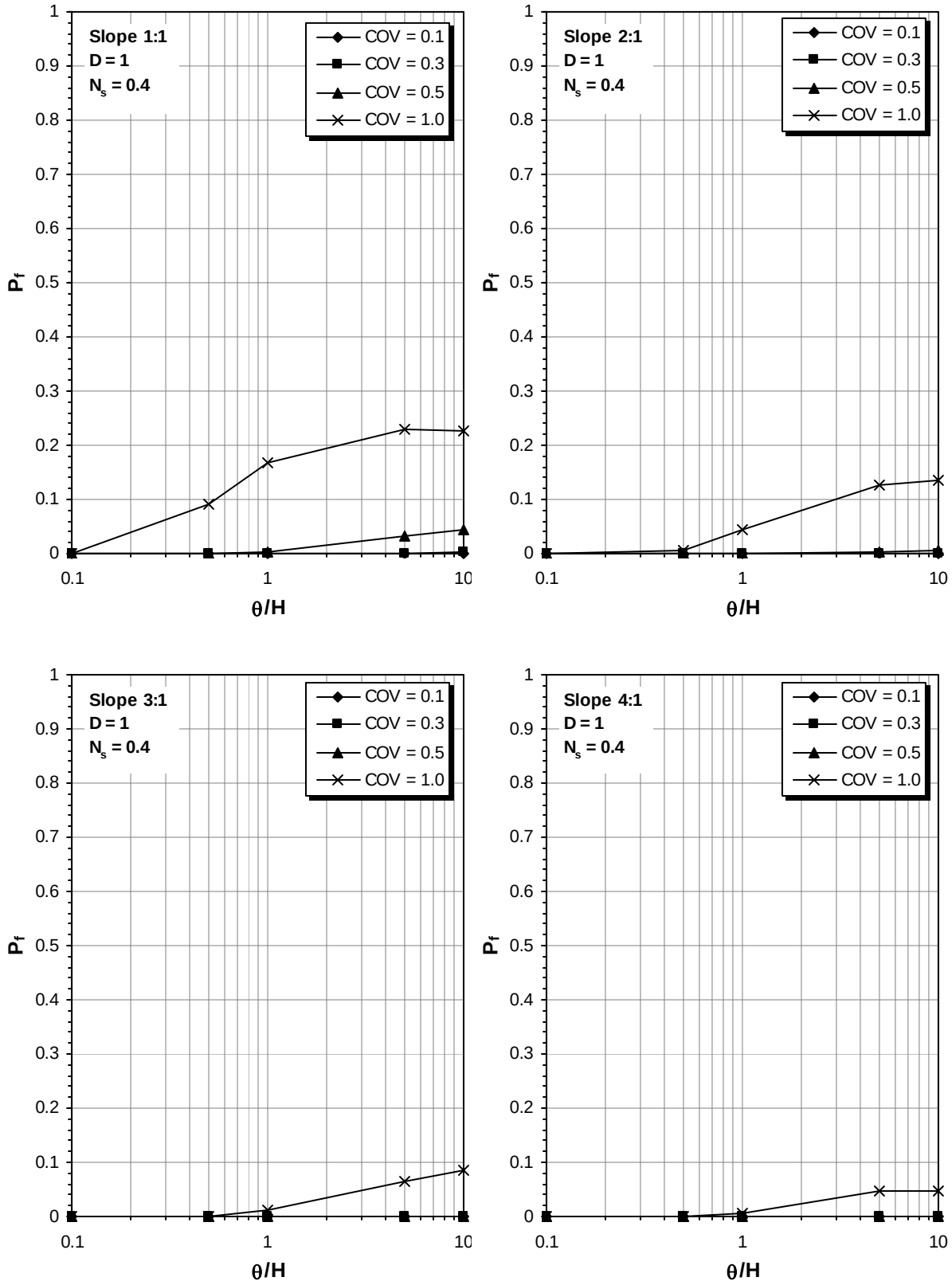
Slope 1:1
D = 1
N_s = 0.4
COV = 0.1
COV = 0.3
COV = 0.5
COV = 1.0
P_f
θ/H
Slope 2:1
D = 1
N_s = 0.4
Slope 3:1
D = 1
N_s = 0.4
Slope 4:1
D = 1
N_s = 0.4

D = 1; N_s = 0.4

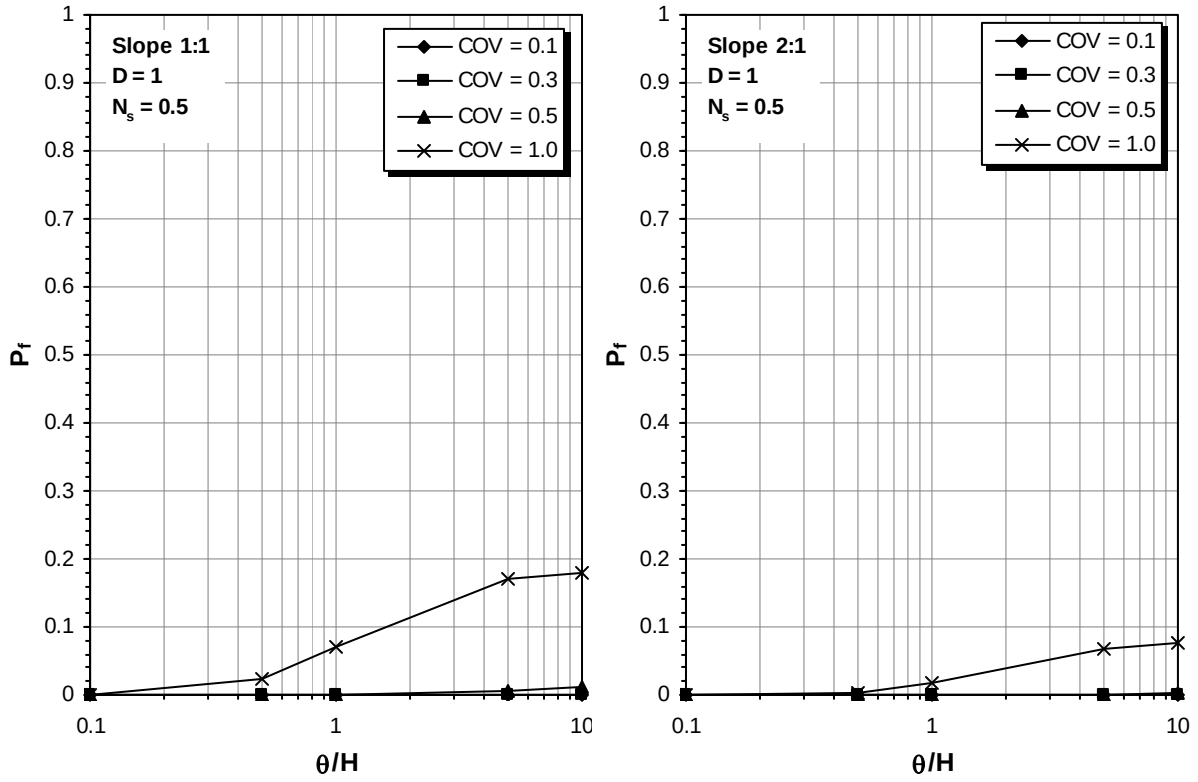
Slope 1:1
D = 1
N_s = 0.5
COV = 0.1
COV = 0.3
COV = 0.5
COV = 1.0
P_f
θ/H
0
0.1
0.2
0.3
0.4
0.5
0.6
0.7
0.8
0.9
1
0.1
1
10

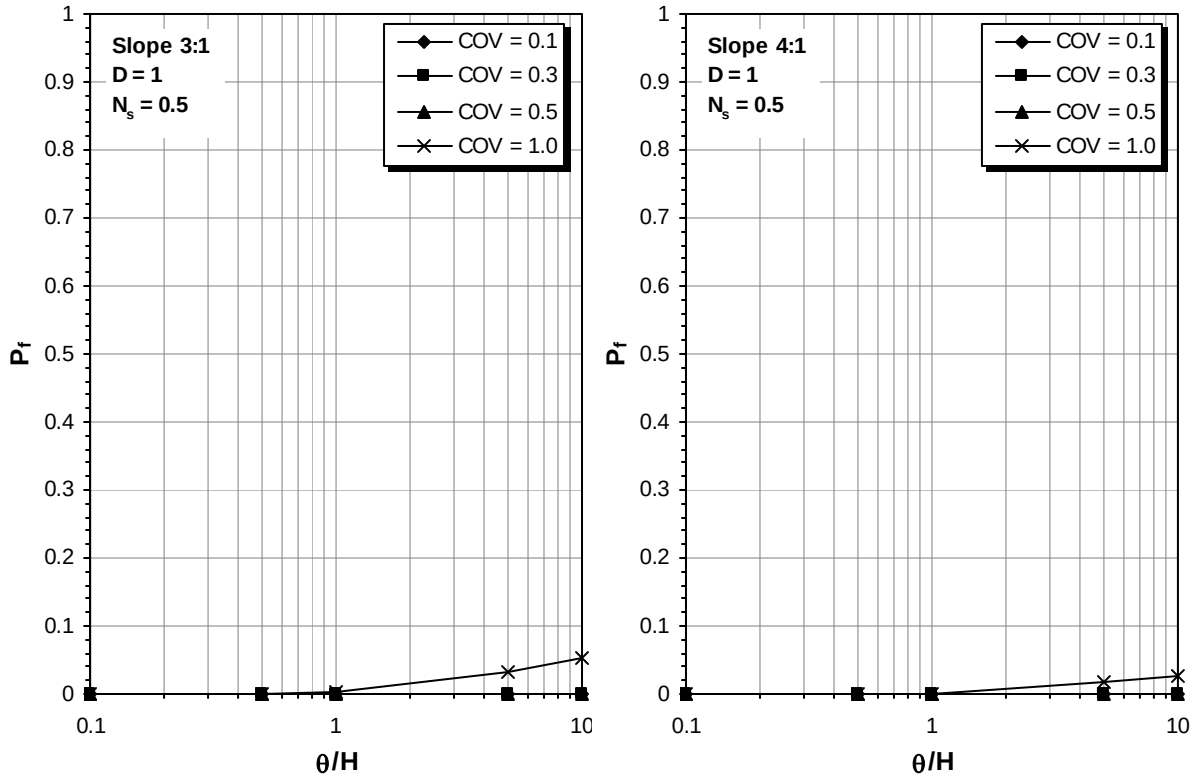
Slope 3:1
D = 1
N_s = 0.5
COV = 0.1
COV = 0.3
COV = 0.5
COV = 1.0
P_f
θ/H
0
0.1
0.2
0.3
0.4
0.5
0.6
0.7
0.8
0.9
1
0.1
1
10

D = 1; N_s = 0.5

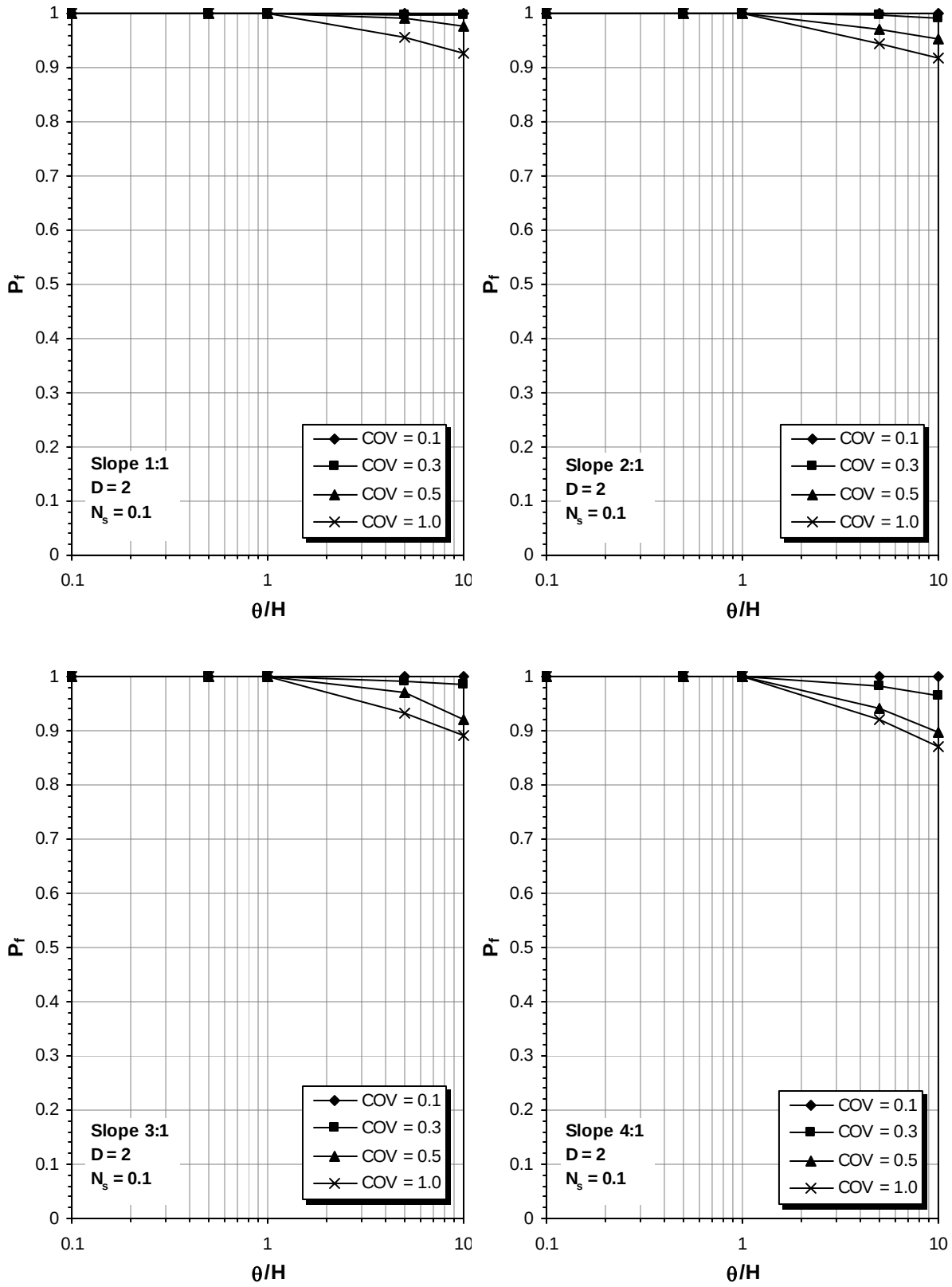
Slope 1:1
D = 2
Ns = 0.1
Slope 2:1
D = 2
Ns = 0.1
Slope 3:1
D = 2
Ns = 0.1
Slope 4:1
D = 2
Ns = 0.1
COV = 0.1
COV = 0.3
COV = 0.5
COV = 1.0
Pf
θ/H
0
0.1
0.2
0.3
0.4
0.5
0.6
0.7
0.8
0.9
1
0.1
1
10

D = 2; N_s = 0.1

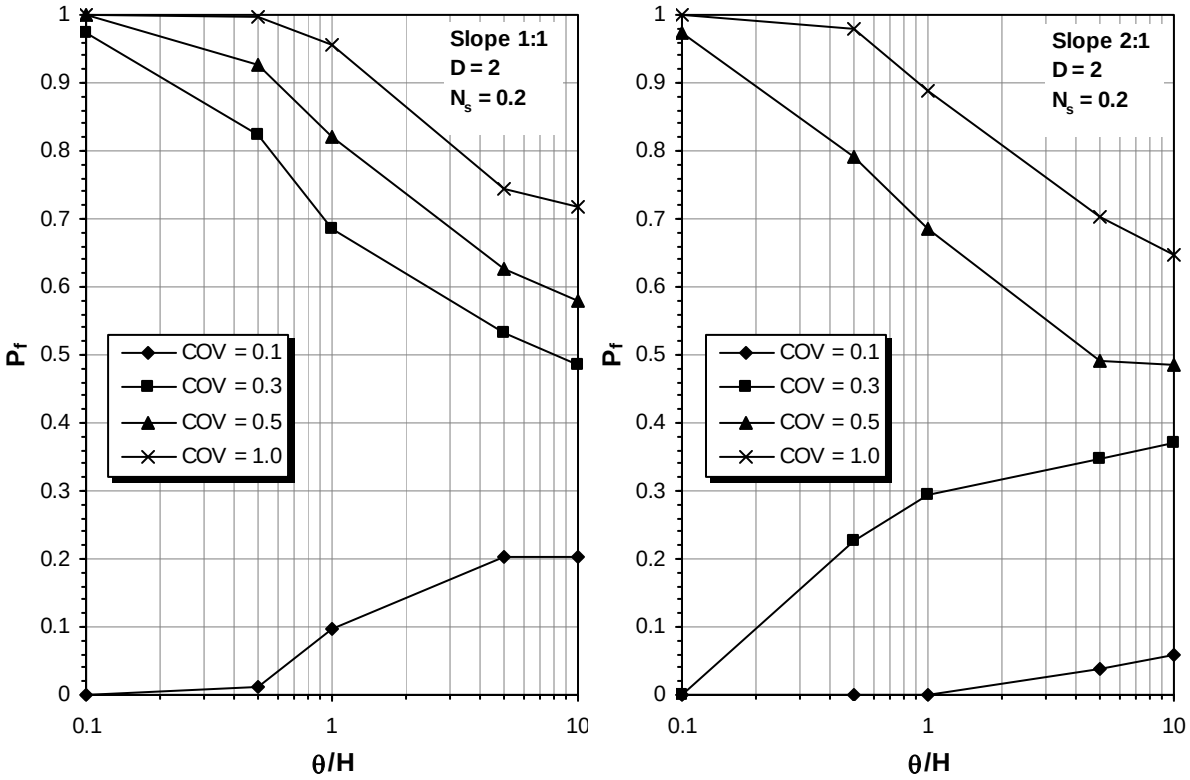
Slope 1:1
D = 2
Ns = 0.2
Slope 2:1
D = 2
Ns = 0.2
COV = 0.1
COV = 0.3
COV = 0.5
COV = 1.0
Pf
θ/H
0
0.1
0.2
0.3
0.4
0.5
0.6
0.7
0.8
0.9
1
0.1
1
10

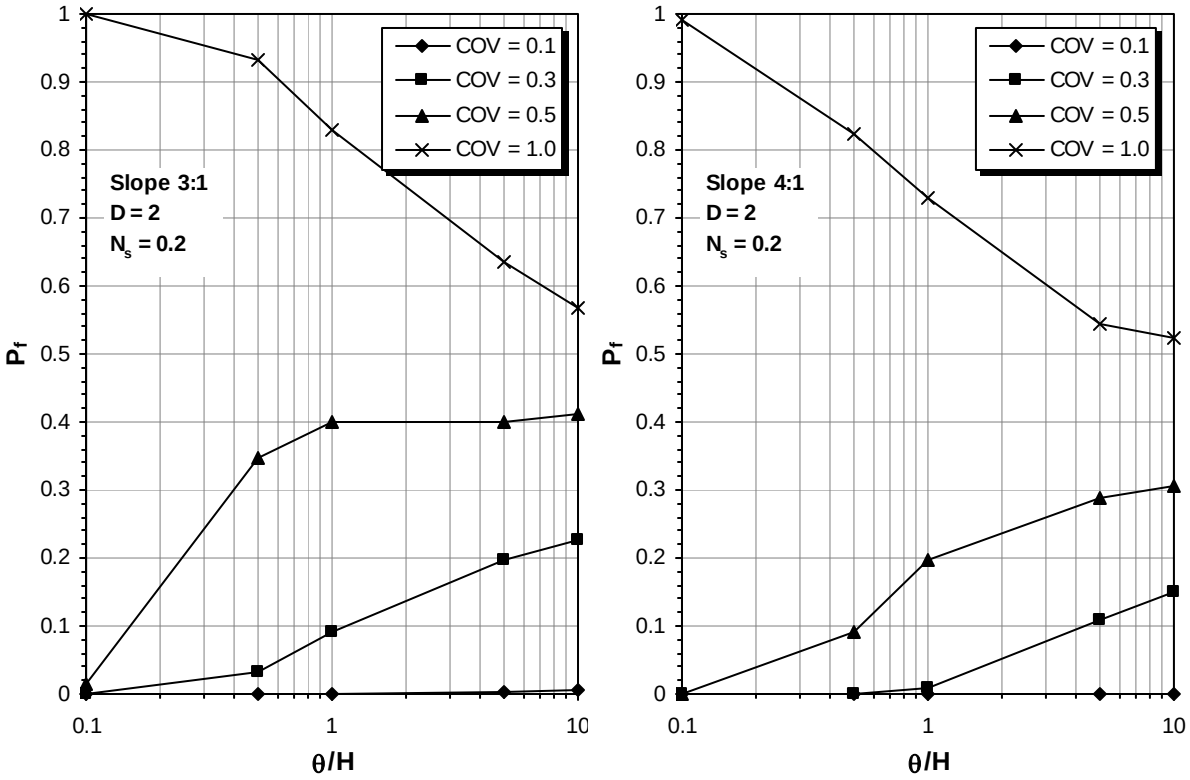
Slope 3:1
D = 2
Ns = 0.2
Slope 4:1
D = 2
Ns = 0.2
COV = 0.1
COV = 0.3
COV = 0.5
COV = 1.0
Pf
θ/H
0
0.1
0.2
0.3
0.4
0.5
0.6
0.7
0.8
0.9
1
0.1
1
10

D = 2; N_s = 0.2

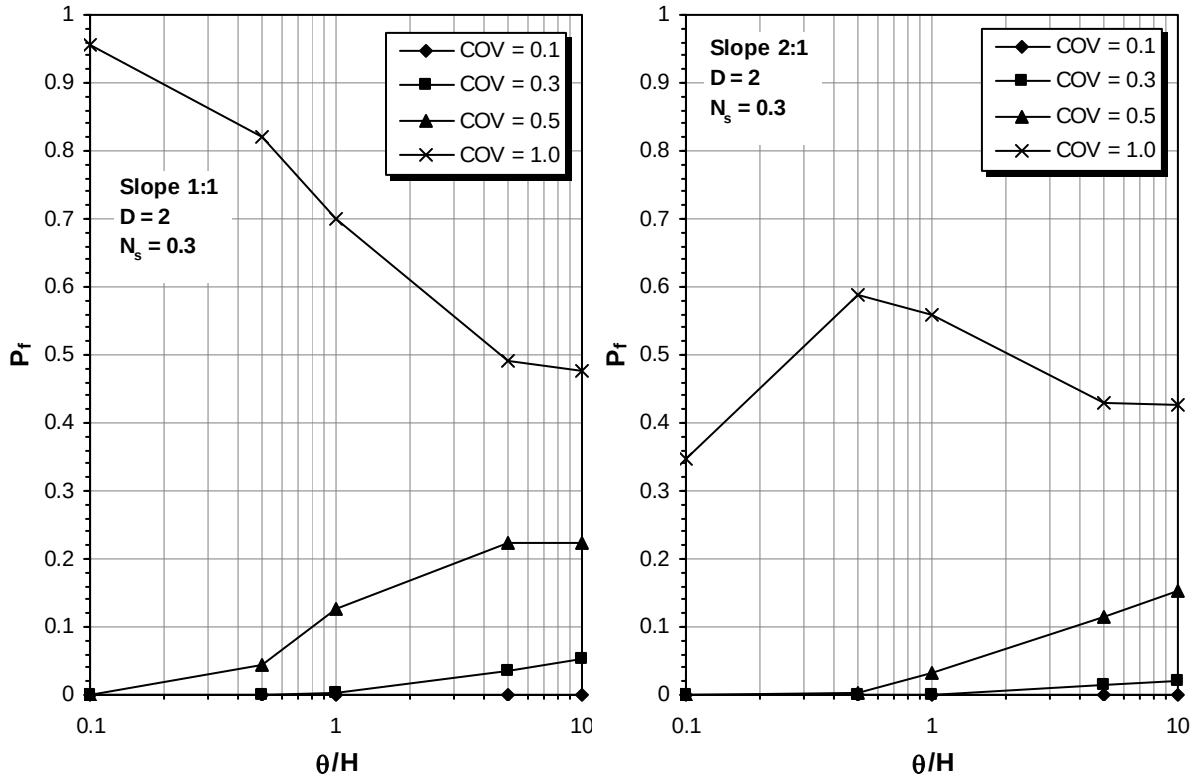
Slope 1:1
D = 2
N_s = 0.3
COV = 0.1
COV = 0.3
COV = 0.5
COV = 1.0
P_f
θ/H
Slope 2:1
D = 2
N_s = 0.3
COV = 0.1
COV = 0.3
COV = 0.5
COV = 1.0
P_f
θ/H

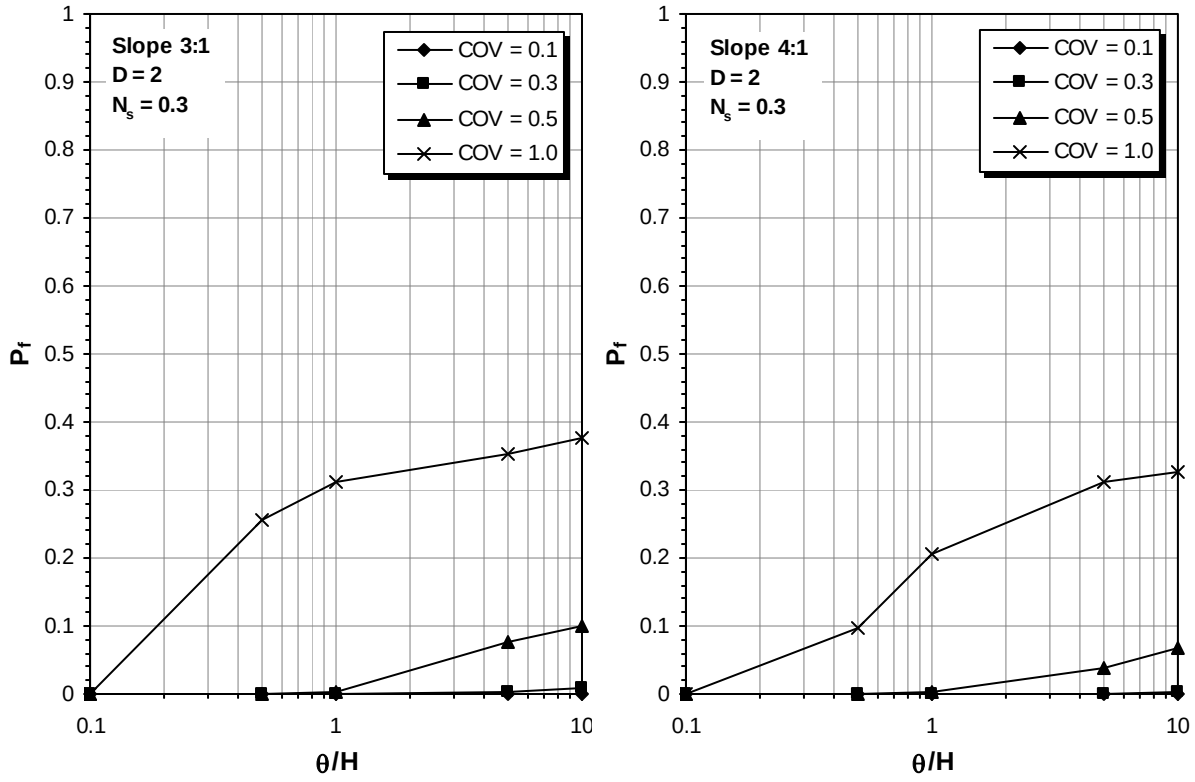
Slope 3:1
D = 2
N_s = 0.3
COV = 0.1
COV = 0.3
COV = 0.5
COV = 1.0
P_f
θ/H
Slope 4:1
D = 2
N_s = 0.3
COV = 0.1
COV = 0.3
COV = 0.5
COV = 1.0
P_f
θ/H

D = 2; N_s = 0.3

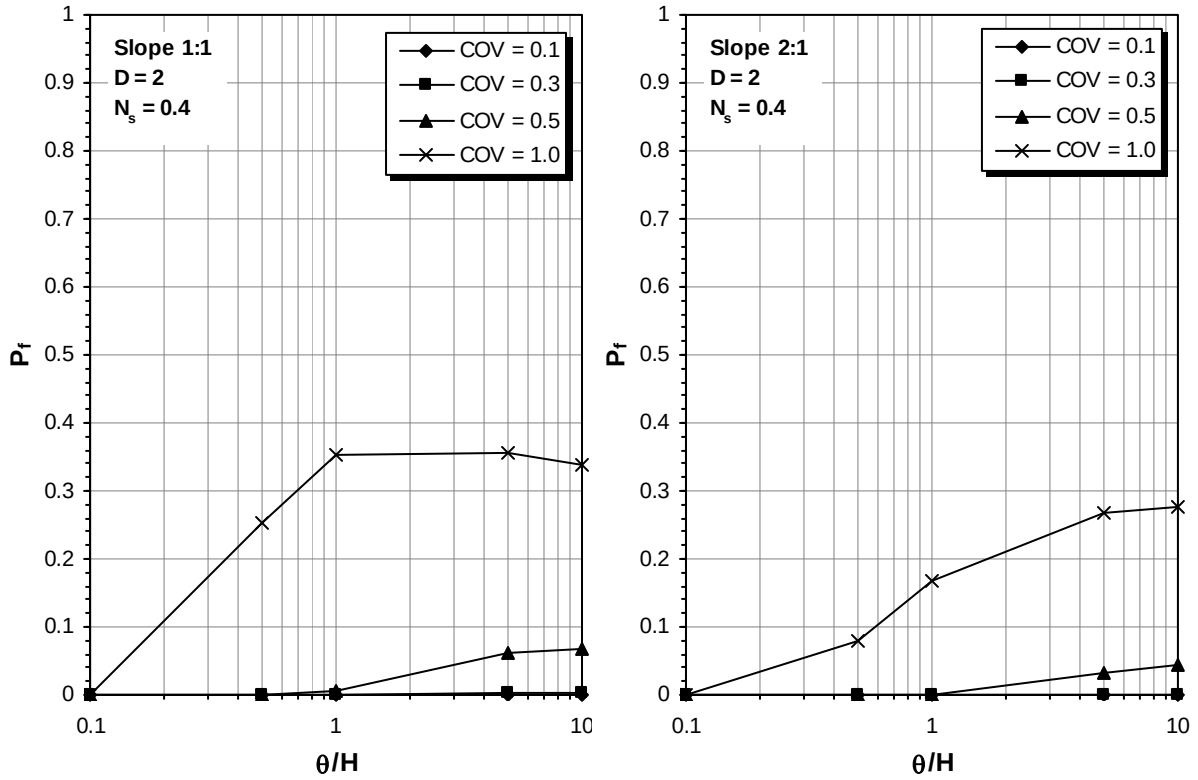
Slope 1:1
D = 2
N_s = 0.4
COV = 0.1
COV = 0.3
COV = 0.5
COV = 1.0
P_f
θ/H
0
0.1
0.2
0.3
0.4
0.5
0.6
0.7
0.8
0.9
1
0.1
1
10

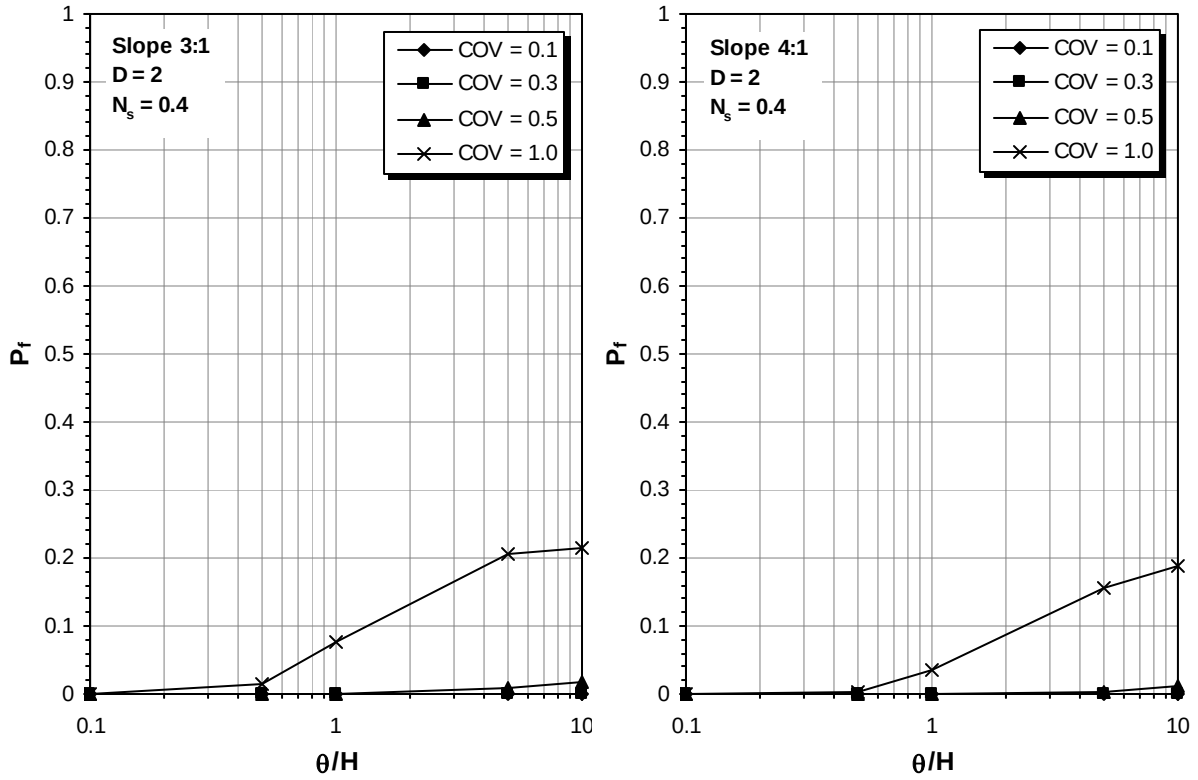
Slope 3:1
D = 2
N_s = 0.4
COV = 0.1
COV = 0.3
COV = 0.5
COV = 1.0
P_f
θ/H
0
0.1
0.2
0.3
0.4
0.5
0.6
0.7
0.8
0.9
1
0.1
1
10

Slope 2:1
D = 2
N_s = 0.4
COV = 0.1
COV = 0.3
COV = 0.5
COV = 1.0
P_f
θ/H
0
0.1
0.2
0.3
0.4
0.5
0.6
0.7
0.8
0.9
1
0.1
1
10

Slope 4:1
D = 2
N_s = 0.4
COV = 0.1
COV = 0.3
COV = 0.5
COV = 1.0
P_f
θ/H
0
0.1
0.2
0.3
0.4
0.5
0.6
0.7
0.8
0.9
1
0.1
1
10

D = 2; N_s = 0.4

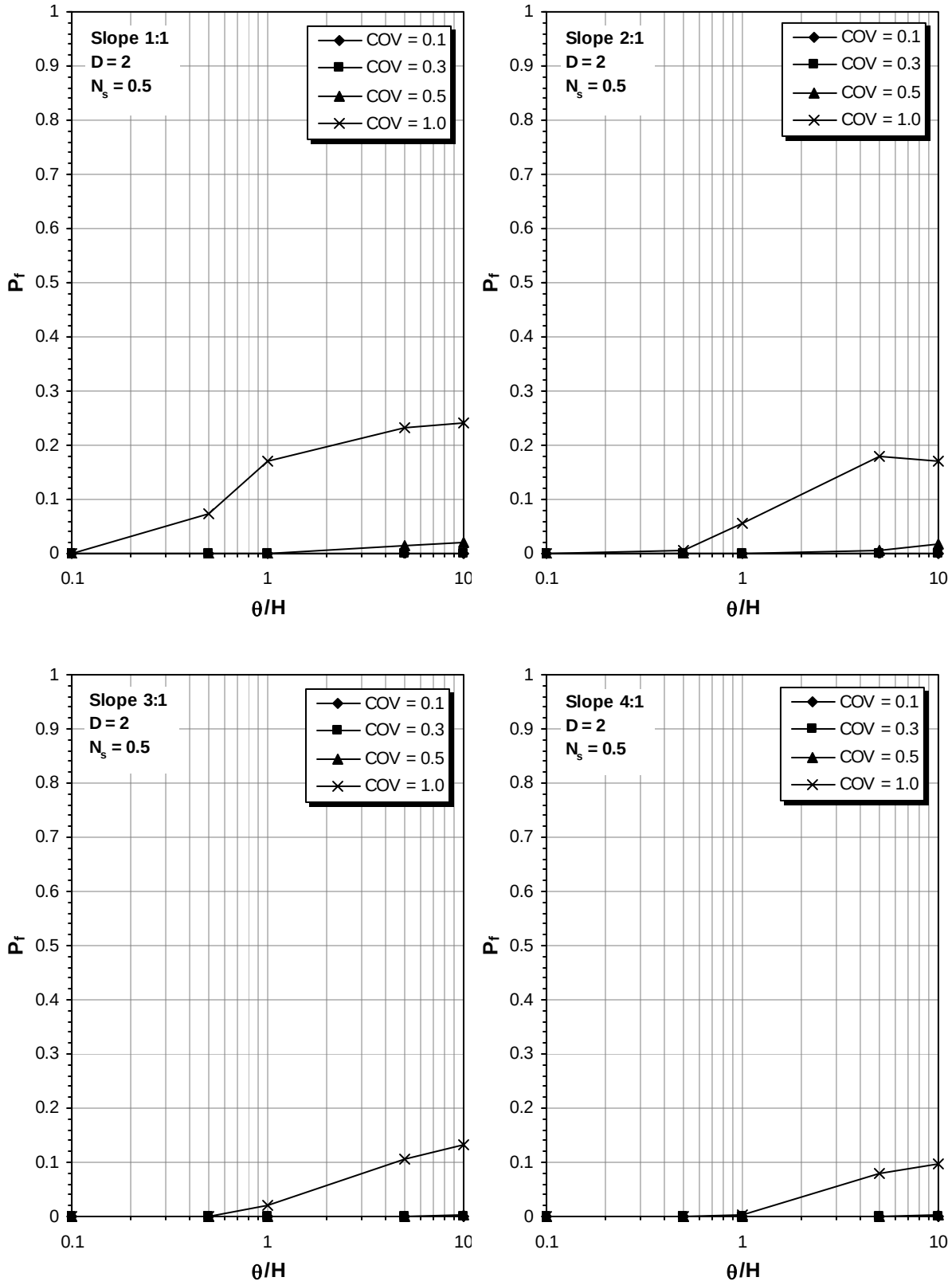
Slope 1:1
D = 2
N_s = 0.5
COV = 0.1
COV = 0.3
COV = 0.5
COV = 1.0
P_f
θ/H
Slope 2:1
D = 2
N_s = 0.5
Slope 3:1
D = 2
N_s = 0.5
Slope 4:1
D = 2
N_s = 0.5

D = 2; N_s = 0.5

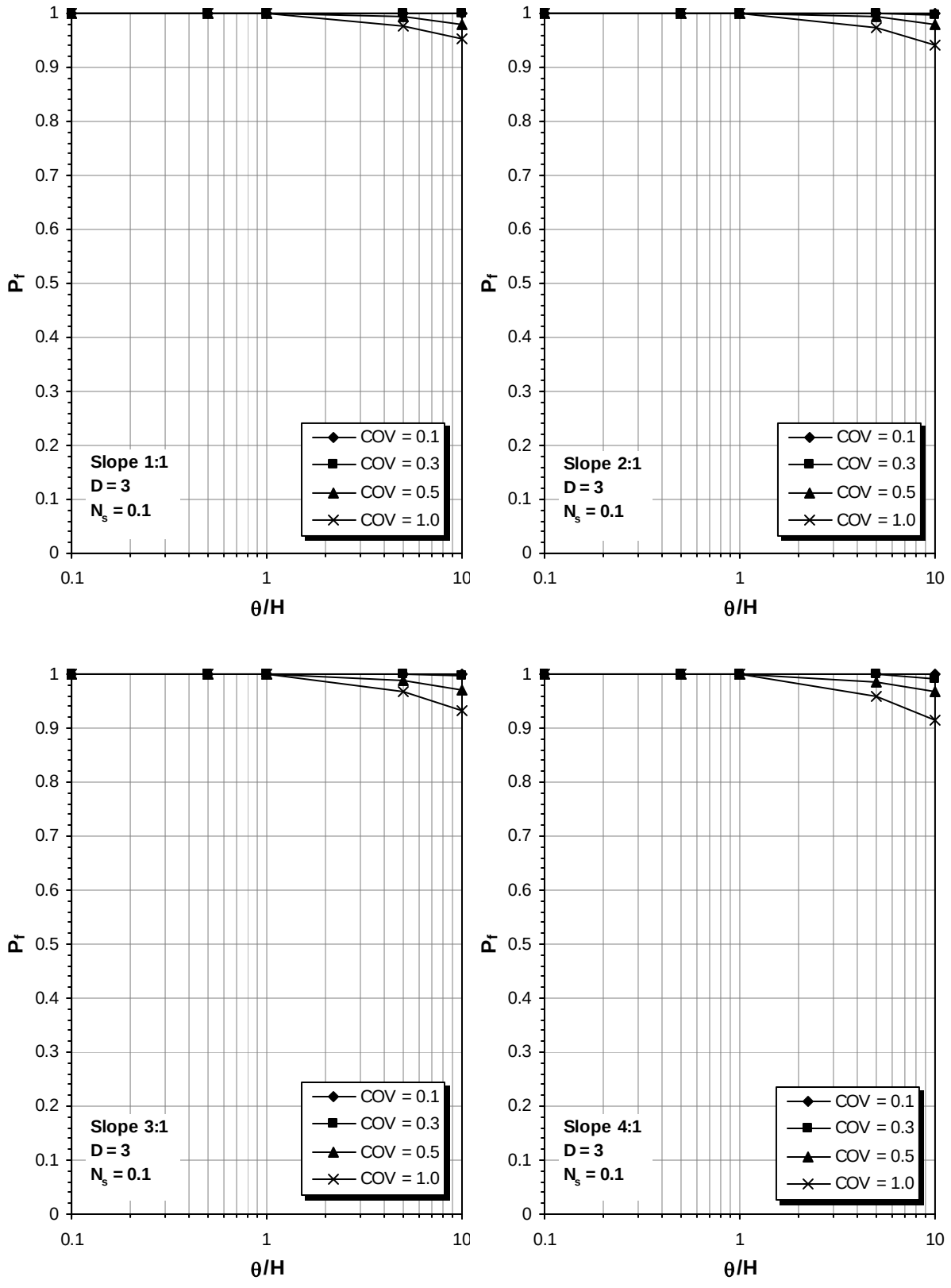
Slope 1:1
D = 3
Ns = 0.1
Slope 2:1
D = 3
Ns = 0.1
Slope 3:1
D = 3
Ns = 0.1
Slope 4:1
D = 3
Ns = 0.1
COV = 0.1
COV = 0.3
COV = 0.5
COV = 1.0
Pf
θ/H
0
0.1
0.2
0.3
0.4
0.5
0.6
0.7
0.8
0.9
1
0.1
1
10

D = 3; N_s = 0.1

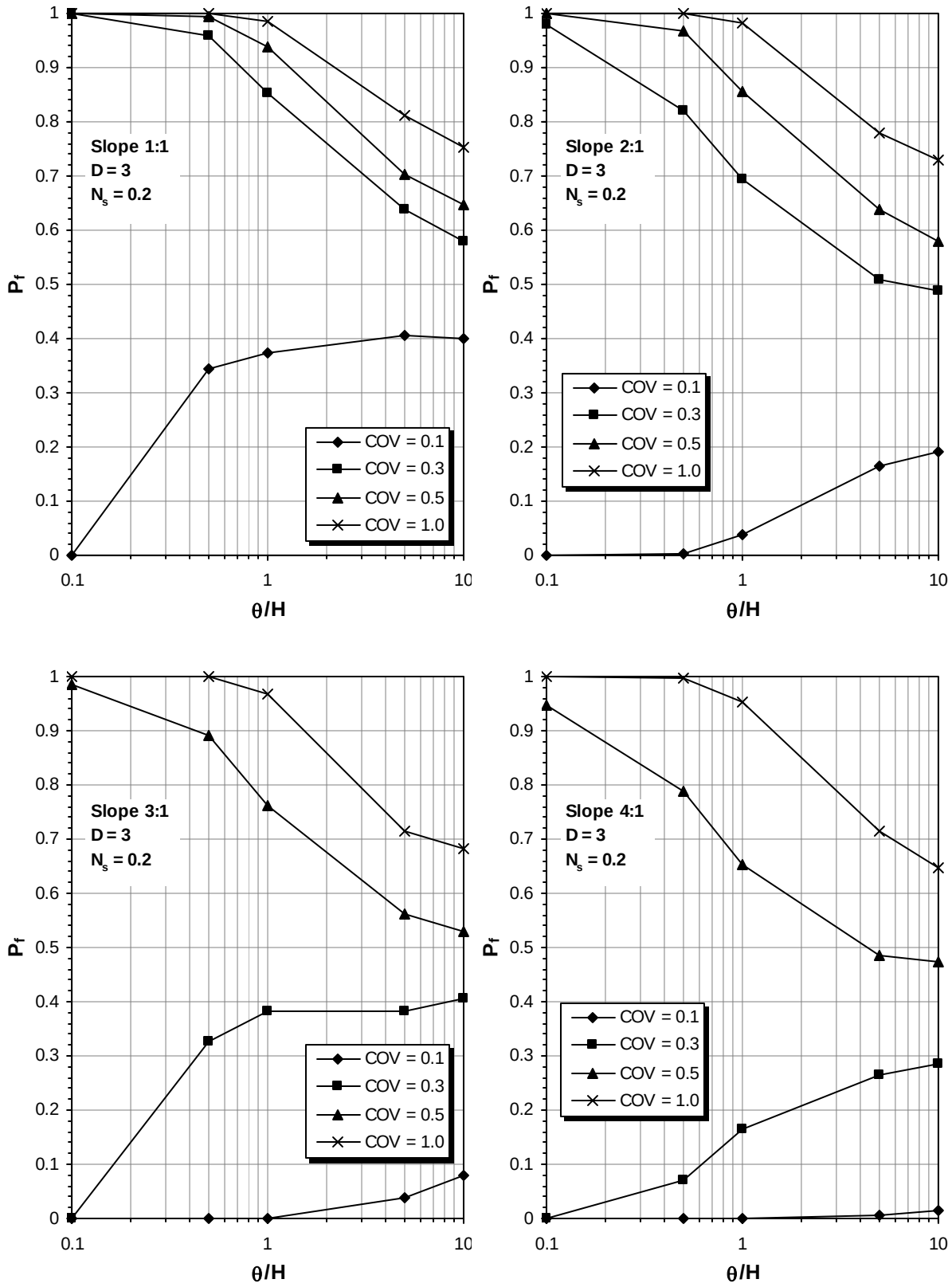
Slope 1:1
D = 3
N_s = 0.2
Slope 2:1
D = 3
N_s = 0.2
Slope 3:1
D = 3
N_s = 0.2
Slope 4:1
D = 3
N_s = 0.2
COV = 0.1
COV = 0.3
COV = 0.5
COV = 1.0
P_f
θ/H
0
0.1
0.2
0.3
0.4
0.5
0.6
0.7
0.8
0.9
1
0.1
1
10

D = 3; N_s = 0.2

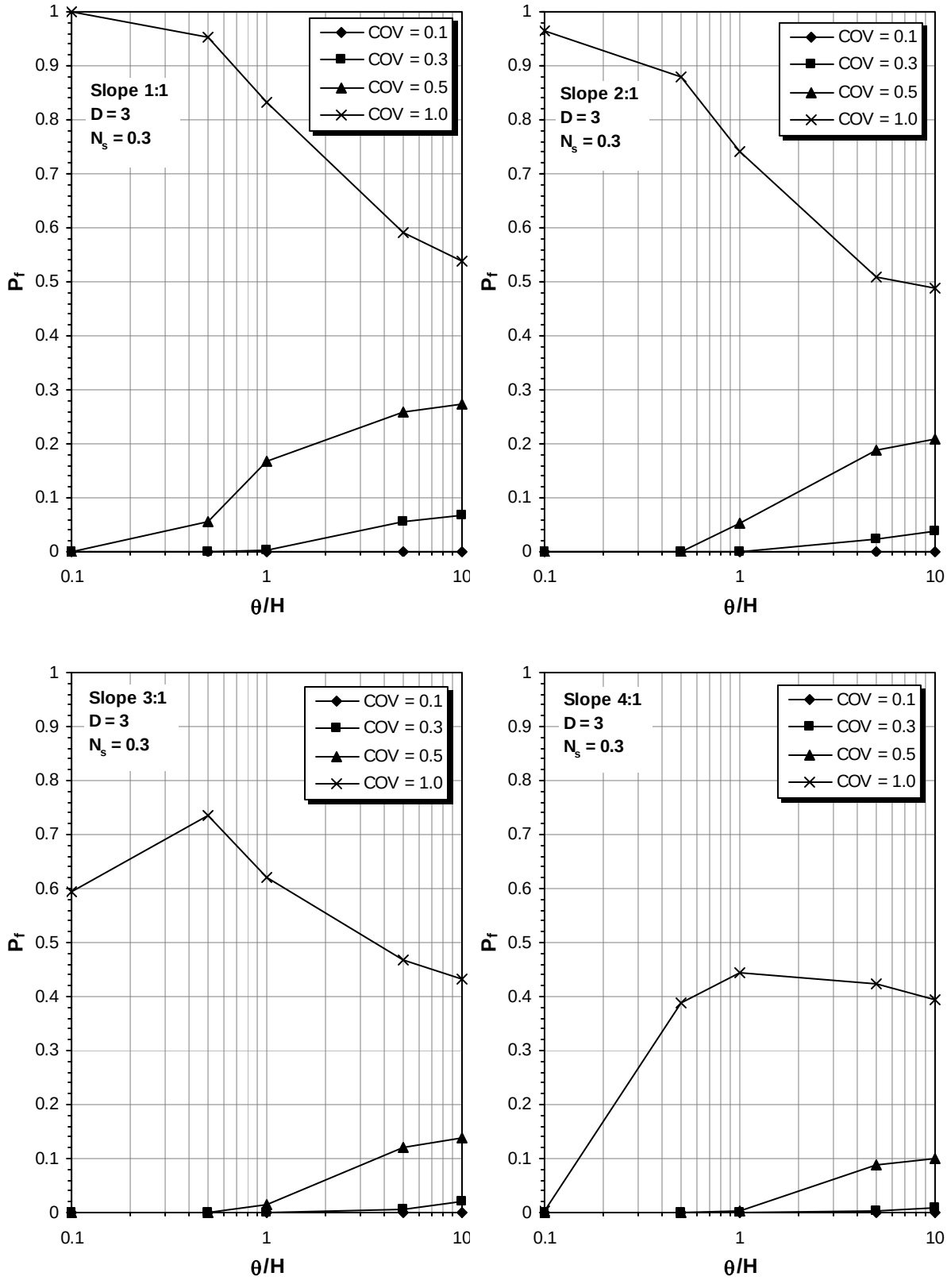
Slope 1:1
D = 3
Ns = 0.3
Slope 2:1
D = 3
Ns = 0.3
Slope 3:1
D = 3
Ns = 0.3
Slope 4:1
D = 3
Ns = 0.3
COV = 0.1
COV = 0.3
COV = 0.5
COV = 1.0
Pf
θ/H
0
0.1
0.2
0.3
0.4
0.5
0.6
0.7
0.8
0.9
1
0.1
1
10

D = 3; N_s = 0.3

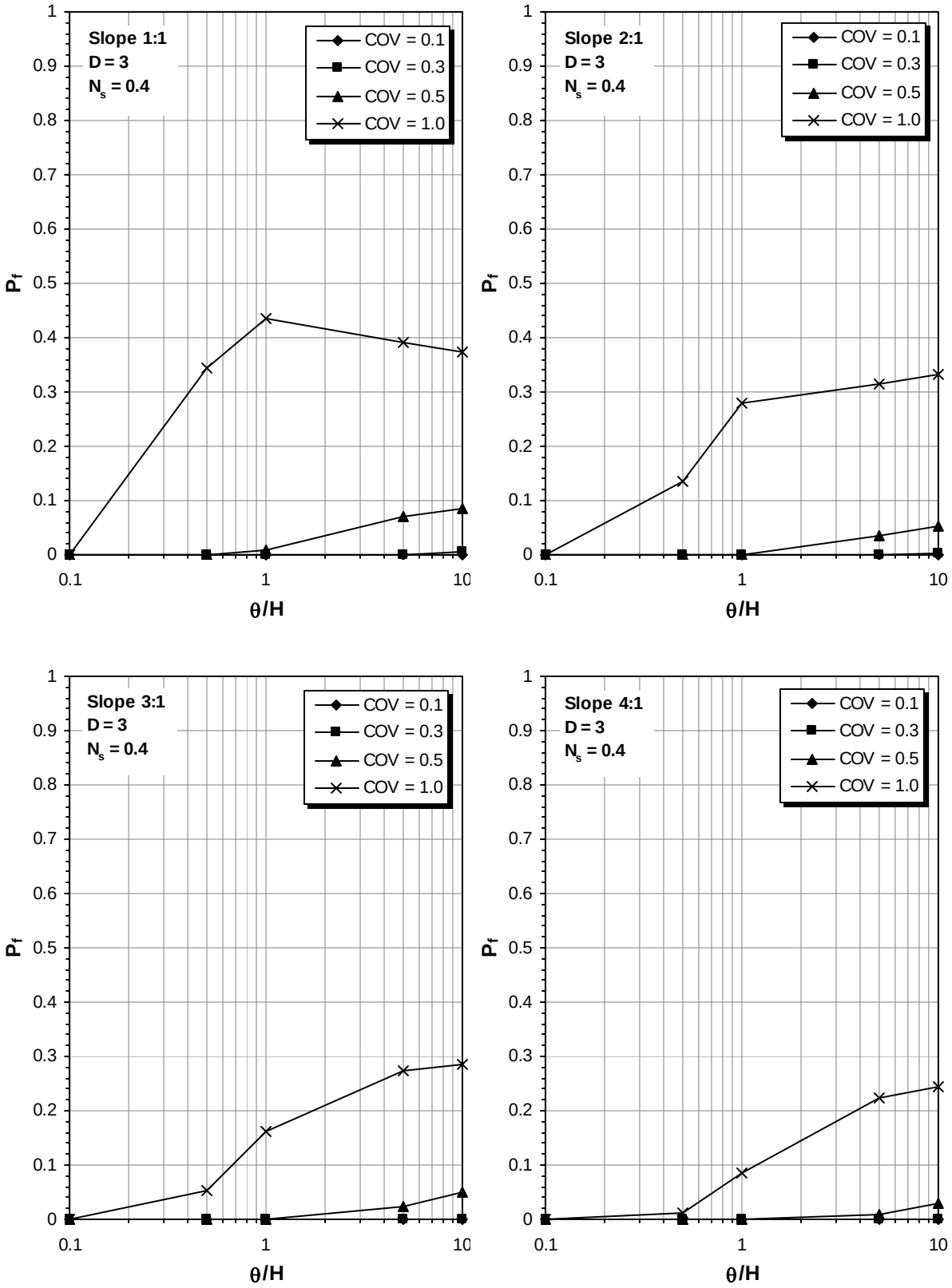
Slope 1:1
D = 3
Ns = 0.4
COV = 0.1
COV = 0.3
COV = 0.5
COV = 1.0
Pf
θ/H
Slope 2:1
D = 3
Ns = 0.4
Slope 3:1
D = 3
Ns = 0.4
Slope 4:1
D = 3
Ns = 0.4

D = 3; N_s = 0.4

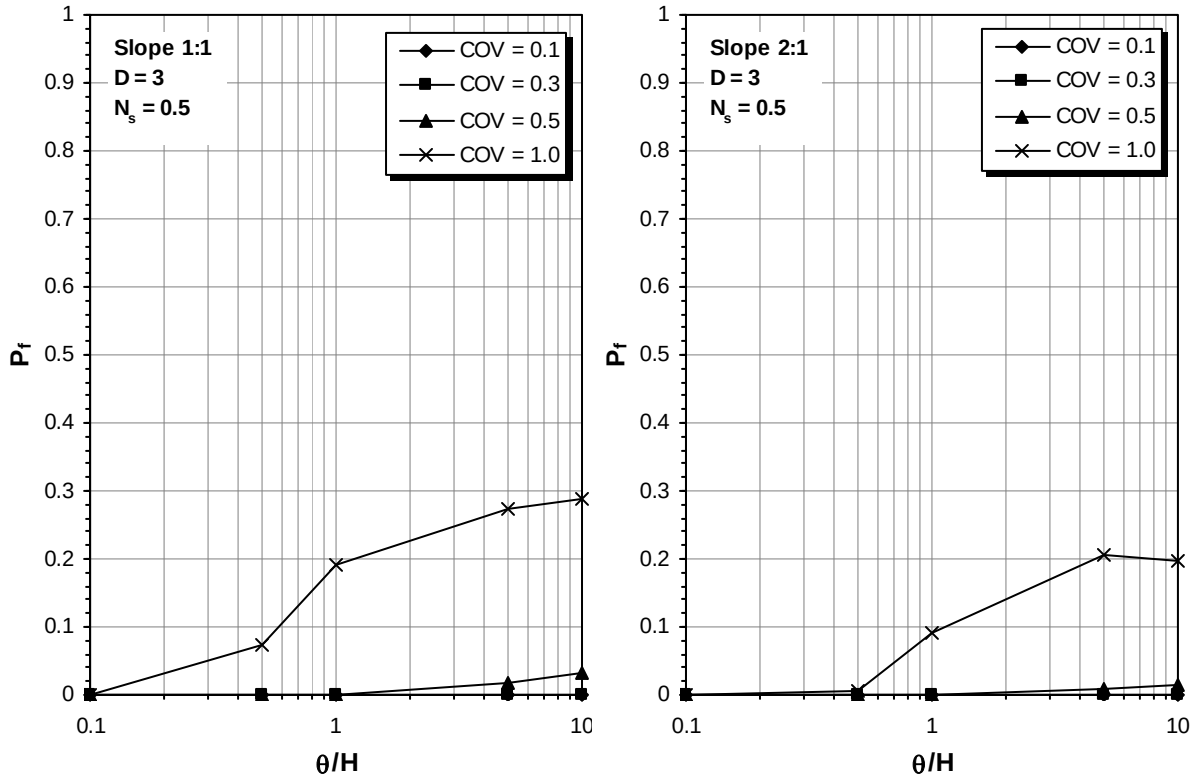
Slope 1:1
D = 3
N_s = 0.5
COV = 0.1
COV = 0.3
COV = 0.5
COV = 1.0
P_f
θ/H
0
0.1
0.2
0.3
0.4
0.5
0.6
0.7
0.8
0.9
1
0.1
1
10

Slope 2:1
D = 3
N_s = 0.5
COV = 0.1
COV = 0.3
COV = 0.5
COV = 1.0
P_f
θ/H
0
0.1
0.2
0.3
0.4
0.5
0.6
0.7
0.8
0.9
1
0.1
1
10

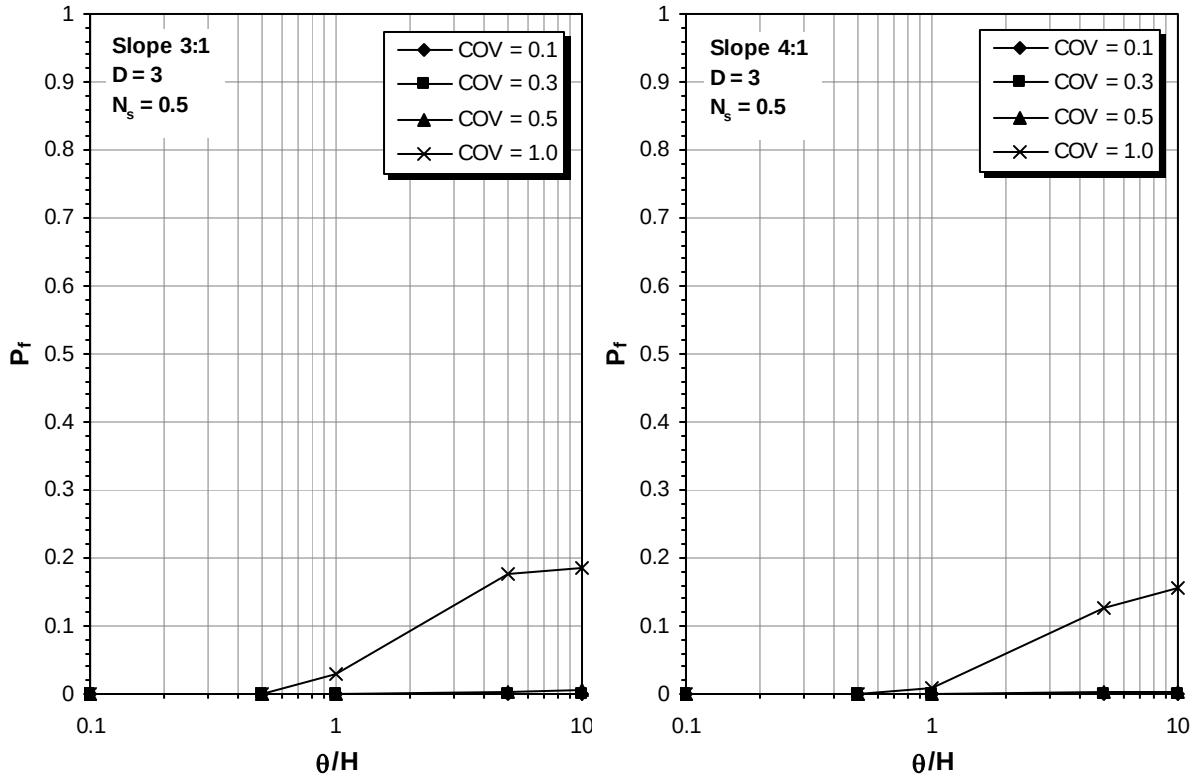
Slope 3:1
D = 3
N_s = 0.5
COV = 0.1
COV = 0.3
COV = 0.5
COV = 1.0
P_f
θ/H
0
0.1
0.2
0.3
0.4
0.5
0.6
0.7
0.8
0.9
1
0.1
1
10

Slope 4:1
D = 3
N_s = 0.5
COV = 0.1
COV = 0.3
COV = 0.5
COV = 1.0
P_f
θ/H
0
0.1
0.2
0.3
0.4
0.5
0.6
0.7
0.8
0.9
1
0.1
1
10

D = 3; N_s = 0.5